



Politechnika Wroclawska

FIELD OF SCIENCE: NATURAL SCIENCES

DISCIPLINE OF SCIENCE: PHYSICAL SCIENCES

DOCTORAL DISSERTATION

MAGNETIC RESPONSE OF COMPOSITES OF MAGNETIC NANOPARTICLES IN DIELECTRIC MATRICES TO THE ALTERNATING FIELD OF THE MICROWAVE FREQUENCY RANGE

Mgr inż. Kacper Brzuszek

Supervisor/Supervisors:

Dr hab. inż. Andrzej Janutka, prof. PWr

Assistant supervisor:

**Keywords: micromagnetic simulations, supermagnetism, superferromagnetism,
superparamagnetism, power conversion, magnetic nanoparticles**

WROCŁAW 2024

RODZICOM I BRATU
ZA WSPARCIE

STRESZCZENIE/ABSTRACT

Streszczenie

Przedstawiony cykl artykułów poświęcony jest teoretycznemu przewidywaniu parametrów odpowiedzi dynamicznej nanostrukturalnych magnetyków na zmienne pole magnetyczne bardzo wysokiej częstotliwości i o wysokiej amplitudzie, analizowanych jako materiały na rdzenie magnetyczne. Potencjalnym polem zastosowań tzw. wysokoczęstościowych nanokompozytów magnetycznych są mikroprzetworniki napięcia (konwertery mocy) do integrowania z układami mikroelektronicznymi. Kluczową ze względu na straty mocy (na prądach wirowych) własnością analizowanych struktur magnetycznych jest wysoki opór elektryczny, związany z separacją nanocząstek oraz małe rozmiary (metalicznych) nanocząstek. Za pomocą symulacji mikromagnetycznych wyznaczono przebiegi czasowe funkcji odpowiedzi magnetycznej (magnetyzacji) układów superferromagnetycznych i superparamagnetycznych (siatek nanocząstek ferromagnetycznych w matrycach dielektrycznych) oraz antyferromagnetycznego izolatora.

Rozważone zostały możliwości wzmocnienia odpowiedzi dynamicznej za pomocą statycznego pola porządkującego, wyboru kształtu nanocząstek magnetycznych, zastosowania rotującego pola wymuszającego zamiast liniowo spolaryzowanego. Trudnościami symulacji były: sformułowanie modelu mikromagnetycznego superferromagnetyka, uwzględnienie fluktuacji termicznych w dynamice superparamagnetyków, uwzględnienie złożonej anizotropii w wielodomenowej strukturze dwupodsieciowego antyferromagnetyka. Wyniki pozwoliły stwierdzić, że

1. zależność od częstości funkcji odpowiedzi warstw kompozytów superferromagnetycznych na dynamiczne pole magnetyczne jest podobna jak odpowiedzi jednorodnych ferromagnetyków, jednak nieliniowe efekty odpowiedzi dynamicznej silnie zależą od struktury kompozytu;
2. wartość przenikalności magnetycznej kompozytów superparamagnetycznych w zakresie mikrofalowej częstości może być kilkukrotnie większa od przenikalności magnetycznej próżni, co uzasadnia ich potencjalne zastosowanie w konwersji mocy;
3. tak zwany *performance factor* (iloczyn podatności magnetycznej i częstości χf) antyferromagnetycznego izolatora może osiągać wartości porównywalne do układów ferromagnetycznych, co uzasadnia rozważenie antyferromagnetyków jako materiałów magnetycznych do zastosowań w ekstremalnie wysokich częstotliwościach.

Abstract

The presented series of papers is devoted to the theoretical prediction of the dynamic response parameters of nanostructured magnets to alternating magnetic fields of very high frequency and high amplitude, analyzed as materials for magnetic cores. A potential field of application of so-called high-frequency magnetic nanocomposites is voltage microconverters for integration into micro-electro-mechanical systems. The key property of the analyzed magnetic structures, due to power losses (on eddy currents), is the high electrical resistance associated with the separation of nanoparticles and the small size of (metallic) nanoparticles. Using micromagnetic simulations, the time courses of the magnetic response functions (magnetization) of superferromagnetic and superparamagnetic systems (lattices of ferromagnetic nanoparticles in dielectric matrices) and an antiferromagnetic insulator were determined.

The possibilities of enhancing the dynamical response with a static ordering field, choice of the shape of magnetic nanoparticles, use of a rotating driving field instead of a linearly polarized one were considered. The difficulties of the simulations were the formulation of a model of a micromagnetic superferromagnet, the consideration of thermal fluctuations in the dynamics of superparamagnets, the consideration of complex anisotropy in the multi-domain structure of a two-lattice antiferromagnet. The results made it possible to conclude that

1. the frequency dependence of the response function of superferromagnet composite layers to a dynamic magnetic field is similar to the response of homogeneous ferromagnets, but the nonlinear effects of the dynamic response strongly depend on the structure of the composite;
2. the value of the magnetic permeability of superparamagnet composites in the microwave frequency range can be several times greater than the magnetic permeability of a vacuum, which justifies their potential use in power conversion;
3. the so-called *performance factor* (the product of magnetic susceptibility and frequency χf) of an antiferromagnet insulator, can reach values comparable to ferromagnet systems, justifying the consideration of antiferromagnets as magnetic materials for applications at extremely high frequencies.

Contents

Streszczenie/abstract	v
Table of Content	xi
Author's papers	1
I Introduction	3
1 Objectives and motivation	5
2 High frequency magnetic composites	7
2.1 <i>On-chip</i> power conversion	7
2.2 Magnetic cores and magnetic composite cores	8
3 Elements of macroscopic description of magnetization dynamics	11
3.1 Dynamical equation of magnetization in ferromagnets and supermagnets	11
3.1.1 Landau-Lifshitz-Gilbert equation	11
3.1.2 Determination of macroscopic material parameters from experi- mental data	12
3.2 Linear response of ferromagnets and supermagnets to an external dy- namical field	13
3.2.1 Ferromagnetic resonance	13
3.2.2 Dynamic magnetic permeability and the Snoek limit	16
3.2.3 Thermal fluctuations of the magnetic moment of a ferromagnetic particle and dynamical response in the presence of fluctuations . .	17
4 Key findings of the dissertation	23
4.1 High-frequency magnetic response of superferromagnetic nanocompos- ites – [P1]	23
4.2 High-frequency magnetic response of superparamagnetic composites of spherical Fe ₆₅ Co ₃₅ nanoparticles – [P2]	26
4.3 High-frequency magnetic response of superparamagnetic composites of spherical Fe and Fe ₃ O ₄ nanoparticles – [P3]	28
4.4 High-Frequency Magnetic Response of Arrays of Planar Fe ₆₅ Co ₃₅ Nan- odots: Effects of Bias Field and Thermal Fluctuations – [P4]	30
4.5 High-frequency magnetic response of crystalline and nanocrystalline antiferromagnetic NiO – [P5]	32

II	Articles	33
III	Summary	79
5	Summary and general conclusions	81
6	Acknowledgements	83
IV	Appendix	87
A	High-frequency magnetic composites	89
	Bibliography	I
	List of figures	XII

Author's papers

Doctoral series

1. K. Brzuszek and A. Janutka. “High-frequency magnetic response of superferromagnetic nanocomposites”. In: *Journal of Magnetism and Magnetic Materials*, vol. 543, (2022), p. 168608. DOI: 10.1016/j.jmmm.2021.168608 – [P1];
2. K. Brzuszek, C. A. Ross, and A. Janutka. “High-frequency magnetic response of superparamagnetic composites of spherical Fe₆₅Co₃₅ nanoparticles”. In: *Journal of Magnetism and Magnetic Materials*, vol. 573, (2023), 170651. DOI: 10.1016/j.jmmm.2023.170651 – [P2];
3. K. Brzuszek, C. A. Ross, and A. Janutka. “High-frequency magnetic response of superparamagnetic composites of spherical Fe and Fe₃O₄ nanoparticles”. DOI: 10.2139/ssrn.4709514 – [P3];
4. K. Brzuszek, C. A. Ross, and A. Janutka. “High-Frequency Magnetic Response of Arrays of Planar Fe₆₅Co₃₅ Nanodots: Effects of Bias Field and Thermal Fluctuations”. In: *IEEE Transactions on Magnetics*, vol. 59, no. 11 (2023), 7100306. DOI: 10.1109/TMAG.2023.3313871 – [P4];
5. K. Brzuszek, C. A. Ross, and A. Janutka. “High-frequency magnetic response of crystalline and nanocrystalline antiferromagnetic NiO”. in: *AIP Advances*, vol. 14, no. 2 (Feb. 2024), p. 025222. DOI: 10.1063/9.0000781 – [P5];

Other

1. A. Janutka and K. Brzuszek. “Domain-wall-assisted giant magnetoimpedance of thin-wall ferromagnetic nanotubes”. In: *Journal of Magnetism and Magnetic Materials*, vol. 465, (2018), pp. 437–449. DOI: 10.1016/j.jmmm.2018.06.007;
2. A. Janutka and K. Brzuszek. “Domain-wall-assisted asymmetric magnetoimpedance in ferromagnetic nanostripes”. In: *Journal of Physics D: Applied Physics*, vol. 52, (2018). DOI: 10.1088/1361-6463/aae6b4;
3. A. Janutka and K. Brzuszek. “Double-Vortex-Assisted Asymmetric Magnetoreactance in H-Shaped Nanomagnets”. In: *IEEE Magnetics Letters*, vol. 10, (2019), pp. 1–5. DOI: 10.1109/LMAG.2019.2912964;
4. A. Janutka and K. Brzuszek. “Giant magnetoreactance in magnetic nanowires”. In: *Journal of Magnetism and Magnetic Materials*, vol. 515, (2020), p. 167297. DOI: 10.1016/j.jmmm.2020.167297;

PART I:
INTRODUCTION

Chapter 1

Objectives and motivation

The transmission of electrical energy inside increasingly complex electronic circuits is becoming a problem for the development of automation systems. Especially for applications requiring weight reduction (aviation, but also aerospace), high-performance microdevices are needed to convert the parameters of electric current. Micro-powerconverters (transformers and inductors) are a promising alternative to electronic power conversion systems. The use of magnetic cores in them can improve the characteristics of these devices. However, miniaturization of power converters is associated with the need to raise the operating frequency to compensate for magnetic field fluxes that decrease with size. Another potential application of magnetic materials operating at high frequencies are the stators of electric micromotors.

In metallic magnets, as the frequency increases, the level of power losses increases exponentially, and the main component is the losses associated with the creation of eddy currents. A proposal for reducing losses are magnetic nanocomposites consisting of two phases:

- a dielectric matrix that increases the average resistance of the material, thereby reducing currents flowing through the composite and, hence, eddy current losses;
- the actual magnetic material (usually ferromagnetic) in the form of nanoparticles.

With a significant concentration of magnetic nanoparticles, the matrix can be doped with magnetic ions and change its magnetic properties, leading to the formation of a superferromagnetic phase – a phase with the desired high saturation magnetization. Unfortunately, this is associated with a significant reduction in electrical resistance, especially in the high frequency range. At sufficiently low concentrations, nanoparticles only interact with each other through a magnetostatic field, forming a superparamagnetic phase. Despite close to zero average saturation magnetization, superparamagnetic materials are now being considered for high-frequency applications, including microconverter cores.

The purpose of this dissertation is to determine the parameters of the high-frequency magnetic response of the supermagnetic phases of periodic magnetic nanoparticle systems – materials considered optimal for high-frequency applications, i.e., those containing no rare earth elements and with the highest possible saturation magnetization. Numerical simulations of ideally periodic systems make it possible to determine the limits of magnetic response enhancement, in isolation from technological limitations on the quality of nanostructured materials.

As a result of the study, we conclude that

1. the frequency-dependent function of the response of layered superferromagnetic composites to a dynamic magnetic field from the microwave range is similar to the response of homogeneous ferromagnets, but the nonlinear effects of the dynamic

- response strongly depend on the structure of the composite;
2. the amplitude of the magnetic permeability of superparamagnetic composites in the microwave frequency range can be several times higher than the magnetic permeability of a vacuum, which justifies their potential use in power conversion;
 3. the so-called *performance factor* (product of magnetic susceptibility and frequency, χf) of an antiferromagnetic insulator in the sub-THz frequency range can reach values comparable to ferromagnetic systems, which justifies consideration of antiferromagnets as magnetic materials for applications at extremely high frequencies.

Chapter 2

High frequency magnetic composites

2.1 *On-chip* power conversion

The expansion of electronic circuits results in high power consumption and requires the transmission of electric current over distances that are significant in the scale of the components of these circuits. Miniaturization of electronics leads to the need for efficient voltage microconverters (power converters). Nowadays, converting circuits of so-called power electronics are sometimes replaced by high-performance microinductors and microtransformers. While the use of magnetic cores is an obvious way to improve the efficiency of power conversion in transformers for electrical engineering applications, the miniaturization required in electronics is related to the significant difficulty of integrating magnetic components. The miniaturized converter must operate at very high frequencies to compensate for the low values of magnetic flux which results from the limited winding area. However, high magnetic permeability materials used in transformer cores are good conductors of electric current, and the inhomogeneities present in them, moving under the action of the external magnetic field, generate eddy currents (further locally amplified by the skin effect) and therefore power losses. Increasing exponentially with frequency, these losses can lead to complete uselessness of the magnetic core.

To characterize the quality of the magnetic core, one notices that the converted power is proportional to the electromotive force and, in the case of a linear or weakly nonlinear core response, to the product of the frequency and amplitude of the magnetic field flux.

$$P \propto f\Phi.$$

The conversion efficiency is the ratio of the transferred power to the power generated in the primary circuit of the converter, i.e. the power in the secondary circuit plus the value of the total power loss P_s :

$$\eta = \frac{P}{P + P_s}.$$

The parameter P_s is the sum of the contributions from eddy current losses and the so-called magnetic hysteresis losses (resulting from the core remagnetization itself - independent of the creation of eddy currents).

In past years, advances have been made in the topic of on-chip power conversion: [DWL+23; HWZ+21; MSS+15; WDS+16].

Appendix A contains notable information on content and manufacturing of magnetic composites applicable in high frequencies.

2.2 Magnetic cores and magnetic composite cores

In power conversion, the goal is to maximize the induced electromotive force while minimizing power losses. Losses P_s are divided into magnetic losses (so-called hysteresis losses P_h) and eddy current losses P_{ec} (arising from dynamical changes in the spatial magnetic structure – domains) – ([KBF+13; PWKF18]).

$$P_s = P_h + P_{ec}.$$

In the high-frequency (subGHz) frequency range, the Steinmetz scaling algorithm ([NSSP19; SSNW07]) is used to describe losses in complex magnetic cores (composites), hysteresis loops can be analyzed using the same approach [VK14].

$$P = p_1 f^x B_m^{\beta-\alpha x} + p_2 f^{2x} B_m^{\beta-2\alpha x},$$

where

- f is the frequency of the driving field of amplitude of B_m ;
- exponent of the power of the frequency refers to the (non)linearity of the response. For $x = 1$, a linear response is analyzed;
- two terms of the Steinmetz equation ([Ste92]) are summed to take into account possible nonlinearities;
- $p_1, p_2, x, \beta, \alpha$ are fitting coefficients, unique for each material.

The general idea behind this equation is to represent the losses as an electromotive force multiplied by a certain constant derived from the geometry of the system, material parameters, etc., which constants can be fitted to the experimental results as ([VK14]) $k f^m B^n$.

Magnetic losses are proportional to the area covered by the hysteresis loop (cf. fig. 2.1 and eq. (2.2.1)) in the $M - H$ plot.

$$P_h \propto \int B dH \quad (2.2.1)$$

The shape and width of the (dynamic) hysteresis loop can strongly depend on the remagnetization frequency.

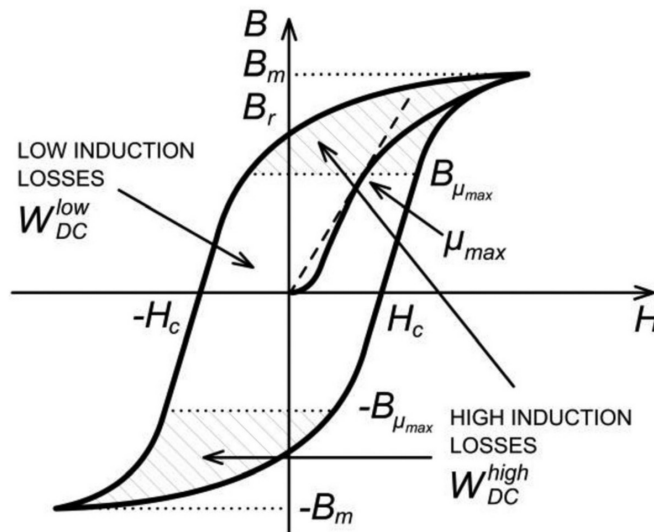


Figure 2.1: Hysteresis losses are directly related to area of hysteresis – [PWKF18]

Eddy currents are formed [KTPT92] due to the time-varying vector potential of the magnetic field:

$$\vec{j} = -\frac{\partial \vec{A}}{\partial t}$$

In magnetic composites, the losses associated with them can be divided into parts related to charge flows between magnetic particles and flows within the particles:

$$P_{ec} = P_{inter} + P_{intra}$$

and these losses are due to electrical resistance, cf. fig. 2.2.

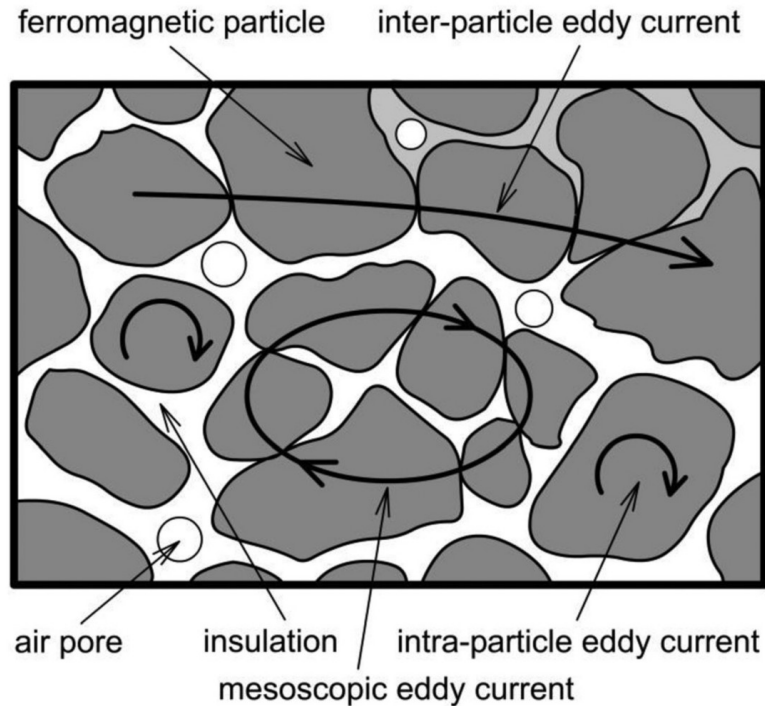


Figure 2.2: Possible paths of eddy currents in magnetic nanocomposite – origin of eddy currents losses – [PWKF18]

Finite element method is used to simulate magnetic materials. Numerical calculations are costly - requiring significant resources and time, so possible other ways to analyze eddy current losses are being sought. An analysis of (semi-analytical) methods for cuboidal iron nanoparticles in an epoxy resin matrix has been carried out in [CRD21]. The analysis used the homogenization method ([Iga17]). A subtype of eddy current losses associated with inter-particle flows are *excess losses* - associated with the forced movement of domain walls between large, encompassing multiple magnetic particles domains [Ber88; KBF+13]. However, eddy current models are very complex, involving the full system of Maxwell's equations, and the approximations used to solve them can fail especially in the range of high frequencies and large amplitudes of driving fields.

Chapter 3

Elements of macroscopic description of magnetization dynamics

3.1 Dynamical equation of magnetization in ferromagnets and supermagnets

3.1.1 Landau-Lifshitz-Gilbert equation

The dynamical equation of the normalized magnetization \hat{m} is the Landau-Lifshitz-Gilbert equation ([Gil04; Gil55; LL37]) of the form

$$\frac{\partial \hat{m}}{\partial t} = \overbrace{\gamma \hat{m} \times \vec{H}_{\text{eff}}}^{\text{Prec.}} - \overbrace{\alpha \hat{m} \times \frac{\partial \hat{m}}{\partial t}}^{\text{Diss.}},$$

whose right-hand side contains the precession and dissipation terms. The effective magnetic field \vec{H}_{eff} is determined from the density of the Hamiltonian as the

$$\vec{H}_{\text{eff}} \equiv -\frac{1}{\mu_0 M_s} \frac{\delta \mathcal{H}_{\text{sum}}}{\delta \hat{m}}.$$

The energy density of a ferromagnet is given by the sum of the following contributions:

1. exchange energy density

$$\mathcal{H}_{\text{ex}} = A (\nabla \hat{m})^2.$$

2. single-ion magnetocrystalline anisotropy energy density:

$$\mathcal{H}_{\text{an}} = \begin{cases} K_1 \sin^2(\theta) + K_2 \sin^4(\theta) + \dots & \text{Uniaxial anisotropy} \\ K_0 + K_1 (\alpha_1^2 \alpha_2^2 + \alpha_2^2 \alpha_3^2 + \alpha_3^2 \alpha_1^2) + K_2 (\alpha_1^2 \alpha_2^2 \alpha_3^2) & \text{Cubic anisotropy,} \end{cases}$$

where

- θ is the angle between magnetization and easy axis;
- α_i is the cosine of angle between magnetization and the i -th axis of the cubic crystal;

3. demagnetization energy density

$$\mathcal{H}_d \approx -\frac{\mu_0}{2} \vec{H}_d \cdot \vec{M}.$$

$$\vec{H}_d(r) \equiv -\int_V \frac{\rho(\vec{r}')(\vec{r}' - \vec{r})}{4\pi |\vec{r} - \vec{r}'|^3} d\vec{r}' + \int_S \frac{\sigma(\vec{r}')(\vec{r}' - \vec{r})}{4\pi |\vec{r} - \vec{r}'|^3} d\vec{r}',$$

where $\rho(\vec{r}) \left(\equiv -M_s \vec{\nabla} \cdot \vec{m}(\vec{r}) \right)$ and $\sigma(\vec{r}) \left(\equiv M_s \vec{m}(\vec{r}) \cdot \hat{n}(\vec{r}) \right)$ denotes, respectively, volume and surface density of magnetic charges;

4. Zeeman energy density – effect of external field on magnetization

$$\mathcal{H} = -M_s \vec{H} \cdot \hat{m}.$$

In superferromagnets ([P1]), the dynamics of magnetization is described by the LLG equation as well, but the inhomogeneity of the structure is incorporated as the inhomogeneity of the equation's parameters. In the case of superparamagnets ([P2; P3; P4]), magnetization is non-zero only in the region of magnetic particles, and it disappears in the area of the (non-magnetic) matrix. In case of superantiferromagnets ([P5]) nanoparticles (and domains in bulk) do not interact with each other due to zero demagnetization field.

3.1.2 Determination of macroscopic material parameters from experimental data

The magnetic subsystem of a superferromagnet includes magnetic particles and a dielectric matrix. Thus, micromagnetic simulations require knowledge of the macroscopic parameters of the magnetic subsystem: anisotropy constants, exchange stiffness, both for the region of metallic nanoparticles (we can use here parameters of the bulk magnetic material which are known), and for the matrix region. Determination of the magnetic parameters of the matrix requires their extraction from experimental data with the help of a magnetic model of the inhomogeneous medium. We use the model of random magnetic anisotropy (RMA model – [ABC78]). The model assumes that there is local magnetic anisotropy in a granular magnetic medium with a random orientation of the anisotropy axis due to the local distribution of the magnetite grains. In RMA model developed by Herzer ([Her05]), there is also global anisotropy, i.e. the granular structure of the magnetic composite is not completely independent of the magnetization state of the system during its solidification. According to the RMA model, the average random anisotropy constant scales with the number N of magnetic particles, forming a local anisotropic structure. It proposes the existence of an effective exchange constant (spin stiffness), depending on the anisotropy constants and value of the coercivity field, transverse to the easy axis of global anisotropy. The relationship between the magnetization of nanoparticles and the matrix and the resultant magnetization of the system, as well as the relationship between the spin stiffnesses of the nanoparticles, the matrix and the effective spin stiffness of the system are part of the RMA model, and they allow us to determine the corresponding material constants of the magnetic substructure of the dielectric matrix when formulating numerical model of the superferromagnetic nanocomposite.

If in the volume $V_{\text{ex}} \left(\equiv L_{\text{ex}}^3 \right)^1$ there are $N \left(\equiv \left[\frac{L_{\text{ex}}}{D} \right]^3 \right)$ grains, where D denotes the size of the grain (magnetic nanoparticle)², with different anisotropy directions, then, for a finite number of N , there is a certain local axis of easy magnetization. The average

¹ L_{ex} stands for *magnetic correlation length* – it's a *renormalized* exchange length contrary to *basic* exchange length λ_{ex} . Former can be obtained by substituting local anisotropy constant K_1 by it's averaged value $\langle K_1 \rangle$ [Her05].

²In consideration, we assume cubical nanoparticles of edge length equals to D

constant of uniaxial anisotropy can be determined as

$$\langle K_1 \rangle = \frac{|K_1|}{\sqrt{N}} = |K_1| \left(\frac{D}{L_{\text{ex}}} \right)^{\frac{2}{3}}$$

In addition, there may be global anisotropy of the superferromagnetic system characterized by the constant K_u . The content of the magnetic phase in the composite formed of cubic nanoparticles is determined by the ratio of its volume to the total volume, eq.

$$x \equiv \frac{D^3}{(D + \Lambda)^3},$$

where Λ is the distance between nanoparticles.

There is also a critical ratio of the magnetic phase content x_c , above which spontaneous magnetization occurs in the system. Renormalizing the magnetic phase content ratio into

$$x_p \equiv \frac{1 - x}{1 - x_c},$$

such that

$$\begin{aligned} x_p &\xrightarrow{x \rightarrow x_c^+} 0, \\ x_p &\xrightarrow{x \rightarrow 1^-} 1. \end{aligned}$$

The effective exchange constant of the composite is given by

$$\bar{A}_{\text{ex}} = \left(\frac{x_p \sqrt{K_u} K_1^2 D^3}{\mu_0 \bar{M}_s H_{\text{cy}}} \right)^{\frac{2}{3}},$$

where H_{cy} is the coercivity field for the hysteresis obtained when the field is aligned along the direction of the hard axis ([WMZL12]) and K_1 denotes unique anisotropy axis of given nanoparticle.

Knowing the material parameters of the nanoparticles, the magnetic parameters of the matrix will be obtained from the following relations

$$\begin{aligned} M_s^d &= \frac{\bar{M}_s - x_p M_s^m}{1 - x_p} \\ A_{\text{ex}}^d &= \frac{\left(x_p^{-\frac{1}{3}} - 1 \right)^2 \bar{A}_{\text{ex}} A_{\text{ex}}^m}{\left(x_p^{-\frac{1}{3}} \sqrt{A_{\text{ex}}^m} - \sqrt{\bar{A}} \right)^2}. \end{aligned}$$

3.2 Linear response of ferromagnets and supermagnets to an external dynamical field

3.2.1 Ferromagnetic resonance

Magnetic resonance ([Coe10; KM18; Yal13]) occurs when an alternating magnetic field of frequency equal to the Larmor frequency is applied. If a constant field B and transverse

to it alternating field $b(t)$ of high frequency act on the magnetic moment, the Larmor frequency

$$f_L \equiv \frac{\gamma B}{2\pi}$$

determines the amplitude of dynamical response. In thin ferromagnetic layers, in the situation of a driving field directed along the axis of magnetization and a constant field directed in the plane of the layer along the hard axis, resonance occurs in the dynamical response at a certain value of the Larmor frequency. An important role for the resonance is played by the demagnetization field, which forces the magnets to order in the plane of the layer and can be included into effective description by means of uniaxial anisotropy (of the easy plane type) by introducing demagnetization factors.

For simple magnets geometries, the demagnetization field is of the form $-\bar{N}\vec{M}$, where \bar{N} is the tensor of demagnetization factors, which is diagonal $\bar{N} \equiv \begin{bmatrix} N_x & 0 & 0 \\ 0 & N_y & 0 \\ 0 & 0 & N_z \end{bmatrix}$ ³.

The overall field inside takes the form

$$\vec{H}_{\text{tot}} = \frac{\text{Outer field}}{\mu_0} \vec{B} + \vec{b}(t) - \frac{\text{Demagnetization field}}{NM} \vec{M} \quad (3.2.1)$$

Assuming that the driving field is weak ($b \ll B$), in the linear approximation, the magnetization can be expressed as $\vec{M} \approx M_s \hat{k} + \frac{\vec{m}(t)}{M}$ – we assume that $\vec{B} \parallel \hat{k}$. Then the demagnetization field is of the form

$$\vec{H}_d = -\mu_0 [N_x m_x \hat{i} + N_y m_y \hat{j} + N_z (m_z + M_s) \hat{k}]$$

The oscillating components of \vec{m} satisfy the linearized equations (where $H_0 (\equiv \frac{B}{\mu_0}) \parallel OZ$)⁴

$$\begin{aligned} \frac{dm_x}{dt} &= \gamma_0 (m_y H_z - M H_y) = \gamma_0 [H_0 + (N_y - N_z) M] m_y \\ \frac{dm_y}{dt} &= \gamma_0 (-m_x H_z + M H_x) = -\gamma_0 [H_0 + (N_x - N_z) M] m_x \end{aligned}$$

The frequencies of oscillatory solutions (eigenvalues of the matrix of coefficients) of the above system of equations can be found under the condition of zero determinant

$$\begin{vmatrix} i\omega & \gamma_0 [H_0 + (N_y - N_z) M] \\ -\gamma_0 [H_0 + (N_x - N_z) M] & i\omega \end{vmatrix} = 0$$

In particular, the frequencies of ferromagnetic resonance (FMR) are ([Kit48; Kit51]).

$$\omega_0^2 = \gamma_0^2 [H_0 + [N_x - N_z] M] [H_0 + (N_y - N_z) M]$$

³Here and hereafter the symbol $\bar{\cdot}$ over N is omitted.

⁴In literature γ is sometimes used in context of γ_0 . It is therefore important to clearly state their values used in this dissertation:

$$\begin{aligned} \gamma &\equiv 1.76 \cdot 10^{11} \text{ Hz T}^{-1} \\ \gamma \mu_0 = \gamma_0 &\equiv 2.21 \cdot 10^5 \text{ m A}^{-1} \text{ s}^{-1}. \end{aligned}$$

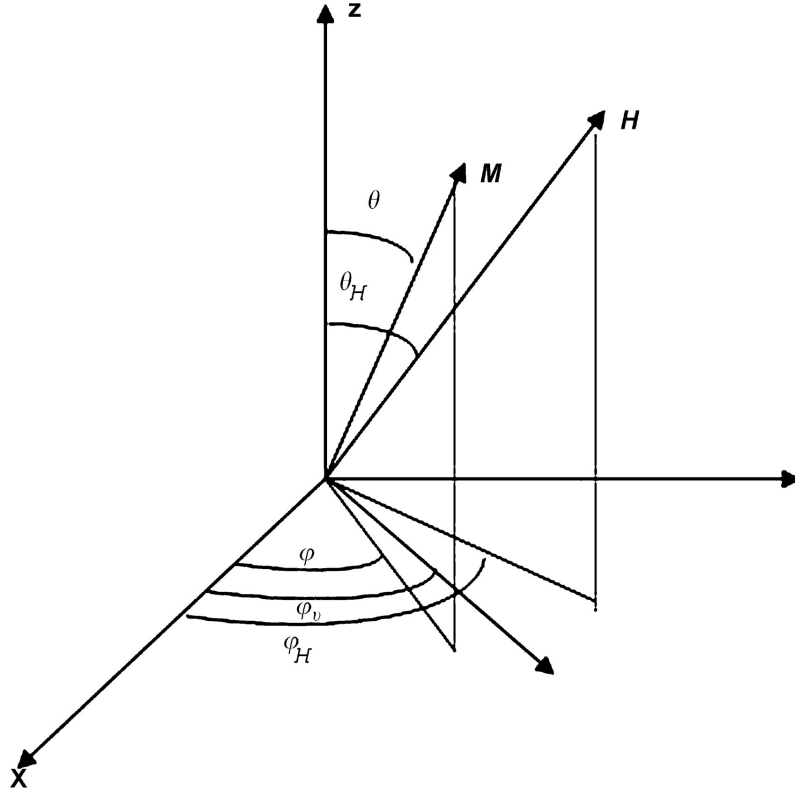


Figure 3.1: Angles for determining ferromagnetic resonance frequencies from eq. (3.2.2) – [DDF07]

The presence of magnetocrystalline anisotropy also affects the resonance frequency – it provides an additional term to the eq. (3.2.1) of the vector length $H_u \equiv \frac{2K_u}{M_s}$. In the paper [DDF07] the following form of the equation for the ferromagnetic resonance frequency is suggested (the angles are the same as those on fig. 3.1):

$$\left(\frac{\omega}{\gamma_0}\right)^2 = [H_0 \cos(\varphi_0 - \varphi_H) - H_u \sin^2(\varphi_0) + H_{\text{eff}}] [H_0 \cos(\varphi_0 - \varphi_H) + H_u \cos(2\varphi_0)], \quad (3.2.2)$$

where $H_{\text{eff}} \equiv M_s - \frac{2K_{\perp}}{M_s}$ with K_{\perp} being the perpendicular anisotropy constant relative to the plane of the layer (PMA – Perpendicular Magnetic Anisotropy)⁵.

In the case of a sphere where all directions are equal (so $N_{x|y|z} = \frac{1}{2}$), the FMR frequency is given by the

$$\omega_0 = \gamma_0 \left(H_0 + \frac{2K_u}{M_s} \right).$$

For more complicated systems, for example, with magnetocrystalline cubic anisotropy, one can find the relevant relations in the literature, e.g. [Coe10].

Ferromagnetic resonance excitation is a useful tool for studying magnetic properties (saturation magnetization, easy axis directions and values of anisotropy constants) – ([FPW16; SML+21; Yal13]). Simultaneously, the magnetic resonance frequency limits the operating frequency range of materials for magnetic cores of power converters, which is associated with a significant phase shift of the magnetic response with respect to

⁵In general, the effect of PMA on FMR frequency is more complicated, but this is beyond the scope of this dissertation.

the driving field in the vicinity of resonance. The phase shift is accompanied by the occurrence of dynamic hysteresis, and therefore power losses for core remagnetization.

3.2.2 Dynamic magnetic permeability and the Snoek limit

Let us consider a single-domain ferromagnet in an alternating magnetic field directed along the versor \hat{y} , that is, $\vec{H}(t) = [0, H_y(t), 0]$ with amplitude $\text{Amp}(H_y)$ transverse to the direction of magnetization (easy axis OX). In order to describe the oscillations of magnetization around the equilibrium state $\hat{m} = [1, 0, 0]$, we introduce a complex dynamic parameter $m_+(t) \equiv m_y(t) + im_z(t)$.

Solution of the linearized equation of motion of the form

$$m_+(t) = [A_y(\omega) + iA_z(\omega)] \sin(\omega t) + [C_y(\omega) + iC_z(\omega)] \cos(\omega t)$$

leads, through a Fourier transform, to the dependence of the dynamic magnetic susceptibility/permeability on the frequency

$$\mu(\omega) \equiv \frac{m_+(\omega)}{H_y(\omega)} = \frac{M_s}{\text{Amp}(H_y)} \left\{ A_y(\omega) + C_z(\omega) + i[A_z(\omega) - C_y(\omega)] \right\}.$$

Introducing quantities

$$\begin{aligned} \omega_1 &\equiv \gamma_0 \left(\frac{2K_u}{\mu_0 M_s} + M_s \right), \\ \omega_2 &\equiv \gamma_0 \frac{2K_u}{\mu_0 M_s} \end{aligned}$$

one can write the real and imaginary parts of the dynamic permeability as

$$\begin{aligned} \mu'(\omega) &= \gamma_0 M_s \frac{(\omega - \omega_1)(\omega^2 - \omega_1 \omega_2) + \alpha^2 \omega^2 (\omega + \omega_2)}{(\omega^2 - \omega_1 \omega_2)^2 + \alpha^2 \omega^2 (\alpha^2 \omega^2 + \omega_1^2 + \omega_2^2)}, \\ \mu''(\omega) &= \gamma_0 M_s \frac{\alpha \omega \{ \omega [(1 + \alpha^2) \omega - \omega_2] - \omega_1 (\omega - \omega_1) \}}{(\omega^2 - \omega_1 \omega_2)^2 + \alpha^2 \omega^2 (\alpha^2 \omega^2 + \omega_1^2 + \omega_2^2)}, \end{aligned}$$

Zeroes of $\mu'(\omega)$ and $\mu''(\omega)$ are very close to the frequency of ferromagnetic resonance $\omega_{\text{res}} \equiv \sqrt{\omega_1 \omega_2}$.

It should be emphasized that, unlike in the previous subsection, ferromagnetic resonance in the absence of a constant *ordering* field is considered here, and this resonance arises from the choice of frequency of the driving field. The quantity

$$\tan(\delta_\omega) \equiv \frac{\mu''(\omega)}{\mu'(\omega)}$$

is a performance characteristic of the magnetic material called the tangent of the loss angle. In the case of magnetic layers, $\text{Amp}[m_z] \ll \text{Amp}[m_y]$ and

$$\begin{aligned} \mu'(\omega) &\approx M_s \frac{\text{Amp}[m_y](\omega)}{\text{Amp}(H_y)} \cos(\delta_\omega) \\ \mu''(\omega) &\approx M_s \frac{\text{Amp}[m_y](\omega)}{\text{Amp}(H_y)} \sin(\delta_\omega) \end{aligned}$$

Then the magnetic losses can also be characterized by the ratio $\frac{\text{Amp}[m_z](\omega)}{\text{Amp}[m_y](\omega)}$, and the angle of deviation of magnetization from the plane of the layer is close to the loss angle.

In the low-frequency limit $\omega \rightarrow 0$, the real part of the magnetic susceptibility tends toward the value of $\mu'(\omega \rightarrow 0) = \gamma_0 \frac{M_s}{\omega_2} = \mu_0 \frac{M_s^2}{2K_u}$, i.e.

$$(\mu' - 1)\omega_{\text{res}} = (\gamma_0 M_s)^2 \left(1 + \frac{H_{\text{an}}}{M_s} \right).$$

This is the Snoek [AD08; Sno48] relation which defines the maximum value of the real part of the magnetic susceptibility (reached in the low-frequency limit), called the Snoek limit. Its breakthrough would be considered an overcome of fundamental difficulty in improving magnetic materials.

3.2.3 Thermal fluctuations of the magnetic moment of a ferromagnetic particle and dynamical response in the presence of fluctuations

The benchmark for studying the dynamics of superparamagnetic composites is the Brown's theory of thermal fluctuations in a single-domain ferromagnetic particle. For nanoparticles with very small volume, the fluctuations of their magnetic moments are very strong even at temperatures well below room temperature and cannot be ignored in the analysis of the dynamical response.

Brown's theory [Bro63] is based on a distribution function $w(\hat{m}, t, T)$, which is expressed with the magnetic moment orientation angles θ and ϕ : $\frac{\vec{M}}{|\vec{M}|} = \hat{m} = [\sin \theta \cos \phi, \sin \theta \sin \phi, \cos \theta]$. For particles with uniaxial anisotropy $w(\theta, \phi, t, T) = w(\theta, t, T)$.

The dynamical equation of the distribution function obtained from the Larmor equation (Landau-Lifshitz-Gilbert for a homogeneous system) within Fokker-Planck scheme ([Fok14; Pla17]), we mean assuming the presence of drift and diffusion terms in the equation and specifying of the correlation functions of the magnetic field components given as ([Bro63])

$$\langle H_{\text{th},i}(t), H_{\text{th},j}(t + \tau) \rangle = \frac{2\alpha k_B T}{\gamma_0 \mu_0 M_s} \delta_{ij} \delta(\tau).$$

An algebra leads to a Smoluchowski-type evolution equation [Smo16a; Smo16b]:

$$\frac{\partial w}{\partial t} = \frac{\partial}{\partial y} \left[(1 - y^2) \left(h \frac{\partial \mathcal{H}}{\partial y} w + D \frac{\partial w}{\partial y} \right) \right],$$

where:

- $y \equiv \cos \theta$;
- \mathcal{H} is the Hamiltonian of macrospin;
- coefficients (of diffusion and drift) are given by

$$h \equiv \frac{\gamma \alpha}{M(1 + \alpha^2)}; \quad D \equiv \frac{h k_B T}{V}.$$

Separating the variables and expanding the angular part of the distribution function with Legendre polynomials $P_l(y)$ one obtains

$$w(\theta, t, T) = w_0(\theta, T) + \exp\left(-\frac{V\mathcal{H}(\theta)}{k_B T}\right) \sum_{l=1}^{\infty} A_l P_l(\cos \theta) \exp(-p_l t),$$

where

$$p_l = \frac{hk_B T}{V} l(l+1) \quad w_0(\theta, T) = \frac{\exp\left(-\frac{V\mathcal{H}(\theta)}{k_B T}\right)}{Z}$$

$$Z = 2 \exp\left(-\frac{V\mathcal{H}(0)}{k_B T}\right) \quad A_l(y) \equiv \frac{2l+1}{2} \exp\left(-\frac{V\mathcal{H}(y)}{k_B T}\right) P_l(y)$$

The dynamical response of a magnetic particle is determined in two fundamental temperature regimes. In the high-temperature regime (the low-energy-barrier regime $KV \ll k_B T$), for this purpose, one uses the autocorrelation function of the magnetization:

$$\frac{\langle \delta M_z(t) \delta M_z(0) \rangle}{M^2} = \int_{-1}^1 \int_{-1}^1 y y' w(y, y', t) w_0(y') dy' dy = \frac{1}{3} \exp(-p_l t),$$

where $w(y, y', t)$ is the distribution function at the initial condition of state y' being filled – the density of transition probability.

In the high-energy-barrier regime $KV \gg k_B T$ (low-temperature regime), the magnetic moment of the particle weakly deviates from its equilibrium states, and the dynamical equation of the distribution function takes the form of a continuity equation

$$\frac{\partial w}{\partial t} = \frac{1}{2\pi} \frac{\partial I}{\partial y},$$

(the probability of occupancy of the magnetization state flows over time similarly to the particle fluid). The stationary solution of the evolution equation of the distribution function is $I = \text{const}$, which means that the distribution function satisfies the linear equation

$$\sin \theta \left(h \frac{\partial \mathcal{H}}{\partial \theta} w + D \frac{\partial w}{\partial \theta} \right) = \frac{I}{2\pi} \quad (3.2.3)$$

If a probability current of density I flows between the low-energy macrospin states $\theta \approx 0$ and $\theta \approx \pi$ (W_1 and W_2 , respectively) filled with probabilities

$$W_1(t) \approx \frac{2\pi w(0, t, T)}{\exp\left(-\frac{V\mathcal{H}(0)}{k_B T}\right)} \int_0^{\theta_1} \exp\left(-\frac{V\mathcal{H}(\theta)}{k_B T}\right) \sin \theta d\theta$$

$$W_2(t) \approx \frac{2\pi w(\pi, t, T)}{\exp\left(-\frac{V\mathcal{H}(\pi)}{k_B T}\right)} \int_{\theta_2}^{\pi} \exp\left(-\frac{V\mathcal{H}(\theta)}{k_B T}\right) \sin \theta d\theta,$$

where θ_1 and θ_2 are certain *cutoff parameters* associated with the width of the potential well, then the probability current density has the form

$$I = -\dot{W}_1 = \dot{W}_2.$$

Integration of eq. (3.2.3) leads to the form

$$w(\theta_2, t, T) \exp\left(\frac{V\mathcal{H}(\theta_2)}{k_B T}\right) - w(\theta_1, t, T) \exp\left(\frac{V\mathcal{H}(\theta_1)}{k_B T}\right) = -\frac{VI}{2\pi k_B T h} \int_{\theta_1}^{\theta_2} \frac{w(\theta, t, T) \exp\left(\frac{V\mathcal{H}(\theta)}{k_B T}\right)}{\sin \theta} d\theta,$$

which makes it possible to write a master equation describing the evolution of a macrospin between two discrete states

$$\dot{W}_1 - \dot{W}_2 = -\frac{2h \exp\left(-\frac{VK}{k_B T}\right)}{I_m} [W_2(2K + \mu_0 H_z M) - W_1(2K - \mu_0 H_z M)], \quad (3.2.4)$$

where

$$I_m \equiv \sqrt{\frac{2\pi k_B T}{-V\mathcal{H}''(\theta_m)}} \approx \sqrt{\frac{\pi k_B T}{VK}}, \quad \mathcal{H}(\theta_m) \equiv \max\{\mathcal{H}(\theta)\}.$$

The master equation is solved with the constraint $W_1 + W_2 = 1$. Through the definition of averaged magnetic moment $\langle m_y \rangle = W_1 - W_2$, given the above constraint, the master equation (eq. (3.2.4)) can be formulated as the evolution equation of averaged moment

$$\frac{d\langle m_y \rangle}{dt} = -\tau^{-1} \langle m_y \rangle + \Theta H_y(t), \quad (3.2.5)$$

where

- the relaxation factor of τ^{-1} is given by

$$\tau^{-1} \equiv \frac{2\gamma\alpha}{1 + \alpha^2} \frac{4K}{M_s} \sqrt{\frac{KV}{\pi k_B T}} \exp\left(-\frac{KV}{k_B T}\right);$$

- the coefficient of the effect of the external field on the state of the macrospin Θ – by

$$\Theta = \frac{1}{\tau} \frac{\mu_0 M_s}{4K}.$$

For $H_y(t) = H \sin(\omega t)$, the specific solution to eq. (3.2.5) takes form

$$\langle m_y(t) \rangle = \frac{\mu_0 M_s H}{4K} \frac{\tau^{-1}}{\sqrt{\omega^2 + \tau^{-2}}} \sin(\omega t + \phi), \quad \phi \equiv -\arctan\left(\frac{1}{\omega\tau}\right).$$

The amplitude of the response function

$$\langle m_y \rangle_\omega = \frac{\mu_0 M_s H}{4K} \frac{\tau^{-1}}{\sqrt{\omega^2 + \tau^{-2}}} \quad \text{dla } KV \gg k_B T$$

determines dynamic susceptibility.

In the high-temperature regime (low barrier regime – $KV \ll k_B T$), the amplitude of the response can be determined by the Fourier transform of the autocorrelation function. One finds

$$\langle m_y \rangle_\omega = \frac{V\mu_0 M_s H}{3k_B T} \frac{\tau_1^{-1}}{\sqrt{\omega^2 + \tau_1^{-2}}},$$

where

$$\tau_1^{-1} = \frac{2\gamma\alpha}{M_s(1 + \alpha^2)} \frac{k_B T}{V}.$$

Analyzing the amplitude of the dynamical response as a function of temperature for a fixed frequency, one finds

$$\begin{aligned}\langle m_y \rangle_\omega &\xrightarrow{\tau \rightarrow 0} 0, \\ \langle m_y \rangle_\omega &\xrightarrow{\tau \rightarrow \infty} 0.\end{aligned}$$

The temperature at which the $\langle m_y \rangle_\omega$ reaches its maximum is called the paramagnetic blocking point. The paramagnetic blocking effect is a special case of the phenomenon of **stochastic resonance**, i.e. reaching the temperature maximum of amplitude of the dynamical response of a classical bistable system subject to thermal fluctuations, which can be considered as random changes in the height of the potential barrier separating two local minima of this potential. In the simplest case of a single particle described by the dynamic equation [GHJM98]

$$\dot{x}(t) = -V'(x) + A_0 \cos(\Omega t + \varphi) + \xi(t),$$

where

- (symmetrical) potential is given by

$$V(x) = -\frac{a}{2}x^2 + \frac{b}{4}x^4; \quad (3.2.6)$$

- ' marks spatial derivative;
- driving field of amplitude A_0 , frequency Ω and phase shift φ is applied;
- fluctuations (of thermal origin) are characterized by white noise of gaussian function with zero mean. This white noise's correlation function is of the form of

$$\langle \xi(t)\xi(0) \rangle = 2D\delta(t)$$

with intensity $D \sim T$.

A scheme of cyclic dynamics described by the above equation and the (numerically determined) average value of the dynamical parameter (as shown on fig. 3.2) as a function of temperature (for three different ratios between A_0 , distance between minimas from fig. 3.3 and height of potential well) are shown on basis of [GHJM98].

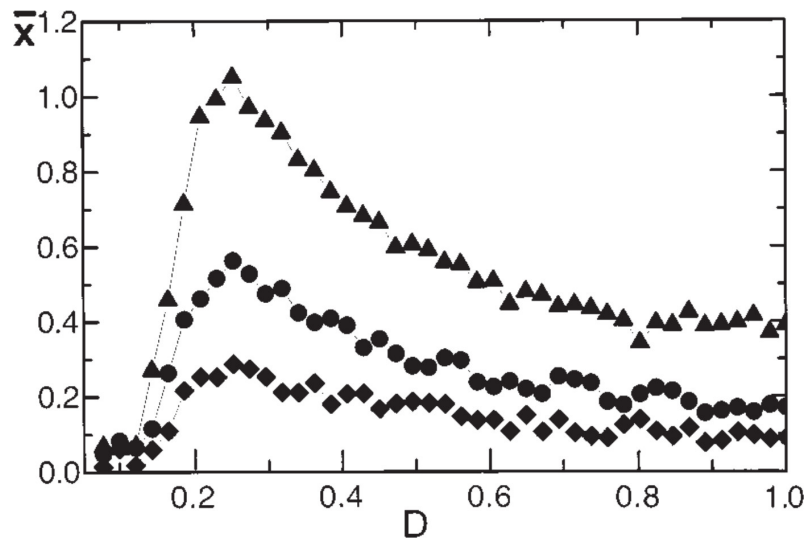


Figure 3.2: Average amplitude \bar{x} is a function of noise intensity D – [GHJM98]

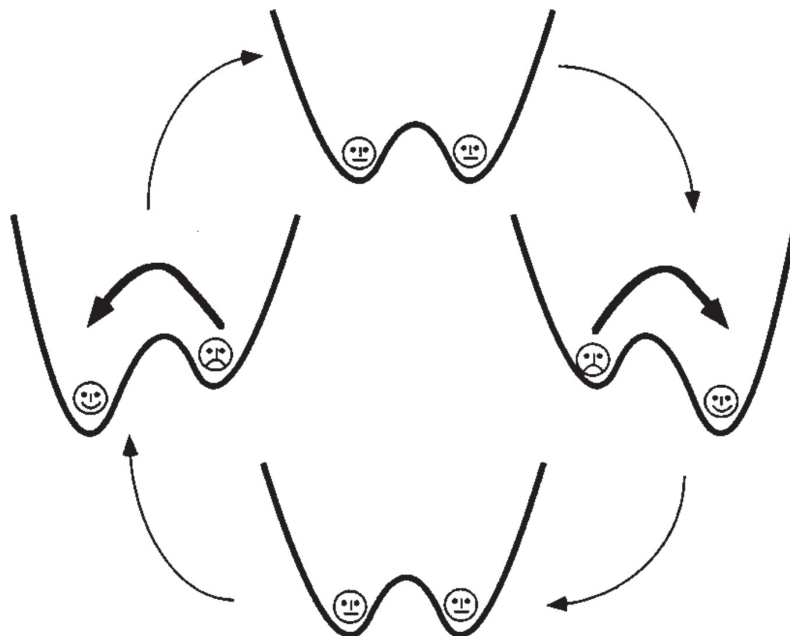


Figure 3.3: Transformation of wells given by eq. (3.2.6) – [GHJM98]

Chapter 4

Key findings of the dissertation

The dissertation consists of five papers, devoted to micromagnetic simulations of the dynamical response of supermagnetic phases, summarized below. The papers are referred to with their designations: [P1] – [P5].

4.1 High-frequency magnetic response of superferromagnetic nanocomposites – [P1]

Results were published in K. Brzuszek and A. Janutka. “High-frequency magnetic response of superferromagnetic nanocomposites”. In: *Journal of Magnetism and Magnetic Materials*, vol. 543, (2022), p. 168608. DOI: 10.1016/j.jmmm.2021.168608 attached on page 35.

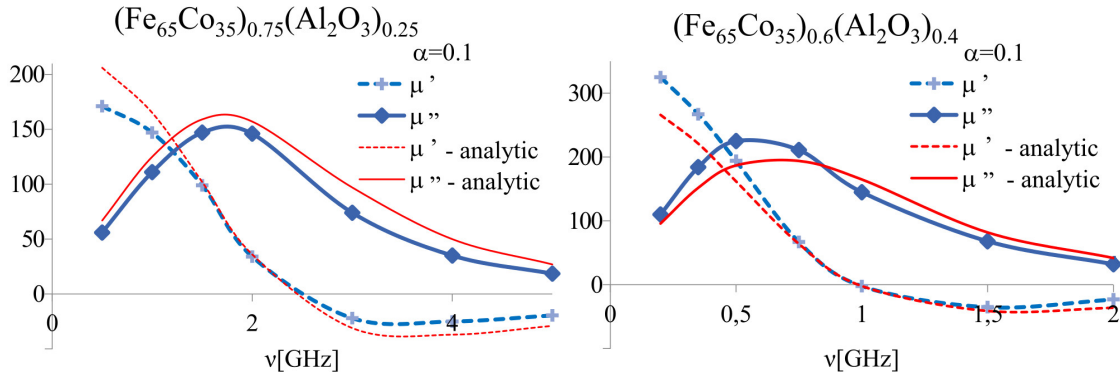
In the paper, a micromagnetic model of a layered superferromagnetic nanocomposite was formulated and its response to an alternating magnetic field with frequencies in the subGHz and GHz range was simulated. For superferromagnets literature data was used to obtain magnetic parameters of their matrices. For this purpose, specific, following from the random magnetic anisotropy (RMA) model, relations between material parameters of magnetic particles and matrices and measurable quantities (saturation magnetization, transverse and longitudinal coercivity fields, size and concentration of nanoparticles) were used.

The relaxation of magnetization of the trilayers of $(\text{Fe}_{65}\text{Co}_{35})_{0.75}(\text{Al}_2\text{O}_3)_{0.25}$, $(\text{Fe}_{65}\text{Co}_{35})_{0.57}(\text{SiO}_2)_{0.43}$, $(\text{Co})_{0.42}(\text{MgF}_2)_{0.58}$ and five-layers of $(\text{Fe}_{65}\text{Co}_{35})_{0.6}(\text{Al}_2\text{O}_3)_{0.4}$ of magnetic cubical nanoparticles from a disordered state shows the long-range (super)ferromagnetic ordering present, with distinct domain structures.

The magnetic response to an alternating field directed in the plane of the layer transverse to the axis of easy magnetization (that is lying in the plane as well) turned out to be typical of ferromagnetic layers, with a characteristic frequency plot of the real and imaginary part of the magnetic susceptibility. Details of the dynamics of composites of different materials and different granularity deviate from each other. In simulations, we observe the stability or oscillatory motion of the domain walls in successive cycles of the dynamical response.

The strength of the exchange coupling between the nanoparticles affects the amplitude of the dynamical response function and the dynamical permeability. In fig. 4.1 plots of the frequency dependence of the real and imaginary parts of the magnetic permeability are presented – values obtained from simulations of superferromagnet (blue lines) exceed theoretical values (red lines) for one of the analyzed superferromagnetic nanocomposites.

For the real part of the magnetic permeability, this is a very desirable violation of Snoek's limit (fig. 4.1b) on the magnetic permeability of ferromagnetic systems. Unfortunately, the accompanying increase in the imaginary part of the magnetic permeability is an undesirable effect, associated with a phase shift of the magnetic response function with respect to the driving field, and therefore with an increase in power losses.



(a) $(\text{Fe}_{65}\text{Co}_{35})_{0.75}(\text{Al}_2\text{O}_3)_{0.25}$ – values obtained from simulation are below analytical values – no breakthrough
 (b) $(\text{Fe}_{65}\text{Co}_{35})_{0.6}(\text{Al}_2\text{O}_3)_{0.4}$ – values obtained from simulations **exceed** analytical values – breakthrough on the Snoek limit

Figure 4.1: Comparison of analytical and simulated values of magnetic permeability components for two selected superferromagnetic composites – breakthrough on the Snoek limit

In the dynamics of $(\text{Co})_{0.42}(\text{MgF}_2)_{0.58}$ at a given amplitude of the driving field, the domain structure and superferromagnetic state are destroyed. Thus, the system is unstable to the driving field, which is due to large local (nanoparticle's) anisotropy constant $K_1 = 4.5 \cdot 10^5 \text{ J m}^{-3}$ dominant over in-the-plane uniform easy axis anisotropy $K_u = 2 \cdot 10^3 \text{ J m}^{-3}$ and easy plane magnetostatic anisotropy $K = -2 \cdot 10^5 \text{ J m}^{-3}$. For remaining three composites the easy plane anisotropy dominates with a value more than one order of magnitude higher than next-highest anisotropy.

Interesting observations relate to the response of magnetic composites to a magnetic field rotating in the plane of the layer. Such a magnetic response remains stable at higher values of the driving field than in the case of a linearly polarized driving field. Important for the stability of the composite response is the mobility of domain walls, which depends on their length, and the value of the effective Gilbert damping constant α of the composite material, For a very strong rotating magnetic field of 2 kA m^{-1} , micromagnetic simulations for $(\text{Fe}_{65}\text{Co}_{35})_{0.6}(\text{Al}_2\text{O}_3)_{0.4}$ showed the occurrence of a regime of chaotic frequency response of magnetization and a regime of rotation of magnetization in the plane of the magnetic layer (the time course of in-the-plane components of the normalized magnetization are plotted on fig. 4.2). Periodic rotation of magnetization seen is a very strong dynamical response that can be used in high-frequency power conversion.

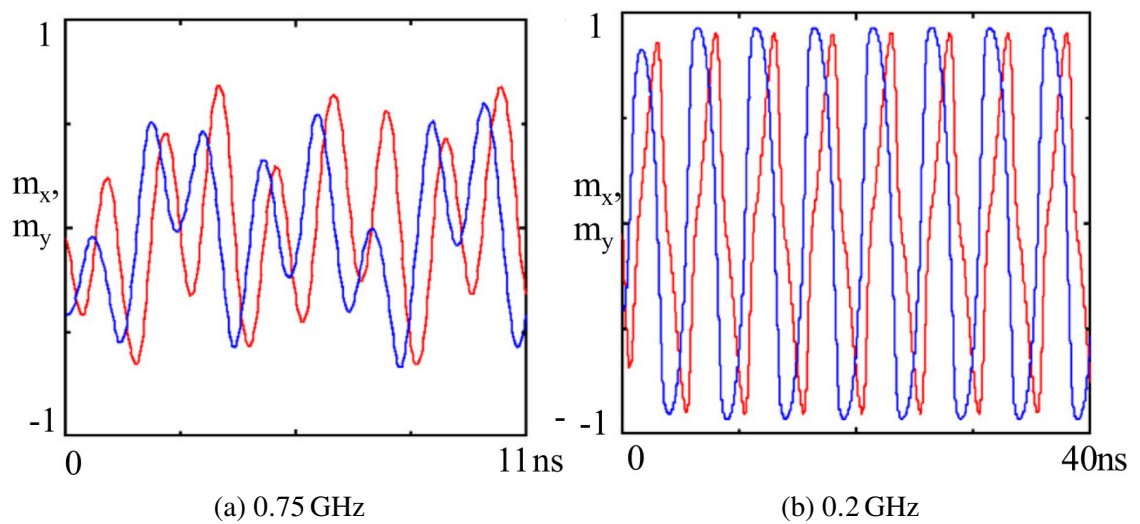


Figure 4.2: Strong response of $(\text{Fe}_{65}\text{Co}_{35})_{0.6}(\text{Al}_2\text{O}_3)_{0.4}$ to the rotating field of 2 kA m^{-1} in the plane, components of m_x and m_y are shown.

4.2 High-frequency magnetic response of superparamagnetic composites of spherical $\text{Fe}_{65}\text{Co}_{35}$ nanoparticles – [P2]

Results were published in K. Brzuszek, C. A. Ross, and A. Janutka. “High-frequency magnetic response of superparamagnetic composites of spherical $\text{Fe}_{65}\text{Co}_{35}$ nanoparticles”. In: *Journal of Magnetism and Magnetic Materials*, vol. 573, (2023), 170651. DOI: 10.1016/j.jmmm.2023.170651 attached on page 47.

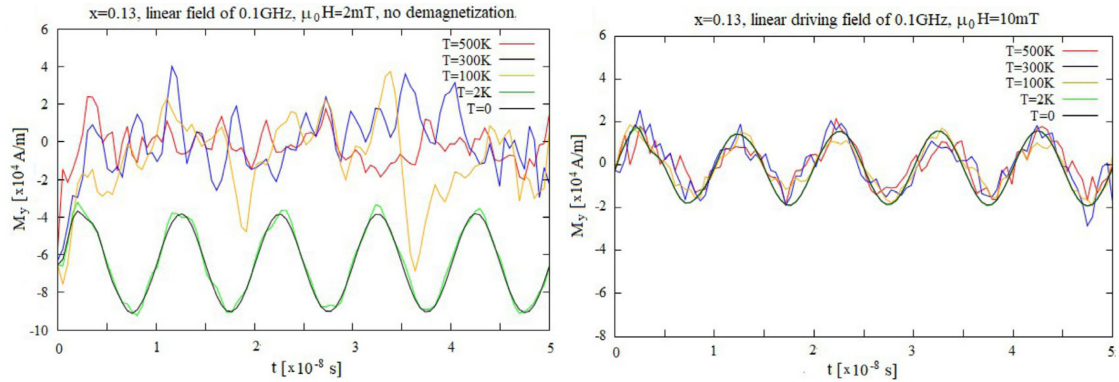
The dynamical response of superparamagnetic systems of a similar type to these considered in [P1] though of a lower concentration of nanoparticles in the dielectric matrix, was simulated in the next paper. With sufficiently high dilution of nanoparticles, such systems are superparamagnetic, or strictly speaking, form *super dipolar glasses* due to long-range magnetostatic interactions (dipole-dipole interactions) between the nanoparticles. These interactions are relatively weak, but important for the dynamical magnetic response. Due to the relatively low energy of the magnetocrystalline anisotropy of nanoparticles (remagnetization energy) relative to the thermal energy $k_B T$, the magnetic ordering of the systems is unstable to thermal fluctuations of the magnetic moments of nanoparticles. A measure of stability of the nanoparticle magnetization is the blocking temperature defined as in eq. (4.2.1)

$$T_B \equiv \frac{KV}{k_B}. \quad (4.2.1)$$

Realistic modeling of the dynamics of superparamagnetic systems therefore requires consideration of their temperature. While the linear dynamical response of a single magnetic particle in the presence of thermal fluctuations is described analytically within the framework of the Neel-Brown model [Bro59; Bro63; Néé49a; Néé49b], the application of magnetic composites as core materials requires the use of strong magnetic fields, which is associated with the need to go beyond the linear response approximation. In addition, magnetostatic interactions between nanoparticles have a significant effect on the high-frequency dynamics, stabilizing the magnetic system, especially in the high temperature range. The mentioned stabilization can be seen from fig. 4.3 where we plot the magnetic response function of a system of nanoparticles $\text{Fe}_{65}\text{Co}_{35}$ with 5 nm diameter and volume fraction of magnetic material $x = 13\%$, to a linearly polarized driving field of amplitude H . The time courses of the response function of the system without dipole-dipole interactions (fig. 4.3a) and in the presence of these interactions (fig. 4.3b) are compared.

From fig. 4.3 one notices a strong magnetic response in 0 K, which is due to the nonlinearity of the magnetic response (Neel-Brown theory predicts the disappearance of the dynamical response at $T = 0$ K). Note that the shift of the function of the response function in the system without magnetostatic interactions (black and green lines on the fig. 4.3a) is due to the size limitation of the simulated system ($4 \times 4 \times 4$ nanoparticles), in which total magnetic moment at equilibrium can be unequal to zero for particular history of the magnetic structure relaxation.

The paper also analyzes the dynamical response of the system in the presence of a strong static field transverse to the driving field. The presence of such a field allows one for intensifying the amplitude of the dynamical response at zero temperature. In the high temperature range, the static field makes it possible to significantly reduce thermal fluctuations of time oscillations of the response function.



(a) No demagnetization field – response separation and chaos in the low barrier regime (b) With the demagnetization field – one can see the stabilization of the response

Figure 4.3: Response of superparamagnetic composite as a function of system temperature – highlighting low and high energy barrier regimes

While the values of the relative magnetic permeability of superferromagnetic composites reach hundreds, in the case of superparamagnetic composites they are at most several times higher than the magnetic permeability of vacuum. However, these are still significant values, justifying the use of magnetic cores in voltage converters.

4.3 High-frequency magnetic response of superparamagnetic composites of spherical Fe and Fe₃O₄ nanoparticles – [P3]

Results were published in K. Brzuszek, C. A. Ross, and A. Janutka. “High-frequency magnetic response of superparamagnetic composites of spherical Fe and Fe₃O₄ nanoparticles”. DOI: 10.2139/ssrn.4709514 attached on page 57.

We continue the study of the response of superparamagnetic systems to a strong driving field. Compared to [P2] nanoparticles, iron and magnetite nanoparticles are of very strong (cubic) magnetocrystalline anisotropy, so their magnetic moments do not undergo significant thermal fluctuations. Magnetite is distinguished from other nanoparticle material considered by a considerably lower value of saturation magnetization, thus, the interactions of nanoparticles of Fe₃O₄ are weaker than those of nanoparticles of Fe₆₅Co₃₅ or Fe. Based on the example of magnetite, we can see the dependence of the dynamical magnetic response on size (diameter) of the nanoparticles due to the size dependence of the magnetostatic (dipole-dipole) interaction of the nanoparticles. The stabilization of the dynamical response at high temperatures, as described in the [P2], significantly depends on the diameter of the nanoparticles, which is visualized in the time courses of the response function fig. 4.4 for the 9 nm nanoparticle system (fig. 4.4a) and 12 nm (fig. 4.4b).

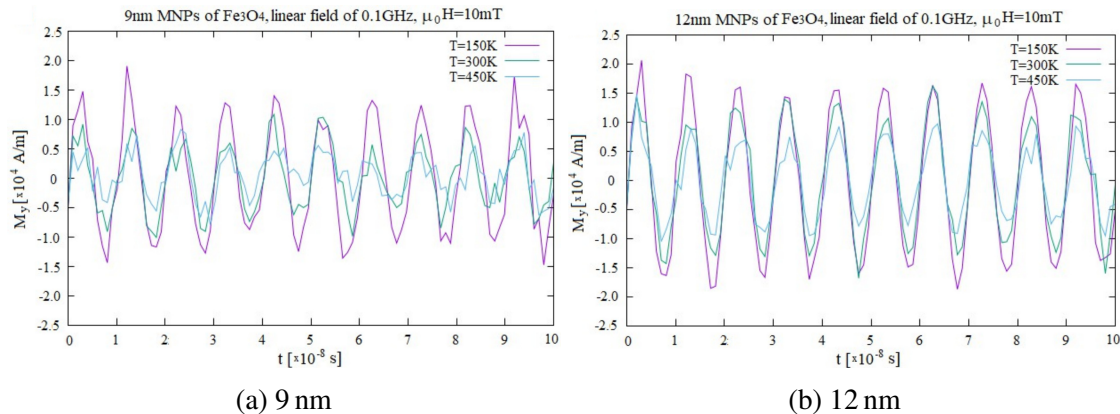


Figure 4.4: Stabilization of the response of Fe₃O₄ as a function of nanoparticle size and temperature

With increase of the diameter of nanoparticles, their magnetic moment increases, and therefore the strength of magnetostatic interactions increases. However, simulations show a limitation on the response efficiency with regard to size of nanoparticles. As shown by $M - H$ plots (4.5), strong magnetostatic interactions lead to opening of a dynamical hysteresis loop, a phenomenon unfavorable for the use of composites as magnetic cores, which is accompanied by power losses.

These losses were determined by averaging numerous $M - H$ plots (fig. 4.5) into singular loops as shown on fig. 4.6. Then area of these loops were calculated, results are shown in table 4.1.

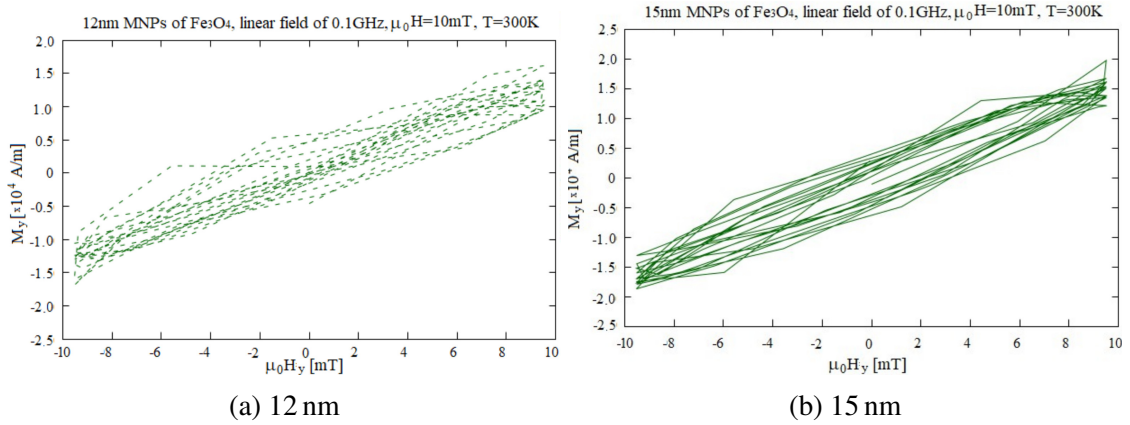


Figure 4.5: Dynamical hystereses for different sizes of nanoparticles of Fe₃O₄ – an increase in size leads to opening the hysteresis loop and therefore to an increase in losses

Table 4.1: Calculated power losses of Fe₃O₄ nanoparticles of different sizes

d [nm]	9	12	15
P [J m ⁻³]	19.3	58.4	101.2

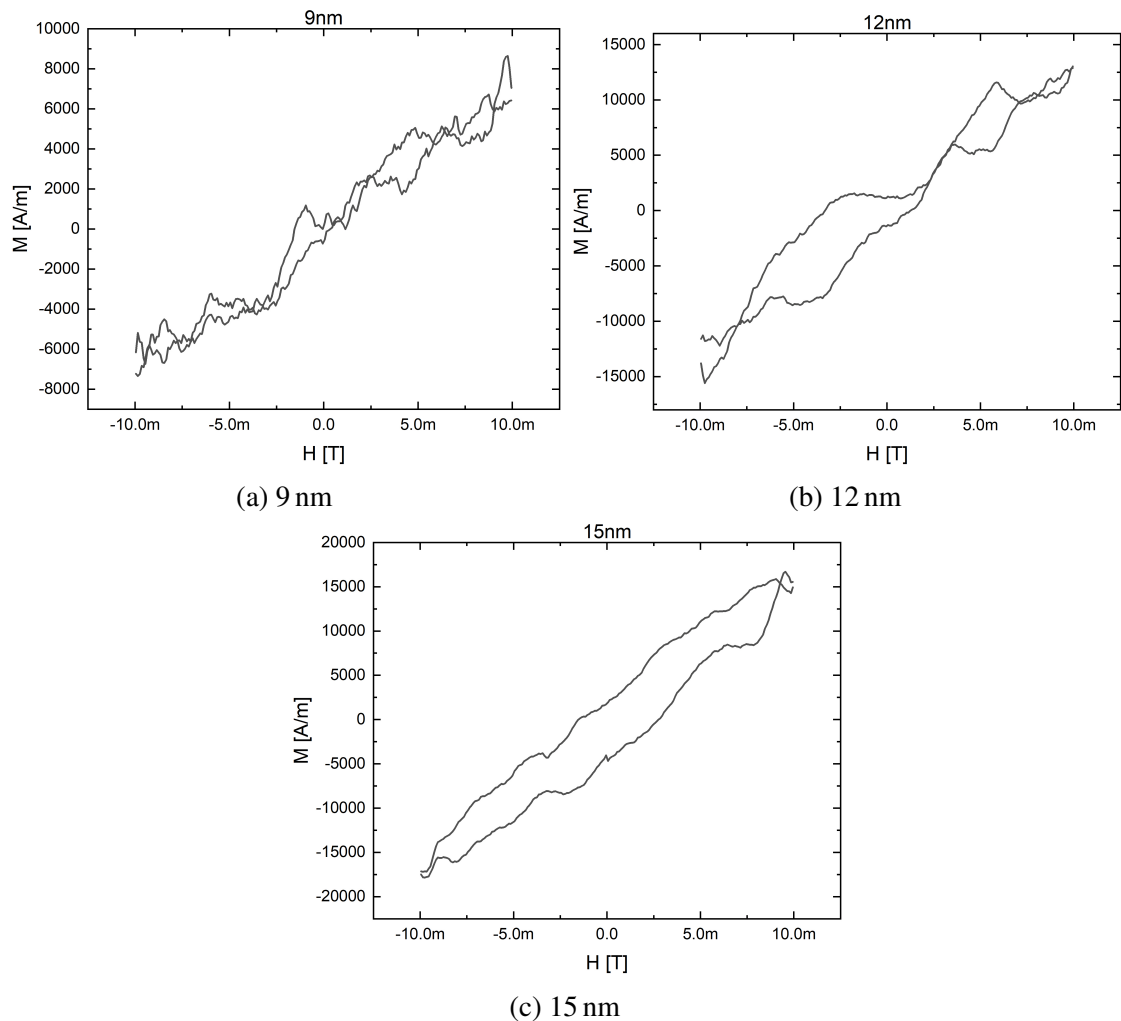


Figure 4.6: Averaged loops of hystereses for different sizes of nanoparticles of Fe₃O₄

4.4 High-Frequency Magnetic Response of Arrays of Planar $\text{Fe}_{65}\text{Co}_{35}$ Nanodots: Effects of Bias Field and Thermal Fluctuations – [P4]

Results were published in K. Brzuszek, C. A. Ross, and A. Janutka. “High-Frequency Magnetic Response of Arrays of Planar $\text{Fe}_{65}\text{Co}_{35}$ Nanodots: Effects of Bias Field and Thermal Fluctuations”. In: *IEEE Transactions on Magnetics*, vol. 59, no. 11 (2023), 7100306. DOI: 10.1109/TMAG.2023.3313871 attached on page 67.

This paper deals with the high-frequency magnetic response of periodic structures of planar $\text{Fe}_{65}\text{Co}_{35}$ nanomagnets. The flattened shape of nanomagnets is associated with anisotropy of the easy plane type of magnetostatic origin. As in ferromagnetic layers, this shape anisotropy allows resonant enhancement of the response in the presence of an additional static field transverse to the driving field. The phenomenon of occurrence of the maximum in dependence of amplitude of the response function on the static field is called ferromagnetic resonance (FMR) and it was described in section 3.2.1 of this dissertation. The purpose of the work [P4] was to verify the usefulness of the FMR effect for enhancing the response of superparamagnetic magnetic dot systems.

For a multilayer system of magnetic nanodiscs with magnetocrystalline anisotropy in random directions in the plane of the layers, whose equilibrium state is visualized on fig. 4.7, we notice the dynamical response to a linear driving field in the plane of the nanodot layers to be resonant in nature. Figure 4.8 shows the dependence of the magnetic response amplitude on the static transverse field. Of interest is considerable shift of the resonance frequency (threefold increase) compared to that predicted for a homogeneous ferromagnetic layer of $\text{Fe}_{65}\text{Co}_{35}$.

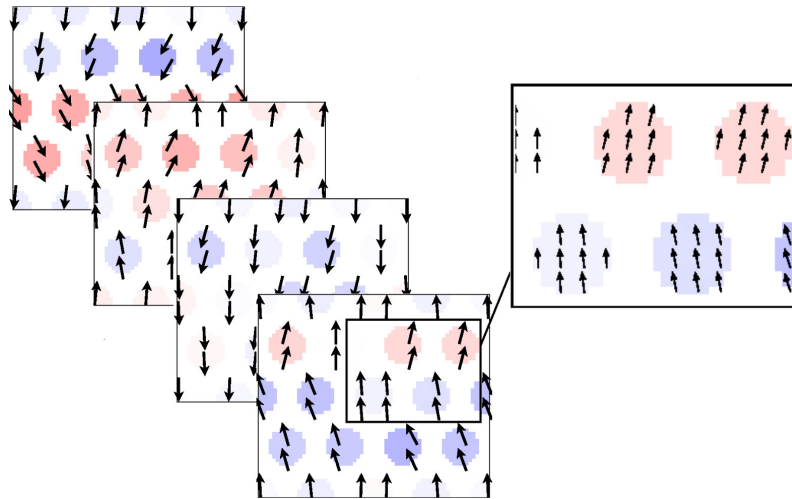


Figure 4.7: Relaxed magnetization for an array of $4 \times 4 \times 4$ nanodiscs with a diameter of 5 nm and a height of 1 nm (RIA-I). Random orientations of the anisotropy axes

Simultaneously, the static transverse field plays a role in enhancing the magnetic response and stabilizing it at high (room) temperature. Despite small volume of nanoparticles, therefore low anisotropy energy, in the resonant range, the response function has a sinusoidal time course at room temperature.

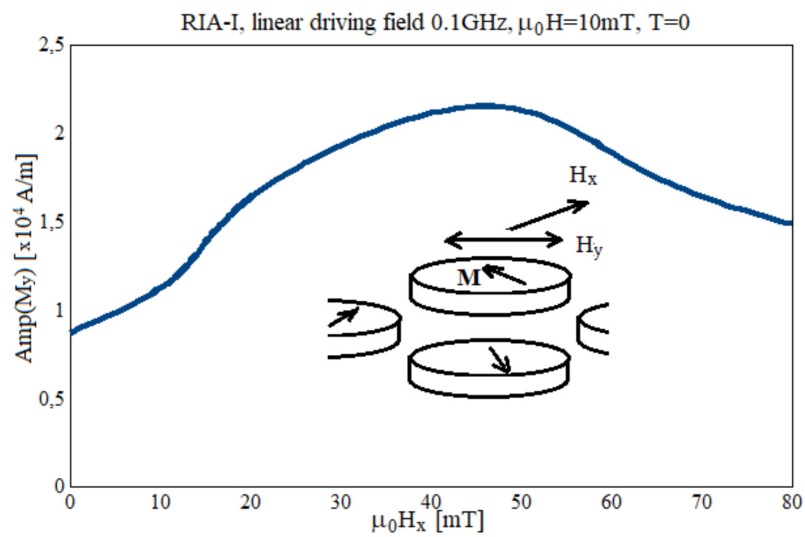


Figure 4.8: Response amplitude function for RIA-I as a function of perpendicular field

4.5 High-frequency magnetic response of crystalline and nanocrystalline antiferromagnetic NiO – [P5]

Results were published in K. Brzuszek, C. A. Ross, and A. Janutka. “High-frequency magnetic response of crystalline and nanocrystalline antiferromagnetic NiO”. in: *AIP Advances*, vol. 14, no. 2 (Feb. 2024), p. 025222. doi: 10.1063/9.0000781 attached on page 73.

The interest in antiferromagnets as magnetic core materials for high-frequency applications is due to very high (terahertz) frequency of antiferromagnetic resonance (a phenomenon analogous to FMR). The working range for magnetic cores is the region of frequencies much lower than the resonance frequency, where the real part of the dynamical susceptibility is relatively large and the imaginary part is small. In this paper, a micromagnetic model of NiO was formulated on the basis of microscopic parameters of exchange interaction and magnetocrystalline anisotropy. The model was used to numerically simulate the dynamical response of the non-conducting antiferromagnet NiO in the frequency range up to 100 GHz. Quite a lot of measured data on the magnetic susceptibility of nickel oxide monocrystals are available, but interpreted within the framework of a historical model with biaxial anisotropy. In our study, the presence of multiple antiferromagnetic domains is taken into account. The simulated model can also be treated as a model of superantiferromagnet, since antiferromagnetic particles practically do not interact with each other (their demagnetization field is zero), and, on the other hand, antiferromagnetic domains in the bulk material are not of magnetostatic origin (unlike in ferromagnets), but they result from structural disorder (the presence of dislocations). The simulations confirmed the linear nature of the response of the antiferromagnet to a relatively strong magnetic field of an amplitude of 200 mT even. They showed that, despite low magnetic susceptibility, the product of frequency and magnetic susceptibility of a multi-domain antiferromagnet can reach values comparable to those achievable for superparamagnetic systems considered in [P2; P3; P4].

PART II:
ARTICLES



Contents lists available at ScienceDirect

Journal of Magnetism and Magnetic Materials

journal homepage: www.elsevier.com/locate/jmmm

Research articles

High-frequency magnetic response of superferromagnetic nanocomposites

Kacper Brzuszek, Andrzej Janutka*

Department of Theoretical Physics, Wrocław University of Science and Technology, 50-370 Wrocław, Poland



ARTICLE INFO

Keywords:

Superferromagnetism
Power conversion
Micromagnetic simulations
Ferromagnetic resonance
High-frequency magnetic response

ABSTRACT

Studies of the dynamical response of thin-film composites of magnetic nanoparticles embedded in dielectric matrices to the oscillatory magnetic field of the microwave-frequency range are performed using numerical simulations. Four soft-magnetic systems; $(\text{Co})_{0.42}(\text{MgF}_2)_{0.58}$, $(\text{Fe}_{65}\text{Co}_{35})_{0.57}(\text{SiO}_2)_{0.43}$, $(\text{Fe}_{65}\text{Co}_{35})_{0.75}(\text{Al}_2\text{O}_3)_{0.25}$, $(\text{Fe}_{65}\text{Co}_{35})_{0.6}(\text{Al}_2\text{O}_3)_{0.4}$, typical of a class of "high-frequency ferromagnetic nanocomposites" are simulated. The necessary micromagnetic parameters are extracted from data within the model of random magnetic anisotropy (RMA). Those materials are candidates for use in micro-converters of power (inductors and transformers) due to their high saturation magnetization, high resistivity, and absence of intra-grain magnetic domains. Thus, they are able to create a high magnetic flux at low power losses. The simulations allow for an inspection into details of the spatial distribution of the oscillating magnetization. We predict noticeable differences in the ferromagnetic resonance (FMR) in different composites which are related to the shape of the static hysteresis. Operating ranges of the driving-field amplitude are related to the hysteresis width. Next to FMR, we analyze the magnetic response via the oscillatory motion of domain walls in a longitudinal field. Besides the response to the alternating field of a constant direction, we study the magnetization dynamics driven by in-the-plane-rotating field. Such a field can drive the magnetization rotations which are a strong-response (nonlinear) mode potentially useful for efficient power conversion.

1. Introduction

Limitations of the semiconductor-based power electronics motivate the interest in the layers of soft-magnetic properties with a high resistivity for microinductors and transformers to be operated at high (near-microwave) frequencies [1–3]. This is because the miniaturization of the power converters is connected to a decrease of the magnetic flux which has to be compensated by an increase of the frequency [4,5]. The constant challenge in the field is the reduction of the power loss due to the fast remagnetizations. Present magnetic-core microconverters of power utilize the effect of the ferromagnetic resonance (FMR), while, being operated at considerably-lower frequencies than the FMR frequency, in a region far from the maximum of spin losses. Another way of the power conversion utilizes the oscillatory motion of domain walls (DWs) in a magnetic layer, however, its frequency is limited by the eddy-current (excess) losses and the skin effect [6]. Hence, the improvement of the high-frequency magnetic materials is related to the increase of the FMR frequency and/or the decrease of the electrical resistivity at the high permeability. Unfortunately, the Snoek and Acher laws are strong constraints impeding the former, while, the metallicity of the soft ferromagnets impedes the later [7–9].

For a long time, hopes for producing highly-permeable materials for the power conversion at low losses are connected with composites of high-magnetization nanoparticles embedded in dielectric matrices [1–3,10,11]. The major advantage of the magnetic-metal-dielectric nanocomposites is a very-high resistivity, (the residual-conductivity mechanism is related to the electron tunneling through the dielectric barriers between the metallic nanoparticles). Reducing the volume content of the metallic phase suppresses the inter-grain eddy currents, thus, reducing losses, (at a larger microwave permeability than that of ferrites [12]). Simultaneously, the magnetic grains (nanoparticles) are monodomain and small enough to suppress the circulation of the electric charge (due to eddy currents) or skin effect inside them, (unlike in ferrites [13] or other industrial soft-magnetic (micro)composites [11, 14]). On the other hand, the nonuniform spatial distribution of the magnetic moments can lead to deviations of FMR in the nanocomposites from typical of the films of homogeneous ferromagnets, which gives some hope for breaking the Snoek/Acher limit of the permeability value.

Nowadays, the class of manufactured ferromagnetic metal-dielectric nanocomposites is rich, and methods for enhancing the uniaxial anisotropy of their films (in order to increase the frequency of FMR)

* Corresponding author.

E-mail address: Andrzej.Janutka@pwr.edu.pl (A. Janutka).<https://doi.org/10.1016/j.jmmm.2021.168608>

Received 14 January 2021; Received in revised form 22 September 2021; Accepted 25 September 2021

Available online 9 October 2021

0304-8853/© 2021 The Authors. Published by Elsevier B.V. This is an open access article under the CC BY license (<http://creativecommons.org/licenses/by/4.0/>).

are established; oblige deposition or deposition in a magnetic field [8]. In spite of this, at present, the operating regime of the nanogranular-core inductors is limited to MHz frequencies well below the microwave region, (they utilize FMR due to in-the-plane field), [15–17]. Independent of the eddy-current losses, the frequency is limited by spin losses and a decrease of the permeability. In the present paper, we explore the potential of several magnetic nanocomposites in terms of strengthening the magnetic response at the microwave frequencies via numerical simulations.

Manufacturing nanocomposite magnets is a complex process and it is not standardized. Possible clustering of the magnetic nanoparticles can result in creating paths for eddy-current conducting. Inhomogeneities of the magnetic ordering can result in the coexistence of different dynamical processes; FMR and DW motion, independent of the orientation of the driving field. Identifying the occurrence of these imperfections in the high-frequency dynamics requires the support from the knowledge of the dynamical response of the ideal systems, whereas, popular analytical models of FMR and oscillatory DW motion are oversimplified when applied to the nanocomposite [9]. Full experimental characterization of the radio-frequency properties is challenging since it requires performing different measurements in a wide range of frequencies. The simulations are helpful in completing data of particular experiments. We perform micromagnetic simulations of microwave dynamics of in-the-plane magnetized films of several magnetic-metal–dielectric nanocomposites of the “ultimate” purity. We mean the systems of uniformly dispersed magnetic nanoparticles in a uniform dielectric matrix without any electrical current, thus, with losses of the spin origin only. We study the magnetization oscillations driven by the magnetic longitudinal or transverse in-the-plane field as well as by in-the-plane-rotating field. We have three particular goals; checking the applicability of the analytical description of the transverse-field-driven FMR, determining the efficiency of DW-assisted response to the longitudinal driving field, and validating the strength and checking the periodicity of the response to rotating in-the-plane field.

High permeability of the nanogranular magnets requires the saturation magnetization of the system as a whole to be high, thus, the volume percentage of the magnetic phase has to be large at the expense of the distance of the granule separation. This results in an outflow of the spin density outside the metallic component into the dielectric matrix, making the spin system continuous and ferromagnetically ordered [18]. The basic role is believed to be played by (oxygen) vacancies in the matrix [19]. Note a similarity to an effect of appearance of the magnetization at the surface of nanoparticles of oxide (non-ferromagnetic) materials [20]. Detailed description of the magnetic ordering in metal–dielectric nanocomposites is performed within the models of the random magnetic anisotropy (RMA), which, developed for the amorphous magnets [21], is also a canonical approach to describing the nanogranular ferromagnets [22–24]. The analysis of the parameters of magnetic properties from data of static measurements allows us for formulating a “micromagnetic” model of the layered nanocomposites. Due to a smooth leakage of the spin from the ferromagnetic nanoparticles (small gradient of the magnetization), the demagnetizing field in the material body is negligible, however, the shape-anisotropy field of the easy-plane type (that confines the magnetization to the layer plane in the static case) is not.

In Section 2, we formulate the micromagnetic model of the metal–dielectric nanocomposite. Section 3 is devoted to characterizing the ordering in terms of the static hysteresis. The dynamical properties are studied in Section 4, and conclusions are summarized in Section 5.

2. Model

The dynamics of the ferromagnetic media is described with the Landau–Lifshitz–Gilbert (LLG) equation of the evolution of magnetization $\mathbf{M} = M_s \mathbf{m}$, (M_s denotes the saturation magnetization)

$$-\frac{\partial \mathbf{m}}{\partial t} = \frac{2\gamma A_{ex}}{M_s} \mathbf{m} \times \Delta \mathbf{m} + \gamma \mathbf{m} \times (\mathbf{B}_{an} + \mathbf{B})$$

$$- \alpha \mathbf{m} \times \frac{\partial \mathbf{m}}{\partial t}, \quad (1)$$

the coefficients of whom are dependent on the spatial coordinates. Here, \mathbf{B}_{an} and \mathbf{B} denote the anisotropy field (relevant to local crystal structure) and an external field applied. The parameters; γ , α denote the gyromagnetic factor and the Gilbert damping constant, respectively. The random orientation of the crystallographic axes of the ferromagnetic nanoparticles results in a random distribution of the magnetic anisotropy directions within the layer. Inside the magnetic nanoparticles, values of the saturation magnetization $M_s = M_s^{(m)}$, the exchange stiffness $A_{ex} = A_{ex}^{(m)}$ and the anisotropy field $|\mathbf{B}_{an}| = |\mathbf{B}_{an}^{(m)}|$ are assumed to be almost the same as in the bulk of the ferromagnetic material. However, a leakage of a small amount of the spin from the nanoparticles into the dielectric matrix results in the formation of a continuous system of ferromagnetically-interacting magnetic moments. We evaluate values of $M_s = M_s^{(d)}$, $A_{ex} = A_{ex}^{(d)}$, $|\mathbf{B}_{an}| = |\mathbf{B}_{an}^{(d)}|$ relevant to the dielectric matrix, based on experimental data. Whereas, primary analysis of the experiments use mean values of the magnetization and of the exchange stiffness, we extract values relevant to the nanoparticles and to the matrix, applying the RMA model of structural ferromagnets [21–23].

For simplicity of the numerical discretization of the medium, we consider the ferromagnetic inclusions to be cubes of the edge length of D , ordered into a cubic lattice (of the lattice constant $D + \Lambda$) and we exclude the magnetostatic effects of the nanoparticle shape from the considerations. While, the RMA models are universal, the magnetostatics is very sensitive to the geometrical details. Beyond the nanoparticle shape and the diameter distribution, including the demagnetization requires detailed knowledge on the distribution of spin in the vicinity of the metal–dielectric interface whose changes are not jumpwise in real systems, (our test simulations including the demagnetization field with the sharp boundaries between the matrix and nanoparticles led to unphysical results).

All the necessary factors to determine the magnetic properties are believed to be contained in effective parameters of the RMA model: average saturation magnetization \bar{M}_s , effective exchange stiffness \bar{A}_{ex} , a constant of the local anisotropy K_l (relevant to the nanoparticles), the constant of the global uniaxial anisotropy K_u , which are available from literature data. Knowing additionally the bulk values of the micromagnetic parameters for the inclusion material, we extract the values relevant to the dielectric matrix with dependence on the volume fraction of the ferromagnetic material x . For this purpose, first, we define the volume fraction of the dense ferromagnetic phase $x_p \equiv D^3 / (D + \Lambda)^3$. Noticing the existence of a critical value of the volume fraction of the ferromagnetic material x_c , (the composite is spontaneously magnetized for $x \in (x_c, 1]$), we estimate $x_p \equiv (x - x_c) / (1 - x_c)$, which satisfies $x_p \rightarrow_{x \rightarrow x_c^+} 0$ and $x_p \rightarrow_{x \rightarrow 1^-} 1$.

The effective exchange stiffness is evaluated with

$$\bar{A}_{ex} = \left(\frac{x_p \sqrt{K_u} K_l^2 D^3}{\mu_0 \bar{M}_s H_{cy}} \right)^{2/3}, \quad (2)$$

based on the formulas of the RMA model, where H_{cy} denotes the coercive field of the “transverse hysteresis” which is obtained with the field directed onto the magnetically-hard axis (y axis) [25]. From the relationships

$$\begin{aligned} \bar{M}_s &= x_p M_s^{(m)} + (1 - x_p) M_s^{(d)}, \\ \frac{D + \Lambda}{\sqrt{\bar{A}_{ex}}} &= \frac{D}{\sqrt{A_{ex}^{(m)}}} + \frac{\Lambda}{\sqrt{A_{ex}^{(d)}}} \end{aligned} \quad (3)$$

we extract

$$\begin{aligned} M_s^{(d)} &= \frac{\bar{M}_s - x_p M_s^{(m)}}{1 - x_p} \\ A_{ex}^{(d)} &= \frac{(x_p^{-1/3} - 1)^2 \bar{A}_{ex} A_{ex}^{(m)}}{(x_p^{-1/3} \sqrt{A_{ex}^{(m)}} - \sqrt{\bar{A}})^2}. \end{aligned} \quad (4)$$

At the nanoparticle–matrix interface, we apply the exchange-stiffness value of $A_{ex}^{(m)}$.

Finally, the anisotropy field can be written in the form

$$\mathbf{B}_{an} = \frac{2K_1}{M_s} (\mathbf{m} \cdot \hat{n}) \hat{n} + \frac{2K_u}{M_s} (\mathbf{m} \cdot \hat{i}) \hat{i} + \frac{2K}{M_s} (\mathbf{m} \cdot \hat{k}) \hat{k}, \quad (5)$$

where \hat{n} is a randomly-oriented unit vector that is constant inside each nanoparticle, K_1 is the anisotropy constant of the magnetic-component material, which is equal to zero in the matrix, K_u is constant in whole the magnetic medium, and $K \equiv -\mu_0 \bar{M}_s^2 / 2$ denotes the constant of the effective easy-plane anisotropy.

In our numerical simulations, the choice of the magnetic nanoparticle material is motivated by the highest possible saturation magnetization and the simplicity of the chemical composition, as well as by the absence of the rare earth content. The highest available magnetization is offered by $\text{Fe}_{65}\text{Co}_{35}$, while, Co nanoparticles are also attractive in terms of the above criteria. Note that, while of a very high magnetization, Fe is not described with our model because of its cubic anisotropy. The requirement of a high strength of the uniaxial anisotropy of the nanocomposite is related to the technique of manufacturing rather than to the nanoparticle material and K_u value in our simulations is dictated by the availability of experimental data. The same concerns the Gilbert damping constant which is extremely sensitive to the quality of the magnetic structure and its realistic value is far from one of the pure material. We use the relatively-high value $\alpha = 0.1$, which is quite typical of magnetic nanosystems with significant structural imperfections.

3. Statics

With relevance to films of four composites of magnetic nanoparticles in dielectric matrices; $(\text{Co})_{0.42}(\text{MgF}_2)_{0.58}$, $(\text{Fe}_{65}\text{Co}_{35})_{0.57}(\text{SiO}_2)_{0.43}$, $(\text{Fe}_{65}\text{Co}_{35})_{0.75}(\text{Al}_2\text{O}_3)_{0.25}$, $(\text{Fe}_{65}\text{Co}_{35})_{0.6}(\text{Al}_2\text{O}_3)_{0.4}$, we have performed numerical investigations of the longitudinal and transverse hysteresis loops, (the hysteresis due to in-the-plane magnetic field longitudinal or transverse with respect to the easy axis). In our simulations, the magnetic-metal inclusions are considered to be identical cubes homogeneously distributed inside a dielectric. The shapes of the inclusions do not play any role since the magnetostatic effects (the shape anisotropies) are completely neglected. Otherwise, the magnetostatics would critically influence the ordering, which is not in line with assumptions of the RMA model, of whom the local-anisotropy and global-anisotropy parameters $k_1 = K_1/\sqrt{N}$, (where N denotes the number of coupled grains), and K_u are the only anisotropy constants including effects of all possible anisotropy origins. From the coercivity measurements, the shape anisotropy of nanoparticles in superferromagnetic composites is known to be inconsistent with that of the isolated nanoparticles, which is due to a smooth change of the magnetic-moment density at the nanoparticle–matrix interfaces (lack of the magnetic surface charges) [19].

Based on literature data (of experiments analyzed within the RMA model), using (2)–(4), we have extracted the sets of material parameters of the films. For $(\text{Co})_{0.42}(\text{MgF}_2)_{0.58}$, the constant of randomly oriented uniaxial anisotropy of Co inclusions is $K_1 = 4.5 \cdot 10^5 \text{ J/m}^3$, while, the in-the-plane uniform easy-axis anisotropy is reported to take $K_u = 2.0 \cdot 10^3 \text{ J/m}^3$. An additional easy-plane anisotropy of the magnetostatic origin is related to the constant $K = -2.0 \cdot 10^5 \text{ J/m}^3$. The saturation magnetization and the exchange stiffness for the inclusions and for the matrix are $M_s^{(m)} = 1.4 \cdot 10^6 \text{ A/m}$, $M_s^{(d)} = 2.4 \cdot 10^5 \text{ A/m}$, $A_{ex}^{(m)} = 3.3 \cdot 10^{-11} \text{ J/m}$, $A_{ex}^{(d)} = 7.3 \cdot 10^{-14} \text{ J/m}$. The average diameter of the magnetic inclusion (the length of edge of the magnetic cube) is $D = 3.3 \text{ nm}$, which, via a given volume ratio of the metal to dielectric content in the composite, determines the spacing between the surfaces of the closest inclusions $\Lambda = 1.9 \text{ nm}$, [26,27]. We simulate a square of $166.4\text{nm} \times 166.4 \text{ nm}$ of the 15.6 nm -thick film (the thickness of three nanoparticle monolayers), applying the finite-difference method with

the grid-discretization size of $0.65\text{nm} < \sqrt{\bar{A}_{ex}/K}$, (we utilize OOMMF package switching the demagnetization field off).

The thickness of the layers is taken to be higher than the effective exchange length of the system $\sqrt{\bar{A}_{ex}/(K_u^2 + k_1^2)^{1/4}} \approx \sqrt{\bar{A}_{ex}/K_u}$. With relevance to the simulations of the dynamical response (next section), for all the studied metal–dielectric films, we have taken quite high value of the Gilbert damping constant $\alpha = 0.1$, which is supported by measurements of composites of FeCo nanoparticles [28–30].

For $(\text{Fe}_{65}\text{Co}_{35})_{0.6}(\text{Al}_2\text{O}_3)_{0.4}$, the parameters are following: $K_1 = 1.5 \cdot 10^4 \text{ J/m}^3$, $K_u = 5.0 \cdot 10^2 \text{ J/m}^3$, $K = -1.4 \cdot 10^5 \text{ J/m}^3$, $M_s^{(m)} = 1.9 \cdot 10^6 \text{ A/m}$, $M_s^{(d)} = 1.25 \cdot 10^5 \text{ A/m}$, $A_{ex}^{(m)} = 1.7 \cdot 10^{-11} \text{ J/m}$, $A_{ex}^{(d)} = 3.0 \cdot 10^{-14} \text{ J/m}$, $D = 2.3 \text{ nm}$ and $\Lambda = 1.2 \text{ nm}$, [25]. We simulate a square of $182\text{nm} \times 182 \text{ nm}$ of the 17.5 nm -thick film (the thickness of five nanoparticle monolayers), with the grid-discretization size of 0.7 nm .

For $(\text{Fe}_{65}\text{Co}_{35})_{0.75}(\text{Al}_2\text{O}_3)_{0.25}$, the parameters are following: $K_1 = 1.5 \cdot 10^4 \text{ J/m}^3$, $K_u = 2.8 \cdot 10^3 \text{ A/m}$, $K = -1.3 \cdot 10^6 \text{ J/m}^3$, $M_s^{(m)} = 1.9 \cdot 10^6 \text{ A/m}$, $M_s^{(d)} = 1.0 \cdot 10^5 \text{ A/m}$, $A_{ex}^{(m)} = 1.7 \cdot 10^{-11} \text{ J/m}$, $A_{ex}^{(d)} = 1.5 \cdot 10^{-14} \text{ J/m}$, $D = 3.9 \text{ nm}$ and $\Lambda = 1.3$, [25]. We simulate a square of $166.4\text{nm} \times 166.4 \text{ nm}$ of the 15.6nm -thick film (the thickness of three nanoparticle monolayers), with the grid-discretization size of 0.65 nm .

For $(\text{Fe}_{65}\text{Co}_{35})_{0.57}(\text{SiO}_2)_{0.43}$, the parameters are following: $K_1 = 1.5 \cdot 10^4 \text{ J/m}^3$, $K_u = 2.9 \cdot 10^3 \text{ A/m}$, $K = -5.8 \cdot 10^5 \text{ J/m}^3$, $M_s^{(m)} = 1.9 \cdot 10^6 \text{ A/m}$, $M_s^{(d)} = 6.3 \cdot 10^5 \text{ A/m}$, $A_{ex}^{(m)} = 1.7 \cdot 10^{-11} \text{ J/m}$, $A_{ex}^{(d)} = 1.1 \cdot 10^{-13} \text{ J/m}$, $D = 3.92 \text{ nm}$ and $\Lambda = 2.32 \text{ nm}$, [31–33]. We simulate a square of $199.68\text{nm} \times 199.68 \text{ nm}$ of the 18.72 nm -thick film (the thickness of three nanoparticle monolayers), with the grid-discretization size of 0.78 nm .

The simulations of the hysteresis loops have been performed starting from a zero-field state of the system that is relaxed from the randomly-magnetized state. Domain structures appear despite lack of the magnetostatic interactions as a consequence of the competing complex exchange interactions and RMA. Note that the initial states of our finite systems are not perfectly magnetized in the easy direction. This is because the RMA magnets are “systems with memory”, thus, there is a large number of equilibria for any given external field including zero. Properties typical of the reentrant spin glass (overcooled states) have been observed for metal–dielectric nanocomposites [34,35]. The loops of longitudinal and transverse hysteresis, (we mean the hystereses due to the action of in-the-plane field longitudinal or transverse to the easy magnetization direction - $m_x(H_x)$ or $m_y(H_y)$ curves, respectively) are presented in Fig. 1, (we plot halfloops only). For a wide range of the field considered, in majority of the systems, the complete magnetization is not reached, while, the system “remembers” the initial (zero-field) state. Resulting hysteresis curves (except for $(\text{Fe}_{65}\text{Co}_{35})_{0.75}(\text{Al}_2\text{O}_3)_{0.25}$) reveal a nonzero slope beyond the loop area (for the field above the coercivity), similar to ones of [36,37].

The coercive fields (of the transverse and longitudinal hysteresis) are found to be relatively low for each of the four materials, however, the strict condition of the soft magnetism, the coercive field of the longitudinal hysteresis lower than 1kA/m is fulfilled by one of the composites only; $(\text{Fe}_{65}\text{Co}_{35})_{0.6}(\text{Al}_2\text{O}_3)_{0.4}$. The longitudinal-hysteresis shape for $(\text{Co})_{0.42}(\text{MgF}_2)_{0.58}$ is different from those of the $\text{Fe}_{65}\text{Co}_{35}$ -based composites, whereas, the materials of the later group differ significantly from each other in the coercive field.

The transverse hysteresis loops are very narrow (transverse coercivities are low) or even not clearly seen with the field-resolution of Fig. 1. The systems behave similar to the Stoner–Wohlfarth model of the magnetic particle which predicts the absence of the transverse hysteresis and the presence of the rectangular-shaped loop of the longitudinal hysteresis. Some literature on the corresponding nanocomposites reports clearly resolved loops of the transverse hysteresis of the real magnets. They are attributed to large scale of the probed systems, which is related to local deviations of the easy magnetization axis from the average and cannot be reproduced within our simulations. However, the way of the material deposition is crucial in terms of the local distribution of the anisotropy. Specific-angle-oblique sputtering allows for producing

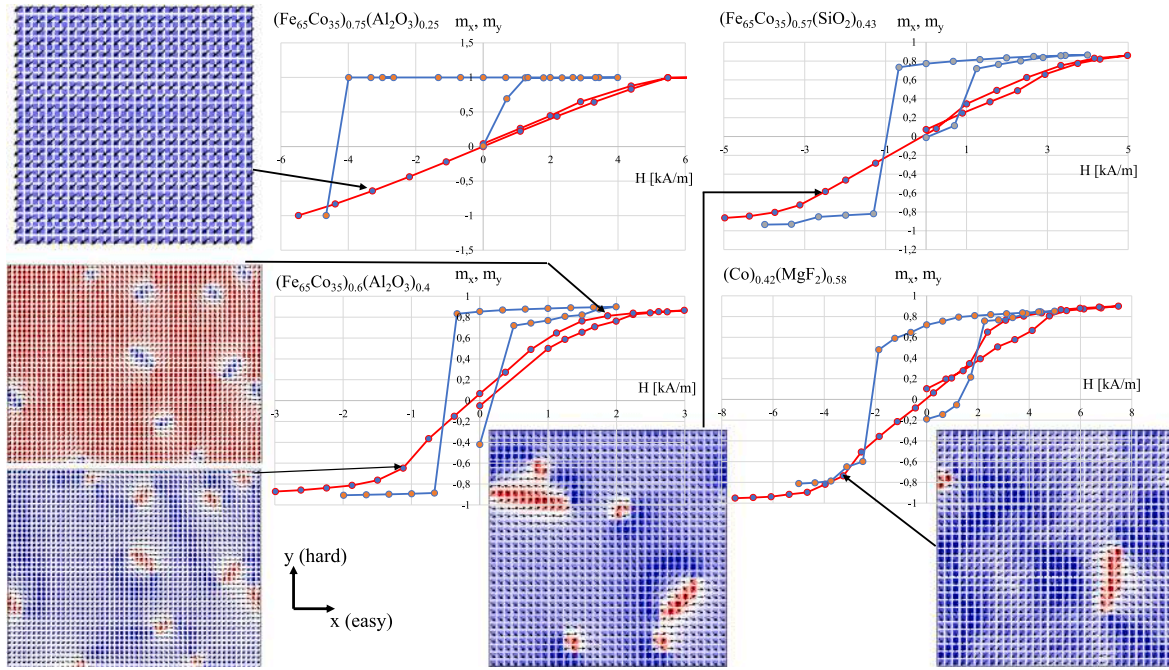


Fig. 1. Hysteresis curves $m_x(H_x)$ (blue lines; “longitudinal hysteresis”) and $m_y(H_y)$ (red lines; “transverse hysteresis”) of the four simulated systems, and snapshots of the magnetization (the colors indicate the direction and intensity of the m_y -component) at the indicated points of the “transverse-hysteresis” curve.

nanocomposites of the Stoner–Wohlfarth-like hystereses [38]. That hysteresis type is claimed to support the view of dominance of the exchange inter-particle interactions over the dipole–dipole ones [39].

Looking at the snapshots of the transverse component of the magnetization relevant to the transverse reversal modes (Fig. 1), one sees the clearly resolved domains except for $(\text{Co})_{0.42}(\text{MgF}_2)_{0.58}$ of whom the random anisotropy is strong enough to prevent uniform demagnetization in the hard plane (yz -plane). The strong random anisotropy causes a non-rectangular shape of the longitudinal-hysteresis loop; the remanence magnetization $m_r = M_r/M_s$ (called a squareness ratio) of the longitudinal hysteresis loop is visibly smaller than one. It is not for $\text{Fe}_{65}\text{Co}_{35}$ -based structures, however, there are differences in the remagnetization of particular-composition systems. For the magnetically-hardest of the composites; $(\text{Fe}_{65}\text{Co}_{35})_{0.75}(\text{Al}_2\text{O}_3)_{0.25}$, we have found the plot of $m_y(H_y)$ dependence to be a straight line for up to $|m_y| \approx 1$ while the ordering to be uniform (a Stoner–Wohlfarth-like behavior). For magnetically-softest $(\text{Fe}_{65}\text{Co}_{35})_{0.57}(\text{SiO}_2)_{0.43}$ and $(\text{Fe}_{65}\text{Co}_{35})_{0.6}(\text{Al}_2\text{O}_3)_{0.4}$, the domain structure is durable against the transverse field and complete magnetization reversal using the transverse field requires the application of a field that exceeds the longitudinal coercivity value, (the corresponding red curves in Fig. 1 differ in shape from the Stoner–Wohlfarth turn). This is related to very narrow minima of the energy of $(\text{Fe}_{65}\text{Co}_{35})_{0.75}(\text{Al}_2\text{O}_3)_{0.25}$ compared to the remaining composites. From the comparison of snapshots in Fig. 2(g) and 2 (h), we notice transition between the stripe and maze domains with changing the concentration of the magnetic component, which has been previously observed (using MFM) in superferromagnetic nanocomposites with perpendicular magnetic anisotropy (PMA) [35]. The field-induced shrinking of the stripe domains into the separate bubbles (an incomplete remagnetization in the snapshots of Fig. 1 for the magnetically softer systems) has been observed (with MOKE) for an in-plane-magnetized nanocomposite [37].

4. High-frequency dynamics

We have simulated the magnetization dynamics driven with alternating longitudinal, transverse, and in-the-plane rotational field of the microwave frequencies. Correspondingly, the magnetic response can

follow from FMR or the oscillatory DW motion or a mixture of both (or a rotational mode of FMR). The driving field is applied to the (zero-field) magnetization states of the beginning points in the hysteresis curves of Fig. 1.

Relatively-strong driving fields are considered, having in mind the composite application to the power conversion. The amplitudes of the flux density in microinductors are typically considered in the range of ~ 0.01 – 0.1T [15,40–42], which corresponds, via the permeability of ~ 100 to the driving field of ~ 0.1 – 1.0kA/m .

We neglect the skin effect. Despite a tunneling conductivity is present in real nanocomposites, its value is about four orders of magnitude lower than for bulk metals [26,43–45]. Thus, the potential decrease of the skin depth due to the frequency increase (up to GHz) is compensated by the decrease of the conductivity and the skin depth remains of the μm range [46].

4.1. Driving by in-the-plane transverse field

The alternating in-the-plane transverse field drives the oscillations of the magnetization components m_y , m_z (perpendicular to the easy axis). For the field amplitude of 0.2 kA/m , we plot the frequency dependence of the response amplitudes of; $(\text{Fe}_{65}\text{Co}_{35})_{0.75}(\text{Al}_2\text{O}_3)_{0.25}$ in Fig. 2(a), $(\text{Fe}_{65}\text{Co}_{35})_{0.6}(\text{Al}_2\text{O}_3)_{0.4}$ in Fig. 2(d), $(\text{Fe}_{65}\text{Co}_{35})_{0.57}(\text{SiO}_2)_{0.43}$ in Fig. 3(a), and for $(\text{Co})_{0.42}(\text{MgF}_2)_{0.58}$ in Fig. 3(d). The square-shaped spatial windows chosen for performing the calculations is pointed out in the snapshots in Figs. 2(g), (h), 3(g). Those single-domain windows are considered in order to simulate conditions of measurement of the dynamical permeability at its maximum (in a single-domain state). In the plots and in the text below, amplitudes of oscillating quantities are denoted as $\text{Amp}(\cdot)$, while, the angular frequency reads $\omega \equiv 2\pi\nu$. For $(\text{Co})_{0.42}(\text{MgF}_2)_{0.58}$, the total transverse magnetization of the system is plotted, because of a specific dynamical response of the layer. As seen from the snapshots in Fig. 3j, the out-of-plane component of the magnetization in the layer of $(\text{Co})_{0.42}(\text{MgF}_2)_{0.58}$ almost does not oscillate inside the magnetic nanoparticles of the composite except in a small number of them, (unlike in the snapshots of $(\text{Fe}_{65}\text{Co}_{35})_{0.57}(\text{SiO}_2)_{0.43}$ layer for instance, Fig. 3i). Such a behavior does not coincide with the classic description of FMR (by Kittel) and,

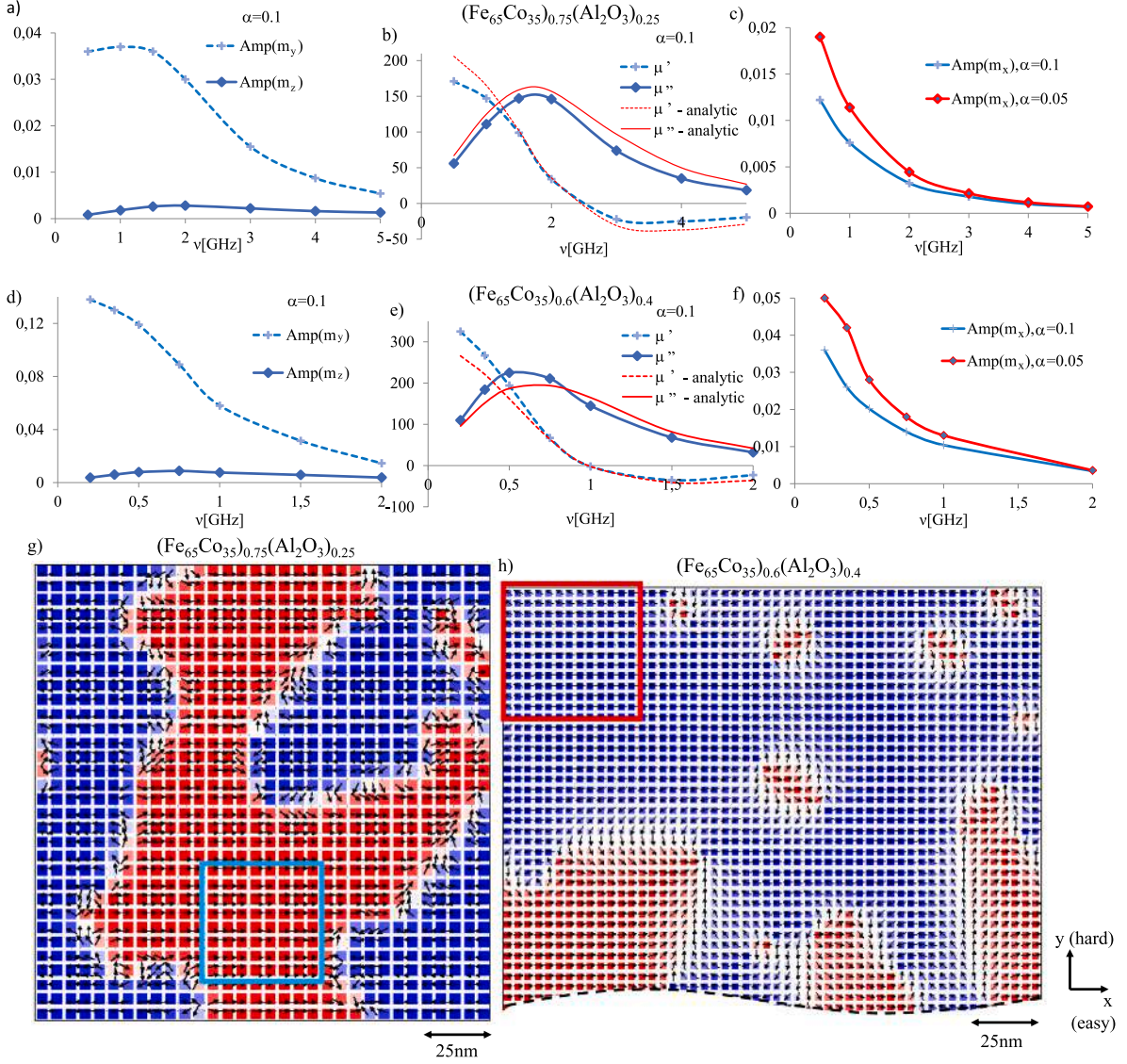


Fig. 2. Simulated dynamical response to the alternating transverse field: frequency dependence of the amplitudes of the magnetization components m_y , m_z (a), the real and imaginary permeabilities μ' , μ'' (b) for $(\text{Fe}_{65}\text{Co}_{35})_{0.6}(\text{Al}_2\text{O}_3)_{0.4}$ layer, and the same for $(\text{Fe}_{65}\text{Co}_{35})_{0.75}(\text{Al}_2\text{O}_3)_{0.25}$; (d), (e), respectively. Dynamical response from both the materials to the alternating longitudinal field: frequency dependence of the amplitude of the magnetization component m_x ; (c), (f). Equilibrium ordering in $(\text{Fe}_{65}\text{Co}_{35})_{0.75}(\text{Al}_2\text{O}_3)_{0.25}$; (g), and $(\text{Fe}_{65}\text{Co}_{35})_{0.6}(\text{Al}_2\text{O}_3)_{0.4}$; (h). The colors in (g), (h) and their intensity are related to the m_x component of the magnetization. The transverse-field response is established for indicated in (g), (h) spatial windows.

(similar to domain nonuniformity in Section 3), it is due to very strong RMA in $(\text{Co})_{0.42}(\text{MgF}_2)_{0.58}$.

Consider FMR due to an alternating field $\mathbf{B}(t)/\mu_0 = [0, H_y(t), 0]$ of an amplitude $\text{Amp}(H_y)$, using the complex dynamical parameter $m_+(t) \equiv m_y(t) + im_z(t)$. When considering the single-domain state/area of a ferromagnet, the linearization of (1) around $\mathbf{m} = [1, 0, 0]$ allows one for finding the particular solution in the form $m_+(t) = [A_y(\omega) + iA_z(\omega)] \sin(\omega t) + [C_y(\omega) + iC_z(\omega)] \cos(\omega t)$ and, via its Fourier transform, the permeability

$$\mu(\omega) \equiv \frac{m_+(\omega)}{H_y(\omega)} = \frac{M_s}{\text{Amp}H_y} \left\{ A_y(\omega) + C_z(\omega) + i [A_z(\omega) - C_y(\omega)] \right\}. \quad (6)$$

Upon denoting $\omega_1 \equiv \gamma_0 \left(\frac{2K_u}{\mu_0 M_s} + M_s \right)$ and $\omega_2 \equiv \gamma_0 \frac{2K_u}{\mu_0 M_s}$, the real and imaginary parts of the permeability read

$$\mu'(\omega) = \gamma_0 M_s \frac{(\omega - \omega_1)(\omega^2 - \omega_1\omega_2) + \alpha^2\omega^2(\omega + \omega_2)}{(\omega^2 - \omega_1\omega_2)^2 + \alpha^2\omega^2(\alpha^2\omega^2 + \omega_1^2 + \omega_2^2)}$$

$$\mu''(\omega) = \gamma_0 M_s \frac{\alpha\omega \{ \omega [(1 + \alpha^2)\omega - \omega_2] - \omega_1(\omega - \omega_1) \}}{(\omega^2 - \omega_1\omega_2)^2 + \alpha^2\omega^2(\alpha^2\omega^2 + \omega_1^2 + \omega_2^2)} \quad (7)$$

Zero of $\mu'(\omega)$ and maximum of $\mu''(\omega)$ are close to the FMR frequency $\sqrt{\omega_1\omega_2}$. The angle of the out-of-plane deviation of the magnetization δ_ω is directly related to the loss tangent;

$$\tan(\delta_\omega) = \frac{\text{Amp}[m_z](\omega)}{\text{Amp}[m_y](\omega)} = \frac{\mu''(\omega)}{\mu'(\omega)}. \quad (8)$$

Noticing that $\text{Amp}(m_z) \ll \text{Amp}(m_y)$, we verify the application of the FMR description to the nanocomposites via utilizing the relationships $\mu'(\omega) \approx \frac{M_s}{\text{Amp}(H_y)} \text{Amp}[m_y](\omega) \cdot \cos(\delta_\omega)$ and $\mu''(\omega) \approx \frac{M_s}{\text{Amp}(H_y)} \text{Amp}[m_y](\omega) \cdot \sin(\delta_\omega)$. The amplitudes of magnetization components averaged over a spatial window in a single-domain area are determined from the simulations and multiplied by sine or cosine of the calculated with (8) values of δ_ω . Thus, we evaluate the permeability with dependence on the frequency and compare its plot to the permeability curve calculated with (7), dashed and solid lines in Figs. 2(b), (e), 3(b), respectively. For $(\text{Co})_{0.42}(\text{MgF}_2)_{0.58}$, since the dynamics appeared in our simulations to

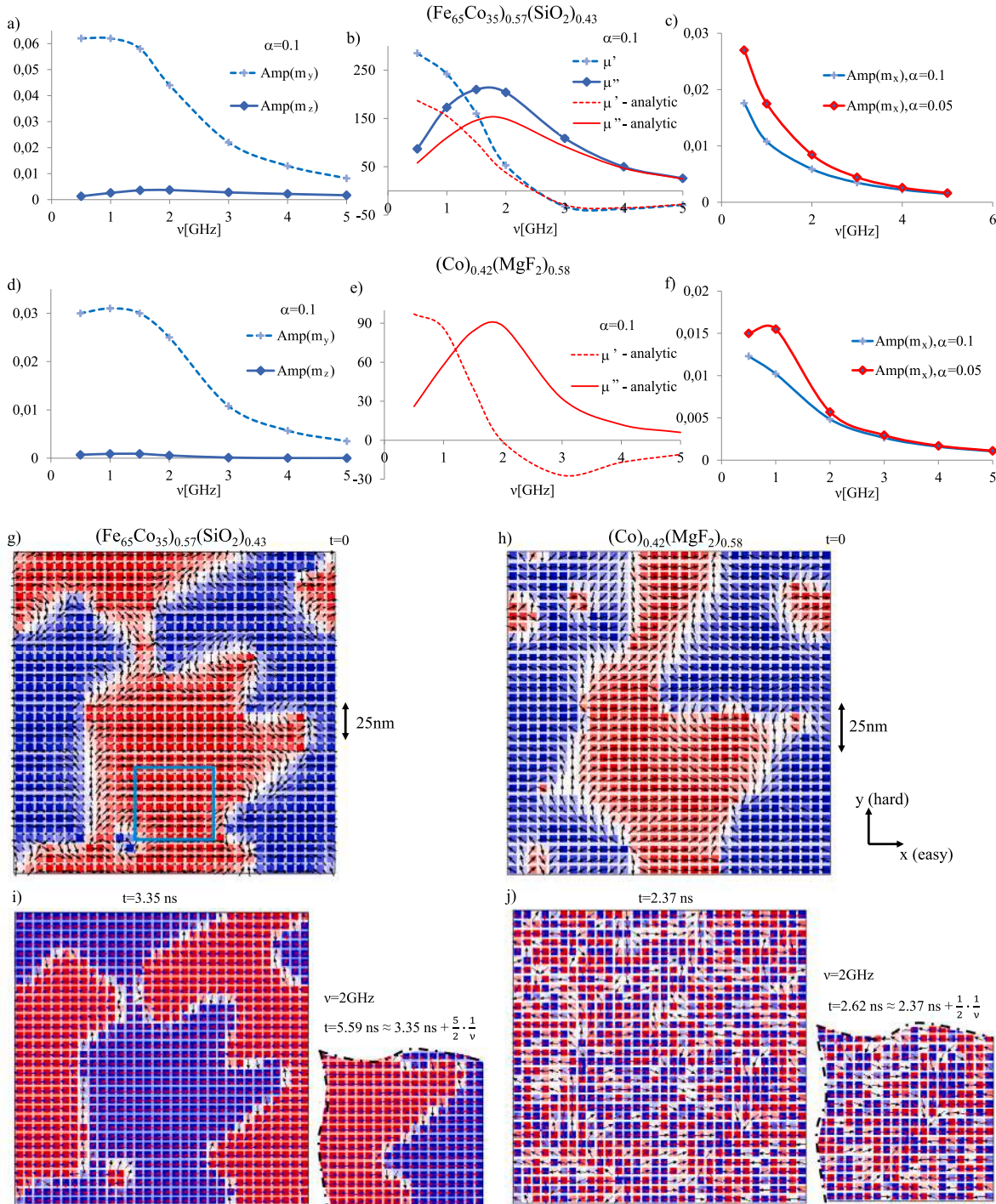


Fig. 3. Dynamical response to the alternating transverse field: frequency dependence of the amplitudes of the magnetization components m_y , m_z (a), the real and imaginary permeabilities μ' , μ'' (b) for $(\text{Fe}_{65}\text{Co}_{35})_{0.57}(\text{SiO}_2)_{0.43}$ layer, and the same for $(\text{Co})_{0.42}(\text{MgF}_2)_{0.58}$; (d), (e), respectively. Dynamical response from both the materials to the alternating longitudinal field: frequency dependence of the amplitude of the magnetization component m_x ; (c), (f). Equilibrium ordering in $(\text{Fe}_{65}\text{Co}_{35})_{0.57}(\text{SiO}_2)_{0.43}$; (g), and $(\text{Co})_{0.42}(\text{MgF}_2)_{0.58}$; (h). The colors in (g), (h) and their intensity are related to the m_x component of the magnetization. The transverse-field response is established for indicated in (g), (h) spatial windows. Bottom line: snapshots of z -component of the magnetization during the transverse-field-driven oscillations for $(\text{Fe}_{65}\text{Co}_{35})_{0.57}(\text{SiO}_2)_{0.43}$; (i), (the color intensity is increased via dividing M_x by 1000), and for $(\text{Co})_{0.42}(\text{MgF}_2)_{0.58}$; (j), (the color intensity is increased via dividing M_x by 100).

be far from usual FMR as mentioned above, in Fig. 3(e), the analytical permeability curves are plotted only.

While similar, the simulation and analytical curves in Figs. 2(b), (e), 3(b) differ from each other. In Fig. 3(b), (the plot for $(\text{Fe}_{65}\text{Co}_{35})_{0.57}(\text{SiO}_2)_{0.43}$) and in Fig. 2(e), (the plot for $(\text{Fe}_{65}\text{Co}_{35})_{0.6}(\text{Al}_2\text{O}_3)_{0.4}$), a relatively large $\sim 10\%$ differences in simulation and analytical values of the real part of the low-frequency permeability are found. Such an considerable increase of the real part of the permeability above the

analytical value is connected to the breakdown of the Snoek law. Unfortunately, the simulation value of the imaginary part of the permeability is increased compared to the analytical one as well and the loss tangent at sub-GHz frequencies remains large.

Experimental curves of the dynamical permeability for relevant materials are qualitatively similar to ours while, they are better fitted to the analytical curves [28,31]. This is possibly because, the damping

constant is a fitting parameter in the experimental works. The permeability values (so as the damping constant and FMR frequency) can be very strongly influenced by the presence of a substrate and depend on the thickness of the magnet [28]. The most stable in terms of the parameters (and especially similar to our model systems) are multilayered granular films and we have found a good correspondence of the permeability curves for the FeCo-SiO₂ composite (Fig. 3(b)) to the experimental data on relevant multilayered system, (up to small differences in the composition and size of the nanoparticles), [47]. Note that low thickness of the interlayer (comparable to the interparticle distances) is crucial for the frequency dependence of the permeability [48].

4.2. Driving by longitudinal field and by rotating field

In the system driven with the alternating longitudinal field $\mathbf{B}(t)/\mu_0 = [H_x(t), 0, 0]$, DWs perform the oscillatory motion which leads to the oscillations of the longitudinal magnetization of the system as a whole. For the frequencies close to the resonance point and higher, the driven oscillations of the m_x -component of the magnetization are found to be of a very low amplitude. However, according to Figs. 2(c), (f), 3(c), (f), in the sub-GHz range, the oscillations (for $\text{Amp}(H_x) = 0.2$ kA/m) rapidly become significant, of the amplitude comparable to the amplitude of the m_y -component when the system is driven with the transverse field of the same amplitude. The increase of the amplitude of the DW oscillations with decreasing the frequency is usual in ferromagnets [49–51]. While frequency of the efficient FMR-based response is limited at the top by the increase of the loss tangent, the frequency of the efficient DW-assisted response is limited at the bottom by the increase of the DW-motion amplitude close to the domain size.

For all the systems, we have found the increase of the longitudinal permeability with decreasing the Gilbert damping constant (Fig. 2(c), (f), 3 (c), (f)). This suggests the related DW motion to be viscous at the certain time scale of the period of oscillations (similar to the constant DW motion below the Walker breakdown). The strongest longitudinal response has been found for $(\text{Fe}_{65}\text{Co}_{35})_x(\text{Al}_2\text{O}_3)_{1-x}$ systems. Larger amplitude $\text{Amp}(m_x)$ at the composition factor $x = 0.6$ is compensated by the higher saturation magnetization at $x = 0.75$, hence, the hysteretic losses in both magnets are expected to be similar. Lower amplitude of magnetization oscillations in $(\text{Fe}_{65}\text{Co}_{35})_{0.75}(\text{Al}_2\text{O}_3)_{0.25}$ is an advantage with regard to the stability of the domain structure. It allows for the application of stronger driving field than usable for $(\text{Fe}_{65}\text{Co}_{35})_{0.6}(\text{Al}_2\text{O}_3)_{0.4}$. However, large volumetric percentage of the metallic phase in the former system is a disadvantage in terms of the requirement of a high resistivity, which is especially important for the case of the DW-assisted response because of the excess losses.

At the microscale, a very strong rotating field can be created with a pair of mutually-perpendicular coils which method is utilized for omnidirectional wireless power transfer [52,53]. Such a field drives the magnetization rotation and possibly causes the overlap of FMR with significant oscillations of the DW positions. For sufficiently-low frequency and high amplitude of the driving field, the response of the layer to (in-the-plane) rotating field becomes nonlinear, which limits the operating ranges of the field frequency and amplitude. We have performed the simulations for the field amplitude of up to 2 kA/m and frequency down to 0.5 GHz for $(\text{Fe}_{65}\text{Co}_{35})_{0.57}(\text{SiO}_2)_{0.43}$, $(\text{Co})_{0.42}(\text{MgF}_2)_{0.58}$, and for $(\text{Fe}_{65}\text{Co}_{35})_{0.75}(\text{Al}_2\text{O}_3)_{0.25}$, roughly establishing that the driven oscillations of in-the-plane components of the magnetization remain sinusoidal in principle, however, for the later system, weakly-visible nonlinear features appear in the plot of $m_x(t)$ in Fig. 4(d) (the blue line).

For the magnetically-softest $(\text{Fe}_{65}\text{Co}_{35})_{0.6}(\text{Al}_2\text{O}_3)_{0.4}$, the nonlinear character of the magnetization oscillations in the rotating field of 2kA/m (well above the longitudinal coercive field of Fig. 1 but below the saturating transverse field) is clearly seen in the range of frequencies of our study (see Fig. 4(f), (g)). At 0.2 GHz, instead of the magnetization oscillations, we see in-the-plane rotations of it with

some nonlinear features. Notice that in the vicinity of the linear-resonance frequency, at 0.75 GHz, under the strong rotating field of 2kA/m, the magnetization oscillations are chaotic. Thus, there is an upper-limit of the frequency on using the strong rotating field (in the regime of the nonlinear response) to the power conversion. On the other hand, at the relatively-low frequency 0.2 GHz, the amplitudes of the dynamical response have increased from $\text{Amp}(m_y) = 0.14$ at the rotating field 0.2kA/m (or the driving transverse field $\text{Amp}(H_y) = 0.2$ kA/m) to $\text{Amp}(m_y) > 0.9$ and $\text{Amp}(m_x) \approx \text{Amp}(m_y)$ at the rotating field of 2kA/m. Such a large oscillation amplitude is related to complete in-the-plane rotations of the magnetization, which we call below a nonlinear rotational mode. The amplitude of the simultaneous out-of-the-plane (nonlinear) oscillations (extracted from Fig. 4(h)) provides an information on the strength of the spin loss (dissipation). The ratio $\eta \equiv \text{Amp}(m_z)/\text{Amp}(m_y) < 0.03$ at the rotating field 2.0kA/m of 0.2 GHz frequency is comparable to one of the linear-response regime, in particular, to the case of the driving with the transverse-field of the amplitude of 0.2kA/m at the same frequency 0.2 GHz.

In Appendix, we apply van der Pol approach to the ferromagnetic nonlinear resonance at the rotating field. Note that, the geometry of our oscillating ferromagnet is different from a widely studied nonlinear-resonant (PMA) system in a rotating in-the-plane field by the presence of an in-the-plane anisotropy [54,55], (we focus on the high-frequency FMR configuration). Despite, established analytical methods to treat the nonlinear resonance are devoted to weakly-nonlinear oscillations which is not the case of $(\text{Fe}_{65}\text{Co}_{35})_{0.6}(\text{Al}_2\text{O}_3)_{0.4}$ at 0.2 GHz and 2.0 kA/m for instance, there is a transition between the weak- and strong-nonlinear regimes with changing the frequency/amplitude of the driving field. Also, in Appendix, simulations of a simplified uniform system of the effective parameters of $(\text{Fe}_{65}\text{Co}_{35})_{0.6}(\text{Al}_2\text{O}_3)_{0.4}$ are sketched. We find the highly-nonlinear oscillations at 0.2 GHz in the nanocomposite (Fig. 4(g)) to be well described with the uniform effective model (Fig. 6(e)). At the resonant frequency of 0.75 GHz and the strong rotating field 2.0 kA/m, the magnetization oscillations in the nanocomposite become chaotic (Fig. 4(f)), whereas, some transient (while not chaotic) behavior at the same frequency is found in the uniform model as well (Fig. 6(d)). It should be noted that the transient behavior of the anisotropic ferromagnets under the rotating field has been studied within the Melnikov method in [56], with especial attention to our case of in-the-plane easy-axis anisotropy. However, numerical evaluations were performed in a different range of parameters ($K/K_u \sim 1$, $\alpha = 0.01$) than ours ($K/K_u \sim 100$, $\alpha = 0.1$), which are crucial for values of the Melnikov function.

Evaluating the hysteretic loss, we plot the Zeeman energy with dependence on time in Fig. 5. The Zeeman energy oscillates with the amplitude that corresponds to the average volumetric power loss $\bar{P}_V \sim \text{Amp}(E_Z)$ via

$$\bar{P}_V = \frac{\nu}{V} \int_0^{1/\nu} \left| \frac{dE_Z}{dt} \right| dt. \quad (9)$$

In Fig. 5(a), (b), the time course of the Zeeman energy is shown for $(\text{Fe}_{65}\text{Co}_{35})_{0.6}(\text{Al}_2\text{O}_3)_{0.4}$ layer excited by different-amplitude longitudinal fields. The Zeeman-energy amplitude $\text{Amp}(E_Z)$ significantly increases with the field so as the volumetric power loss (the hysteretic loss), from $\bar{P}_V = 20$ W/s·m³·ν at $|\mathbf{B}|/\mu_0 = 0.2$ kA/m to $\bar{P}_V = 300$ W/s·m³·ν at $|\mathbf{B}|/\mu_0 = 2$ kA/m). The time dependence of the Zeeman energy of the transverse-field-excited system is plotted in Fig. 5(c), showing a quite large amplitude of the energy oscillations. According to Fig. 5(d), the amplitude of the Zeeman energy (thus, the hysteretic loss) of the system in the rotating field of 2.0 kA/m; ($\bar{P}_V = 80$ W/s·m³·ν) is reduced compared to those in the longitudinal (or even transverse) fields of the amplitude of 2.0kA/m (Fig. 5(b), (c)).

In the present system, the hysteretic losses are comparable or smaller than ones evaluated from data on nanogranular magnets, albeit, to the best of our knowledge, data are available for at least an order of magnitude smaller frequencies than considered here [57]. More

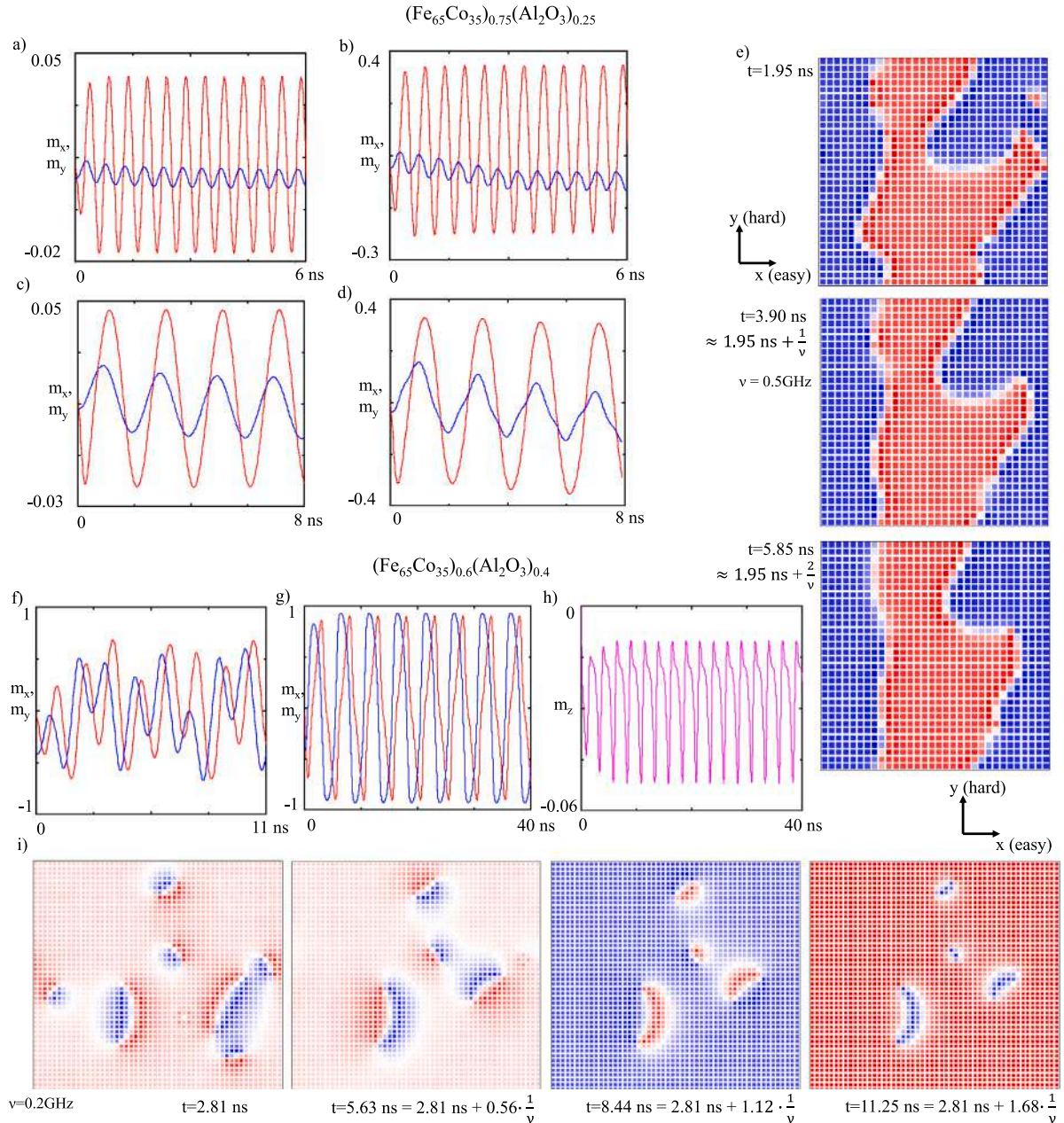


Fig. 4. Time dependence of the longitudinal (blue curve) and transverse in-the-plane (red curve) components of the magnetization of $(\text{Fe}_{65}\text{Co}_{35})_{0.75}(\text{Al}_2\text{O}_3)_{0.25}$ oscillating in a rotating in-the-plane field of 2 GHz and 0.2 kA/m (a), 2 GHz and 2 kA/m (b), 0.5 GHz and 0.2 kA/m (c), 0.5 GHz and 2 kA/m (d) and the snapshots from the later evolution (e). The same for $(\text{Fe}_{65}\text{Co}_{35})_{0.6}(\text{Al}_2\text{O}_3)_{0.4}$ at 0.75 GHz and 2 kA/m (f), 0.2 GHz and 2 kA/m (g), with the time dependence of the perpendicular component (h) and the snapshots from the later evolution (i). In the snapshots, the colors indicate the magnetization projection onto the easy axis (m_x component).

importantly, in an alternating (sub-GHz) field of a constant direction, the eddy-current losses are believed to dominate over the hysteretic ones, despite the resistivities of the nanocomposites are large. In the rotating field, our simulations predict the magnetization rotation without or with a minor movement of DWs (see the snapshots in Fig. 5(i)). When, the direction of the domain magnetization is rotating with a constant phase shift with respect to the field and that phase shift is close to $\pi/2$, (the domain magnetization is remaining perpendicular to the field), there is no reason for DWs to move, thus, for inducing the eddy currents. The stability of the domain structure under this high rotating field is confirmed by the time periodicity of the magnetization-component plot in Fig. 4(g). In contrast, the instability of the domain structure in the linearly-polarized (longitudinal or transverse) field

of the corresponding amplitude and frequency is seen from the perturbation of the periodicity in the magnetization plots of Fig. 5(b), (c).

5. Conclusions

The loss tangent of the transverse-field-driven dynamics has been found to be large for all the $\text{Fe}_{65}\text{Co}_{35}$ -based composites at the GHz and sub-GHz frequencies ($\tan(\delta_\omega) \sim 0.1$ or higher). The transverse-field-driven dynamics of the $(\text{Co})_{0.42}(\text{MgF}_2)_{0.58}$ layer does not coincide with the classic description of FMR since, inside magnetic domains, the out-of-plane magnetization component was visibly nonuniform. Therefore, instead the loss tangent, we evaluate the ratio of the amplitudes of the magnetization components $\eta \equiv \text{Amp}(m_z)/\text{Amp}(m_y)$, which is a characteristic of the spin loss as well. At the driving frequency 0.2 GHz

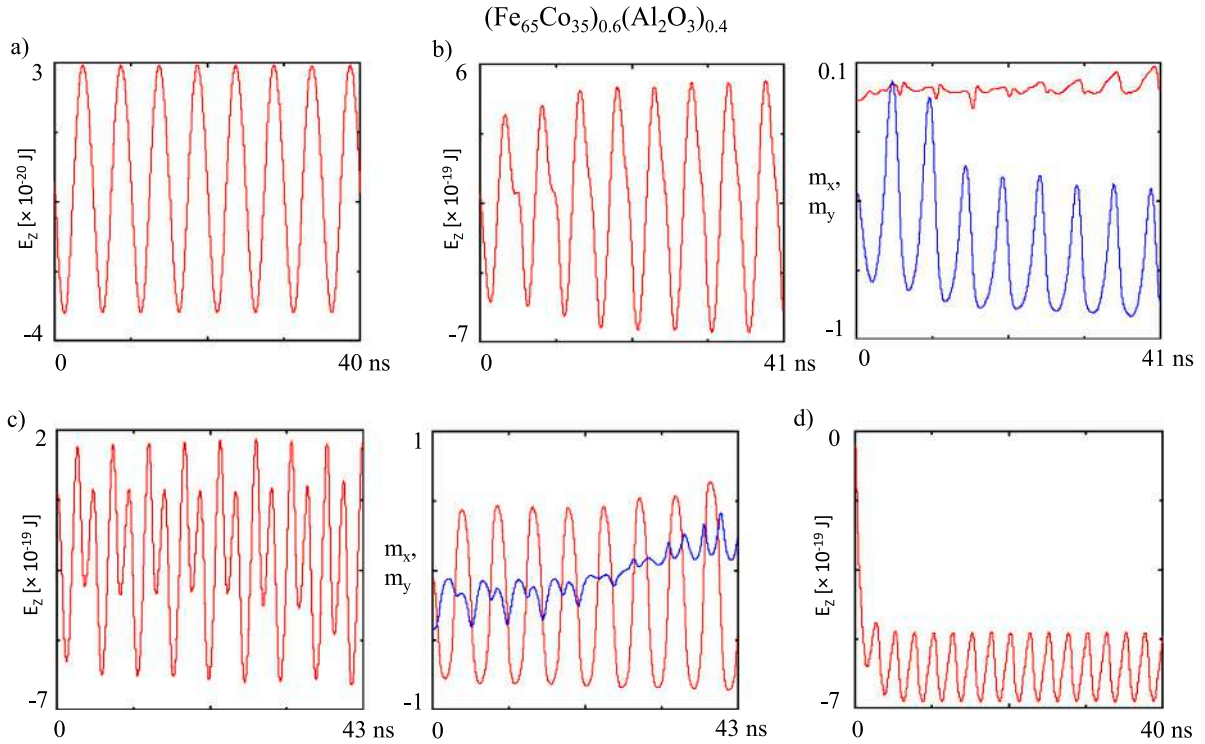


Fig. 5. Time dependence of the Zeeman energy of $(\text{Fe}_{65}\text{Co}_{35})_{0.6}(\text{Al}_2\text{O}_3)_{0.4}$ under 0.2 GHz alternating field longitudinal to the easy axis of the field amplitude 0.2 kA/m (a), 2.0 kA/m [(b) - left plot], 0.2 GHz alternating field transverse to the easy axis of the field amplitude 2.0 kA/m [(c) - left plot], 0.2 GHz in-the-plane rotating field of 2.0 kA/m (d). Additionally, the time dependence of the magnetization m_x (blue line) and m_y (red line) components of the overall magnetization at the longitudinal [(b) - right plot] and transverse [(c) - right plot] driving field of the amplitude of 2.0 kA/m and frequency 0.2 GHz.

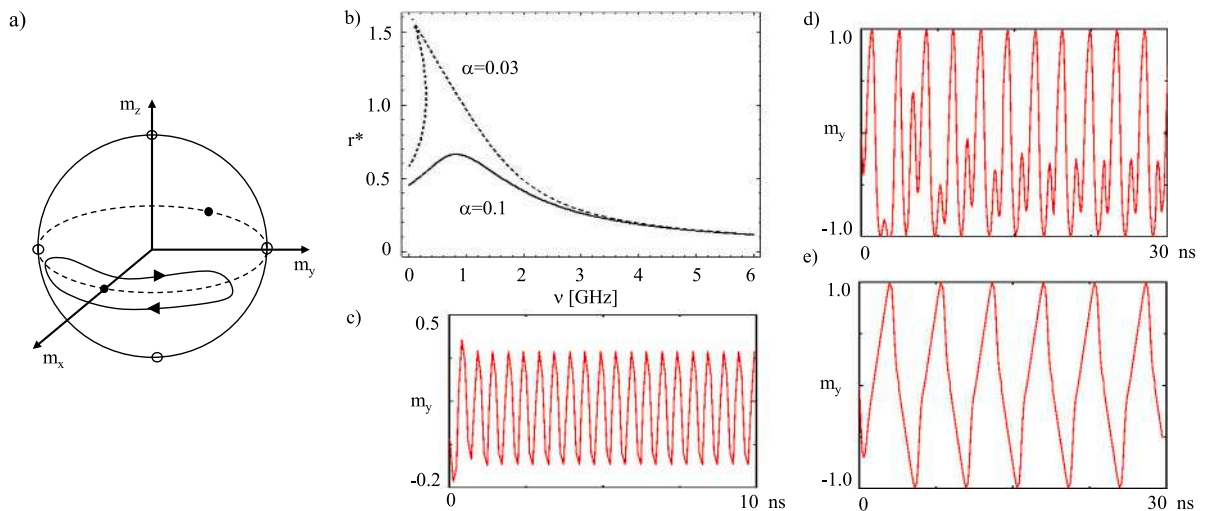


Fig. 6. Stable (filled dots) and unstable (open dots) critical points of the LL equation on the unit sphere and a trajectory of the weakly-nonlinear magnetization oscillations (a). Analytically determined equilibrium value of the radius of the phase-space trajectory with dependence on the frequency of the rotating (2 kA/m) field for $(\text{Fe}_{65}\text{Co}_{35})_{0.6}(\text{Al}_2\text{O}_3)_{0.4}$, with different Gilbert-damping constants (b), and simulated with a simplified model of $(\text{Fe}_{65}\text{Co}_{35})_{0.6}(\text{Al}_2\text{O}_3)_{0.4}$ (a uniform ferromagnet) time dependence of the transverse in-the-plane component (m_y) of the magnetization under the 2kA/m rotating field of $\nu = 2$ GHz (c), $\nu = 0.75$ GHz (d), and $\nu = 0.2$ GHz (e).

for $(\text{Fe}_{65}\text{Co}_{35})_{0.6}(\text{Al}_2\text{O}_3)_{0.4}$ and at 0.5 GHz for the remaining of the studied systems, $\eta = 0.02 \div 0.05$; (Figs. 2(a), (d), 3(a), (d)). Thus, we have not managed to avoid a relatively high spin loss in the transverse magnetic response at sub-GHz frequencies and the power conversion with the transverse mode of the sub-GHz range is on the limit of efficiency.

Unlike for the cores of large-scale transformers, lowered remanent magnetization M_r (the squareness ratio $m_r \equiv M_r/M_s < 1$, as found for $(\text{Co})_{0.42}(\text{MgF}_2)_{0.58}$) is a not an advantage for the microinductors in general. The design of the later includes directing the driving field

relative to the axes of the magnetic anisotropy. The requirement of a low anisotropy for the core materials is not applicable to the energy conversion that utilizes FMR. A high (close to one) squareness ratio of the $\text{Fe}_{65}\text{Co}_{35}$ -based composites ensures the DW-assisted dynamical response to the longitudinal field to be the strongest possible, whereas, a close-to-zero surface area of the transverse-hysteresis loops of all the composites studied is related to the largest possible amplitude of the FMR-assisted response to the transverse field.

The longitudinal-field-driven (DW-assisted) response in different composites is found to be significant in the sub-GHz range, while,

rapidly weakening with increase of the frequency. In the field of a given amplitude, the magnetically-softest the system is, (the lower volume of the metallic phase is), the higher amplitude of the DW oscillations is reached. It is due to the increased DW width in the soft magnets, thus, the increased DW mobility, (according to the classic prediction for DW in a constant field by Schryer and Walker [58]). That increase of the DW-oscillation amplitude in $(\text{Fe}_{65}\text{Co}_{35})_{0.6}(\text{Al}_2\text{O}_3)_{0.4}$ compensates a decrease of the saturation magnetization relative to $(\text{Fe}_{65}\text{Co}_{35})_{0.75}(\text{Al}_2\text{O}_3)_{0.25}$ when evaluating the longitudinal permeability in the regime of the linear response. However maximum of the DW-oscillation amplitude, thus, maximum of the driving field is limited by average size of the domains. Therefore, a lower amplitude of the DW oscillations in the magnetically-hardest $(\text{Fe}_{65}\text{Co}_{35})_{0.75}(\text{Al}_2\text{O}_3)_{0.25}$ than in the other layers is noticeable with regard to the stability of the DW structure, whereas, in the magnetically-softest $(\text{Fe}_{65}\text{Co}_{35})_{0.6}(\text{Al}_2\text{O}_3)_{0.4}$, the domain-structure instability in a longitudinal field of the amplitude $\text{Amp}(H_x) = 2.0$ kA/m or higher manifests in chaotic oscillations of the magnetization. On the other hand, low volume of the metallic phase in the later system is an advantage in terms of increasing the resistivity, thus, limiting the excess loss of the longitudinal magnetic response.

Periodic rotations of the magnetization in the layer of $(\text{Fe}_{65}\text{Co}_{35})_{0.6}(\text{Al}_2\text{O}_3)_{0.4}$ are achievable in a sufficiently-strong rotating field below a frequency of a threshold to the chaotic magnetic response. We have found the amplitude of in-the-plane magnetization oscillations at $|\mathbf{H}| = 2$ kA/m and $\nu = 0.2$ GHz to be higher (the magnetization continuously rotates almost in-the-plane) than the amplitude of $m_y(t)$ at the magnetic response to the transverse field of the corresponding amplitude $\text{Amp}(H_y) = 2$ kA/m. The characteristic of the spin loss of the rotation-excited mode $\eta \approx 0.02$ is comparable to one of the linear (rotational or transverse) excitation modes at the field (or field amplitude) of 0.2 kA/m. Moreover, the nonlinear rotational mode of the magnetization in $(\text{Fe}_{65}\text{Co}_{35})_{0.6}(\text{Al}_2\text{O}_3)_{0.4}$ layer is accompanied by a lower hysteretic loss than necessary for exciting the longitudinal mode with the alternating field of equal amplitude. However, the most promising fact about this mode is the dynamical stability of the domain structure in contrast to the case of driving with the strong linearly-polarized (longitudinal or transverse) field. It is related to withholding the excess loss which is the main power loss in the soft magnets at high frequencies. Utilizing the driven rotations of the nanocomposite magnetization seems to be a big chance for increasing the efficiency of the integrated power converters.

CRedit authorship contribution statement

Kacper Brzuszek: Investigation, Validation, Visualization. **Andrzej Janutka:** Conceptualization, Investigation, Supervision, Writing – original draft.

Declaration of competing interest

The authors declare that they have no known competing financial interests or personal relationships that could have appeared to influence the work reported in this paper.

Acknowledgment

Calculations have been carried out using resources provided by Wrocław Centre for Networking and Supercomputing (<http://wcss.pl>), grant No. 450.

Appendix. Nonlinear ferromagnetic resonance in a rotating field

Reduce (1) for the case of a homogeneous magnetization into

$$-\frac{\partial \mathbf{m}}{\partial t} = \gamma \mathbf{m} \times (\mathbf{B}_{an} + \mathbf{B}) - \alpha \mathbf{m} \times \frac{\partial \mathbf{m}}{\partial t}, \quad (10)$$

where $\mathbf{B}_{an} = \frac{2K_u}{M_s}(\mathbf{m} \cdot \hat{i})\hat{i} - \mu_0 \bar{M}_s(\mathbf{m} \cdot \hat{k})\hat{k}$. At zero external field ($\mathbf{B} = 0$), the critical points of (10) are $\mathbf{m} = [\pm 1, 0, 0]$ or $\mathbf{m} = [0, \pm 1, 0]$ or $\mathbf{m} = [0, 0, \pm 1]$ of whom only those of the first pair (dark dots on the unit sphere in Fig. 6(a)) are stable equilibria. These stability points are of the center type in the case of the absence of the spin dissipation, hence, the surrounding magnetization trajectories should form closed loops (orbits) on the sphere, (Fig. 6(a)).

In order to determine amplitudes of the driven oscillations of the magnetization components in a rotating field, we expand y - and z -components of Eq. (10) around $\mathbf{m} = [1, 0, 0]$ in m_y, m_z , up to the third order. We apply the van der Pol transform

$$\begin{aligned} u(t) &= m_y(t) \cos(\omega t) - \sqrt{\frac{\omega_1}{\omega_2}} m_z(t) \sin(\omega t), \\ v(t) &= m_y(t) \sin(\omega t) + \sqrt{\frac{\omega_1}{\omega_2}} m_z(t) \cos(\omega t). \end{aligned} \quad (11)$$

and write down the dynamical equations of u and v . Averaging them over the period of the driving field, thus, exchanging $u \rightarrow \bar{u} \equiv \frac{1}{T} \int_0^T u(t) dt$, $v \rightarrow \bar{v} \equiv \frac{1}{T} \int_0^T v(t) dt$, and transforming the averages into $r \equiv \sqrt{\bar{u}^2 + \bar{v}^2}$, $\phi \equiv \arctan(\bar{v}/\bar{u})$, one arrives at the autonomous equations

$$\begin{aligned} r\dot{r} &= -\frac{\alpha(\omega_1 + \omega_2)}{2(1 + \alpha^2)} r^2 - \frac{\sqrt{\omega_1 \omega_2}}{8(1 + \alpha^2)} \sin(2\phi) \cos(2\phi) r^4 \\ &\quad - \frac{\gamma_0 \text{Amp}(H)}{2(1 + \alpha^2)} \sqrt{\frac{\omega_1}{\omega_2}} \frac{\cos(\phi) r}{1 - \frac{1}{8} r^2}, \\ [\tan(\phi)]\dot{\phi} &= \omega r^2 + \frac{\sqrt{\omega_1 \omega_2}}{1 + \alpha^2} r^2 - \frac{3\sqrt{\omega_1 \omega_2}}{8(1 + \alpha^2)} \cos(2\phi) r^4 \\ &\quad - \frac{\gamma_0 \text{Amp}(H)}{2(1 + \alpha^2)} \sqrt{\frac{\omega_1}{\omega_2}} \frac{\sin(\phi) r}{1 - \frac{3}{8} r^2}. \end{aligned} \quad (12)$$

Since $r = \sqrt{m_y^2 + \frac{\omega_1}{\omega_2} m_z^2}$, the critical points $[r^*(\omega), \phi^*(\omega)]$ (the solutions for $\dot{r} = 0$, $\dot{\phi} = 0$) determine the amplitude of the oscillations of the m_y -component of the magnetization; $r^*(\omega) = \text{Amp}(m_y)$. In Fig. 6(b), $r^*(\omega)$ is plotted for the parameters $\{\bar{M}_s, K_u\}$ of the $(\text{Fe}_{65}\text{Co}_{35})_{0.6}(\text{Al}_2\text{O}_3)_{0.4}$ composite. The plot shows the dependence of r^* on ω to be unique for the damping constant $\alpha = 0.1$, whereas, a non-uniqueness typical of nonlinear resonance (the transition to chaos) is present for $\alpha \leq 0.03$.

We have verified the above analytical predictions on nonlinear FMR simulating the uniform ferromagnetic layer of the parameters $\{\bar{M}_s, K_u, \bar{A}_{ex}\}$ of $(\text{Fe}_{65}\text{Co}_{35})_{0.6}(\text{Al}_2\text{O}_3)_{0.4}$ and of $\alpha = 0.1$ in a rotating in-the-plane field, ($\bar{M}_s = 4.8 \cdot 10^5$ A/m, $K_u = 5.0 \cdot 10^2$ J/m³, $\bar{A}_{ex} = 1.6 \cdot 10^{-11}$ J/m). At $\nu = 2$ GHz, we have found weakly-nonlinear oscillations of the magnetization whose amplitude coincides quite well with $r^*(2\pi\nu)$, as seen from the comparison of Fig. 6(b) and 6 (c). However, at low frequencies (close to or lower than resonant frequency), the oscillations are not weakly-nonlinear [the formula for $r^*(\omega)$ does not apply anymore and the magnetization vector performs full rotations in the XY-plane instead, (see Fig. 6(d), (e)).

References

- [1] C.R. Sullivan, D.V. Harburg, J. Qiu, C.G. Levey, D. Yao, Integrating magnetics for on-chip power: a perspective, IEEE Trans. Power Electron. 28 (2013) 4342–4353, <http://dx.doi.org/10.1109/TPEL.2013.2240465>.
- [2] M. Aragchini, et al., A technology overview of the PowerChip development program, IEEE Trans. Power Electron. 28 (2013) 4182–4201, <http://dx.doi.org/10.1109/TPEL.2013.2237791>.
- [3] R.J. Kaplar, J.C. Neely, D.L. Huber, L.J. Rashkin, Generation-After-Next Power Electronics: Ultrawide-bandgap devices, high-temperature packaging, and magnetic nanocomposite materials, IEEE Power Electron. Mag. 4 (2017) 36–42, <http://dx.doi.org/10.1109/PEL.2016.2643098>.

- [4] V. Korenivski, GHz magnetic film inductors, *J. Magn. Magn. Mater.* 215–216 (2000) 800–806, [http://dx.doi.org/10.1016/S0304-8853\(00\)00292-4](http://dx.doi.org/10.1016/S0304-8853(00)00292-4).
- [5] C.O. Mathuna, N. Wang, S. Kulkarni, S. Roy, Review of integrated magnetics for power supply on chip (PwrSoC), *IEEE Trans. Power Electron.* 27 (2012) 4799–4816, <http://dx.doi.org/10.1109/TPEL.2012.2198891>.
- [6] E.A. Perigo, B. Weidenfeller, P. Kollar, J. Fuzer, Past, present, and future of soft magnetic composites, *Appl. Phys. Rev.* 5 (2018) 031301, <http://dx.doi.org/10.1063/1.5027045>.
- [7] D.-S. Xue, F.-S. Li, X.-L. Fan, X.-S. Wen, Bianisotropy picture of higher permeability at higher frequencies, *Chin. Phys. Lett.* 25 (2008) 4120–4123, <http://dx.doi.org/10.1088/0256-307X/25/11/077>.
- [8] C.-H. Jiang, X.-L. Fan, D.-S. Xue, High frequency magnetic properties of ferromagnetic thin films and magnetization dynamics of coherent precession, *Chin. Phys. B* 24 (2015) 057504, <http://dx.doi.org/10.1088/1674-1056/24/5/057504>.
- [9] A.N. Lagarkov, K.N. Rozanov, High-frequency behavior of magnetic composites, *J. Magn. Magn. Mater.* 321 (2009) 2082–2092, <http://dx.doi.org/10.1016/j.jmmm.2008.08.099>.
- [10] S. Ohnuma, H. Fujimori, S. Mitani, T. Masumoto, High-frequency magnetic properties in metal-nonmetal granular films, *J. Appl. Phys.* 79 (1996) 5130–5135, <http://dx.doi.org/10.1063/1.361531>.
- [11] J.M. Silveyra, E. Ferrara, D.L. Huber, T.C. Monson, Soft magnetic materials for a sustainable and electrified world, *Science* 362 (2018) eaao195, <http://dx.doi.org/10.1126/science.aao195>.
- [12] R.C. Pullar, Hexagonal ferrites: A review of the synthesis, properties and applications of hexaferrite ceramics, *Prog. Mater. Sci.* 57 (2012) 1191–1334, <http://dx.doi.org/10.1016/j.pmatsci.2012.04.001>.
- [13] D. Polder, J. Smit, Resonance phenomena in ferrites, *Rev. Modern Phys.* 25 (1953) 89–90, <http://dx.doi.org/10.1103/RevModPhys.25.89>.
- [14] T.N. Lamichhane, L. Sethuraman, A. Dalagan, H. Wang, J. Keller, M.P. Paranthaman, Additive manufacturing of soft magnets for electrical machines—a review, *Mater. Today Phys.* 15 (2020) 100255, <http://dx.doi.org/10.1016/j.mtphys.2020.100255>.
- [15] D.S. Gardner, G. Schrom, F. Paillet, B. Jamieson, T. Karnik, S. Borkar, Review of on-chip inductor structures with magnetic films, *IEEE Trans. Magn.* 45 (2009) 4760–4766, <http://dx.doi.org/10.1109/TMAG.2009.2030590>.
- [16] D. Yao, C.G. Levey, R. Tian, C.R. Sullivan, Microfabricated V-groove power inductors using multilayer Co–Zr–O thin films for very-high-frequency DC–DC converters, *IEEE Trans. Power Electron.* 28 (2013) 4384–4394, <http://dx.doi.org/10.1109/TPEL.2012.2233760>.
- [17] L. Wang, Y. Wang, H. Zhang, Z. Zhong, L. Wang, D. Peng, F. Bai, Integrated on-chip solenoid inductors with nanogranular magnetic cores, *IEEE Trans. Magn.* 52 (2016) 8400604, <http://dx.doi.org/10.1109/TMAG.2015.2514095>.
- [18] V.N. Kondratyev, H.O. Lutz, Shell effect in exchange coupling of transition metal dots and their arrays, *Phys. Rev. Lett.* 81 (1998) 4508–4511, <http://dx.doi.org/10.1103/PhysRevLett.81.4508>.
- [19] X. Bao, et al., Excellent microwave absorption of FeCo/ZnO composites with defects in ZnO for regulating the impedance matching, *J. Alloys Compd.* 769 (2018) 512–520, <http://dx.doi.org/10.1016/j.jallcom.2018.08.036>.
- [20] S.A. Makhlof, F.T. Parker, F.E. Spada, A.E. Berkowitz, Magnetic anomalies in NiO nanoparticles, *J. Appl. Phys.* 81 (1997) 5561–5563, <http://dx.doi.org/10.1063/1.364661>.
- [21] R. Alben, J.J. Becker, M.C. Chi, Random anisotropy in amorphous ferromagnets, *J. Appl. Phys.* 49 (1978) 1653–1658, <http://dx.doi.org/10.1063/1.324881>.
- [22] G. Herzer, Grain size dependence of coercivity and permeability in nanocrystalline ferromagnets, *IEEE Trans. Magn.* 26 (1990) 1397–1402, <http://dx.doi.org/10.1109/20.104389>.
- [23] K. Suzuki, G. Herzer, J.M. Cadogan, The effect of coherent uniaxial anisotropies on the grain-size dependence of coercivity in nanocrystalline soft magnetic alloys, *J. Magn. Magn. Mater.* 177 (1998) 949–950, [http://dx.doi.org/10.1016/S0304-8853\(97\)00987-6](http://dx.doi.org/10.1016/S0304-8853(97)00987-6).
- [24] G. Herzer, Modern soft magnets: Amorphous and nanocrystalline materials, *Acta Mater.* 61 (2013) 718–734, <http://dx.doi.org/10.1016/j.actamat.2012.10.040>.
- [25] S. Wang, J. Ma, X. Zhang, J. Li, Magnetic softness and interparticle exchange interactions of $(\text{Fe}_{65}\text{Co}_{35})_{1-x}(\text{Al}_2\text{O}_3)_x$ ($x = 0 - 0.50$) nanogranular films, *Thin Sol. Films* 520 (2012) 5046–5052, <http://dx.doi.org/10.1016/j.tsf.2012.03.025>.
- [26] K.D. Coonley, G.J. Mehan, C.R. Sullivan, U.J. Gibson, Evaporatively deposited Co–MgF₂ granular materials for thin-film inductors, *IEEE Trans. Magn.* 36 (2000) 3463–3465, <http://dx.doi.org/10.1109/20.908861>, <http://dx.doi.org/10.1063/1.2190719>.
- [27] V. Ionescu, M. Osiac, C.P. Lungu, O.G. Pompilian, I. Jecu, I. Mustata, G.E. Iacobescu, Morphological and structural investigations of Co–MgF₂ granular thin films grown by thermionic vacuum arc, *Thin Sol. Films* 518 (2010) 3945–3948, <http://dx.doi.org/10.1016/j.tsf.2010.02.035>.
- [28] G. Lu, H. Zhang, J.Q. Xiao, X. Tang, Z. Zhong, F. Bai, High-frequency properties and thickness-dependent damping factor of – thin films, *IEEE Trans. Magn.* 48 (2012) 3654–3657, <http://dx.doi.org/10.1109/TMAG.2012.2200096>.
- [29] S. Wang, X. Zhang, J. Li, J. Ma, J. Huang, Enhanced magnetic softness and high-frequency characteristics of $\text{Fe}_{51.1}\text{Co}_{48.9}\text{B-Al}_2\text{O}_3$ nanogranular films, *Scr. Mater.* 65 (2011) 45–48, <http://dx.doi.org/10.1016/j.scriptamat.2011.03.010>.
- [30] Y. Wang, H. Zhang, D. Wen, Z. Zhong, F. Bai, Magnetic and high frequency properties of nanogranular CoFe–TiO₂ films, *J. Appl. Phys.* 113 (2013) 17A316, <http://dx.doi.org/10.1063/1.4795325>.
- [31] S. Ge, D. Yao, M. Yamaguchi, X. Yang, H. Zuo, T. Ishii, D. Zhou, F. Li, Microstructure and magnetism of FeCo–SiO₂ nano-granular films for high frequency application, *J. Phys. D: Appl. Phys.* 40 (2007) 3660–3664, <http://dx.doi.org/10.1088/0022-3727/40/12/016>.
- [32] D. Yao, S. Ge, X. Zhou, H. Zuo, Grain size dependence of coercivity in magnetic metal–insulator nanogranular films with uniaxial magnetic anisotropy, *J. Appl. Phys.* 107 (2010) 073902, <http://dx.doi.org/10.1063/1.3357399>.
- [33] X. Ou, J. He, Z. Xia, J. An, J. Hao, S. He, D. Zhao, Fabrication and magnetic properties of strip-patterned FeCoB–SiO₂ nanoparticle films for GHz application, *Mater. Sci. Eng. B* 242 (2019) 69–74, <http://dx.doi.org/10.1016/j.mseb.2019.03.009>.
- [34] W. Kleemann, O. Petravic, Ch. Binek, G.N. Kakazei, Yu.G. Pogorelov, J.B. Sousa, S. Cardoso, P.P. Freitas, Interacting ferromagnetic nanoparticles in discontinuous Co₈₀Fe₂₀–Al₂O₃ multilayers: From superspin glass to reentrant superferromagnetism, *Phys. Rev. B* 63 (2001) 134423, <http://dx.doi.org/10.1103/PhysRevB.63.134423>.
- [35] A.A. Stashkevich, et al., Brillouin light scattering observation of the transition from the superparamagnetic to the superferromagnetic state in nanogranular (SiO₂)Co films, *J. Appl. Phys.* 104 (2008) 093912, <http://dx.doi.org/10.1063/1.3009339>.
- [36] S. Bedanta, et al., Superferromagnetic domain state of a discontinuous metal insulator multilayer, *Phys. Rev. B* 72 (2005) 024419, <http://dx.doi.org/10.1103/PhysRevB.72.024419>.
- [37] N. Chowdhury, S. Bedanta, S. Sing, W. Kleemann, Controlling the size and relaxation dynamics of superferromagnetic domains, *J. Appl. Phys.* 117 (2015) 153907, <http://dx.doi.org/10.1063/1.4918670>.
- [38] Y. He, Y. Wang, Z. Zhong, H. Zhang, F. Bai, High-frequency magnetic loss in nanogranular FeCoTiO films with different histories of induced uniaxial anisotropy, *IEEE Trans. Magn.* 54 (2018) 2800905, <http://dx.doi.org/10.1109/TMAG.2018.2842430>.
- [39] S.M. Ryabchenko, A.A. Timopheev, V.M. Kalita, A.F. Lozenko, P.A. Trotsenko, V.A. Stephanovich, M. Munakata, Intergranular interactions in nanogranular (CoFe)_x–(SiO₂)_{1-x} films with temperature and angular variations in coercivity, *Low Temp. Phys.* 36 (2010) 682–692, <http://dx.doi.org/10.1063/1.3490833>.
- [40] G.R. Khan, C.R. Sullivan, Nanogranular nickel iron thin films for high frequency power applications, in: Proc. of 2013 Twenty-Eighth Annual IEEE Appl. Power Electronics Conf. and Expo, APEC, 2013, pp. 1638–1643, <http://dx.doi.org/10.1109/APEC.2013.6520516>.
- [41] A.J. Hanson, J.A. Belk, S. Lim, C.R. Sullivan, D.J. Perreault, Measurements and performance factor comparisons of magnetic materials at high frequency, *IEEE Trans. Power Electron.* 31 (2016) 7909–7925, <http://dx.doi.org/10.1109/TPEL.2015.2514084>.
- [42] Y. He, Z. Zhang, R. Wu, W. Guo, H. Zhang, F. Bai, On-chip coupled inductors with a novel spliced anisotropic and isotropic magnetic core for inductance and coupling enhancement, *Sol. State. Electron.* 164 (2020) 107699, <http://dx.doi.org/10.1016/j.sse.2019.107699>.
- [43] P. Zukowski, T. Koltunowicz, J. Partyka, Yu.A. Fedotova, A.V. Larkin, Electrical properties of nanostructures (CoFeZr)_x+(Al₂O₃)_{1-x} with use of alternating current, *Vacuum* 83 (2009) S275–S279, <http://dx.doi.org/10.1016/j.vacuum.2009.01.081>.
- [44] W. Li, Y. Sun, C.R. Sullivan, High-frequency resistivity of soft magnetic granular films, *IEEE Trans. Magn.* 41 (2005) 3283–3285, <http://dx.doi.org/10.1109/TMAG.2005.854720>.
- [45] K. Ikeda, T. Suzuki, T. Sato, FeNiSiO/SiO₂ multi-layer granular magnetic films with high-resistivity, *Trans. Mater. Res. Soc. Jpn.* 934 (2009) 9–13, <http://dx.doi.org/10.14723/tmrsj.34.9>.
- [46] L.Z. Wu, J. Ding, H.B. Jiang, C.P. Neo, L.F. Chen, C.K. Ong, High frequency complex permeability of iron particles in a nonmagnetic matrix, *J. Appl. Phys.* 99 (2006) 083905.
- [47] K. Ikeda, T. Suzuki, T. Sato, CoFeSiO/SiO₂ multilayer granular films with very narrow ferromagnetic resonant linewidth, *IEEE Trans. Magn.* 45 (2009) 4290–4293, <http://dx.doi.org/10.1109/TMAG.2009.2023616>.
- [48] H. Geng, et al., Soft magnetic property and high-frequency permeability of [Fe₈₀Ni₂₀–O/TiO₂]_n multilayer thin films, *J. Alloys Compd.* 576 (2013) 13–17, <http://dx.doi.org/10.1016/j.jallcom.2013.04.128>.
- [49] A. Janutka, K. Brzuszek, Domain-wall-assisted giant magnetoimpedance of thin-wall ferromagnetic nanotubes, *J. Magn. Magn. Mater.* 465 (2018) 437–449, <http://dx.doi.org/10.1016/j.jmmm.2018.06.007>.
- [50] A. Janutka, K. Brzuszek, Domain-wall-assisted asymmetric magnetoimpedance in ferromagnetic nanostripes, *J. Phys. D: Appl. Phys.* 52 (2019) 035003, <http://dx.doi.org/10.1088/1361-6463/aae6b4>.
- [51] A. Janutka, K. Brzuszek, Giant magnetoreactance in magnetic nanowires, *J. Magn. Magn. Mater.* 515 (2020) 167297, <http://dx.doi.org/10.1016/j.jmmm.2020.167297>.

- [52] L. Xie, Y. Shi, Y.T. Hou, W. Lou, Wireless power transfer and applications to sensor networks, *IEEE Wirel. Commun.* 20 (2013) 140–145, <http://dx.doi.org/10.1109/MWC.2013.6590061>.
- [53] B.-J. Che, G.-H. Yang, F.-Y. Meng, K. Zhang, J.-H. Fu, Q. Wu, L. Sun, Omnidirectional non-radiative wireless power transfer with rotating magnetic field and efficiency improvement by metamaterial, *Appl. Phys. A* 116 (2014) 1579–1586, <http://dx.doi.org/10.1007/s00339-014-8409-0>.
- [54] H. Suhl, The nonlinear behavior of ferrites at high microwave signal levels, *Proc. IRE* 44 (1956) 1270–1284, <http://dx.doi.org/10.1109/JRPROC.1956.274950>.
- [55] G. Bertotti, C. Serpico, I.D. Mayergoyz, Nonlinear magnetization dynamics under circularly polarized field, *Phys. Rev. Lett.* 86 (2001) 724–727, <http://dx.doi.org/10.1103/PhysRevLett.86.724>.
- [56] C. Serpico, M. d'Aquino, A. Quercia, S. Perna, I.D. Mayergoyz, Transient chaos in nanomagnets subject to elliptically polarized AC applied fields, *IEEE Trans. Magn.* 55 (2019) 4300305, <http://dx.doi.org/10.1109/TMAG.2018.2865574>.
- [57] G. Khan, *Design and Synthesis of Soft Magnetic Materials for High Frequency Power Applications*, ProQuest Dissertations Publishing, 2013, 1553172.
- [58] N.L. Schryer, L.R. Walker, The motion of 180° domain walls in uniform dc magnetic fields, *J. Appl. Phys.* 45 (1974) 5406–5421, <http://dx.doi.org/10.1063/1.1663252>.



Contents lists available at ScienceDirect

Journal of Magnetism and Magnetic Materials

journal homepage: www.elsevier.com/locate/jmmm

Research article

High-frequency magnetic response of superparamagnetic composites of spherical Fe₆₅Co₃₅ nanoparticlesKacper Brzuszek^a, Caroline A. Ross^b, Andrzej Janutka^{a,*}^a Department of Theoretical Physics, Wrocław University of Science and Technology, 50-370, Wrocław, Poland^b Department of Materials Science and Engineering, Massachusetts Institute of Technology, Cambridge, MA 02139, USA

ARTICLE INFO

Keywords:

Superparamagnetism
Power conversion
Micromagnetic simulations
Microwave frequency

ABSTRACT

The response of composites of magnetic nanoparticles (MNPs) with randomly-oriented magnetocrystalline anisotropy axes to a linearly-polarized ac field or a rotating field is studied with regard to the concept of using superparamagnetic nanocomposites as core materials for high (sub-GHz and GHz) frequency power conversion devices. We perform micromagnetic simulations of systems of spherical 5nm-diameter nanoparticles of Fe₆₅Co₃₅ with two different concentrations arranged periodically within a dielectric matrix, including thermal fluctuations of the magnetization within the stochastic thermal field. Because the particles are closely packed, the effect of surface anisotropy is neglected. The dependence of the amplitude of the magnetic response function on temperature is determined. We show the inapplicability of Brown's classic theory of thermal excitations in single-domain magnetic particles for given material parameters even in the absence of the magnetostatic field. Magnetostatic interactions of MNPs are found to be necessary for stabilizing the dynamical magnetic response in the high temperature (low-energy-barrier) range. They allow for driving magnetization oscillations at room temperature with amplitude comparable to the zero-temperature case. Dynamical (hysteretic and residual) losses are discussed.

1. Introduction

Early interest in composites consisting of magnetic particles embedded in dielectric matrices was related to microwave absorption. Absorbing composite materials exhibit a broadened dielectric permittivity of the matrix and a large magnetic resonance width due to eddy-current-assisted dynamics of the domain structure inside sufficiently large particles (microparticles of ferrites for instance) [1,2]. In contrast, low-loss magnetization dynamics in nanoscale metallic/dielectric assemblies has gained attention for applications in high-frequency power conversion. In very small magnetic particles, the eddy currents and the skin effect are suppressed both because the particle lacks an internal domain structure, and due to charge confinement when the diameter is lower than the metallic mean free path of the electrons. A finite spacing of the nanoparticles provides a dielectric barrier for the electrons and suppresses interparticle currents, thus suppressing the mechanisms that lead to excess loss.

In power converters, current-assisted losses are the major problem at high (microwave) frequencies. To enable on-chip power conversion, elevating the operating frequency is crucial for miniaturization of inductors and transformers in order to compensate for reduced values of the magnetic flux [3–6]. Superferromagnetic (SFM) composites, in

which magnetic nanoparticles (MNPs) interact to form a ferromagnetic assembly [7,8], are therefore interesting for low loss, high frequency applications [9]. Creation of the SFM state requires the MNPs to be densely packed in order to interact, which makes the interparticle tunneling barriers narrow and results in unwanted particle clustering. This raises the tunneling conductivity and paths for direct conductance can appear. Moreover, SFM is mediated by magnetic-ion dopants in the nonmagnetic matrix which can create conducting paths themselves. An electric-field-driven transition between metal and insulator states within the SFM phase has been observed, which is accompanied by breaking the conducting paths [10].

These facts have redirected interest towards the application of superparamagnetic (SPM) nanocomposites to high-frequency power conversion despite the expected lower permeability and its strong sensitivity to temperature compared to that of SFM nanocomposites [11,12]. The temperature dependence of the magnetic response is governed by the size dependence of the anisotropy of MNPs [7,13,14]. A higher anisotropy raises the energy barrier and suppresses thermally-induced reversal, whereas a higher temperature sensitivity of the magnetic properties is promoted in the regime where the energy barrier is low relative to the thermal energy. Increasing the particle volume and/or

* Corresponding author.

E-mail address: Andrzej.Janutka@pwr.edu.pl (A. Janutka).<https://doi.org/10.1016/j.jmmm.2023.170651>

Received 9 January 2023; Received in revised form 14 March 2023; Accepted 19 March 2023

Available online 24 March 2023

0304-8853/© 2023 The Authors. Published by Elsevier B.V. This is an open access article under the CC BY-NC-ND license (<http://creativecommons.org/licenses/by-nc-nd/4.0/>).

doping the particles provides a path to the latter regime, as shown in Refs. [15–17], where strong changes in the temperature dependence of the susceptibility have been reported.

For power conversion, small nanoparticles (of a diameter below the electronic mean free path; below 10 nm) are of interest. These particles exhibit increased anisotropy due to magnetostatic effects from irregularities in shape, and oxidation can modify the exchange interactions within a surface layer leading to a surface spin glass ordering [18,19]. The anisotropy of MNPs can be modified through fabrication methods, and the question arises whether the magnetic response characteristics, i.e. the permeability of the engineered SPM MNP composites could be adequate to allow their use as core materials in power conversion devices. Engineering the surfaces of MNPs suspended in fluids via coating has been reported to considerably influence the effective anisotropy, hence controlling the Brown or Neel mechanism of thermal relaxation [20]. The effective anisotropy in surface-modified nanoparticles of low diameter has been reduced to be close to that of the bulk crystalline material [21–23]. Moreover, in systems of close-packed nanoparticles, the magnetostatic effect of the particle-shape imperfections is suppressed by the magnetostatic interparticle interactions [24].

This article uses a modeling approach to determine the limitations of the high-frequency magnetic response of composites consisting of high-moment SPM nanoparticles to both a linearly-polarized alternating field and a rotating field, with regard to the power conversion applications. For these applications, we focus on nanocomposites with relatively high driving fields and with magnetic fractions that yield a SPM response, and in the frequency range of 0.1–1.0 GHz. We perform micromagnetic simulations of an idealized composite consisting of monodisperse and periodically-distributed nanoparticles with bulk-like material parameters and with randomly oriented uniaxial magnetocrystalline anisotropy. The simulated systems are cubical assemblies of order 100 of small (5 nm) spherical nanoparticles of $\text{Fe}_{65}\text{Co}_{35}$, (a material of high saturation magnetization), influenced by a stochastic thermal field. We compare the simulated dynamics to those predicted within Brown's classic approach to thermal fluctuations in the single-domain magnetic particle [25]. The theory predicts the relaxation of the nanoparticles to be dominated by the Brownian mechanism (a continuous macrospin rotation) at sufficiently high temperature, unlike the typical approach of treating MNP relaxation using the Neel model, i.e. a macrospin flipping between two low-energy states [26]. In immobilized MNPs, the Brownian dynamics correspond to a low magnetic anisotropy energy, whereas, in fluid suspended MNPs, the Brownian mechanism of the relaxation is based on the magnetically-driven mechanical rotation of the nanoparticles which requires the magnetic anisotropy to be strong [27].

In [28], we described the high-frequency magnetic response of layers of SFM composites of $\text{Fe}_{65}\text{Co}_{35}$ nanoparticles at ferromagnetic resonance (FMR) conditions in the presence of a strong in-plane anisotropy. In the present work, we focus our simulations on systems in which the volumetric ratio of the magnetic component is below the threshold for SFM, which is reported (e.g. for $(\text{Fe}_{65}\text{Co}_{35})_x(\text{Al}_2\text{O}_3)_{1-x}$, [29]) to be about 50%. This provides the opportunity to directly compare the magnetic response in both SPM and SFM cases. In particular, we verify the efficiency of the magnetic response of SPM nanocomposites to a rotating field, which has been found to be higher than the response to a linear driving field in SFM layers [28].

Below the threshold ratio, in the regime of zero net magnetization, the correlation between the orientations of the nanoparticle magnetizations is caused by magnetostatic (dipole) interactions. Collective thermal behaviors typical of canonical spin glasses, ZFC-FC splitting and a temperature cusp in the susceptibility are well known features of nanoparticle composites [7]. Based on simulation snapshots, we distinguish an intermediate regime of the volumetric ratio of the magnetic content which is lower than that necessary for establishing the SFM state while higher than that relevant to the SPM phase

[7,8,30]. In this intermediate regime, the orientations of the nanoparticle magnetizations are dominated by magnetostatic interactions, leading, in the case of a periodic spatial distribution of the nanoparticles, to noncollinear multisublattice ordering. We call such a multisublattice state a super spin glass (SSG) because in practical systems, structural disorder is expected to destroy the sublattices, inducing a disordered collective state via interparticle interactions [31–34]. Both systems under consideration are closely packed, which counteracts the particle-surface-induced anisotropy. We consider whether the enhanced dipole interparticle interactions modify the dynamical susceptibility relative to that of the SPM phase.

In Section 2, we formulate the micromagnetic model of the dynamics of SSG and SPM nanocomposites. The model is applied in Sections 3 and 4 to determining the static ordering and investigating the driven high-frequency dynamics, respectively. Conclusions are collected in Section 5.

2. Model

The dynamics of a lattice of SPM nanoparticles is described by the stochastic Landau-Lifshitz-Gilbert (sLLG) equation of the normalized magnetization $\mathbf{M} = M\mathbf{m}$ of the nanoparticles, (here, M denotes the saturation magnetization of the nanoparticles),

$$-\frac{\partial \mathbf{m}}{\partial t} = \frac{2\gamma A_{ex}}{M} \mathbf{m} \times \Delta \mathbf{m} + \gamma_0 \mathbf{m} \times (\mathbf{H}_{an} + \mathbf{H}_{ms} + \mathbf{H} + \mathbf{H}_{th}) - \alpha \mathbf{m} \times \frac{\partial \mathbf{m}}{\partial t}. \quad (1)$$

Outside the nanoparticles, in the dielectric matrix, the magnetization is equal to zero. Here, \mathbf{H}_{an} , \mathbf{H}_{ms} and \mathbf{H} denote the magnetocrystalline anisotropy field, the magnetostatic (demagnetization) field and an external applied field, respectively. The orientation of the axes of the magnetocrystalline anisotropy is randomly assigned for each of the MNPs. The anisotropy field is related to the anisotropy constant K via $|\mathbf{H}_{an}| = 2K/\mu_0 M$. The parameters γ , A_{ex} and α denote the gyromagnetic factor, the exchange stiffness and the Gilbert damping constant, $\gamma_0 \equiv \gamma\mu_0$, where μ_0 represents the vacuum permeability.

In our numerical simulations, the nanoparticles are spherical in shape, of equal diameters, and uniformly distributed on a cubic lattice of $4 \times 4 \times 4$ particles satisfying periodic boundary conditions at each boundary of the cubic simulation box. A random (thermal) field \mathbf{H}_{th} satisfies the correlation property

$$\langle H_{thi}(t)H_{thj}(t+\tau) \rangle = \frac{2k_B T \alpha}{\gamma \mu_0^2 M} \delta_{ij} \delta(\tau). \quad (2)$$

In the micromagnetic simulations, after N time steps of length Δt , the relevant thermal field is given by the formula

$$\mu_0 \mathbf{H}_{th}(N \Delta t) = \sqrt{2k_B T \alpha / \gamma M \Delta V \Delta t} \mathbf{s}(N \Delta t), \quad (3)$$

where ΔV denotes the volume of the computational cell, and $\mathbf{s}(t)$ is a vector of random orientation and of components drawn from a normal distribution at each time step [35,36].

In the regime of low volume concentration of the magnetic phase (i.e. a large distance between nanoparticles), the evolution of the magnetization orientations is treated by applying Brown's approach to the dynamics of the single-domain particles with easy-axis anisotropy, using the Fokker-Planck equation [25]. The effects of the magnetostatic interparticle interactions are weak perturbations. Brown distinguishes two basic temperature regimes. In the low-temperature regime (the high energy barrier regime), the particle can be reduced to a two-level (classical) system, discretizing the relevant master equation (Neel-type relaxation). On average, the evolution of the particle magnetization in a single (let us say y -axis) direction $\langle m_y \rangle = W_1 - W_2$, ($W_{1(2)}$ denotes the probability of the occupation of the $m_y = 1$ ($m_y = -1$) state and $W_1 + W_2 = 1$). It is governed by the dynamical Eq. (23) of the Appendix, which can be rewritten in the form

$$\frac{d\langle m_y \rangle}{dt} = -\tau^{-1} \langle m_y \rangle + \Theta H_y(t). \quad (4)$$

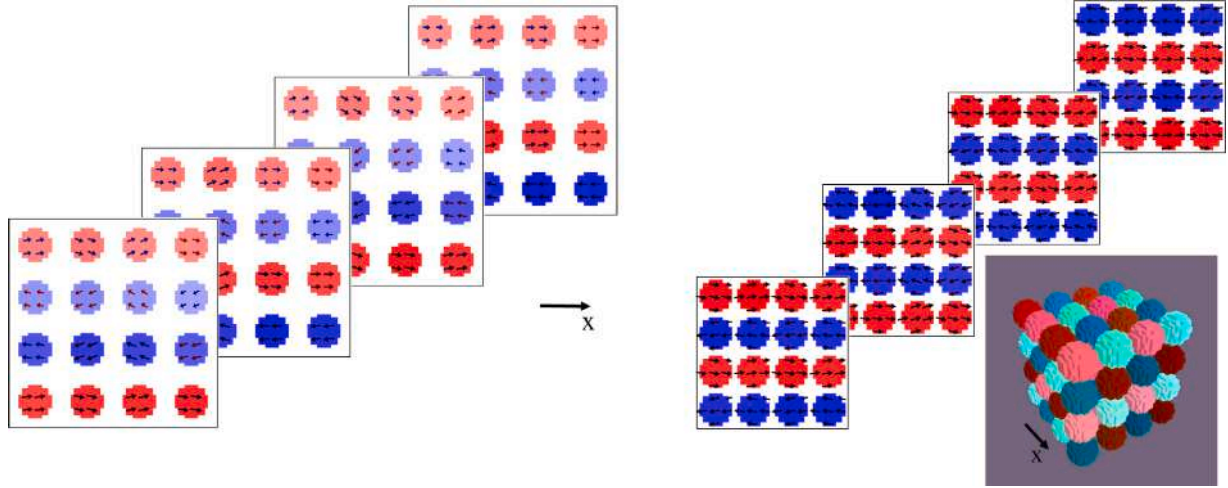


Fig. 1. Magnetic ordering in system of $4 \times 4 \times 4$ nanoparticles of $\text{Fe}_{65}\text{Co}_{35}$ of 5 nm diameter in consecutive planes of the nanoparticle lattice, at a volumetric ratio of the magnetic phase content of (a) $x = 0.13$, and (b) $x = 0.3$. The colors and their intensity indicate the magnetization projection onto the x -axis.

The relaxation rate

$$\tau^{-1} = \frac{2\gamma\alpha}{M(1+\alpha^2)} 4K \sqrt{\frac{KV}{\pi k_B T}} e^{-KV/k_B T} \quad (5)$$

is dependent on the particle volume V . The coefficient of the inhomogeneous term reads $\Theta = \tau^{-1} \mu_0 M / 4K$. For $H_y(t) = H \sin(\omega t)$, the particular (long-term) solution to (4) takes the form

$$\langle m_y(t) \rangle = \frac{\mu_0 M H}{4K} \frac{\tau^{-1}}{\sqrt{\omega^2 + \tau^{-2}}} \sin(\omega t + \phi), \quad (6)$$

$$\phi = -\arctan(1/\omega\tau).$$

The response to a linearly polarized field of SPM with a random distribution of the magnetic anisotropy axes is obtained by averaging the projections of the amplitudes of the nanoparticle response $\langle m_y \rangle_\omega$ to the field projected onto the easy axes of the particles $\langle m_y \rangle_\omega \equiv \int_0^{\pi/2} \langle m_y \rangle_\omega \cos^2 \vartheta \sin \vartheta d\vartheta$, where $\cos \vartheta = \mathbf{H}_{an} / |\mathbf{H}_{an}| \cdot \mathbf{H} / |\mathbf{H}| = H_y / |\mathbf{H}|$. Thus,

$$\overline{\langle m_y \rangle_\omega} = \frac{\langle m_y \rangle_\omega}{3} = \frac{\text{Amp}(M_y)}{M}, \quad (7)$$

where (here and below), $\text{Amp}(\dots)$ denotes the amplitude of any oscillating value, $M \equiv M(T)$ denotes the length of the vector of magnetization of the nanoparticle material and $M \rightarrow_{T \rightarrow 0} M_s$.

A rotating field in the XY -plane makes all in-plane directions of the nanoparticle anisotropy equivalent in terms of the magnetic response. Thus, the response function of the system of randomly oriented MNPs is an average

$$\overline{\langle m_y \rangle_\omega} = \frac{1}{2\pi} \int_0^\pi \int_{-\pi/2}^{\pi/2} \langle m_y \rangle_\omega \cos^2 \varphi \sin^3 \vartheta d\varphi d\vartheta$$

$$= \frac{\langle m_y \rangle_\omega}{3}. \quad (8)$$

In the high-temperature, low energy barrier regime, the amplitude of the linear magnetic response of a single-domain particle to the longitudinal AC field is described with the formula

$$\langle m_y \rangle_\omega = \frac{V \mu_0 M H}{3 k_B T} \frac{\tau_1^{-1}}{\sqrt{\omega^2 + \tau_1^{-2}}}, \quad (9)$$

where, the (Brown's) relaxation rate reads

$$\tau_1^{-1} = \frac{2\gamma\alpha}{M(1+\alpha^2)} \frac{k_B T}{V}. \quad (10)$$

3. Static ordering

We consider systems of spherical $\text{Fe}_{65}\text{Co}_{35}$ nanoparticles of 5 nm diameter which form a cubic lattice with randomly aligned crystalline (uniaxial) anisotropy axes. We simulate arrays of $4 \times 4 \times 4$ nanoparticles at the volumetric ratio of the metallic phase $x = 0.13$ (an interparticle distance of 3 nm) and $x = 0.3$ (an interparticle distance of 1 nm) under periodic boundary conditions. Numerical parameters of $\text{Fe}_{65}\text{Co}_{35}$ are: the uniaxial-anisotropy constant $K = 1.5 \cdot 10^4 \text{ J/m}^3$, the exchange stiffness $A_{ex} = 1.7 \cdot 10^{-11} \text{ J/m}$, and the Gilbert damping constant $\alpha = 0.1$. The damping is significantly higher than that of bulk ferromagnetic $\text{Fe}_{65}\text{Co}_{35}$ to account for imperfections of the nanoparticle shapes. The temperature dependence of the magnetization is approximated as $M(T) = M_s(1+T/2T_C)\sqrt{1-T/T_C}$ with a saturation magnetization $M_s = 1.9 \cdot 10^6 \text{ A/m}$ and a Curie temperature of $T_C = 950 \text{ K}$. The grid discretization size is 0.5 nm.

At zero temperature, for $x = 0.13$, the zero-field relaxation from a disordered state leads to a SPM state of the nanoparticle magnetizations that match closely the orientations of the crystalline anisotropy axes. However, correlations of the ordering of neighboring nanoparticles are seen from Fig. 1(a). They are due to dipole interparticle interactions and manifest as a non-arbitrary choice of the orientations of the nanoparticle magnetization from two opposite directions along the easy axis. For $x = 0.3$, our system of periodically aligned nanoparticles is found to prefer a noncollinear multisublattice ordering due to the dominance of the dipole interactions over the magnetocrystalline anisotropy, (Fig. 1(b)). We call the latter ordering the SSG state as described in the Introduction. The distinction is made here between the SSG and SPM phases in terms of ordering in the static magnetization configuration. Note that some features, a maximum in the temperature dependence of the magnetization (spin-glass freezing vs. paramagnetic blocking) and the divergence of the susceptibility at zero temperature can be seen for zero-field-cooled states of both SPM and SSG, therefore, the experimental distinction between the two phases is subtle [32,37].

We have verified that the ordering is independent of the size of the system by simulating arrays of up to 8^3 nanoparticles. Further, for $x = 0.3$, reducing the grid-discretization size to 0.25 nm, the system relaxed to an almost uniformly-magnetized state which turned out to be unstable to a weak oscillating field. Because of the presence of metastable equilibria, memory effects typical of the spin glasses, in particular, discrepancies between the field-cooled and zero-field-cooled states are expected to exist in the SSG regime.

4. High-frequency dynamics

We next simulate the magnetization dynamics of the SPM and SSG systems of nanoparticles of $\text{Fe}_{65}\text{Co}_{35}$ driven by an alternating linearly-polarized or rotating field as a function of temperature. Our purpose is to verify the applicability of Brown's approach to evaluating the amplitude of the high-frequency magnetic response and to maximize the response with respect to the frequency, amplitude and polarization mode of the driving field. Also, for direct verification of the theory, we simulate the driven dynamics of the SPM system without the demagnetization field, thus, without interparticle interactions.

We consider cubic arrays of $4 \times 4 \times 4$ nanoparticles of 5 nm diameter $\text{Fe}_{65}\text{Co}_{35}$ at a volumetric ratio of $x = 0.13$ (the SPM case) and $x = 0.3$ (the SSG case), applying periodic boundary conditions and including thermal fluctuations. In our temperature-dependent micromagnetic simulations, (utilizing the MuMax³ package, [38]), we apply adaptive time stepping with a lower limit of the time step. The rule for the lower limitation on the time step is the subject of a long-term debate. A condition that the thermal exchange length $l_{ex}^{th} \equiv \sqrt{A_{ex}/\mu_0 M H_{th}}$ should be larger than the grid discretization size has been proposed in Ref. [39] and utilized in the present paper, despite its questioning in Refs. [40,41]. Written according to (3),

$$\Delta t = \frac{2\alpha M(T)k_B T (l_{ex}^{th})^4}{\gamma A_{ex}^2 \Delta V} > \frac{2\alpha M(T)k_B T \Delta V^{1/3}}{\gamma A_{ex}^2} \equiv \Delta t_1,$$

the minimum time step cannot tend to zero without the size of the computational cell tending to zero. Thus, for a given cell size, there is a lower limit on the time step. On the other hand, the time step should be as low as possible and other approaches require the convergence of the numerical solutions to the stochastic LLG equation upon reducing the time step [42]. We attribute the choice of the method to the size of the magnetic system. For relatively large mesoscopic magnets, the ordering energy is large compared to the thermal energy in a wide range of temperature, thus, the condition of high energy barriers is satisfied and thermal fluctuations do not destabilize the ordering (i.e. the dynamics is dominated by non-thermal effects). Then, the thermal exchange length is not expected to play a role unlike the magnetostatic and magnetocrystalline anisotropy exchange lengths. Small MNPs of the nanocomposites under consideration are of low magnetic energy compared to the thermal energy except in a narrow range of very low temperatures. In order to be exchange ordered, the nanoparticle has to be discretized with a cell size below the thermal exchange length.

For a discretization size of 0.5 nm (which is sufficiently small to allow for modeling spherically-shaped MNPs of 5 nm diameter) and a damping constant of $\alpha = 0.1$, we find $\Delta t_1(100 \text{ K}) = 5 \cdot 10^{-15} \text{ s}$ and $\Delta t_1(500 \text{ K}) = 2 \cdot 10^{-14} \text{ s}$. In our simulations, the time step is close to its minimum value Δt_1 for a given temperature. We did not find significant effects of the time-step limitation in the low-temperature range of $T < 100 \text{ K}$.

4.1. Dynamical response of the superparamagnet

The SPM system in the presence of linearly-polarized ac or rotating field is simulated. Additionally, we consider the cases of absence or presence of the demagnetization field. At low temperatures, in the absence of the demagnetization field, the driving field required to excite a magnetic response is considerably reduced. We note the condition of low external field (linear response) reads $\mu_0 H \ll \mu_0 H_a \equiv 2K/M_s = 16 \text{ mT}$.

We study the action of a linearly-polarized field of frequencies of 0.1 GHz and 1.0 GHz on SPM. In this range, the response function amplitude rapidly decreases with frequency becoming low compared to thermal fluctuations. The field amplitude is $\mu_0 H = 10 \text{ mT}$ in majority

of simulations when the demagnetization field is present. In that case, a high value of the driving field (close to the anisotropy field $\mu_0 H_a$) is necessary in order to excite magnetization oscillations in the SPM which are visible over the thermal-fluctuation background. Simulations were also performed in the absence of the demagnetization for field amplitude of $\mu_0 H = 2 \text{ mT}$.

In order to demonstrate the methodology, in Figs. 2(a) and 2(b), we have plotted time dependence of the response function (magnetization component parallel to the driving field) at the driving frequency of 0.1 GHz for different temperatures, comparing the response curve in the presence of temperature fluctuations to dynamically averaged curve (smoothed using the Bezier scheme). Curve smoothing is necessary in order to provide numerical data and all the magnetization curves from the temperature simulations below Fig. 2(b) are smoothed in this way.

In Fig. 2(c), we see the smoothed time dependent response for a series of temperatures between zero and 500 K, which show a weak influence of temperature on the response amplitude. This result is in contrast to the case of noninteracting particles, for which a regular (time-periodic) dynamical response is absent in the temperature regime corresponding to a low energy barrier $KV \ll k_B T$ from Figs. 3(a) and 3(b), however, we notice some weakly-nonlinear behavior of the response function at $T = 2 \text{ K}$ in Figs. 3(b), 3(c). For MNPs under consideration, the temperature of the threshold between the high- and low-energy-barrier regimes is $KV/k_B = 71 \text{ K}$, which is lower than the operating temperature of any high-frequency devices. Thus, magnetostatic interactions play an important stabilizing role in the dynamical response, at the expense of lowered sensitivity to the driving field (i.e. excitation requires a driving field of increased amplitude).

In the high energy barrier regime $KV \gg k_B T$, one can expect to find a stochastic resonance, which manifests with a maximum of the temperature dependence of the response amplitude and with vanishing response at $T = 0$, according to the general theory of thermal excitations in classical two-state systems and in single-domain magnetic particles in particular [43–48]. Theoretical curves of the temperature dependence of the response amplitude of noninteracting (Brown's) particle systems are plotted in Fig. 3(d). Particle interactions are believed to shift the temperature of the relevant maximum (the blocking temperature). It should be stressed that the effect of blocking is not seen from our simulations. Seen from Figs. 2(c), 3(a)–(c), an unexpected feature of the response of both the magnetostatically-interacting and noninteracting systems is the nonvanishing amplitude at $T = 0$, which is in contrast to Brown's theory (Fig. 3(d)). Also, simulations of the noninteracting systems do not confirm the analytical prediction of the (time-periodic) magnetic response in the low-energy-barrier (high-temperature) regime.

We have plotted dynamical field-magnetization (H-M) curves for the SPM of $x = 0.13$ in the presence of the magnetostatic interactions at $T = 0$ and $T = 300 \text{ K}$, applying Bezier smoothing. These curves are shown in Fig. 2(d) and they do not form well defined (dynamical) hysteresis loops even for $T = 0$. On average, they are non-hysteretic, though widened by thermal fluctuations. Thus, hysteresis loss is negligible, though temperature dependent residual loss should be taken into account with regard to power-conversion applications of the magnetic nanocomposite. In contrast, an earlier prediction from the macrospin approach (using rate-equation in the high-energy-barrier regime, kinetic Monte-Carlo simulations, or Landau-Lifshitz equation) is the appearance of dynamical hysteresis loop due to the dipole interactions [49–53].

4.2. Dynamical response at bias perpendicular field

Within the macrospin approach, the effect on a single-domain particle of the application of a constant field additional to the rotating field and normal to the rotation plane has been previously studied analytically [54]. By analogy, we have examined the influence of an additional perpendicular field on the amplitude of the dynamical in-plane

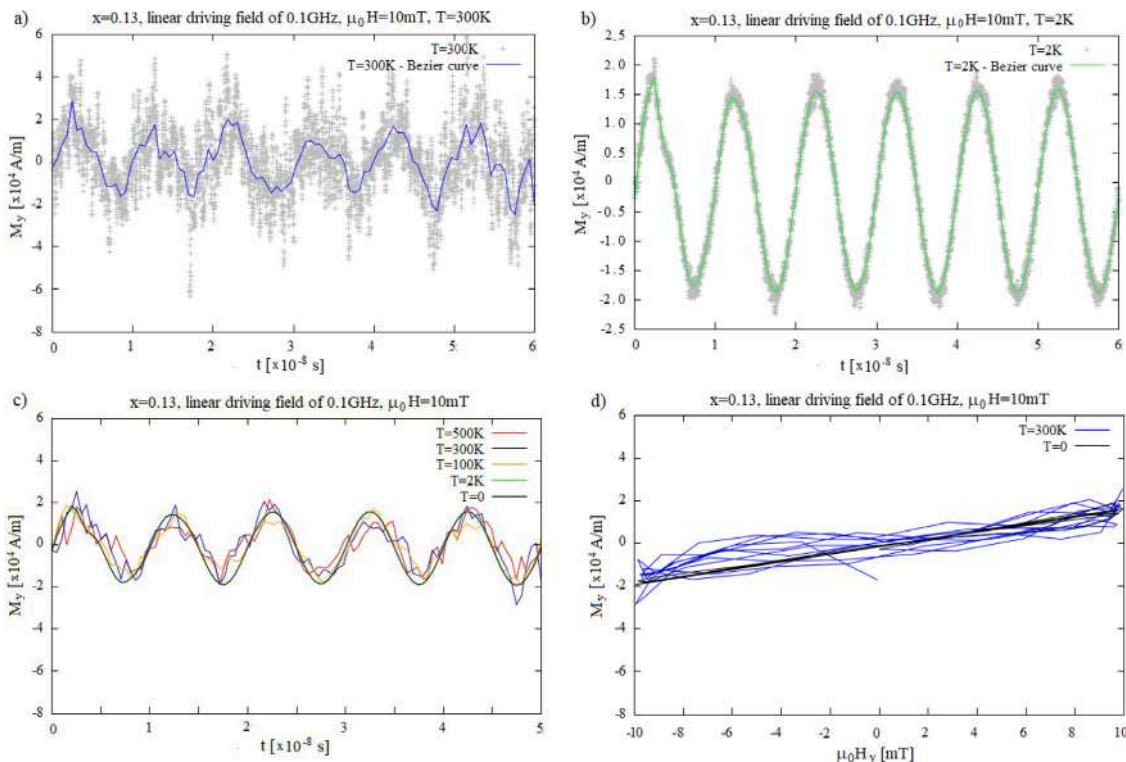


Fig. 2. (a), (b) Comparison of numerical data and Bezier-scheme smoothed curves of the time dependence of the magnetization component parallel to the linearly-polarized driving field of frequency 0.1 GHz for SPM ($x = 0.13$), at (a) temperature $T = 300\text{ K}$, (b) $T = 2\text{ K}$. In (c), Bezier smoothed curves of the time dependence of magnetization for a series of temperatures, and (d) the corresponding (Bezier smoothed) dynamical H-M curves for $T = 0$ and $T = 300\text{ K}$ showing absence of a dynamical hysteresis loop.

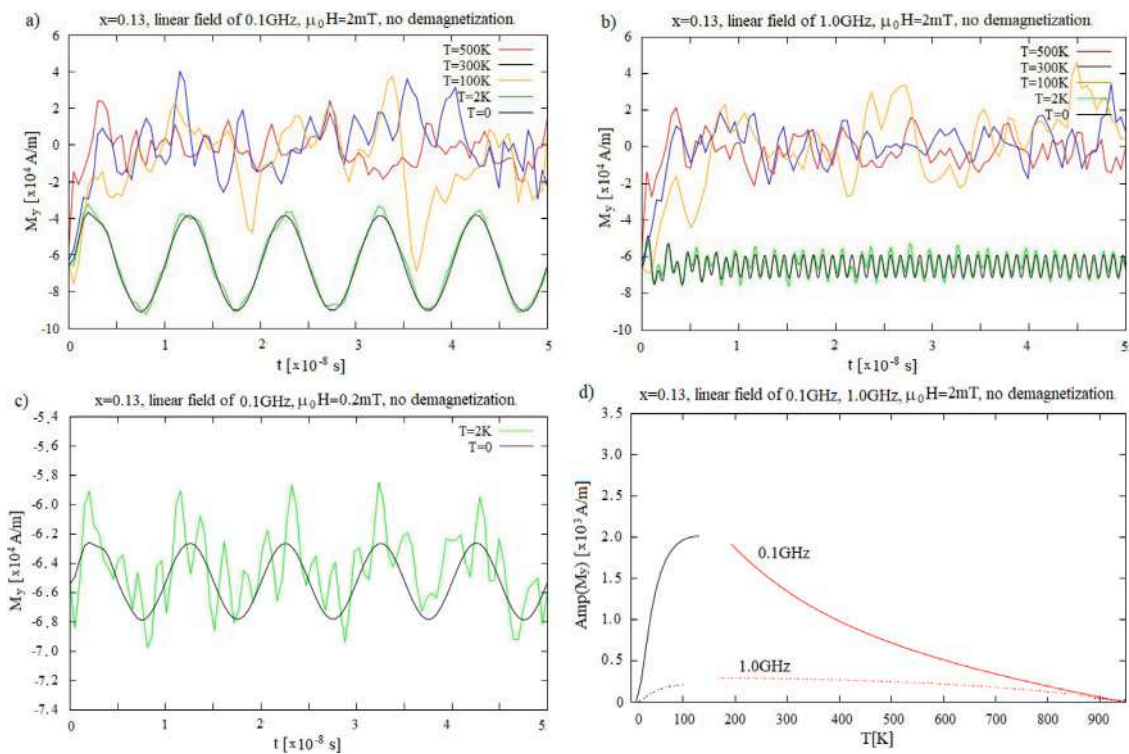


Fig. 3. (a)–(c) Time dependence of the magnetization component parallel to the linearly-polarized driving field for the SPM nanocomposite ($x = 0.13$) in the absence of the demagnetization field at (a) a driving frequency of 0.1 GHz and amplitude of 2 mT , (b) 1.0 GHz and 2 mT , (c) 0.1 GHz and 0.2 mT . (d) Theoretical value of magnetic response amplitude of a single nanoparticle obtained within Brown's macrospin approach; in the high-energy-barrier regime of temperatures — black curves, the low-energy-barrier regime of temperatures — red curves. All curves in (a)–(c) are smoothed with a Bezier scheme.

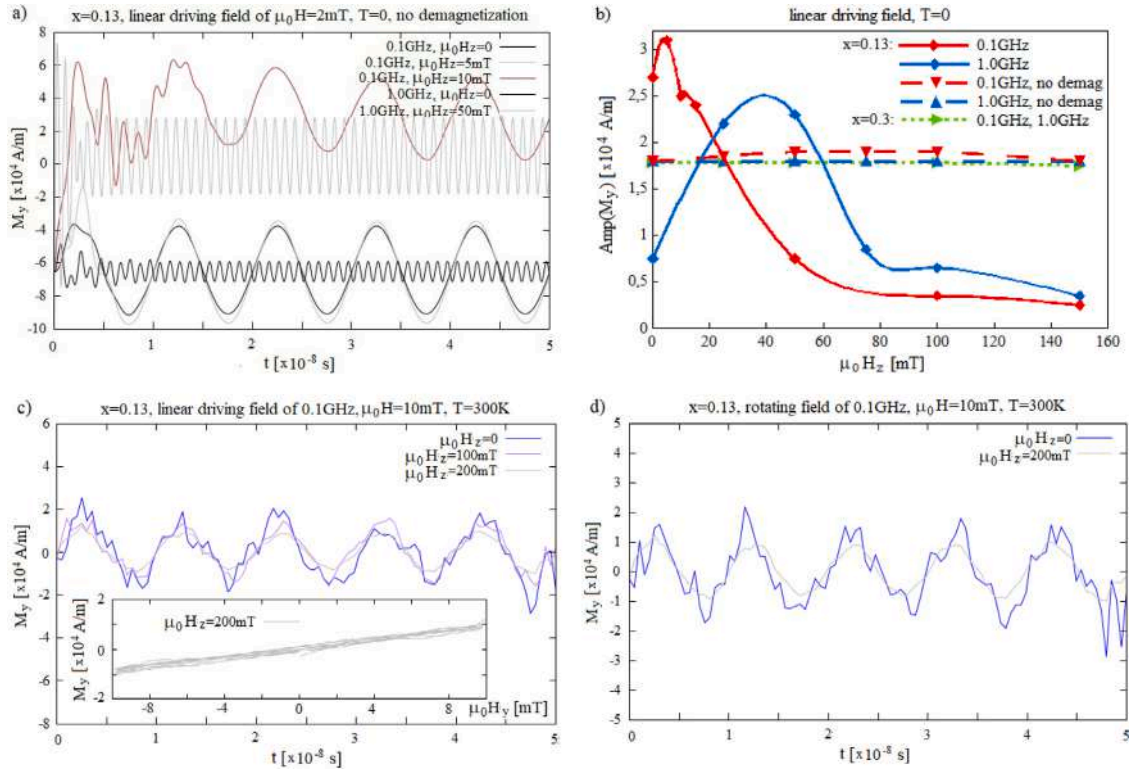


Fig. 4. (a) Time dependence of the magnetization component parallel to the linearly-polarized driving field for the SPM nanocomposite ($x = 0.13$) in the absence of the demagnetization field and in the presence of a constant transverse field $\mu_0 H_z$, for $T = 0$. (b) Dependence of amplitude of the magnetization oscillations on a constant transverse field for the SPM nanocomposite ($x = 0.13$) in the absence or presence of the demagnetization field as well as for the SSG nanocomposite ($x = 0.3$) in the presence of the demagnetization field, for $T = 0$. (c)–(d) Time dependence of the magnetization component parallel to the (c) linear driving or (d) rotating field in the XY plane for the SPM nanocomposite ($x = 0.13$) in the presence of the demagnetization field and in the absence or presence of a strong transverse field at $T = 300$ K. Inset of (c): the dynamical H-M curve for a transverse field $\mu_0 H_z = 200$ mT showing the absence of a dynamical hysteresis loop. All curves in (a), (c) and (d) are smoothed using a Bezier scheme.

magnetic response. Our simplified model of the dynamical magnetic response of a single-domain particle in the presence of a constant transverse field is developed assuming the y -axis to be magnetically easy. We express the total applied field in the form $\mathbf{H}(t) = [0, H \sin(\omega t), H_z]$ and in the high energy barrier, low temperature regime, the dynamics of the average magnetization are governed by equations of combined precession and relaxation

$$\frac{d\langle m_x \rangle}{dt} = \gamma_0 H_z \langle m_y \rangle.$$

$$\frac{d\langle m_y \rangle}{dt} = -\gamma_0 H_z \langle m_x \rangle - \tau^{-1} \langle m_y \rangle + \Theta H_y(t), \quad (11)$$

Combining the first-order differential equations into the second-order equation

$$\frac{d^2 \langle m_y \rangle}{dt^2} = -\gamma_0^2 H_z^2 \langle m_y \rangle - \tau^{-1} \frac{d\langle m_y \rangle}{dt} + \Theta \frac{dH_y}{dt}, \quad (12)$$

we find the amplitude of normalized magnetization

$$\langle m_y \rangle_\omega = \frac{\Theta H}{3\sqrt{\omega^2 (1 - \gamma_0^2 H_z^2 / \omega^2)^2 + \tau^{-2}}} \quad (13)$$

Therefore, our toy model predicts resonance at a driving frequency close to $\gamma_0 H_z$.

In Fig. 4, results of the simulations of magnetic response in the presence of the bias transverse field are presented. For zero temperature, the amplitude of the magnetic response of the noninteracting system (without demagnetization field) is seen from Fig. 4(a) to be influenced by the transverse field, while, it is also dependent on the driving frequency. For 0.1 GHz, from Fig. 4(b), we find a small increase of the response amplitude with the bias field up to the resonant value $\mu_0 H_z \approx 4$ mT which corresponds to $2\pi \cdot 0.1 \text{ GHz} = \gamma_0 H_z$. For 1.0 GHz, the response amplitude significantly increases at the resonance field of

$\mu_0 H_z \approx 40$ mT relative to the case of zero bias field. Hence, our simple model is capable of correctly predicting the resonance frequency due to the bias field, however, similar to the analytical model of Section 2, it does not correctly predict the temperature dependence of the response amplitude.

On the other hand, applied to the systems of magnetostatically coupled nanoparticles at high (room) temperature, a strong transverse field plays a “rectifying” role. It is shown in Fig. 4(c), Fig. 4(d) that, due to such bias field of the order of 100 mT, the time dependence of magnetization is smoothed compared to the unbiased case and becomes sinusoidal. The effect is similar in the cases of driving with linear-ac and rotating fields (Figs. 4(c) and 4(d), respectively), and we do not observe the previously reported enhancement of the magnetic response due to applying the rotating field to MNP system instead of linear one [55,56].

The bias field application is related to narrowing the area of the H-M curve of inset of Fig. 4(c), thus, to reducing the previously discussed (thermally-induced) residual loss.

4.3. Dynamical response of the super spin glass

We simulate the response of a system of densely packed MNPs (the SSG phase) of the volumetric composition ratio $x = 0.3$. From Fig. 5(a), one sees the possibility of stabilizing the response course via applying a strong bias field perpendicular to the driving ac field. Because of strong magnetostatic coupling between MNPs, efficient bias field is stronger than in the SPM state (Figs. 4(c) and 4(d)). In spite of the strong MNP coupling, we do not find any clear hysteresis loop in the H-M curves, even for zero temperature (unplotted), in contrast to the macrospin-based approaches of Refs. [49–53]. However, according to Figs. 5(b) and 5(c), thermal fluctuations influence the H-M area covered by the plot influencing the residual loss and, similar to the case of SPM, application of the bias field reduces the hysteresis-like area.

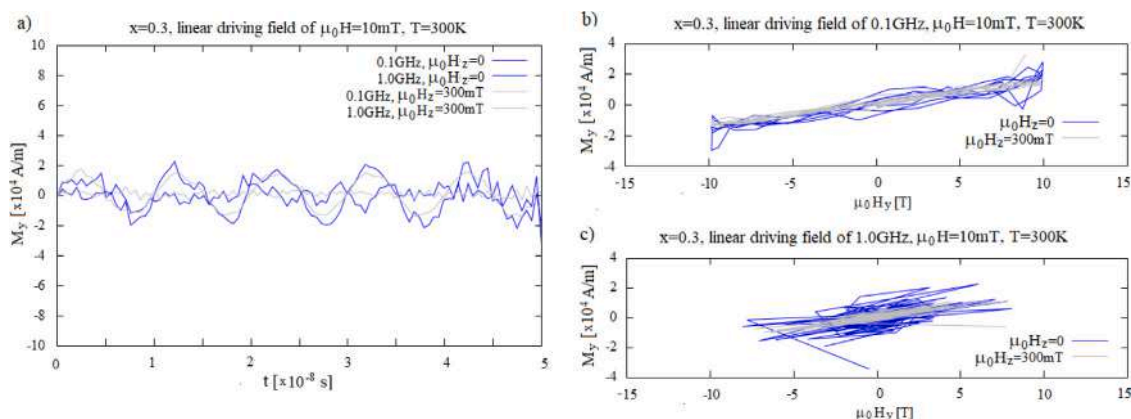


Fig. 5. (a) Time dependence of the magnetization component parallel to the linearly-polarized driving field for the SSG nanocomposite ($x = 0.3$) in the absence and presence of constant transverse field $\mu_0 H_z = 300$ mT, for $T = 300$ K. (b)–(c) The corresponding dynamical H-M curve for the driving frequency of 0.1 GHz (b) and 1.0 GHz (c). All curves are smoothed using a Bezier scheme.

5. Conclusions

For SPM and SSG nanoparticle arrays consisting of $\text{Fe}_{65}\text{Co}_{35}$ MNPs of 5 nm diameter, we have found the dynamical magnetic response to a linearly-polarized ac field to be weakly dependent on temperature. However, in the presence of dipole interactions, the driving field has to be relatively high (quite close to the anisotropy field of 16 mT) in order to excite magnetization oscillations which are visible on the thermal-fluctuation background. In contrast, the magnetization of a model system of noninteracting particles oscillates regularly when driven in the low temperature (high-energy-barrier, $T \ll 71\text{K}$) range, at a relatively low driving amplitude of 2 mT, whereas, in the low-energy-barrier range, the magnetization oscillations are completely dominated by thermal fluctuations of random amplitude. Such a high temperature behavior is not predicted by Brown's theory of thermal fluctuations in single-domain particles. Moreover, the two-state approximation of a monodomain particle in the low temperature regime is not supported by finite-difference simulations in the absence of the magnetostatic field, and in particular, the magnetic response does not vanish in the limit of $T \rightarrow 0$. In the high-energy-barrier range of temperatures, the theoretically predicted values of amplitude of the response function are at least one order of magnitude lower than obtained from low- and zero-temperature simulations of noninteracting MNPs at the same driving field. Hence, the internal structure of the particle magnetization plays a crucial role in the driven dynamics for a given magnetic material and structure parameters of the nanocomposite.

The dynamical susceptibility of all the MNP systems under study is a real value since we do not see any stable phase shifts in the time dependent magnetization relative to the driving field nor do we find dynamical hysteresis loops. The susceptibility can be evaluated using simulation data for the systems driven with linearly-polarized field as

$$\chi = \frac{\text{Amp}(M_y)}{H}. \quad (14)$$

For the SPM system of interacting particles ($x = 0.13$), with the data of Fig. 2(a), we obtain $\chi \approx 2.3$ for the frequency of 0.1 GHz and zero temperature. Correspondingly, for the SSG ($x = 0.3$), at 0.1 GHz and $T = 0$, we estimate the susceptibility to take a similar value ($\chi \approx 2.3$) as that of the SPM (unplotted data). At room temperature, the susceptibilities of SPM and SSG are comparable as well ($\chi \approx 2$), while the regularity (i.e. a sinusoidal time dependence) of the response curves can be improved via the application of a bias transverse field. The bias field required is lower for SPM than for SSG. Hence, decreasing the density of particles (decreasing x down to 0.13) does not lead to any considerable weakening of the dynamical magnetic response, whereas, a low density of MNPs is advantageous in terms of reducing the electric conductivity via interparticle tunneling. Obtained values of

the high-frequency susceptibility are of the same order of magnitude as those reported for SPM systems of Fe nanoparticles and Fe_3O_4 nanoparticles [57,58]. For an assembly of comparable size Fe MNPs, an experimental value of $\chi = 7.7$ has been reported at a composition ratio $x \approx 0.4$, [59], though corresponding to a much lower driving frequency (in the kHz range).

The sub-GHz susceptibility is two orders of magnitude lower than what is achievable for SFM nanocomposites [28]. However, besides the expected low or zero electrical conductivity and the reduced or eliminated eddy-current loss, we do not observe dynamical hysteresis in the simulations of SPM nor SSG systems, in contrast to the significant hysteretic loss predicted for SFMs. Finally, application of a bias field transverse to the driving field is an efficient method of reducing temperature-dependent residual loss.

Declaration of competing interest

The authors declare that they have no known competing financial interests or personal relationships that could have appeared to influence the work reported in this paper.

Data availability

No data was used for the research described in the article.

Acknowledgments

Calculations have been carried out using resources provided by Wrocław Centre for Networking and Supercomputing, Poland (<http://wcss.pl>), grant No. 450. The authors acknowledge support of a MISTI-Poland award from MIT.

Appendix. Thermal fluctuations in single-domain particle

Let $\mathbf{M}/M \equiv \mathbf{m} = [\sin(\theta) \cos(\varphi), \sin(\theta) \sin(\varphi), \cos(\theta)]$. Brown's theory of thermal fluctuations of the macrospin of a particle is based on evaluating the distribution function $w(\mathbf{m}, t, T)$. Transforming it to spherical variables and considering the case $w(\theta, \varphi, t, T) = w(\theta, t, T)$, one arrives at the evolution equation of the Smoluchowski type

$$\frac{\partial w}{\partial t} = \frac{\partial}{\partial y} \left[(1 - y^2) \left(h' \frac{\partial \mathcal{H}}{\partial y} w + D \frac{\partial w}{\partial y} \right) \right], \quad (15)$$

where $y \equiv \cos(\theta)$, \mathcal{H} denotes the macrospin Hamiltonian, and the dissipation and diffusion coefficients read $h' \equiv \frac{\gamma \alpha}{M(1 + \alpha^2)}$ and $D \equiv \frac{h' k_B T}{V}$, respectively. Applying the method of separation of variables and

expanding the angular part of the distribution function with respect to the Legendre polynomials $P_l(y)$, from (15), one obtains

$$\begin{aligned} w(\theta, t, T) &= w_0(\theta) + e^{-V\mathcal{H}(\theta)/k_B T} \\ &\times \sum_{l=1}^{\infty} A_l P_l[\cos(\theta)] e^{-P_l}, p_l = \frac{h' k_B T}{V} l(l+1) \\ w_0(\theta, T) &= Z^{-1} e^{-V\mathcal{H}(\theta)/k_B T}, Z = 2e^{-V\mathcal{H}(0)/k_B T}. \end{aligned} \quad (16)$$

The coefficients of the expansion A_l are found, for the initial condition $\lim_{t \rightarrow 0} w(\theta, t, T) = \delta[\cos(\theta) - \cos(\theta')] \equiv \delta(y - y')$, to take the form

$$A_l(y') = \frac{2l+1}{2} e^{V\mathcal{H}(y')/k_B T} P_l(y'). \quad (17)$$

The initial condition will be denoted with $w(\theta, t, T) \equiv w(\theta, \theta', t, T)$.

In the high-temperature (low-energy-barrier) regime, the amplitude of the dynamical magnetic response is evaluated via determining the autocorrelation function of the magnetization

$$\begin{aligned} &\langle \delta M_z(t) \delta M_z(0) \rangle / M^2 \\ &= \int_{-1}^1 \int_{-1}^1 y y' w(y, y', t) w_0(y') dy' dy = \frac{1}{3} e^{-P_1 t}. \end{aligned} \quad (18)$$

The formula (9) is obtainable from (18) via the fluctuation-dissipation theorem.

In the high-energy-barrier regime, writing (15) in the form

$$\frac{\partial w}{\partial t} = \frac{1}{2\pi} \frac{\partial I}{\partial y}, \quad (19)$$

one considers a stationary solution ($I = \text{const}$), which is related to the linear equation

$$\sin \theta \left(h' \frac{\partial \mathcal{H}}{\partial \theta} w + D \frac{\partial w}{\partial \theta} \right) = \frac{I}{2\pi}, \quad (20)$$

Here, I represents the intensity of the probability current flowing between discrete macrospin states $\theta \approx 0$ and $\theta \approx \pi$ of the occupation probabilities

$$\begin{aligned} W_1(t) &\approx \frac{w(0, t, T) \cdot 2\pi}{e^{-V\mathcal{H}(0)/k_B T}} \int_0^{\theta_1} e^{-V\mathcal{H}(\theta)/k_B T} \sin \theta d\theta \\ W_2(t) &\approx \frac{w(\pi, t, T) \cdot 2\pi}{e^{-V\mathcal{H}(\pi)/k_B T}} \int_{\theta_2}^{\pi} e^{-V\mathcal{H}(\theta)/k_B T} \sin \theta d\theta, \end{aligned} \quad (21)$$

thus, $I = -\dot{W}_1 = \dot{W}_2$. The integration of (20) leads to

$$\begin{aligned} w(\theta_2, t, T) e^{V\mathcal{H}(\theta_2)/k_B T} - w(\theta_1, t, T) e^{V\mathcal{H}(\theta_1)/k_B T} \\ = -\frac{VI}{2\pi k_B T h'} \int_{\theta_1}^{\theta_2} e^{V\mathcal{H}(\theta)/k_B T} \frac{d\theta}{\sin \theta}. \end{aligned} \quad (22)$$

One arrives at the dynamical equation of the (normalized) magnetic moment

$$\begin{aligned} \dot{W}_1 - \dot{W}_2 &= -\frac{2h' e^{-V\mathcal{K}/k_B T}}{I_m} [W_2 (2K + \mu_0 H_z M) \\ &\quad - W_1 (2K - \mu_0 H_z M)], \end{aligned} \quad (23)$$

where $I_m = \sqrt{\frac{2\pi k_B T}{-V\mathcal{H}''(\theta_m)}} \approx \sqrt{\frac{\pi k_B T}{VK}}$ and $\mathcal{H}(\theta_m) \equiv \max \mathcal{H}(\theta)$, to be solved with the constraint $W_1 + W_2 = 1$.

References

[1] D. Polder, J. Smit, Resonance phenomena in ferrites, *Rev. Modern Phys.* 25 (1953) 89–90, <http://dx.doi.org/10.1103/RevModPhys.25.89>.
[2] E.A. Perigo, B. Weidenfeller, P. Kollar, J. Fuzer, Past, present, and future of soft magnetic composites, *Appl. Phys. Rev.* 5 (2018) 031301, <http://dx.doi.org/10.1063/1.5027045>.
[3] C.R. Sullivan, D.V. Harburg, J. Qiu, C.G. Levey, D. Yao, Integrating magnetics for on-chip power: a perspective, *IEEE Trans. Power Electron.* 28 (2013) 4342–4353, <http://dx.doi.org/10.1109/TPEL.2013.2240465>.
[4] M. Araghchini, et al., A technology overview of the PowerChip development program, *IEEE Trans. Power Electron.* 28 (2013) 4182–4201, <http://dx.doi.org/10.1109/TPEL.2013.2237791>.

[5] R.J. Kaplar, J.C. Neely, D.L. Huber, L.J. Rashkin, Generation-after-next power electronics: ultrawide-bandgap devices, high-temperature packaging, and magnetic nanocomposite materials, *IEEE Power Electron. Mag.* 4 (2017) 36–42, <http://dx.doi.org/10.1109/MPEL.2016.2643098>.
[6] V. Korenivski, GHz magnetic film inductors, *J. Magn. Magn. Mater.* 215–216 (2000) 800–806, [http://dx.doi.org/10.1016/S0304-8853\(00\)00292-4](http://dx.doi.org/10.1016/S0304-8853(00)00292-4).
[7] S. Bedanta, W. Kleemann, Supermagnetism, *J. Phys. D: Appl. Phys.* 42 (2009) 013001, <http://dx.doi.org/10.1088/0022-3727/42/1/013001>.
[8] D. Peddis, P.E. Jonsson, S. Laureti, G. Varvaro, Magnetic interactions: a tool to modify the magnetic properties of materials based on nanoparticles, in: C. Binns (Ed.), *Frontiers of Nanoscience*, vol. 6, Elsevier, 2014, pp. 129–188, <http://dx.doi.org/10.1016/B978-0-08-098353-0.00004-X>.
[9] S. Bedanta, A. Barman, W. Kleemann, O. Petravic, T. Seki, Magnetic nanoparticles: a subject for both fundamental research and applications, *J. Nanomater.* 2013 (2013) 952540, <http://dx.doi.org/10.1155/2013/952540>.
[10] V. Rylkov, A. Sitnikov, S. Nikolaev, A. Emelyanov, K. Chernohlazov, K. Nikiruy, A. Drovosekov, M. Blinov, E. Fadeev, A. Taldenkov, V. Demin, A. Vedeneev, A. Bugaev, A. Granovsky, Properties of nanocomposites with different concentrations of magnetic ions in an insulating matrix, *IEEE Magn. Lett.* 10 (2019) 2509504, <http://dx.doi.org/10.1109/LMAG.2019.2955060>.
[11] D. Hasegawa, H. Yang, T. Ogawa, M. Takahashi, Challenge of ultra high frequency limit of permeability for magnetic nanoparticle assembly with organic polymer—Application of superparamagnetism, *J. Magn. Magn. Mater.* 321 (2009) 746–749, <http://dx.doi.org/10.1016/j.jmmm.2008.11.041>.
[12] J.M. Silveyra, E. Ferrara, D.L. Huber, T.C. Monson, Soft magnetic materials for a sustainable and electrified world, *Science* 362 (2018) <http://dx.doi.org/10.1126/science.aao0195>, eao0195.
[13] F. Bodker, S. Morup, S. Linderoth, Surface effects in metallic iron nanoparticles, *Phys. Rev. Lett.* 72 (1994) 282–285, <http://dx.doi.org/10.1103/PhysRevLett.72.282>.
[14] V. Singh, M.S. Seehra, J. Bonevich, Ac susceptibility studies of magnetic relaxation in nanoparticles of Ni dispersed in silica, *J. Appl. Phys.* 105 (2009) 07B518, <http://dx.doi.org/10.1063/1.3073949>.
[15] F. Fabris, Y.T. Xing, D.F. Franceschini, D.R. Sanchez, M. Alzamora, W.C. Nunes, Effects of postdeposition heat treatment on the structural and magnetic properties of CoFe₂O₄ nanoparticles produced by pulsed laser deposition, *J. Appl. Phys.* 122 (2017) 063901, <http://dx.doi.org/10.1063/1.4985789>.
[16] Y. Slimani, A. Baykal, A. Manikandan, Effect of Cr³⁺ substitution on AC susceptibility of Ba hexaferrite nanoparticles, *J. Magn. Magn. Mater.* 458 (2018) 204–212, <http://dx.doi.org/10.1016/j.jmmm.2018.03.025>.
[17] M.A. Almessiere, Y. Slimani, H. Gungunes, A. Demir Korkmaz, A. Baykal, A.V. Trukhanov, G. Yasin, SrCo_xZr_{1-x}Fe_{12-2x}O₁₉ and SrNi_xZr_{1-x}Fe_{12-2x}O₁₉ hexaferrites: a comparison study of AC susceptibility, FC-ZFC and hyperfine interactions, *Chin. J. Phys.* 66 (2020) 596–605, <http://dx.doi.org/10.1016/j.cjph.2020.05.012>.
[18] R.H. Kodama, A.E. Berkowitz, E.J. McNiff Jr., S. Foner, Surface spin disorder in NiFe₂O₄ nanoparticles, *Phys. Rev. Lett.* 77 (1996) 394–397, <http://dx.doi.org/10.1103/PhysRevLett.77.394>.
[19] B. Martinez, X. Obradors, Ll. Balcells, A. Rouanet, C. Monty, Low temperature surface spin-Glass transition in g-Fe₂O₃ nanoparticles, *Phys. Rev. Lett.* 80 (1998) 181–184, <http://dx.doi.org/10.1103/PhysRevLett.80.181>.
[20] F. Fabris, E. Lima Jr., E. De Biasi, H.E. Troiani, M. Vasquez Mansilla, T.E. Torres, R. Fernandez Pacheco, M.R. Ibarra, F. Goya, R.D. Zysler, E.L. Winkler, Controlling the dominant magnetic relaxation mechanisms for magnetic hyperthermia in bimagnetic core-shell nanoparticles, *Nanoscale* 11 (2019) 3164–3172, <http://dx.doi.org/10.1039/C8NR07834C>.
[21] D. Peddis, F. Orru, A. Ardu, C. Cannas, A. Musinu, G. Piccaluga, Interparticle interactions and magnetic anisotropy in cobalt ferrite nanoparticles: influence of molecular coating, *Chem. Mater.* 24 (2012) 1062–1071, <http://dx.doi.org/10.1021/cm203280y>.
[22] C. Cannas, A. Musinu, A. Ardu, F. Orru, D. Peddis, M. Casu, R. Sanna, F. Angius, G. Diaz, G. Piccaluga, CoFe₂O₄ and CoFe₂O₄/SiO₂ core/shell nanoparticles: magnetic and spectroscopic study, *Chem. Mater.* 22 (2013) 3353–3361, <http://dx.doi.org/10.1021/cm903837g>.
[23] F. Zeb, M. Ishaque, K. Nadeem, M. Kamran, H. Krenn, D.V. Szabo, U. Brossmann, I. Letofsky-Papst, Reduced surface effects in weakly interacting ZrO₂ coated MnFe₂O₄ nanoparticles, *J. Magn. Magn. Mater.* 469 (2019) 580–586, <http://dx.doi.org/10.1021/cm903837g>.
[24] H. Kura, M. Takahashi, T. Ogawa, Extreme enhancement of blocking temperature by strong magnetic dipoles interaction of α-Fe nanoparticle-based high-density agglomerate, *J. Phys. D: Appl. Phys.* 44 (2011) 022002, <http://dx.doi.org/10.1088/0022-3727/44/2/022002>.
[25] W.F. Brown, Thermal fluctuations of a single-domain particle, *Phys. Rev.* 130 (1963) 1677–1686, <http://dx.doi.org/10.1103/PhysRev.130.1677>.
[26] M. Anand, Thermal and dipolar interaction effect on the relaxation in a linear chain of magnetic nanoparticles, *J. Magn. Magn. Mater.* 522 (2021) 167538, <http://dx.doi.org/10.1016/j.jmmm.2020.167538>.
[27] S. Ota, Y. Tanemura, Dynamics of magnetization and easy axis of individual ferromagnetic nanoparticle subject to anisotropy and thermal fluctuations, *J. Magn. Soc. Jpn.* 43 (2019) 34–41, <http://dx.doi.org/10.3379/msjmag.1903R005>.

- [28] K. Brzuszek, A. Janutka, High-frequency magnetic response of superferromagnetic nanocomposites, *J. Magn. Magn. Mater.* 543 (2022) 168608, <http://dx.doi.org/10.1016/j.jmmm.2021.168608>.
- [29] S. S. Wang, J. Ma, X. Zhang, J. Li, Magnetic softness and interparticle exchange interactions of $(\text{Fe}_{65}\text{Co}_{35})_{1-x}(\text{Al}_2\text{O}_3)_x$ ($x = 0-0.50$) nanogranular films, *Thin Solid Films* 520 (2012) 5046-5052, <http://dx.doi.org/10.1016/j.tsf.2012.03.025>.
- [30] D. Peddis, C. Cannas, A. Musinu, G. Piccaluga, Magnetism in nanoparticles: beyond the effect of particle size, *Chem. Europe* 15 (2009) 7822-7829, <http://dx.doi.org/10.1002/chem.200802513>.
- [31] H. Mamiya, I. Nakatani, T. Furubayashi, Blocking and freezing of magnetic moments for iron nitride fine particle system, *Phys. Rev. Lett.* 80 (1998) 177-180, <http://dx.doi.org/10.1103/PhysRevLett.80.177>.
- [32] X. Chen, S. Bedanta, O. Petracic, W. Kleemann, S. Sahoo, S. Cardoso, P.P. Freitas, Superparamagnetism versus superspin glass behavior in dilute magnetic nanoparticle systems, *Phys. Rev. B* 72 (2005) 214436, <http://dx.doi.org/10.1103/PhysRevB.72.214436>.
- [33] K. Hiroi, H. Kura, T. Ogawa, M. Takahashi, T. Sato, Spin-glass like behavior of magnetic ordered state originating from strong interparticle magnetostatic interaction in α -Fe nanoparticle agglomerate, *Appl. Phys. Lett.* 98 (2011) 252505, <http://dx.doi.org/10.1063/1.3602313>.
- [34] K. Hiroi, H. Kura, T. Ogawa, M. Takahashi, T. Sato, Magnetic ordered states induced by interparticle magnetostatic interaction in α -Fe/Au mixed nanoparticle assembly, *J. Phys.: Condens. Matter* 26 (2014) 176001, <http://dx.doi.org/10.1088/0953-8984/26/17/176001>.
- [35] A. Lyberatos, R.W. Chantrell, Thermal fluctuations in a pair of magnetostatically coupled particles, *J. Appl. Phys.* 73 (1993) 6501-6503, <http://dx.doi.org/10.1063/1.352594>.
- [36] A. Vansteenkiste, J. Leliaert, M. Dvornik, M. Helsen, F. Garcia-Sanchez, B. Van Waeyenberge, The design and verification of MuMax3, *AIP Adv.* 4 (2014) 107133, <http://dx.doi.org/10.1063/1.4899186>.
- [37] O. Petracic, X. Chen, S. Bedanta, W. Kleemann, S. Sahoo, S. Cardoso, P.P. Freitas, Collective states of interacting ferromagnetic nanoparticles, *J. Magn. Magn. Mater.* 300 (2006) 192-197, <http://dx.doi.org/10.1016/j.jmmm.2005.10.061>.
- [38] <https://mumax.github.io/>.
- [39] V. Tsiantos, W. Scholz, D. Suess, T. Schrefl, J. Fidler, The effect of the cell size in langevin micromagnetic simulations, *J. Magn. Magn. Mater.* 242-245 (2002) 999-1001, [http://dx.doi.org/10.1016/S0304-8853\(01\)01365-8](http://dx.doi.org/10.1016/S0304-8853(01)01365-8).
- [40] E. Martinez, L. Lopez-Diaz, L. Torres, C.J. Garcia-Cervera, Minimizing cell size dependence in micromagnetics simulations with thermal noise, *J. Phys. D: Appl. Phys.* 40 (2007) 942-948, <http://dx.doi.org/10.1088/0022-3727/40/4/003>.
- [41] M.B. Hahn, Temperature in micromagnetism: cell size and scaling effects of the stochastic Landau-Lifshitz equation, *J. Phys. Commun.* 3 (2019) 075009, <http://dx.doi.org/10.1088/2399-6528/ab31e6>.
- [42] J. Leliaert, J. Mulkers, J. De Clercq, A. Coene, M. Dvornik, B. Van Waeyenberge, Adaptively time stepping the stochastic Landau-Lifshitz-Gilbert equation at nonzero temperature: Implementation and validation in MuMax³, *AIP Adv.* 7 (2017) 125010, <http://dx.doi.org/10.1063/1.5003957>.
- [43] B. McNamara, K. Wiesenfeld, Theory of stochastic resonance, *Phys. Rev. A* 39 (1989) 4854-4869, <http://dx.doi.org/10.1103/PhysRevA.39.4854>.
- [44] M.I. Dykman, D.G. Luchinsky, R. Mannella, P.V.E. McClintock, N.D. Stein, N.G. Stocks, Stochastic resonance: linear response and giant nonlinearity, *J. Stat. Phys.* 70 (1993) 463-478, <http://dx.doi.org/10.1007/BF01053982>.
- [45] Y.L. Raikher, V.I. Stepanov, Stochastic resonance and phase shifts in superparamagnetic particles, *Phys. Rev. B* 52 (1995) 3493-3498, <http://dx.doi.org/10.1103/PhysRevB.52.3493>.
- [46] J.L. Garcia-Palacios, F.J. Lazaro, Langevin-dynamics study of the dynamical properties of small magnetic particles, *Phys. Rev. B* 58 (1998) 14937-14958, <http://dx.doi.org/10.1103/PhysRevB.58.14937>.
- [47] R.W. Chantrell, N. Walmsley, J. Gore, M. Maylin, Calculations of the susceptibility of interacting superparamagnetic particles, *Phys. Rev. B* 63 (2000) 024410, <http://dx.doi.org/10.1103/PhysRevB.63.024410>.
- [48] F. Bodker, M.F. Hansen, C. Bender Koch, K. Lefmann, S. Morup, Magnetic properties of hematite nanoparticles, *Phys. Rev. B* 61 (2000) 6826-6838, <http://dx.doi.org/10.1103/PhysRevB.61.6826>.
- [49] G. Barrera, P. Allia, P. Tiberto, Hysteresis effects in magnetic nanoparticles: a simplified rate-equation approach, *J. Magn. Magn. Mater.* 496 (2020) 165927, <http://dx.doi.org/10.1016/j.jmmm.2019.165927>.
- [50] G. Barrera, P. Allia, P. Tiberto, Dipolar interactions among magnetite nanoparticles for magnetic hyperthermia: a rate-equation approach, *Nanoscale* 13 (2021) 4103-4121, <http://dx.doi.org/10.1039/D0NR07397K>.
- [51] S. Ruta, R. Chantrell, O. Hovorka, Unified model of hyperthermia via hysteresis heating in systems of interacting magnetic nanoparticles, *Sci. Rep.* 5 (2015) 9090, <http://dx.doi.org/10.1038/srep09090>.
- [52] M. Anand, Hysteresis in two dimensional arrays of magnetic nanoparticles, *J. Magn. Magn. Mater.* 540 (2021) 168461, <http://dx.doi.org/10.1016/j.jmmm.2021.168461>.
- [53] N.A. Usov, O.N. Serebryakova, V.P. Tarasov, Interaction effects in assembly of magnetic nanoparticles, *Nanoscale Res. Lett.* 12 (2017) 489, <http://dx.doi.org/10.1186/s11671-017-2263-x>.
- [54] G. Bertotti, C. Serpico, I.D. Mayergoyz, Nonlinear magnetization dynamics under circularly polarized field, *Phys. Rev. Lett.* 86 (2001) 724-727, <http://dx.doi.org/10.1103/PhysRevLett.86.724>.
- [55] M. Bekovic, M. Trlep, M. Jesenik, A. Hamler, A comparison of the heating effect of magnetic fluid between the alternating and rotating magnetic field, *J. Magn. Magn. Mater.* 355 (2014) 12-17, <http://dx.doi.org/10.1016/j.jmmm.2013.11.045>.
- [56] A. Skumiel, P. Kopcansky, M. Timko, M. Molcan, K. Paulovicova, R. Wojciechowski, The influence of a rotating magnetic field on the thermal effect in magnetic fluid, *Int. J. Thermal Sci.* 171 (2022) 107258, <http://dx.doi.org/10.1016/j.ijthermalsci.2021.107258>.
- [57] H. Kura, T. Ogawa, R. Tate, K. Hata, M. Takahashi, Size effect of Fe nanoparticles on the high-frequency dynamics of highly dense self-organized assemblies, *J. Appl. Phys.* 111 (2012) 07B517, <http://dx.doi.org/10.1063/1.3676224>.
- [58] H. Yun, X. Liu, T. Paik, D. Palanisamy, J. Kim, W.D. Vogel, A.J. Viescas, J. Chen, G.C. Papaefthymiou, J.M. Kikkawa, M.G. Allen, C.B. Murray, Size- and composition-dependent radio frequency magnetic permeability of iron oxide nanocrystals, *ACS Nano* 8 (2014) 12323-12337, <http://dx.doi.org/10.1021/nn504711g>.
- [59] M. Kin, H. Kura, T. Ogawa, Core loss and magnetic susceptibility of superparamagnetic Fe nanoparticle assembly, *AIP Adv.* 6 (2016) 125013, <http://dx.doi.org/10.1063/1.4972059>.

High-frequency magnetic response of superparamagnetic composites of spherical Fe and Fe₃O₄ nanoparticles

Kacper Brzuszek^a, Caroline A. Ross^b, Andrzej Janutka^a

^a*Department of Theoretical Physics, Wrocław University of Science and Technology, 50-370 Wrocław, Poland*

^b*Department of Materials Science and Engineering, Massachusetts Institute of Technology, Cambridge, Massachusetts 02139, USA*

Abstract

The response of arrays of magnetic nanoparticles (MNPs) of cubic anisotropy materials (magnetite or iron) to high-frequency (sub-GHz) field is investigated utilizing micromagnetic simulations. Composites of MNPs embedded in dielectric media are of interest as core materials for high-frequency power microconverters with low eddy-current losses. Going beyond the macrospin approximation for MNPs (including internal spin structure), we simulate the magnetization dynamics of arrays of spherical and periodically arranged MNPs under periodic boundary conditions and in the presence of thermal fluctuations of the magnetization within the stochastic thermal field. Analyzing the dependence of the dynamical response on the size of the MNPs, we find the size to be crucial for exciting regular magnetization oscillations at room temperature and reducing hysteresis loss. The efficiency of the dynamical response of composites of high-magnetization-metal (iron) MNPs is compared to that of magnetite nanocomposites. We find the sub-GHz susceptibility of magnetite-containing nanocomposite to be comparable to that of the iron MNPs despite the lower saturation magnetization of Fe₃O₄, (at the volumetric ratio of the magnetic phase of 0.13, susceptibility is $\chi \approx 1.6$ for 5nm Fe and ≈ 1.4 for 12nm Fe₃O₄ MNPs at $T = 300\text{K}$ and frequency of 0.1GHz).

Keywords: superparamagnetism, power conversion, micromagnetic simulations, microwave frequency

¹E-mail address: Andrzej.Janutka@pwr.edu.pl

1. Introduction

Superparamagnetic composites of magnetic nanoparticles (MNPs) embedded in dielectric matrices are considered to be an alternative to soft ferromagnetic materials for high-frequency applications, and in particular, they could serve as core materials for on-chip power converters [1, 2, 3, 4]. The advantages of such nanocomposites are low electrical conductivity due to large spacing of the metallic MNPs, (thus, low excess loss), and a lack of internal domain structure, yielding low or zero intra-particle eddy-current losses. The latter property of MNPs requires their diameter to be very small, while a large separation between the MNPs requires the volumetric ratio of the magnetic phase to be low. Under these conditions, the magnetic response of the superparamagnetic nanocomposites is critically dependent on the saturation magnetization of the MNP material. Motivated by these considerations, we have previously simulated the response of superparamagnetic composites of spherical nanoparticles made of Fe₆₅Co₃₅, a material of with high saturation magnetization and low magnetic anisotropy [5]. MNPs consisting of magnetic metallic elements or alloys are prone to oxidation. In the present paper, we verify by means of micromagnetic simulations whether MNPs of an oxide, mag-

netite (Fe₃O₄) can serve as an alternative material for high-frequency magnetic nanocomposites.

Temperature fluctuations are key factor in the dynamics of superparamagnetic nanoparticles and they have to be included into studies of high-frequency magnetic response. The classic theory of such fluctuations is capable of predicting the dynamical response in the linear regime within the macrospin approximation for magnetic particles [6]. However, the macrospin approximation can be questionable, especially, for high-frequency dynamics. Also, significant response at high frequency may require use of a strong driving field which leads to nonlinear effects in the evolution of the magnetization. Besides the difficulties of applying an analytical approach to nonlinear theory of thermal fluctuations in a magnetic particle, additional complexity is introduced by the magnetostatic interactions between MNPs. A way to avoid these difficulties is performing micromagnetic simulations which take into account thermal fluctuations and we apply the stochastic-Landau-Lifshitz-Gilbert (sLLG) equation to accomplish this aim. Of special interest in the present paper are the zero temperature and room temperature dynamical responses of systems of cubic-anisotropy MNPs since the former case is especially valid to studying breakdown of the macrospin approximation for MNPs, whereas the room temperature case corresponds to the operating conditions for magnetic-nanocomposite-based devices.

In spite of the relatively low saturation magnetization

of oxides, surface anisotropy, and a significant crystalline anisotropy, we consider systems of idealized uniform MNPs of equal sizes that are periodically arranged in space, with random orientations of their crystalline anisotropy axes, with the purpose of determining physical limitations of the magnetic response. Unlike previously simulated $\text{Fe}_{65}\text{Co}_{35}$, magnetite has cubic magnetic anisotropy, which motivates our comparative study of the magnetic response from a system of MNPs of iron which is another cubic material. Among magnetic nanocomposites, arrays of both Fe_3O_4 and Fe nanoparticles are frequently studied because of their low cost for inductive-core applications and potential applicability to hyperthermia treatment [7, 8, 9, 10, 11]. Real systems are affected by clustering of MNPs and by their shape, structure and dispersion. Controlling all these factors simultaneously is challenging, for example larger nanoparticles offer easier control of their shape but a stronger tendency towards clustering [12]. Simulations allow the effects of these factors on the response characteristics to be identified more easily than in an experiment.

A model of the dynamics of cubic-anisotropy MNPs is formulated in Sec. 2 and applied in Sec. 3 to performing micromagnetic simulations of the response to an oscillating magnetic field. Sec. 5. is devoted to summarizing the results.

2. Model

The time evolution of the magnetization of nanocomposite is governed by the sLLG equation

$$-\frac{\partial \mathbf{m}}{\partial t} = \frac{2\gamma A_{ex}}{M} \mathbf{m} \times \Delta \mathbf{m} + \gamma_0 \mathbf{m} \times (\mathbf{H}_{an} + \mathbf{H}_{ms} + \mathbf{H} + \mathbf{H}_{th}) - \alpha \mathbf{m} \times \frac{\partial \mathbf{m}}{\partial t}. \quad (1)$$

Here, we consider the normalized magnetization $\mathbf{m} = \mathbf{M}/|\mathbf{M}| \equiv \mathbf{M}/M$ which is non-zero in the nanoparticles, while it vanishes in the matrix. The magnetization value satisfies $M \rightarrow_{T \rightarrow 0} M_s$, where M_s denotes the saturation magnetization. The fields \mathbf{H}_{an} and \mathbf{H}_{ms} result from the presence of the magnetocrystalline anisotropy and the demagnetization (the magnetostatic field), whereas \mathbf{H} represents the external magnetic field. The axes of the crystalline anisotropy are assumed to be constant within each MNP, but randomly oriented within the nanocomposite. The anisotropy field is related to constant of the cubic anisotropy of the MNP material K_1 . The parameters of the sLLG equation γ , A_{ex} and α denote the gyromagnetic ratio, the exchange stiffness and the Gilbert damping constant, $\gamma_0 \equiv \gamma\mu_0$, where μ_0 represents the vacuum permeability. The exchange field $2A_{ex}\Delta\mathbf{m}/\mu_0M$ is defined locally, inside MNPs, (similar to the anisotropy \mathbf{H}_{an} and thermal \mathbf{H}_{th} fields), since the Laplacian of magnetization $\Delta\mathbf{m}$ is undefined in the area of nonmagnetic matrix. The magnetostatic field which is defined everywhere in the grid determines the long-distance interactions, thus, it determines the dipole-dipole interactions between MNPs.

We consider periodic array (a cubic lattice) of spherical MNPs of equal diameters, which are represented in our numerical simulations by a cubic box of $4 \times 4 \times 4$ nanoparticles with periodic boundary conditions applied to the box. A thermal field \mathbf{H}_{th} randomly fluctuates in time (its value and direction are drawn in each time step), satisfying the correlation property

$$\langle H_{thi}(t)H_{thj}(t+\tau) \rangle = \frac{2k_B T \alpha}{\gamma \mu_0^2 M} \delta_{ij} \delta(\tau). \quad (2)$$

At a time point $t = N\Delta t$, where Δt denotes the time step, the thermal field is equal to

$$\mu_0 \mathbf{H}_{th}(N\Delta t) = \sqrt{2k_B T \alpha / \gamma M \Delta V \Delta t} \mathbf{s}(N\Delta t), \quad (3)$$

where ΔV denotes the volume of the computational cell, and $\mathbf{s}(t)$ is a vector of random orientation and of components drawn from a normal distribution [13, 14]. Thus, during the evolution, both the magnetization and the stochastic (thermal) field are nonuniform within each MNP.

For an isolated MNP of the cubic magnetic anisotropy, the evolution of its macrospin is described with a modified Brown's theory of thermal fluctuations in a single-domain magnetic particle, originally formulated for uniaxial magnets [6]. The cubic-anisotropy version of the theory has been developed in [16, 17, 18]. Considering one of the three easy directions to be parallel to an external (driving) field, one arrives at the temperature dependence of the response function

$$\langle m_y(t) \rangle = \begin{cases} \frac{\mu_0 M H}{4K_1} \frac{\tau_1^{-1} \sin(\omega t + \phi_1)}{\sqrt{\omega^2 + \tau_1^{-2}}} & k_B T \ll K_1 V \\ \frac{\mu_0 M H V}{k_B T} \frac{\tau_2^{-1} \sin(\omega t + \phi_2)}{\sqrt{\omega^2 + \tau_2^{-2}}} & k_B T \gg K_1 V \end{cases}, \quad (4)$$

where $1/\tau_2 \approx 2\gamma\alpha k_B T / MV$ and $\tau_2/\tau_1 \propto (K_1 V / k_B T)^{3/2} e^{-K_1 V / 4k_B T}$. However, the validity of the macrospin approach can be questionable, especially beyond the linear response regime. In the present work, we test systems of MNPs of higher crystalline anisotropy than in Ref. [5], thus, of higher temperature of transition between the high- and low-energy-barrier dynamical regimes, which is equal to $K_1 V / k_B$. On the other hand, the arrays of MNPs that we investigate are different in terms of the saturation magnetization of the nanoparticle material (M_s of iron is much higher than M_s of magnetite), thus, the magnetostatic (dipolar) interactions between MNPs differ in strength. Both the breakdown of the macrospin approximation and the magnetostatic interactions can make the Brown-like picture of the magnetization dynamics inapplicable to the MNP arrays, therefore, we rely on the micromagnetic simulations rather than on an analytical approach.

3. Simulation results

The relaxation and driven dynamics of systems of $4 \times 4 \times 4$ MNPs in which the magnetic-phase has a volumetric ratio

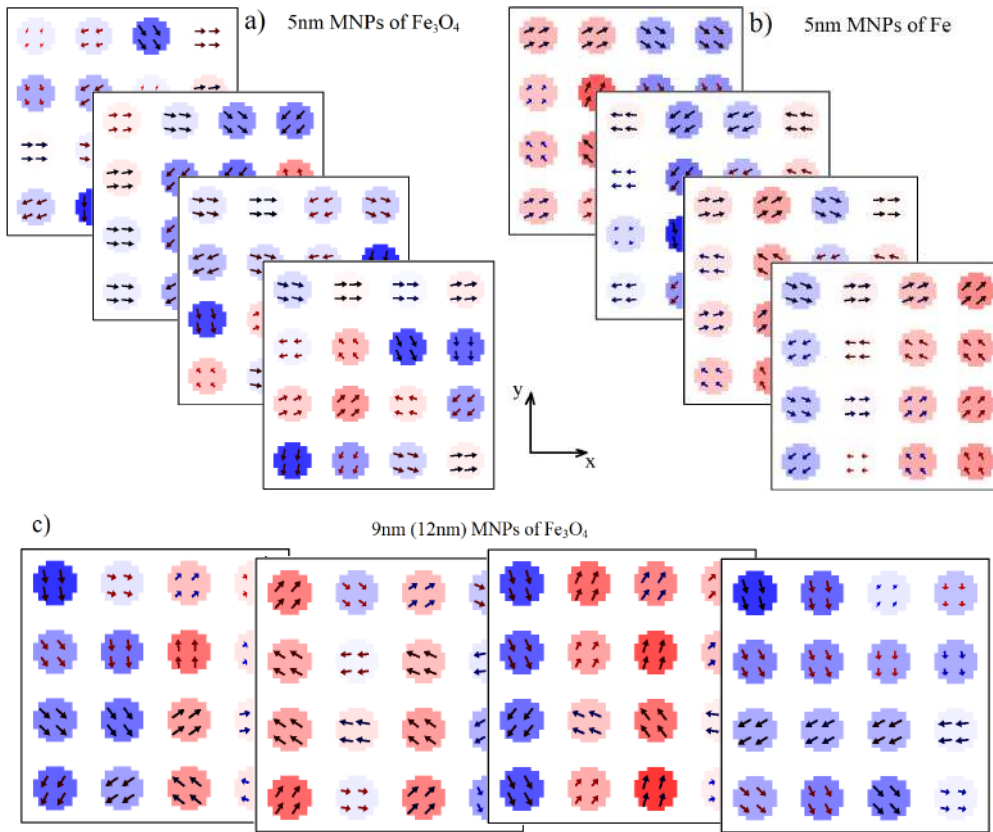


Figure 1: Magnetic ordering in system of 4×4 nanoparticles of Fe_3O_4 and Fe of 5nm diameter in consecutive planes of the nanoparticle lattice, at a volumetric ratio of the magnetic phase content of $x = 0.13$. The colors and their intensity indicate the magnetization projection onto the y -axis.

of 0.13 with periodic boundary conditions were simulated using the MuMax³ package, including thermal fluctuations [19, 14]. We deal with systems of 5nm-diameter MNPs of Fe_3O_4 and Fe as well as systems of 9nm-, 12nm- and 15nm-diameter MNPs of Fe_3O_4 . The material parameters for Fe are: the cubic-anisotropy constant $K_1 = 4.8 \cdot 10^4 \text{J/m}^3$, the exchange stiffness $A_{ex} = 2.0 \cdot 10^{-11} \text{J/m}$, and the saturation magnetization $M_s = 1.7 \cdot 10^6 \text{A/m}$. The grid discretization size is 0.5nm. Thus, a single cell in the micromagnetic model represents a volume containing at least 8 magnetic atoms with a total spin higher than 10, which is important for approximating its magnetic moment with a classical vector, while the cell size is small enough to accurately model the spherical shape of MNPs. Temperature is assumed to modify the magnetization of MNPs following the relation $M(T) = M_s(1 + T/2T_C)\sqrt{1 - T/T_C}$, (following [15]). For Fe_3O_4 , we use different parameters to low-temperature ($T < 120\text{K}$) and high-temperature ($T > 120\text{K}$) regimes, below and above the Verwey transition [9]. Below the Verwey-transition temperature, the anisotropy of magnetite is strong and uniaxial, $K_u = 20 \cdot 10^4 \text{J/m}^3$, and $A_{ex} = 1.2 \cdot 10^{-11} \text{J/m}$, $M_s = 4.0 \cdot 10^5 \text{A/m}$. Above the transition, the anisotropy is cubic, (thus, we modify the numerical model of the low-temperature phase relative to the basic model of Sec. 2), and the parameters take values of $K_1 = -1.1 \cdot 10^4 \text{J/m}^3$, $A_{ex} = 1.2 \cdot 10^{-11} \text{J/m}$, and $M_s = 4.8 \cdot 10^5 \text{A/m}$. Measurements of temperature depen-

dence of the anisotropy parameters of magnetite show that K_1 reaches a minimum at room temperature [20, 21]. In our simulations, for better insight into the role of thermal fluctuations in the magnetization dynamics, we consider a wide range of temperatures $T = 150 \div 450\text{K}$ treating K_1 as constant, thus, maintaining the same starting state of the dynamical simulations for different temperatures. Within this approach, $|K_1|$ is overestimated by a factor of 2 at the ends of the temperature range (at $T = 150\text{K}$ and $T = 450\text{K}$) while it is correct at the most important point $T = 300\text{K}$. The grid discretization size is scaled with the nanoparticle diameter and it takes values of 0.5nm, 0.9nm, 1.2nm and 1.5nm for MNPs of 5nm, 9nm, 12nm and 15nm diameter, respectively. A Gilbert damping constant $\alpha = 0.1$ is taken for all the nanocomposites in order to account for the effects of imperfections of MNP surfaces. Ferromagnetic resonance data for MNP systems and polycrystalline magnets suggest considerably higher damping constants than for bulk magnets [22, 23, 24, 25].

Snapshots of three of the relaxed magnetization structures are presented in Fig. 1. In all the simulated systems, the crystalline anisotropy (uniaxial in magnetite below the Verwey point or cubic in other cases, of randomly oriented easy axes) is strong enough to determine the equilibrium magnetization state, making the magnetization almost parallel to the easy axes inside the nanoparticles. The magnetostatic interactions between MNPs influence

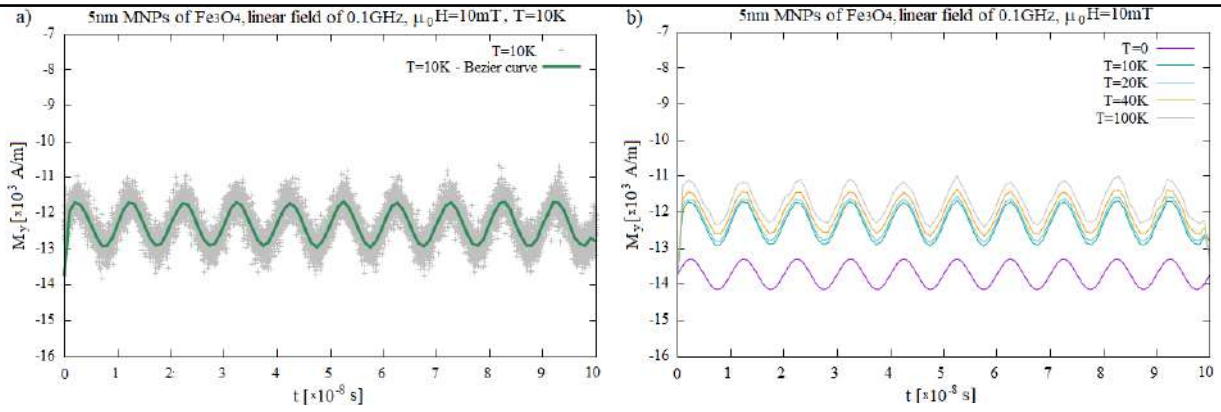


Figure 2: Time dependence of magnetization component parallel to a linearly-polarized driving field of amplitude 10mT and frequency 0.1GHz for an array of 5nm MNPs of Fe_3O_4 with $x = 0.13$ at temperatures below the Verwey point. In (a), a comparison of raw data (grey points) and corresponding smoothed (using Bezier scheme) curve for $T = 10$ K. In (b), all curves for $T > 0$ are smoothed using a Bezier scheme.

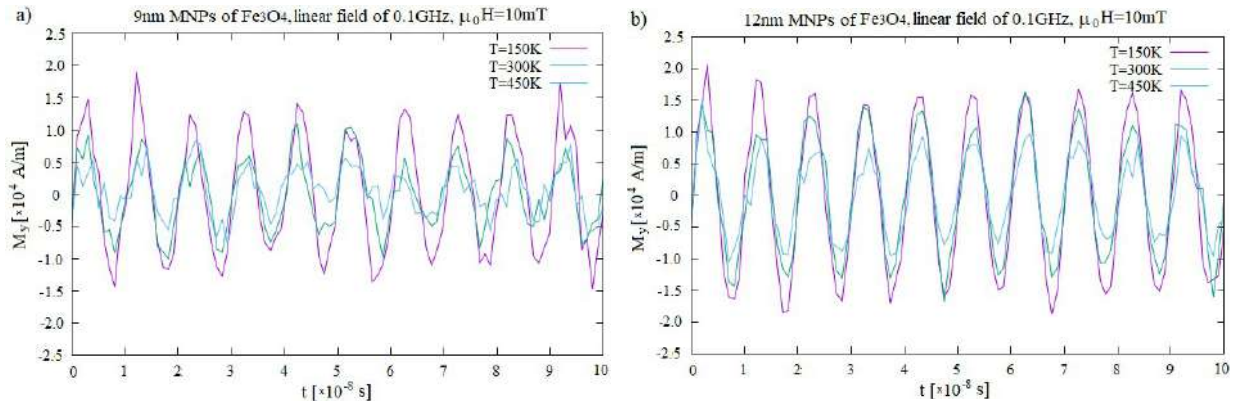


Figure 3: Time dependence of magnetization component parallel to a linearly-polarized driving field of amplitude 10mT and frequency 0.1GHz for array of (a) 9nm MNPs and (b) 12nm MNPs of Fe_3O_4 with $x = 0.13$ at temperatures above the Verwey point. In (a) and (b), all curves in (a) and (b) are smoothed using a Bezier scheme.

the ordering as well, favoring some orientations of the magnetization along the magnetocrystalline easy axes by magnetization of neighboring nanoparticles. The effect of the magnetostatic interactions on the equilibrium states is minor for Fe_3O_4 nanoparticles below the Verwey temperature (Fig. 1(a)) because of low saturation magnetization and high anisotropy constant, (a small total magnetic moment is present due to finite number of MNPs), while, it is stronger for the iron nanoparticle system of the same volumetric ratio $x = 0.13$. In the later case, from Fig. 1(b), we find correlations in the orientations of the magnetic moments of nanoparticles which manifest in a stripe structure of the magnetization similar to that reported for the array of $\text{Fe}_{65}\text{Co}_{35}$ MNPs in Ref. [5]. This is a consequence of a the high saturation magnetization of iron, leading to strong magnetostatic interactions. All the relaxed magnetization structures in Figs. 1(a)-1(c) are used as the initial states for the simulations of dynamical response. With the purpose of simulating high-temperature dynamics, we also relax the magnetite array with the parameters relevant above the Verwey transition, focusing on arrays of larger MNPs of 9nm to 15nm-diameter). An example of the resulting magnetization structure is presented in Fig. 1(c), in which we again find correlations in the orientations of higher magnetic moments of nanoparticles than these of small MNPs of Fig. 1(a).

The dynamics have been simulated for a linearly-polarized driving field of 10mT and of a frequency of 0.1GHz, applying the adaptive time stepping [26], (see details of the numerical method in [5]). The raw-data of the magnetization dependence on time at nonzero temperature is noisy due to thermal fluctuations. The curves in Figs. (2)-(6) were obtained via applying a Bezier smoothing method, following reference [5]. In Fig. 2(a), we demonstrate application of that smooting method. The driving field is strong enough to ensure a magnetic response in magnetostatically interacting systems, and the chosen frequency is not high enough to decrease the amplitude of the response. For the sub-GHz and GHz regimes, we have verified that the response amplitude decreases considerably as the frequency increases, in accordance to data [27]. For 5nm-diameter MNPs of magnetite, below the Verwey point ($T < 120$ K), the time dependence of the magnetization is plotted in Fig. 2(b) for a series of temperatures. We see an almost constant response of the magnet in a whole range of temperatures up to the Verwey point, with magnetization amplitude below 1 kA/m (compared to the saturation magnetization of $0.13M_s = 52$ kA/m). Below the Verwey transition temperature, Fe_3O_4 has a high uniaxial crystalline anisotropy, thus the theoretical temperature for the high-to-low energy-barrier transition is large, $K_u V/k_B = 948$ K in spite of low volume of the MNPs. In consequence, in

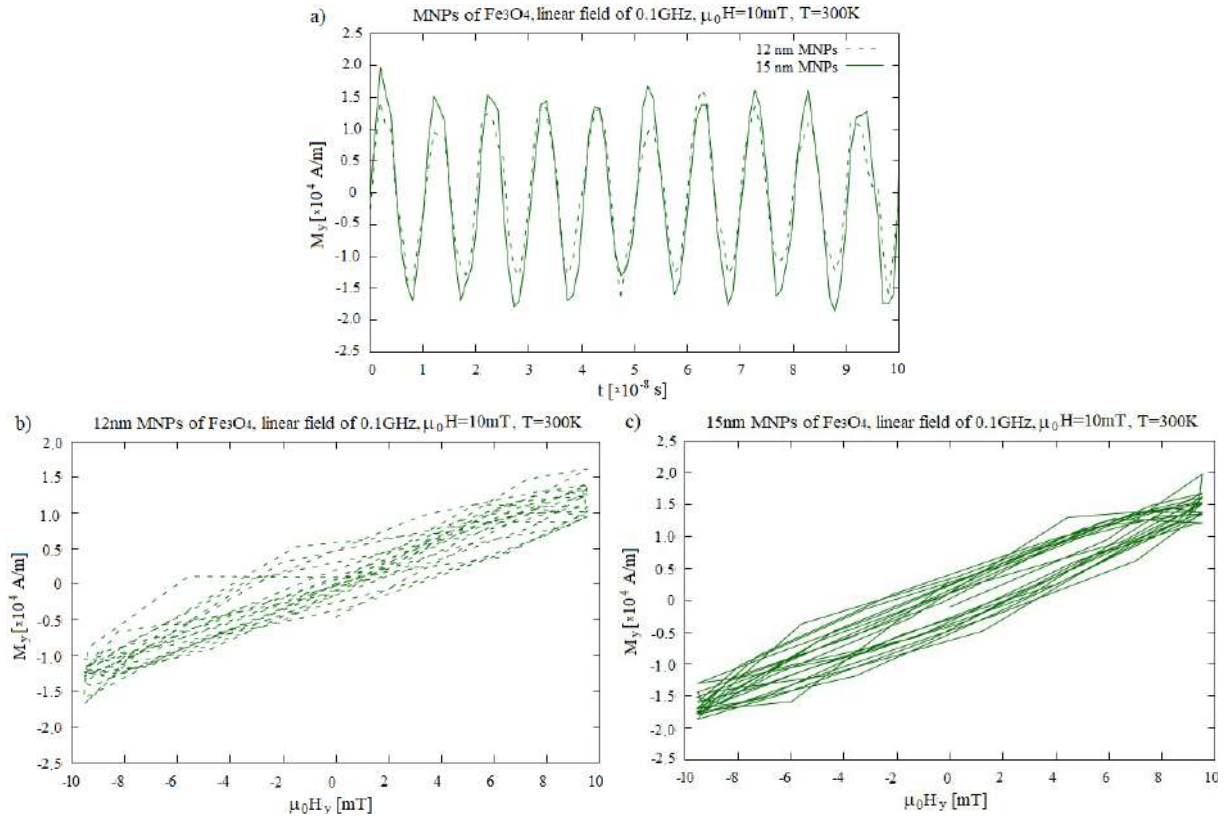


Figure 4: (a) Time dependence of magnetization component parallel to a linearly-polarized driving field of amplitude 10mT and frequency 0.1GHz for array of 12nm MNPs (dash line) and 15nm MNPs (solid line) of Fe_3O_4 with $x = 0.13$ at $T = 300\text{K}$. In (b) and (c), the corresponding dynamical magnetization-field (M - H) curves for time period of 0-100ns. The density of lines in (b) is high at the line crossing the point $[0,0]$ (for 12nm MNPs), whereas in (c), the density of lines creates a hysteresis-like loop (for 15nm MNPs). In (a)-(c), all curves are smoothed using a Bezier scheme.

Fig. 2(b), we do not see much change of the magnetization amplitude with temperature up to $T = 100\text{K}$ (close to the Verwey point), whereas the response function oscillates around a stable equilibrium state that has nonzero magnetization (as shown in Fig. 1(a) and discussed in the Appendix). In contrast, above the Verwey transition temperature, the crystalline anisotropy is cubic and weaker, which leads to a theoretical value of temperature of the high-to-low energy-barrier transition of $|K_1|V/k_B = 52\text{K}$. This suggests that the system is in the low energy barrier regime and thermal fluctuations disrupt the magnetic response of 5nm MNPs of magnetite. The magnetostatic interactions between MNPs are too weak to counteract thermal destabilization of the dynamics. Therefore, to obtain a room temperature response in magnetite we simulate systems of larger nanoparticles, 9nm, 12nm and 15nm diameter.

In Fig. 3(a) and Fig. 3(b), the time dependent response is plotted for magnetite composites of 9nm and 12nm MNPs, respectively, for a series of temperatures: $T = 150\text{K}, 300\text{K}, 450\text{K}$. For 9nm diameter MNPs, we see that thermal fluctuations damp and dephase the driven magnetization oscillations at and above room temperature. For 12nm MNPs of magnetite, the high-to-low energy-barrier transition temperature is as large as $|K_1|V/k_B = 720\text{K}$. The system is in a high energy barrier regime, the

response function amplitude is high and the oscillations are regular. The magnetization of the MNPs is homogeneous in the relaxed state, not influenced by curvature of the MNP surface, even for the MNPs of 12nm diameter. A decrease of amplitude of the response function with temperature in the regime of high-energy-barrier is seen from Fig. 3(b). We consider it as a nonlinear effect since, following equation Eq. (4), in the high-energy-barrier regime, for the magnetic particle (as well as for any classical systems undergoing stochastic resonance), the amplitude of the linear response function vanishes as $T \rightarrow 0$ up to weak oscillations around equilibrium [28, 29].

Motivated by data of Ref. [27], we simulated arrays of magnetite nanoparticles with 12–15nm diameter at room temperature. The data show rapid increase of the imaginary part of the permeability for MNPs with increasing nanoparticle diameter between 12nm and 15nm at a frequency of 0.1GHz. A phase shift between the response functions for arrays of 12nm and 15nm MNPs is not seen from Fig. 4(a). However, from our simulations, we see the appearance of a dynamical hysteresis loop for the 15nm MNP array (Fig. 4(c)). In contrast, for 12nm MNPs, we have found thermal-fluctuation-related widening of the dynamical magnetization-field (M - H) curve which does not form a hysteresis loop (Fig. 4(b)). The shapes of the dynamical hysteresis loops are unstable in the presence

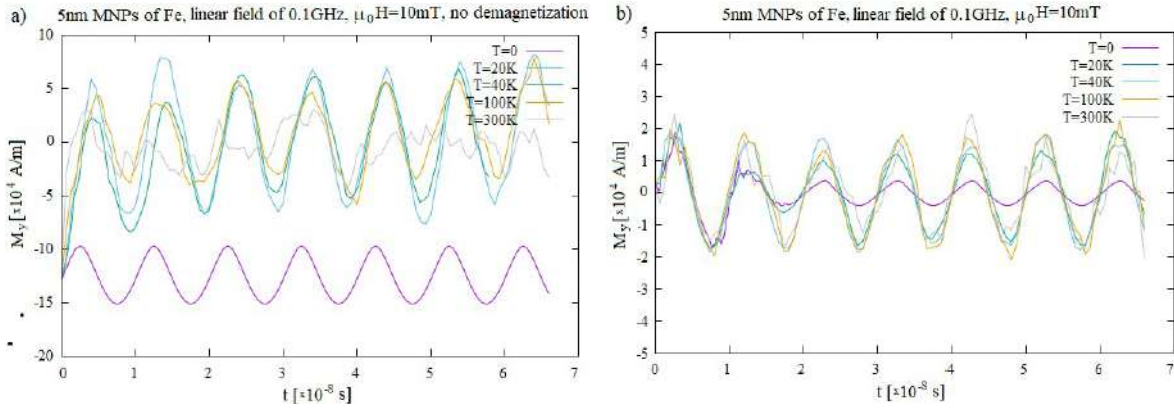


Figure 5: Time dependence of magnetization component parallel to a linearly-polarized driving field of amplitude 10mT and frequency 0.1GHz for array of 5nm MNPs of iron at $x = 0.13$ simulated with the (a) absence and (b) presence of the demagnetization field. In (a) and (b), all curves for $T > 0$ are smoothed using a Bezier scheme.

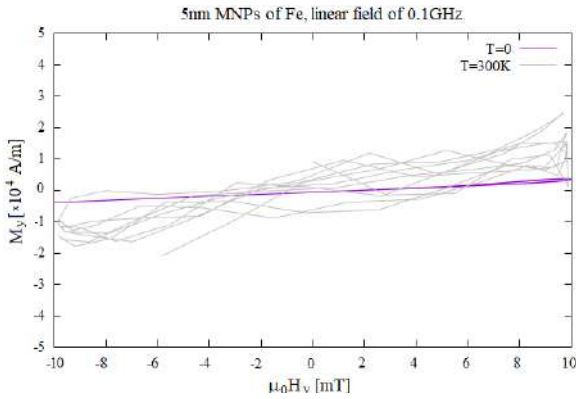


Figure 6: The magnetization-field (M-H) curve of Fe nanoparticle system corresponding to the dynamics in figure 5(b). The grey curve is smoothed using a Bezier scheme.

of thermal fluctuations because we perform limited-term simulations of a single magnetic system not a statistical ensemble of magnets. Nevertheless, the densities of lines representing consecutive periods of the M-H plots are suggestive of a loop in Fig. 4(c), thus of a collective remagnetization of MNPs ensemble, unlike in Fig. 4(b) where there is no loop opening. More details on the M-H curves end evaluation of volumetric power loss, are given in Appendix.

For the purpose of comparison of the dynamics in arrays of different MNPs of cubic anisotropy, we also studied a system of 5nm-diameter MNPs of iron (the temperature of high-to-low energy barrier transition is $|K_1|V/k_B = 228K$). Additionally, we analyze the role of the magnetostatic field by performing simulations in the absence and presence of this interaction field. For both cases, Fig. 5(a) and Fig. 5(b), the amplitude of the magnetic response increases with temperature in the low-temperature range, though it does not vanish in the limit of $T \rightarrow 0$, unlike the behavior expected from the classic description of the magnetic particle response (equation (4)), [6]. This may be understood by considering that the classic (macrospin-approximation-based) Neel-Brown theory of linear magnetic response in the presence of thermal fluctuations is applicable to a driving field much smaller than the thermal

field $H \ll \langle H_{th} \rangle \propto T^{1/2}$, whereas our simulations are beyond the linear regime in the zero-temperature limit. The inclusion of the magnetostatic field results in a decrease of the response function amplitude, however, at high temperatures, in particular at room temperature, the magnetostatic field stabilizes the periodicity of the magnetization vs. time (Fig. 5(a) vs. Fig. 5(b)), similar to [5].

In Fig. 6, the dynamical M-H curve is plotted for the iron nanoparticle system at $T = 0$ and $T = 300K$, which correspond to the magnetization dynamics plotted with purple and grey lines of Fig. 5(b). We notice temperature dependent widening of the M-H plot, which is related to thermally-induced non-hysteretic loss, similar to the M-H curve for an array of magnetite nanoparticles of sufficiently low diameter (Fig. 4(b)). However, the magnetic (not related to eddy current) loss is zero in average (over many cycles) if there is no dynamical hysteresis loop.

4. Conclusions

We have analyzed the response of composites of iron and iron oxide (magnetite) MNPs of cubic crystalline anisotropy to an AC magnetic field of 0.1 GHz. Iron has a large saturation magnetization and high conductivity, whereas magnetite has low conductivity and low saturation magnetization. Both materials have relatively high magnetocrystalline anisotropy, unlike the previously studied $Fe_{65}Co_{35}$ MNPs [5], which had a high conductivity, high saturation magnetization and low uniaxial anisotropy [5].

Thermal fluctuations destabilize the driven oscillations of the magnetization of nanocomposites at room temperature. Stabilization is provided by the dipole-dipole magnetostatic interactions which are strong enough to ensure sinusoidal magnetization changes in the array of Fe MNPs of 5nm diameter. For the arrays of 5nm Fe_3O_4 MNPs, this mechanism for stabilization is inefficient at room temperature because of the low saturation magnetization. The magnetic response can be stabilized against thermal noise by up-shifting the transition temperature from high-to-low energy barrier regime to be above room temperature, by increasing the volume (diameter) of MNPs. This is seen

in 12nm-diameter Fe_3O_4 MNPs which showed stable sinusoidal oscillations of the magnetization. The need for strong crystalline anisotropy in MNPs appears paradoxical since granular materials made of low-anisotropy magnetic particles are expected to be preferable with regard to reducing hysteresis loss. However, for sufficiently small MNPs, we do not find any dynamical hysteresis of composites of MNPs with randomly oriented anisotropy axes from our simulations even for the array of anisotropic Fe nanoparticles (see Fig. 6), and only non-hysteretic loss is important at room temperature.

We note that dynamical hysteresis from composites of magnetite nanoparticles at Hz and sub-kHz regime has been predicted previously (within macrospin approach), however, its area is strongly dependent on the frequency and nanoparticle size (interaction strength) [30, 31]. A very strong dependence of the real and imaginary parts of the susceptibility on frequency and density of the magnetic content has also been found for assemblies of iron nanoparticles [32]. For both nanocomposites of magnetite and iron, there are available experimental data on the dynamical response at sub-GHz and GHz ranges [12, 3]. They show almost zero imaginary part of the susceptibility for sufficiently low MNPs and low volumetric ratio of magnetic content, i.e. without nanoparticle agglomeration. For both magnetite and iron, we have found the amplitude of room-temperature 0.1GHz oscillations of magnetization to be comparable to the maximum amplitude of the formula (4) in the limit of zero frequency; $\sim \mu_0 MH/4K_1$. Hence, the dynamics considered is beyond the regime of applicability of the Neel-Brown theory of linear response. The room temperature susceptibility of the composite of 12nm MNPs of Fe_3O_4 and the volumetric ratio of the magnetic subsystem $x = 0.13$ is found to take $\chi \approx 1.4$ at $T = 300\text{K}$ and frequency of 0.1GHz. A similar susceptibility has been measured for 12.8nm MNPs of magnetite in Ref. [27]. For analogous conditions, despite much higher saturation magnetization of iron than magnetite, the susceptibility of the composite of 5nm MNPs of iron is comparable, $\chi \approx 1.6$ at room temperature. A comparable value of the susceptibility ($\chi \approx 2$) has been found previously for the system of 5nm-diameter nanoparticles of $\text{Fe}_{65}\text{Co}_{35}$ MNPs [5]. However, the mechanism of stabilization of the dynamical response using dipole-dipole nanoparticle interactions can be sensitive to the uniformity of the MNP size and arrangement. For this reason, arrays of sufficiently-large MNPs of Fe_3O_4 (a low-magnetization material) can be even more attractive in terms of inducing strong dynamical response than arrays of high-magnetization metallic nanoparticles. We mention that direct measurements of characteristics of a transformer with a core composed of 35nm MNPs of magnetite still show improvement of the power conversion relative to an air-core transformer up to a frequency of 1GHz [33].

Acknowledgement

Calculations have been carried out using resources provided by Wroclaw Centre for Networking and Supercomputing (<http://wcss.pl>), grant No. 450. The authors acknowledge support of a MISTI-Poland award from MIT.

Appendix

We expand upon several statements of Sec. 3. The equilibrium state of the system of Fe_3O_4 MNPs below the Verwey temperature (Fig. 1(a)) has a net magnetic moment. We see that the response function in Figs. 2(a), 2(b) oscillates around a magnetized state similar to the response function of the system of Fe MNPs simulated in the absence of the demagnetization field (Fig. 5(a)). Because of the absence (for Fe MNPs) or weakness (for Fe_3O_4 MNPs) of the demagnetization field, the equilibrium state of the finite size system is governed by the randomly oriented crystalline anisotropy field, thus, it can be magnetized as a consequence of randomness of the initial magnetization. We have verified the time evolution of the response function in Fig. 2(b) by repeating the simulations with three different equilibrium states relaxed with different initial (disordered) magnetization states. From Fig. 7(a), one sees that independent of possible magnetization of the equilibrium states, the response amplitudes of the system of weakly interacting MNPs are similar.

In Fig. 7(b) and Fig. 7(c), we present details of the M-H curves previously plotted in Fig. 4(b) and Fig. 4(c) respectively. From single-cycle plots of the M-H curves of the system of 15nm MNPs of magnetite (Fig. 7(c)), one notices that the integrals over each cycle of $M_y(H_y)$ function are of the same sign since all single-cycle plots form big loops without crossings. This differs for the single-cycle plots of the M-H curves of the 12nm MNPs of magnetite from Fig. 7(b), which are composed of several loops corresponding to positive or negative contributions to integrals of $M_y(H_y)$ over single cycles. To establish the average magnetic loss per cycle, we have calculated the integrals of $M_y(H_y)$ over 10 cycles for the Fe_3O_4 MNPs of 9nm, 12nm and 15nm diameter. For $T = 300\text{K}$ and frequency of 100MHz, the resulting integral values divided by the time period give the volumetric power loss $P_V = 19.3 \cdot 10^8 \text{W/m}^3$, $58.4 \cdot 10^8 \text{W/m}^3$ and $101.2 \cdot 10^8 \text{W/m}^3$, respectively. These values are comparable to ones found in simulations of high-frequency dynamics of MNP systems and anticipated from measurements at lower frequencies [8, 34].

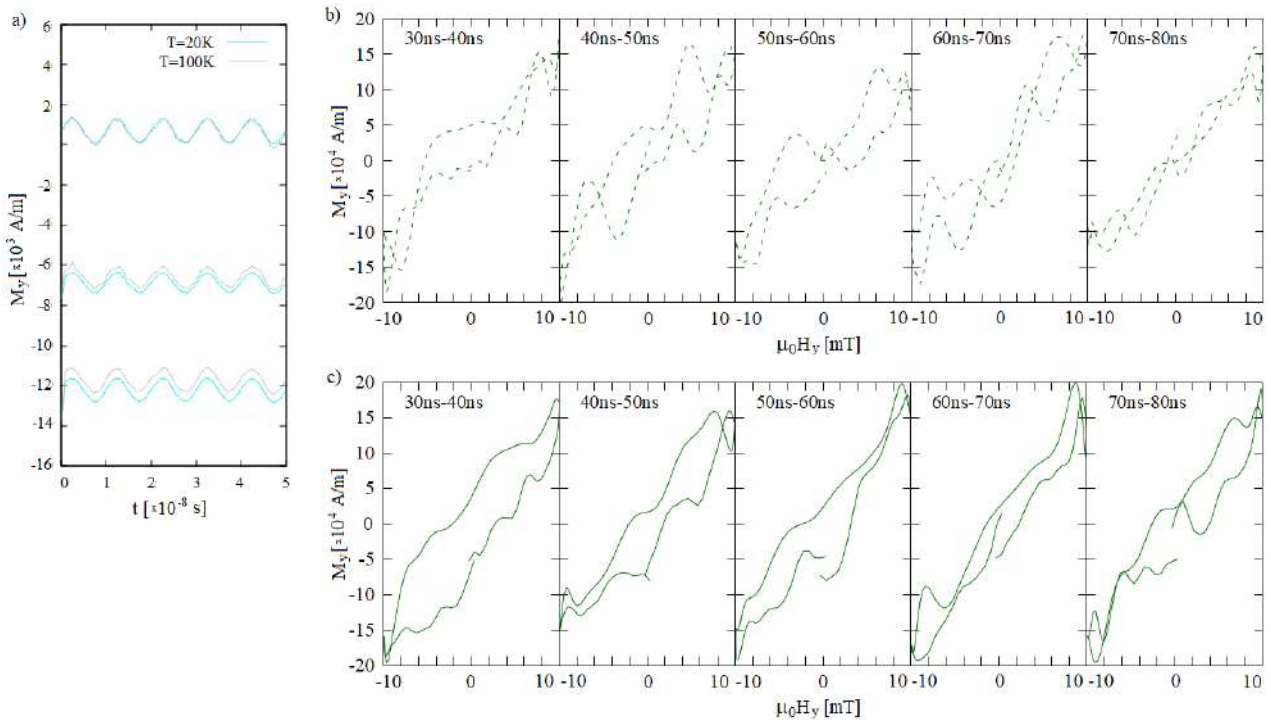


Figure 7: In (a), time dependence of magnetization component parallel to a linearly-polarized driving field of amplitude 10mT and frequency 0.1GHz for an array of 5nm MNPs of Fe_3O_4 with $x = 0.13$ at temperatures below the Verwey point, simulated with three different equilibrium states (expansion of Fig. 2(b)). In (b) and (c), the dynamical magnetization-field (M-H) curves for driving field of amplitude 10mT and frequency 0.1GHz for array of 12nm MNPs (dash line) and 15nm MNPs (solid line) of Fe_3O_4 with $x = 0.13$ at $T = 300\text{K}$ (expansion of Fig. 4(b) and Fig. 4(c) respectively). All curves are smoothed using a Bezier scheme.

References

- [1] M. Araghchini, et al., A technology overview of the PowerChip development program, *IEEE Trans. Power Electron.* 28 (2013) 4182–4201, <https://doi.org/10.1109/TPEL.2013.2237791>
- [2] R. J. Kaplar, J. C. Neely, D. L. Huber, L. J. Rashkin, Generation-after-next power electronics: ultrawide-bandgap devices, high-temperature packaging, and magnetic nanocomposite materials, *IEEE Power Electron. Magazine* 4 (2017) 36–42, <https://doi.org/10.1109/MPEL.2016.2643098>.
- [3] D Hasegawa, H. Yang, T. Ogawa, M. Takahashi, Challenge of ultra high frequency limit of permeability for magnetic nanoparticle assembly with organic polymer—Application of superparamagnetism, *J. Magn. Magn. Mat.* 321 (2009) 746–749, <https://doi.org/10.1016/j.jmmm.2008.11.041>.
- [4] J. M. Silveyra, E. Ferrara, D. L. Huber, T. C. Monson, Soft magnetic materials for a sustainable and electrified world, *Science* 362 (2018) eaao0195, <https://doi.org/10.1126/science.aao0195>.
- [5] K. Brzuszek, C. A. Ross, A. Janutka, High-frequency magnetic response of superparamagnetic composites of spherical $\text{Fe}_{65}\text{Co}_{35}$ nanoparticles, *J. Magn. Magn. Mat.* 573 (2023) 170651, <https://doi.org/10.1016/j.jmmm.2023.170651>.
- [6] W. F. Brown, Thermal fluctuations of a single-domain particle, *Phys. Rev.* 130 (1963) 1677–1686, <https://doi.org/10.1103/PhysRev.130.1677>.
- [7] P. Allia, G. Barrera, P. Tiberto, T. Nardi, Y. Leterrier, M. Sangermano, Fe_3O_4 nanoparticles and nanocomposites with potential application in biomedicine and in communication technologies: Nanoparticle aggregation, interaction, and effective magnetic anisotropy, *J. Appl. Phys.* 116 (2014) 113903, <https://doi.org/10.1063/1.4895837>.
- [8] M. Kin, H. Kura, T. Ogawa, Core loss and magnetic susceptibility of superparamagnetic Fe nanoparticle assembly, *AIP Advances* 6 (2016) 125013, <https://doi.org/10.1063/1.4972059>.
- [9] G. Barrera, P. Tiberto, P. Allia, B. Bonelli, S. Esposito, A. Marocco, M. Pansini, Y. Leterrier, Magnetic Properties of Nanocomposites, *Appl. Sci.* 9 (2019) 212, <https://doi.org/10.3390/app9020212>.
- [10] S. Ganguly, S. Margel, 3D printed magnetic polymer composite hydrogels for hyperthermia and magnetic field driven structural manipulation, *Prog. Polymer Sci.* 131 (2022) 101574, <https://doi.org/10.1016/j.progpolymsci.2022.101574>.
- [11] J. Watt, G. C. Bleier, Z. W. Romero, B. G. Hance, J. A. Bierner, T. C. Monson, D. L. Huber, Gram scale synthesis of $\text{Fe}/\text{Fe}_x\text{O}_y$ core-shell nanoparticles and their incorporation into matrix-free superparamagnetic nanocomposites, *J. Mater. Res.* 33 (2018) 2156–2167, <https://doi.org/10.1557/jmr.2018.139>.
- [12] H. Kura, T. Ogawa, R. Tate, K. Hata, M. Takahashi, Size effect of Fe nanoparticles on the high-frequency dynamics of highly dense self-organized assemblies, *J. Appl. Phys.* 111 (2012) 07B517, <https://doi.org/10.1063/1.3676224>.
- [13] A. Lyberatos, R. W. Chantrell, Thermal fluctuations in a pair of magnetostatically coupled particles, *J. Appl. Phys.* 73 (1993) 6501–6503, <https://doi.org/10.1063/1.352594>.
- [14] A. Vansteenkiste, J. Leliaert, M. Dvornik, M. Helsen, F. Garcia-Sanchez, B. Van Waeyenberge, The design and verification of MuMax³, *AIP Adv.* 4 (2014) 107133, <https://doi.org/10.1063/1.4899186>.
- [15] V. Barsan and V. Kuncser, Exact and approximate analytical solutions of Weiss equation of ferromagnetism and their experimental relevance, *Phil. Mag. Lett.* 97 (2017) 359–371, <https://doi.org/10.1080/09500839.2017.1366081>
- [16] Yu. L. Raikher, V.I. Stepanov, The effect of thermal fluctuations on the FMR line shape in dispersed ferromagnets, *Sov. Phys. JETP* 75 (1992) 764–771.
- [17] Yu. P. Kalmykov, S. V. Titov, W. T. Coffey, Longitudinal complex magnetic susceptibility and relaxation time of superparamagnetic particles with cubic magnetic anisotropy, *Phys. Rev. B* 58 (1998) 3267–3276, <https://doi.org/10.1103/PhysRevB.58.3267>.
- [18] Yu. P. Kalmykov, S. V. Titov, W. T. Coffey, M. Zarifakis, W. J. Dowling, Forced response and dynamic hysteresis of magnetic nanoparticles with mixed uniaxial and cubic anisotropy in superimposed strong ac and dc bias fields, *Phys. Rev. B* 99 (2019) 184414, <https://doi.org/10.1103/PhysRevB.99.184414>.

-
- [19] <https://mumax.github.io/>
- [20] Z. Kakol, J. M. Honig, Influence of deviations from ideal stoichiometry on the anisotropy parameters of magnetite $\text{Fe}_{3(1-\delta)}\text{O}_4$, *Phys. Rev. B* 40 (1989) 9090–9097, <https://doi.org/10.1103/PhysRevB.40.9090>.
- [21] R. Reznicek, V. Chlan, H. Stepankova, P. Novak, M. Marysko, Magnetocrystalline Anisotropy of Magnetite, *J. Phys: Cond. Mat.* 24 (2012) 055501, <https://doi.org/10.1088/0953-8984/24/5/055501>.
- [22] M. Respaud, M. Goiran, J. M. Broto, F. H. Yang, T. Ould Ely, C. Amiens, and B. Chaudret, High-frequency ferromagnetic resonance on ultrafine cobalt particles, *Phys. Rev. B* 59 (1999) R3934–R3937, <https://doi.org/10.1103/PhysRevB.59.R3934>.
- [23] J. Kotzler, D. Gorlitz, F. Wiekhorst, Strong spin-orbit induced Gilbert damping and g-shift in iron-platinum nanoparticles, *Phys. Rev. B* 76 (2007) 104404, <https://doi.org/10.1103/PhysRevB.76.104404>.
- [24] B. K. Kuanr, S.R. Mishra, L. Wang, D. DelConte, D. Neupane, V. Veerakumar, Z. Celinski, Frequency and field dependent dynamic properties of $\text{CoFe}_{2-x}\text{Al}_x\text{O}_4$ ferrite nanoparticles, *Mater. Res. Bulletin* 76 (2016) 22–27, <https://doi.org/10.1016/j.materresbull.2015.11.033>.
- [25] V. Sharma, J. Saha, S. Patnaik, B. K. Kuanr, Synthesis and characterization of yttrium iron garnet (YIG) nanoparticles - Microwave material, *AIP Adv.* 7 (2017) 056405, <https://doi.org/10.1063/1.4973199>.
- [26] J. Leliaert, J. Mulkers, J. De Clercq, A. Coene, M. Dvornik, and B. Van Waeyenberge, Adaptively time stepping the stochastic Landau-Lifshitz-Gilbert equation at nonzero temperature: Implementation and validation in MuMax³, *AIP Adv.* 7 (2017) 125010, <https://doi.org/10.1063/1.5003957>.
- [27] H. Yun, X. Liu, T. Paik, D. Palanisamy, J. Kim, W. D. Vogel, A. J. Viescas, J. Chen, G. C. Papaefthymiou, J. M. Kikkawa, M. G. Allen, C. B. Murray, Size- and composition-dependent radio frequency magnetic permeability of iron oxide nanocrystals, *ACS Nano* 8 (2014) 12323–12337, <https://doi.org/10.1021/nn504711g>.
- [28] M. I. Dykman, D. G. Luchinsky, R. Mannella, P. V. E. McClintock, N. D. Stein, N. G. Stocks, Stochastic resonance: Linear response and giant nonlinearity, *J. Stat. Phys.* 70 (1993) 463–478, <https://doi.org/10.1007/BF01053982>.
- [29] J. L. Garcia-Palacios, F. J. Lazaro, Langevin-dynamics study of the dynamical properties of small magnetic particles, *Phys. Rev. B* 58 (1998) 14937–14958, <https://doi.org/10.1103/PhysRevB.58.14937>.
- [30] P. Poddar, T. Telem-Shafir, T. Fried, G. Markovich, Dipolar interactions in two- and three-dimensional magnetic nanoparticle arrays, *Phys. Rev. B* 66 (2002) 060403(R), <https://doi.org/10.1103/PhysRevB.66.060403>.
- [31] G. Barrera, P. Allia, P. Tiberto, Dipolar interactions among magnetite nanoparticles for magnetic hyperthermia: a rate-equation approach, *Nanoscale* 13 (2021) 4103–4121, <https://doi.org/10.1039/D0NR07397K>.
- [32] T. Ogawa, H. Kura, M. Takahashi, Simultaneous agglomeration of Fe/Au nanoparticles with controllability of magnetic dipole interaction, *Scr. Mater.* 64 (2011) 1067–1070, <https://doi.org/10.1016/j.scriptamat.2011.02.026>.
- [33] S. Li, K. Zhu, L. Ma, B. Wu, W. Zou, F. Liu, A RF Integrated Transformer with Fe_3O_4 Nanoparticles Film, 2021 5th IEEE Electron Devices Technology & Manufacturing Conference (EDTM), Chengdu, China, 2021, pp. 1–3, <https://doi.org/10.1109/EDTM50988.2021.9420979>.
- [34] F. Burrows, C. Parker, R. F. L. Evans, Y. Hancock, O. Hovorka, R. W. Chantrell, Energy losses in interacting fine-particle magnetic composites, *J. Phys. D: Appl. Phys.* 43 (2010) 474010, <https://doi.org/10.1088/0022-3727/43/47/474010>.

High-Frequency Magnetic Response of Arrays of Planar Fe₆₅Co₃₅ Nanodots: Effects of Bias Field and Thermal Fluctuations

Kacper Brzuszek¹, Caroline A. Ross², *Fellow, IEEE*, and Andrzej Janutka¹

¹Department of Theoretical Physics, Wrocław University of Science and Technology, 50-370 Wrocław, Poland

²Department of Materials Science and Engineering, Massachusetts Institute of Technology, Cambridge, MA 02139 USA

Using temperature-dependent micromagnetic simulations, we analyze the magnetic response of arrays of nanoscale disk-shaped particles to linear or rotating fields of sub-GHz and GHz frequency with relevance to designing novel core materials for the on-chip power conversion. The nanodot arrays consist of Fe₆₅Co₃₅ disks of 5 nm (12 nm) diameter and 1 nm (2.4 nm) height arranged in columns that occupy sites of a hexagonal lattice. The volume of smaller (bigger) nanodots corresponds to the low-energy-barrier (high-energy-barrier) regime for thermal excitations at room temperature. A way to increase the amplitude of the response function and stabilize its phase (in order to reduce the residual loss) is to apply a static bias field perpendicular to the driving field. This situation is analyzed numerically for two cases of structure preparation in terms of the crystalline anisotropy in which the uniaxial anisotropy directions of single nanodots are either randomly or uniformly oriented. We predict that the strength of the dynamical response (the susceptibility χ) is comparable to our previously studied (Brzuszek et al., 2023) systems of spherical magnetic nanoparticles (MNPs) of 5 nm diameter ($1.0 < \chi < 2.5$ at 0.1 GHz) in spite of the lowered volumetric ratio of the magnetic subsystem x ($x \geq 0.13$ for MNP arrays versus $x = 0.07$ for magnetic nanodot (MND) arrays), based on ferromagnetic resonance.

Index Terms—Micromagnetic simulations, microwave frequency, power conversion, superparamagnetism.

I. INTRODUCTION

THE need for electric power microconverters for the on-chip power conversion has motivated studies of the high-frequency magnetic response from composites of magnetic nanoparticles (MNPs) embedded in dielectric matrices [2], [3], [4], [5], [6]. Nanogranular structures are insulators (in the absence of electron tunneling between nanoparticles) which allows for reducing or avoiding eddy-current-related loss. This is important because in bulk ferromagnets, eddy-current-related channels of loss dominate over other loss mechanisms at high frequencies. Additionally, confining the magnetic content of the composites to small-volume MNPs minimizes internal domain structure and eddy-currents inside the metallic particles [7].

Motivated by the above, we previously performed numerical investigations of the magnetic response of arrays of spherical MNPs with uniaxial magnetocrystalline anisotropy to linearly polarized or rotating sub-GHz driving fields showing strong effect of thermal excitations on the dynamical susceptibility. Increasing temperature lowered the amplitude of the magnetic response function and increased thermal noise-induced (residual) losses. In [1], we considered nanoparticles of material with high saturation magnetization of $M_s = 1.9 \cdot 10^6$ A/m. Reducing the diameter of the spherical MNPs below 5 nm in order to reduce their magnetic energy (i.e., lowering the temperature at which the system transitions to the low-energy-barrier regime) is challenging because the smaller particles are more seriously affected by deviations

from a spherical shape, which is accompanied by an increase of the magnetostatic energy and limits the performance of the composite [8], [9], [10].

Flat (quasi-2D) MNPs (cylindrical nanodots or disks) are expected to be easier to manufacture than perfect spherical MNPs, and flat MNPs can be of lower energy of the magnetocrystalline anisotropy due to reduced volume. Many systems created for studying fundamental properties of 2-D and 3-D supermagnetic arrays are made of flattened MNPs (called nanoislands or nanodots) in dielectric matrices [11], [12], [13], [14], [15], though, another category are arrays of magnetic nanodots (MNDs) deposited on metallic substrates, e.g., [16]. The development of methods of patterning magnetic media [17], (nanoimprint lithography, and, especially, block copolymer lithography), led to the ability of creating highly periodic arrays of cylindrical MNDs of the diameter well below 10 nm and of pitch size below 20 nm, [18], [19]. Flattening the MNPs results in an easy-plane magnetostatic anisotropy, in addition to the crystalline anisotropy. Therefore, the applicability of Brown's classic theory of thermal excitations in single-domain particles is limited and its numerical verification is required for specific cases. Moreover, excitation of ferromagnetic resonance (FMR) [20] provides a potential opportunity to enhance the magnetic response.

In the present article, we investigate layered systems of MNDs occupying sites of a hexagonal array and stacked to form a hexagonal lattice. With regard to assessing the response, two cases of alignment of in-the-plane easy axes are considered: the random in-plane alignment or parallel alignment of all the easy axes, representing local or global anisotropy, respectively. Performing full micromagnetic simulations instead of applying the commonly used macrospin approximation to MNPs appeared in [1] to be of importance when dealing with the high-frequency dynamics, leading to considerably different dynamics and providing

Manuscript received 3 May 2023; revised 28 July 2023 and 5 September 2023; accepted 6 September 2023. Date of publication 13 September 2023; date of current version 24 October 2023. Corresponding author: A. Janutka (e-mail: andrzej.janutka@pwr.edu.pl).

Color versions of one or more figures in this article are available at <https://doi.org/10.1109/TMAG.2023.3313871>.

Digital Object Identifier 10.1109/TMAG.2023.3313871

0018-9464 © 2023 IEEE. Personal use is permitted, but republication/redistribution requires IEEE permission.

See <https://www.ieee.org/publications/rirights/index.html> for more information.

the need for inclusion of the intraparticle magnetostatic interactions.

This study considers the dynamical magnetic response of arrays of flat Fe₆₅Co₃₅ dots of 5 nm (12 nm) lateral diameter and of 1 nm (2.4 nm) height at a low volumetric ratio of the magnetic content, 0.07. The large spatial separation of the MNDs is chosen to limit tunneling conductivity in the composite. The different cases of MND volume exemplify different regimes of magnetic energies of individual particles, thus, different sensitivities to temperature fluctuations. In particular, the characteristic temperature of the transition to the Brown (low-energy-barrier) regime of dynamics is size dependent. Here, the Brown regime corresponds to a continuous rotation of the magnetization of immobilized MNPs/MNDs [21], unlike the nomenclature used for dispersions of MNPs in fluids.

In Section II, we formulate the micromagnetic model of the dynamics of MND arrays that will be applied to determining the equilibrium zero-temperature orderings in Section III. Section IV is devoted to studying the driven high-frequency dynamics. Conclusions are formulated in Section V.

II. MODEL

We consider a hexagonal lattice of flat MNDs whose dynamics is described with the stochastic Landau–Lifshitz–Gilbert (sLLG) equation

$$-\frac{\partial \mathbf{m}}{\partial t} = \frac{2\gamma A_{\text{ex}}}{M} \mathbf{m} \times \Delta \mathbf{m} + \gamma_0 \mathbf{m} \times (\mathbf{H}_{\text{an}} + \mathbf{H}_{\text{ms}} + \mathbf{H} + \mathbf{H}_{\text{th}}) - \alpha \mathbf{m} \times \frac{\partial \mathbf{m}}{\partial t} \quad (1)$$

where \mathbf{m} is the normalized magnetization related to the magnetization \mathbf{M} via $\mathbf{M} = M\mathbf{m}$ in the MNDs and $\mathbf{M} = 0$ in the dielectric matrix, (M is a function of temperature and it tends to its saturation value M_s following $M \rightarrow_{T \rightarrow 0} M_s$). Here, Δ denotes the Laplace operator. The vectors \mathbf{H}_{an} , \mathbf{H}_{ms} , and \mathbf{H} are the (crystalline) anisotropy field, the magnetostatic (demagnetization) field, and an applied external field, respectively. The axes of the crystalline anisotropy within the dots are assumed to be oriented within the plane of the nanodots. We consider the cases of random or uniform orientation of the easy axes in the plane, where the anisotropy field strength is related to the magnetocrystalline anisotropy constant K via $|\mathbf{H}_{\text{an}}| = 2K/\mu_0 M$. The parameters γ , A_{ex} , and α denote the gyromagnetic factor, the exchange stiffness, and the Gilbert damping constant, respectively, and $\gamma_0 \equiv \gamma\mu_0$, where μ_0 represents the vacuum permeability. The hexagonal lattice of MNDs is simulated by a system of $4 \times 4 \times 4$ cylindrical nanoparticles (grouped in pillars) with periodic boundary conditions. A thermal field \mathbf{H}_{th} satisfies the correlation property

$$\langle H_{\text{th},i}(t) H_{\text{th},j}(t + \tau) \rangle = \frac{2k_B T \alpha}{\gamma \mu_0^2 M} \delta_{ij} \delta(\tau). \quad (2)$$

The application of the thermal field into micromagnetic simulations is based on the relation

$$\mu_0 \mathbf{H}_{\text{th}}(N \Delta t) = \sqrt{2k_B T \alpha / \gamma M \Delta V \Delta t} \mathbf{s}(N \Delta t) \quad (3)$$

where Δt is a time step, ΔV denotes the volume of the computational cell, and $\mathbf{s}(t)$ represents a vector of components drawn from a normal distribution at each time step [22], [23].

Within Brown's theory of thermal fluctuations in single-domain particle [21], the amplitude of the magnetic response to a linearly polarized field $\mathbf{H} = [0, H \sin(\omega t), 0]$ is predicted to be given by

$$\langle m_y \rangle_\omega \propto \frac{\tau^{-1}}{\sqrt{\omega^2 + \tau^{-2}}} \quad (4)$$

where the relaxation rate takes the form

$$\tau^{-1} = \begin{cases} \frac{2\gamma\alpha e^{-KV/k_B T}}{M(1+\alpha^2)} 4K \sqrt{\frac{KV}{\pi k_B T}}, & KV \gg k_B T \\ \frac{2\gamma\alpha}{M(1+\alpha^2)} \frac{k_B T}{V}, & KV \ll k_B T \end{cases} \quad (5)$$

for the linear response regime. Applied to an array of MNDs with random in-the-plane anisotropy, we average the magnetization over their orientations, integrating the magnetization projections onto the direction of the in-plane (driving) field $\langle m_y \rangle_\omega \equiv (2\pi)^{-1} \int_0^{\pi/2} \langle m_y \rangle_\omega \cos^2 \varphi d\varphi$, where $\cos \varphi = \mathbf{H}_{\text{an}}/|\mathbf{H}_{\text{an}}| \cdot \mathbf{H}/|\mathbf{H}| = H_y/|\mathbf{H}|$. This way, we find

$$\frac{\text{Amp}(M_y)}{M(T)} = \frac{\langle m_y \rangle_\omega}{2}. \quad (6)$$

III. ORDERING

We first simulate the relaxation from a disordered state for the MND system with random in-plane anisotropy (RIA) and for one with uniaxial in-plane anisotropy (UIA) system. We start with arrays of 64 cylindrical Fe₆₅Co₃₅ MNDs with diameter of 5 nm and height of 1 nm forming a hexagonal lattice with four layers of MNDs, applying periodic boundary conditions in all directions. The volumetric ratio x of the magnetic material in the composite is $x = 0.07$, based on an interparticle separation in the hexagonal planes of 3 nm and an interplanar spacing of 5 nm. The material parameters for Fe₆₅Co₃₅ include a uniaxial (crystalline) anisotropy constant $K = 1.5 \cdot 10^4$ J/m³ and an exchange stiffness $A_{\text{ex}} = 1.7 \cdot 10^{-11}$ J/m. A relatively high value of the Gilbert damping constant $\alpha = 0.1$ is used in order to imitate possible imperfections of surfaces of the MNDs, in particular, an edge roughness [24], (FMR data for MNP systems and polycrystalline magnets are related to considerably higher damping constants than for bulk magnets [25], [26], [27], [28]). The temperature-dependent magnetization $M(T)$ tends to the saturation value $M_s = 1.9 \cdot 10^6$ A/m as $T \rightarrow 0$, while, for finite temperature, we apply the formula $M(T) = M_s(1 + T/2T_C)(1 - T/T_C)^{1/2}$, [29], where $T_C = 950$ K is the Curie temperature of Fe₆₅Co₃₅. The grid discretization size (the edge length of the cubic finite-difference cell) is 0.5 nm. All the relaxation and dynamics simulations are performed with the MuMax3 package [23].

The relaxed magnetic structure for the 5 nm diameter particles with RIA, denoted as RIA-I, is visualized in Fig. 1(a). The relaxed structure for the same geometry particles with UIA is shown in Fig. 1(b). In Fig. 1(a), we see that the ordering of RIA-I is dominated by the intraparticle anisotropy, while the dipolar interparticle coupling is of low influence. We deduce this from lack of regular multisublattice ordering previously noticed in system of MNPs of a high volumetric ratio of the

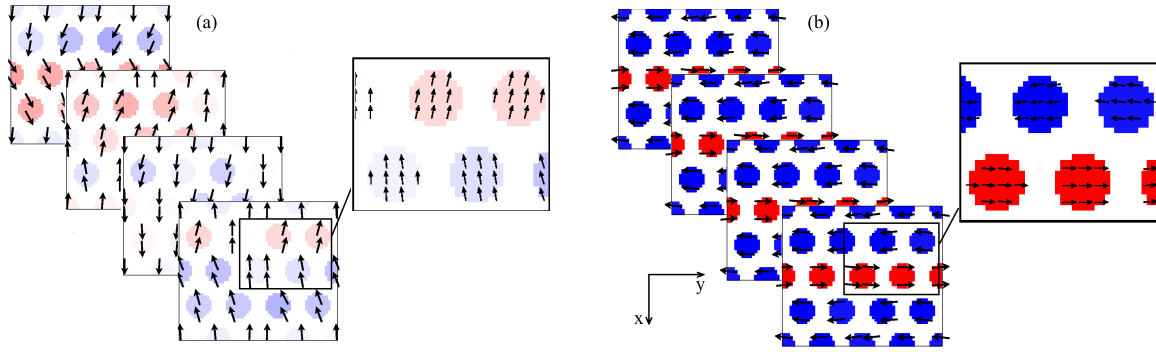


Fig. 1. Magnetic ordering in a model system of $4 \times 4 \times 4$ nanodots of $\text{Fe}_{65}\text{Co}_{35}$ of 5 nm diameter showing consecutive planes of the nanoparticle lattice, at the volumetric ratio of the magnetic phase of $x = 0.07$. (a) Case of random orientations of the easy axes in the plane; RIA-I and RIA-II systems (both relax to the same magnetization state up to rescaling sizes). (b) Case of easy axis of the crystalline anisotropy oriented along the y -direction; UIA system. The colors and their intensity indicate the magnetization projection onto the y -axis.

magnetic phase ($x = 0.3$), that we called a super-spin-glass state in [1]. In Fig. 1(b), for UIA system, the particles are magnetized in rows along the easy axis due to the effect of magnetostatic interactions.

We now consider the relaxed configuration of the rescaled RIA system (RIA-II) which is made up of nanodots with 12 nm-diameter and 2.4 nm-height, maintaining the volumetric ratio of $x = 0.07$ (the interdot distance is 7 nm, the interlayer distance is 12 nm). The grid discretization size is 1.2 nm. RIA-II system remains ordered according to the distribution of crystalline anisotropy axes within the MNDs. Its equilibrium magnetization is similar to that of RIA-I system and the snapshots of Fig. 1(a) are relevant to both RIA-I and RIA-II systems.

IV. HIGH-FREQUENCY DYNAMICS

A. Effect of Field Configuration

The field-driven dynamics of magnetization is simulated for RIA systems I and II and UIA system of $\text{Fe}_{65}\text{Co}_{35}$ nanodots of the previous section. The alternating field is directed in-the-plane, along the y -axis. In the case of UIA, the easy axis is aligned parallel to the alternating field, along the y -axis. With the purpose of determining the dynamical response, we plot the time dependence of longitudinal (M_y) component of the magnetization, starting their evolution from the relaxed (in Section III) state.

For RIA-I system, we performed simulations of the magnetic response at zero temperature plotting the magnetization amplitude with dependence on bias perpendicular field, Fig. 2(a). Based on the plot, the resonant value of the bias field is found to be $\mu_0 H_x = 45$ mT. That resonant field is higher than the crystalline anisotropy field $2K/M_s \approx 16$ mT which satisfies Kittel's classic formula for the resonance frequency

$$\omega_R = \gamma_0 \sqrt{M_s (2K/\mu_0 M_s - |H_x|)} \quad (7)$$

for $\omega_R \rightarrow 0$. Here, M_s denotes the saturation magnetization of bulk $\text{Fe}_{65}\text{Co}_{35}$, while the highest magnetization of the nanocomposite is limited to $x \cdot M_s = 0.07 \cdot M_s$. Note that the condition of a very low driving field (linear response) $\mu_0 H \ll \mu_0 H_a \equiv 2K/M_s$ is not satisfied in our simulations which are focused on a strong response regime. The resonant field can be affected by interparticle magnetostatic interactions

[30], [31]. For instance, large changes in the value of the FMR field with reorientations of equilibrium magnetization state have been reported in systems of magnetostatically interacting MNDs [32].

We do not observe FMR at zero bias field in any of the RIA or UIA systems at elevated frequencies in the range 1.0–7.0 GHz. Fig. 2(b) presents the time dependence of the response function for the example case of RIA-I system at zero temperature, for a series of driving frequencies. The magnetization amplitude monotonically decreases with increasing frequency, whereas, the resonance frequency obtained from Kittel's formula (7) is $\omega_R = \gamma_0 (2K/\mu_0)^{1/2} = 2\pi \cdot 5.4$ GHz for $H_x = 0$. Similar to RIA systems, applying a bias field to the UIA system of 5 nm dots driven with 0.1 GHz frequency, we have found that the bias field corresponding to the maximum in the amplitude of the (nonlinear) response exceeds the field corresponding to the maximum of the linear FMR response $\mu_0 H_x \approx 2K/M_s = 16$ mT, from Fig. 2(c).

We next describe the effect of driving the magnetization dynamics with an in-plane rotating field. Analytical results on single-domain magnetic particles with out-of-plane anisotropy under an in-plane rotating field have predicted a nonlinear enhancement of the magnetic response [33], [34]. In our preceding article [1], we numerically tested the dynamical response of an array of spherical MNPs with random orientations of easy axes to the rotating field, not finding any improvement of the response efficiency relative to the case of a linear driving field. We apply a similar analysis to the case of MNDs where the anisotropy directions are confined to the plane. In Fig. 2(d), we compare the time dependence of the response function for driving with linear and rotating fields of 0.1 GHz for RIA-II system. The rotating field drives a nonsinusoidal response of not higher amplitude than a linear field of the same amplitude independent of the presence or absence of the out-of-plane bias field. A similar result is found for RIA-I system (not shown).

B. Effect of Temperature

A comprehensive study of the effect of thermal fluctuations on the high-frequency magnetic response from arrays of (spherical) MNPs has been performed in [1]. Here, we focus on properties at the bias field of FMR (specific to MNDs).

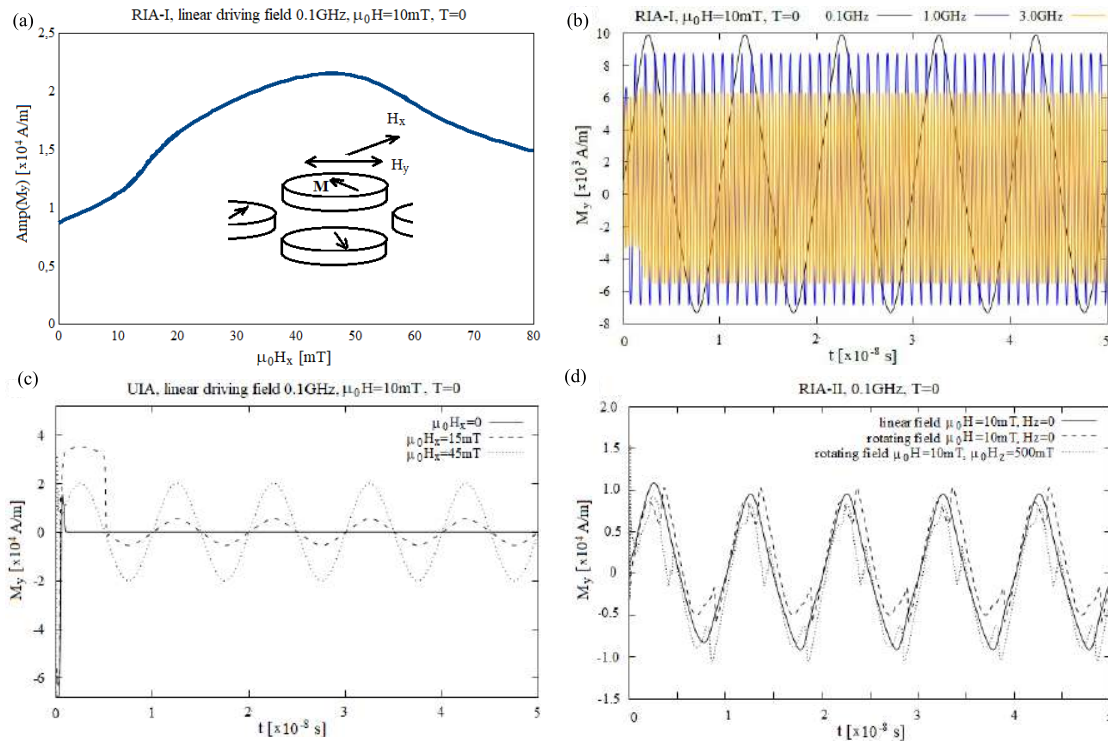


Fig. 2. (a) Response function amplitude of RIA-I system as function of the perpendicular in-plane field, (the field geometry scheme is sketched in the plot area). (b) Time dependence of magnetization component parallel to the linearly polarized driving field of amplitude 10 mT and frequencies 0.1, 1.0, and 3.0 GHz for RIA-I system, at zero temperature. (c) Time dependence of magnetization component parallel to the linearly polarized driving field of amplitude 10 mT and frequency 0.1 GHz for the UIA system in the absence or presence of the transverse bias field in the dot plane. (d) For RIA-II system, time dependence of a magnetization component in the dot plane driven with an in-plane linear field and a rotating field, for both the absence and the presence of an additional out-of-plane bias field.

We perform the temperature-dependent micromagnetic simulations with adaptive time stepping, where the time step is related to a thermal exchange length $l_{\text{ex}}^{\text{th}} \equiv (A_{\text{ex}}/\mu_0 M H_{\text{th}})^{1/2}$. We require $l_{\text{ex}}^{\text{th}}$ to be larger than the grid discretization size [35]. The usual implementation of the thermal field leads to a relationship between the time step Δt and the volume of the computational cell ΔV . Following (2) and (3), the time step is down-limited by:

$$\Delta t = \frac{2\alpha M(T)k_B T (l_{\text{ex}}^{\text{th}})^4}{\gamma A_{\text{ex}}^2 \Delta V} > \frac{2\alpha M(T)k_B T \Delta V^{1/3}}{\gamma A_{\text{ex}}^2}.$$

For sufficiently large magnets, the above condition is believed not to be critical [36], [37], [38], however, in small MNDs, the thermal exchange length plays a similar role as other exchange lengths since thermal energy is comparable to or higher than the magnetic energy.

The method of analyzing output of temperature-dependent simulations of dynamical magnetic response is illustrated in Fig. 3(a), where, we compare the raw data on the time dependence of the magnetization driven with sinusoidal field at a temperature of 20 K to the final plot. The later is obtained via smoothing the magnetization curve with application of the Bezier scheme. All curves from temperature-dependent simulations in the plots below are smoothed this way.

In Fig. 3(b), the time dependence of the longitudinal component of magnetization of RIA-I system is plotted for temperatures $T = 20$ K and $T = 300$ K, both for the absence or presence of a bias field perpendicular to the driving field. From Fig. 3(b), one sees that the bias field influences the

magnetic response at $T = 20$ K, while, its effect is marginal at $T = 100$ K. We note that the transition temperature between high- and low-energy-barrier regimes (theoretical limitation, [21]) is $KV/k_B = 21$ K. In order to verify the role of the energy barrier height on the response of the MND array, we have performed dynamical simulations of RIA-II system, whose MNDs are of 12 nm-diameter and 2.4 nm-height, thus the temperature between high- and low-energy barrier regimes is equal to $KV/k_B = 295$ K. For that system, in Fig. 3(c), we plot the time dependence of the longitudinal component of the magnetization at the same driving field ($\mu_0 H = 10$ mT and 0.1 GHz frequency) as previously considered for RIA-I system. The response amplitudes at low temperatures or zero temperature are comparable in both cases. However, RIA-II system appears to respond more strongly at room temperature than RIA-I system does. Moreover, when a bias field is applied, RIA-II system displays a FMR-related increase of the magnetization amplitude for temperatures up to room temperature at least. In the absence of a bias field ($H_x = 0$), from Fig. 3(c), one sees a higher magnetization amplitude at $T = 300$ K (blue curve) than at $T = 100$ K (solid orange curve). We attribute this thermal enhancement of the dynamical response to the persistence of the high-energy barrier regime up to room temperature.

From the preceding article [1], a strong bias field is known to reduce the residual loss in composites of small MNPs at the expense of reducing the response amplitude. This is confirmed for the arrays of MNDs by the result of a bias field of 100 mT (gray curve of Fig. 3(c) which is of more uniform periodicity

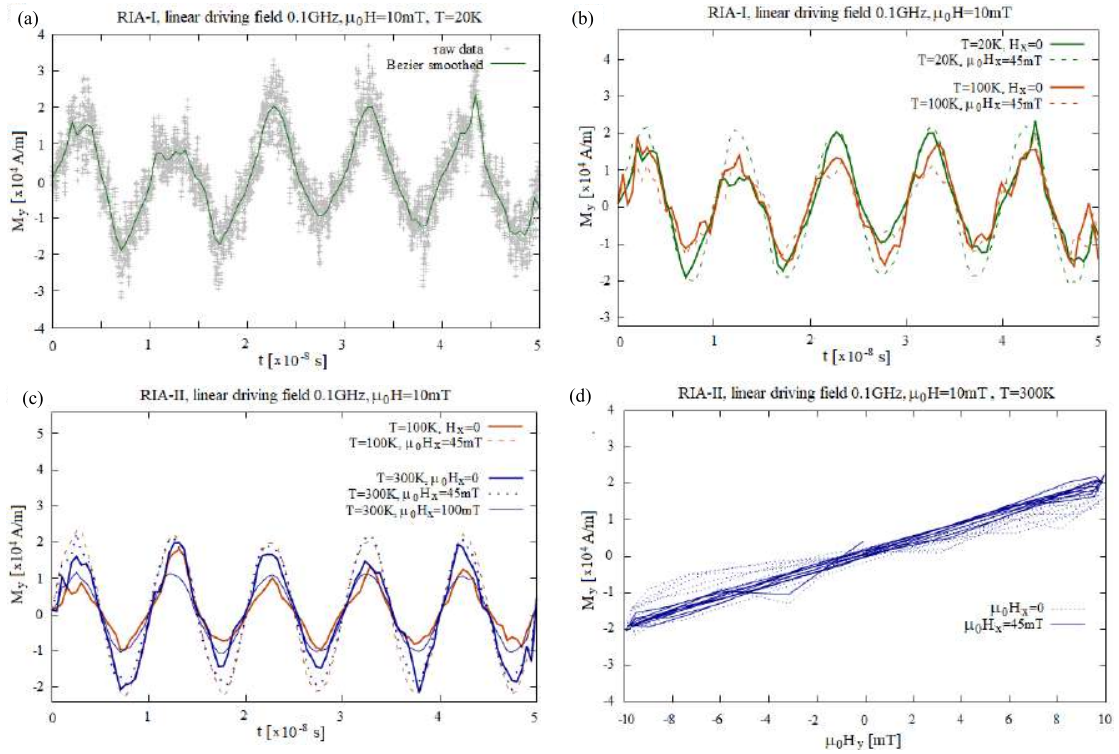


Fig. 3. (a) For RIA-I system, comparison of raw data and Bezier scheme smoothed curves of the time dependence of the magnetization component parallel to the linearly polarized driving field of frequency 0.1 GHz at temperature $T = 20\text{K}$. (b) and (c) Time dependence of magnetization component parallel to a linearly polarized driving field of amplitude 10 mT and frequency 0.1 GHz for RIA arrays of $x = 0.07$ of; (b) nanodots of 5 nm-diameter and 1 nm-height; the RIA-I system, (c) nanodots of 12 nm-diameter and 2.4 nm-height; the RIA-II system. (d) Field-magnetization (H - M) curve of RIA-II system. All curves in (b)–(d) are smoothed using a Bezier scheme.

than the blue (zero-bias field) curve, while having lower amplitude). However, the dashed magenta curve, with a bias field of $\mu_0 H_x = 45$ mT, shows improved periodicity and amplitude compared to the zero-bias case. Accordingly, Fig. 3(d) shows a narrowing of the dynamical field-magnetization curve at a bias field of 45 mT relative to the zero-bias curve. Thus, in arrays of MNDs, an optimum choice of bias field can reduce the residual loss while increasing the response amplitude.

The susceptibility modulus is evaluated as a ratio of the magnetization to the field amplitude

$$\chi = \frac{\text{Amp}(M_y)}{H} \quad (8)$$

The response function is in phase with the linear driving field (i.e., the susceptibility is real) up to weak thermal noise-induced aperiodicity (which is related to a residual loss). For linear driving, based on our simulations, the susceptibility of the 5 nm-diameter MND array with random in-plane magnetic anisotropy (RIA-I system) is $\chi \approx 1.0$ at $T = 100$ K, according to Fig. 3(b), while, it decreases at room temperature. For 12 nm-diameter MNDs (RIA-II system), the susceptibility $\chi \approx 1.5$ at $T = 300$ K, however, applying an in-plane bias field of the resonant value of 45 mT increases the room-temperature susceptibility to above 2.0.

V. CONCLUSION

Numerically studying the field-driven dynamics of systems of flat Fe₆₅Co₃₅ MNDs ordered into hexagonal lattices, we have analyzed the dynamical magnetic response with

relevance to their application as core materials for power conversion. The effects of the size of the MNDs and the orientation of their anisotropy axes were investigated on the response of the array at low volume fraction of the magnetic material and in the absence of an internal domain structure within the MNDs. The anisotropy orientation and the composition ratio x play a dominant role at zero temperature, but the dot size becomes important at elevated temperatures. A lower volume of the MNDs leads to stronger thermal fluctuations and thermal instability of the arrays, manifested by greater variability in their time-dependent magnetization response. In order to maintain sufficient thermal stability and a high amplitude of the response function, it is desirable that the magnetic system be operated in the regime of high-energy barrier, i.e., $T < KV/k_B$. The requirement of a room temperature response provides a lower limit on the volume of MNDs.

For large-volume MNDs (RIA-II system, $KV/k_B = 295$ K), the magnetic response strengthens with increasing temperature between 100 and 300 K, which is typical of superparamagnetic systems in the high-energy barrier regime of thermal excitations, though, the susceptibility does not vanish in the limit $T \rightarrow 0$. At room temperature, the amplitude of the response function can be additionally increased and stabilized against thermal excitations by applying a bias field which drives FMR. Noticeably, in the RIA systems, the resonance field is higher than that predicted by Kittel's classic theory of FMR, and we were unable to simulate zero-field FMR. Moreover, even under a resonance bias field of 45 mT, the

UIA system does not respond more strongly to the ac field compared to the RIA systems and the RIA systems are of interest due to their simpler fabrication process.

Comparing the susceptibilities of the arrays of flat MNDs to that of the arrays of spherical MNPs of [1], we conclude that, due to FMR, the array of flat MNDs gives a response to the alternating field that is as strong as that of small spherical nanoparticles described in the preceding article despite the lower content of the magnetic phase in the composite of MNDs ($x = 0.07$) versus $x \geq 0.13$ for the spherical MNPs in [1]). Using MNDs (quasi-2D islands) instead of spherical MNPs may be important in mitigating the effects of surface roughness and surface strain which reduce magnetism of small nanoparticles.

ACKNOWLEDGMENT

This work was supported by the Wroclaw Center for Networking and Supercomputing, under Grant 450. The authors acknowledge support of a MISTI-Poland award from MIT.

REFERENCES

- [1] K. Brzuszek, C. A. Ross, and A. Janutka, "High-frequency magnetic response of superparamagnetic composites of spherical Fe₆₅Co₃₅ nanoparticles," *J. Magn. Magn. Mater.*, vol. 573, May 2023, Art. no. 170651.
- [2] D. Hasegawa, H. Yang, T. Ogawa, and M. Takahashi, "Challenge of ultra high frequency limit of permeability for magnetic nanoparticle assembly with organic polymer—Application of superparamagnetism," *J. Magn. Magn. Mater.*, vol. 321, no. 7, pp. 746–749, Apr. 2009.
- [3] C. R. Sullivan, D. V. Harburg, J. Qiu, C. G. Levey, and D. Yao, "Integrating magnetics for on-chip power: A perspective," *IEEE Trans. Power Electron.*, vol. 28, no. 9, pp. 4342–4353, Sep. 2013.
- [4] M. Aragchchini et al., "A technology overview of the PowerChip development program," *IEEE Trans. Power Electron.*, vol. 28, no. 9, pp. 4182–4201, Sep. 2013.
- [5] R. J. Kaplar, J. C. Neely, D. L. Huber, and L. J. Rashkin, "Generation-after-next power electronics: Ultrawide-bandgap devices, high-temperature packaging, and magnetic nanocomposite materials," *IEEE Power Electron. Mag.*, vol. 4, no. 1, pp. 36–42, Mar. 2017.
- [6] J. M. Silveyra, E. Ferrara, D. L. Huber, and T. C. Monson, "Soft magnetic materials for a sustainable and electrified world," *Science*, vol. 362, no. 6413, Oct. 2018, Art. no. eaao0195.
- [7] E. A. Périgo, B. Weidenfeller, P. Kollár, and J. Füzér, "Past, present, and future of soft magnetic composites," *Appl. Phys. Rev.*, vol. 5, no. 3, Sep. 2018, Art. no. 031301.
- [8] F. Bødker, S. Mørup, and S. Linderøth, "Surface effects in metallic iron nanoparticles," *Phys. Rev. Lett.*, vol. 72, no. 2, pp. 282–285, Jan. 1994.
- [9] S. Bedanta and W. Kleemann, "Supermagnetism," *J. Phys. D, Appl. Phys.*, vol. 42, no. 1, Jan. 2009, Art. no. 013001.
- [10] V. Singh, M. S. Seehra, and J. Bonevich, "AC susceptibility studies of magnetic relaxation in nanoparticles of Ni dispersed in silica," *J. Appl. Phys.*, vol. 105, no. 7, Apr. 2009, Art. no. 07B518.
- [11] P.-J. Hsu, C.-B. Wu, H.-Y. Yen, S.-S. Wong, W.-C. Lin, and M.-T. Lin, "Electronically patterning through one-dimensional nanostripes with high density of states on single-crystalline Al₂O₃ domain," *Appl. Phys. Lett.*, vol. 93, no. 14, Oct. 2008, Art. no. 143104.
- [12] W.-C. Lin et al., "Nanoscale magnetic configurations of supported Fe nanoparticle assemblies studied by scanning electron microscopy with spin analysis," *Phys. Rev. B, Condens. Matter*, vol. 80, no. 2, Jul. 2009, Art. no. 024407.
- [13] W.-C. Lin et al., "Coverage dependence of magnetic domain structure and magnetic anisotropy in supported Fe nanoparticles on Al₂O₃/NiAl(100)," *J. Appl. Phys.*, vol. 108, no. 3, Aug. 2010, Art. no. 034312.
- [14] D. Miu, S. I. Jinga, B. S. Vasile, and L. Miu, "Out of plane superferromagnetic behavior of quasi two-dimensional Fe/Al₂O₃ multilayer nanocomposites," *J. Appl. Phys.*, vol. 117, no. 7, Feb. 2015, Art. no. 074303.
- [15] S. Bedanta, O. Petravic, and W. Kleemann, "Supermagnetism," in *Handbook of Magnetic Materials*, vol. 23, K. H. J. Buschow, Ed. Amsterdam, The Netherlands: Elsevier, 2015, pp. 1–83.
- [16] W.-C. Lin, H.-Y. Chang, Y.-C. Hu, and C.-C. Kuo, "Dimensionality control and magnetism of Fe on nanopatterned Au(111) surface," *IEEE Trans. Magn.*, vol. 45, no. 10, pp. 4037–4040, Oct. 2009.
- [17] T. R. Albrecht et al., "Bit-patterned magnetic recording: Theory, media fabrication, and recording performance," *IEEE Trans. Magn.*, vol. 51, no. 5, May 2015, Art. no. 0800342.
- [18] Y. Chen and S. Xiong, "Directed self-assembly of block copolymers for sub-10 nm fabrication," *Int. J. Extreme Manuf.*, vol. 2, no. 3, Aug. 2020, Art. no. 032006.
- [19] C. Cummins, G. Pino, D. Mantione, and G. Fleury, "Engineering block copolymer materials for patterning ultra-low dimensions," *Mol. Syst. Des. Eng.*, vol. 5, no. 10, pp. 1642–1657, Dec. 2020.
- [20] C. Kittel, "On the theory of ferromagnetic resonance absorption," *Phys. Rev.*, vol. 73, no. 2, pp. 155–161, Jan. 1948.
- [21] W. F. Brown, "Thermal fluctuations of a single-domain particle," *Phys. Rev.*, vol. 130, no. 5, pp. 1677–1686, Jun. 1963.
- [22] A. Lyberatos and R. W. Chantrell, "Thermal fluctuations in a pair of magnetostatically coupled particles," *J. Appl. Phys.*, vol. 73, no. 10, pp. 6501–6503, May 1993.
- [23] A. Vansteenkiste, J. Leliaert, M. Dvornik, M. Helsen, F. Garcia-Sanchez, and B. Van Waeyenberge, "The design and verification of MuMax³," *AIP Adv.*, vol. 4, no. 10, Oct. 2014, Art. no. 107133.
- [24] H. Min, R. D. McMichael, M. J. Donahue, J. Miltat, and M. D. Stiles, "Effects of disorder and internal dynamics on vortex wall propagation," *Phys. Rev. Lett.*, vol. 104, no. 21, May 2010, Art. no. 217201.
- [25] M. Respaud et al., "High-frequency ferromagnetic resonance on ultra-fine cobalt particles," *Phys. Rev. B, Condens. Matter*, vol. 59, no. 6, pp. R3934–R3937, Feb. 1999.
- [26] J. Kötzler, D. Görlitz, and F. Wiekhorst, "Strong spin-orbit-induced Gilbert damping and *g*-shift in iron-platinum nanoparticles," *Phys. Rev. B, Condens. Matter*, vol. 76, no. 10, Sep. 2007, Art. no. 104404.
- [27] B. K. Kuan et al., "Frequency and field dependent dynamic properties of CoFe_{2-x}Al_xO₄ ferrite nanoparticles," *Mater. Res. Bull.*, vol. 76, pp. 22–27, Apr. 2016.
- [28] V. Sharma, J. Saha, S. Patnaik, and B. K. Kuan, "Synthesis and characterization of yttrium iron garnet (YIG) nanoparticles—Microwave material," *AIP Adv.*, vol. 7, no. 5, May 2017, Art. no. 056405.
- [29] V. Barsan and V. Kuncser, "Exact and approximate analytical solutions of Weiss equation of ferromagnetism and their experimental relevance," *Phil. Mag. Lett.*, vol. 97, no. 9, pp. 359–371, Sep. 2017.
- [30] G. N. Kakazei et al., "In-plane and out-of-plane uniaxial anisotropies in rectangular arrays of circular dots studied by ferromagnetic resonance," *J. Appl. Phys.*, vol. 93, no. 10, pp. 8418–8420, May 2003.
- [31] G. N. Kakazei et al., "Large four-fold magnetic anisotropy in two-dimensional modulated Ni₈₀Fe₂₀ films," *Appl. Phys. Lett.*, vol. 107, no. 23, Dec. 2015, Art. no. 232402.
- [32] R. Verba, G. Melkov, V. Tiberkevich, and A. Slavin, "Collective spin-wave excitations in a two-dimensional array of coupled magnetic nanodots," *Phys. Rev. B, Condens. Matter*, vol. 85, no. 1, Jan. 2012, Art. no. 014427.
- [33] G. Bertotti, C. Serpico, and I. D. Mayergoyz, "Nonlinear magnetization dynamics under circularly polarized field," *Phys. Rev. Lett.*, vol. 86, no. 4, pp. 724–727, Jan. 2001.
- [34] C. Serpico, M. d'Aquino, A. Quercia, S. Perna, and I. D. Mayergoyz, "Transient chaos in nanomagnets subject to elliptically polarized AC applied fields," *IEEE Trans. Magn.*, vol. 55, no. 2, Feb. 2019, Art. no. 4300305.
- [35] V. Tsiantos, W. Scholz, D. Suess, T. Schrefl, and J. Fidler, "The effect of the cell size in Langevin micromagnetic simulations," *J. Magn. Magn. Mater.*, vols. 242–245, pp. 999–1001, Apr. 2002.
- [36] E. Martínez, L. López-Díaz, L. Torres, and C. J. García-Cervera, "Minimizing cell size dependence in micromagnetics simulations with thermal noise," *J. Phys. D, Appl. Phys.*, vol. 40, no. 4, pp. 942–948, Feb. 2007.
- [37] M. B. Hahn, "Temperature in micromagnetism: Cell size and scaling effects of the stochastic Landau-Lifshitz equation," *J. Phys. Commun.*, vol. 3, no. 7, Jul. 2019, Art. no. 075009.
- [38] J. Leliaert, J. Mulkers, J. De Clercq, A. Coene, M. Dvornik, and B. Van Waeyenberge, "Adaptively time stepping the stochastic Landau-Lifshitz-Gilbert equation at nonzero temperature: Implementation and validation in MuMax³," *AIP Adv.*, vol. 7, no. 12, Dec. 2017, Art. no. 125010.

High-frequency magnetic response of crystalline and nanocrystalline antiferromagnetic NiO

Cite as: AIP Advances 14, 025222 (2024); doi: 10.1063/9.0000781

Submitted: 3 October 2023 • Accepted: 5 January 2024 •

Published Online: 12 February 2024



Kacper Brzuszek,¹  Caroline A. Ross,²  and Andrzej Janutka^{1,a)} 

AFFILIATIONS

¹Department of Theoretical Physics, Wrocław University of Science and Technology, 50-370 Wrocław, Poland

²Department of Materials Science and Engineering, Massachusetts Institute of Technology, Cambridge, Massachusetts 02139, USA

Note: This paper was presented at the 68th Annual Conference on Magnetism and Magnetic Materials.

^{a)}Author to whom correspondence should be addressed: Andrzej.Janutka@pwr.edu.pl

ABSTRACT

Performing micromagnetic simulations, we study the efficiency of response of bulk and polycrystalline nickel oxide (NiO) to high-frequency (up to 100 GHz) magnetic fields with relevance to potential application of the antiferromagnet as a core material to high-frequency coils and resonators. NiO is advantageous due to its insulating property and high Néel temperature. Though the dynamical susceptibility of the antiferromagnet is low, the achievable product of susceptibility and frequency (“performance factor”) appears to be relatively high, comparable to that of previously considered superferromagnetic systems. This makes NiO a potential core material for operating at extremely-high (sub-THz) frequency. The influence of thermal fluctuations on the susceptibility is estimated to be weak up to room temperature even for a nanocrystalline antiferromagnet, whereas, the magnetic response is linear for much wider ranges of frequencies and field amplitudes than for ferromagnetic and superferromagnetic systems.

© 2024 Author(s). All article content, except where otherwise noted, is licensed under a Creative Commons Attribution (CC BY) license (<http://creativecommons.org/licenses/by/4.0/>). <https://doi.org/10.1063/9.0000781>

I. INTRODUCTION

Antiferromagnets (AFs) have zero magnetostatic field and their magnetic resonance is in the THz range. Next to THz spintronic applications,^{1,2} interest in an enhanced sub-THz and THz magnetic response is related to chip-to-chip or to-chip wireless power transfer (WPT). Operating at sub-THz range allows for miniaturization of WPT systems relative to RF-based systems.^{3,4} In the THz WPT area, much attention has been focused on controlling radiation via metamaterial based devices (superlenses and shields).^{5–7} With relevance to designing metamaterials, coupling split-ring resonators to AFs has been investigated.^{8,9} A technique of efficient non-radiative transmission called magnetic coupling resonant WPT (MCR-WPT) uses inductive coils coupled to the transmitter and to the receiver.¹⁰ The efficiency of MCR-WPT can be additionally improved via including magnetic cores into the coils.¹¹ At certain levels of miniaturization, the core material has to operate at a sub-THz range of frequencies, which draws our attention to AFs. We also consider the concept of converting electrical power on-chip using magnetic-core inductors or transformers. The smaller the device the higher the operating

frequency has to be in order to compensate for the small value of the magnetic flux. Typically the GHz frequency of the ferromagnetic resonance provides a frequency limitation on use of the ferromagnets or ferromagnet-based composites as core materials. For AFs, the ultimate frequency is shifted up to sub-THz.

Operating ferromagnetic materials at high frequency leads to a fast increase of the eddy-current loss with frequency, which led to the interest in resistive superferromagnets and superparagnets for use as core materials.^{12–15} In AFs, domain wall motion is not driven by an external field and AFs are insulators in the Mott phase. As well as having high electrical resistivity, AFs are advantageous because of their low hysteresis area, thus, low hysteresis loss. The aim of the present paper is numerical determination of the magnetic response of an insulating AF to a sub-THz frequency field of a relatively-high amplitude, thus, verification of its applicability as core material. Although, the total magnetic moment of AFs is zero and inducing significant magnetization requires the application of a high field, operating with several orders of magnitude higher frequency than is usual for ferromagnetic cores can possibly compensate for the lower induced magnetization by enabling a high inductive voltage.

In particular, we consider nickel mono-oxide, a widely studied AF whose major advantage is its high Néel temperature (well above the room temperature) $T_N = 523$ K. An AF core could possibly be made of macroscopic crystals or of nanocrystals. In the first case, the antiferromagnetic-domain structure is determined by crystal defects (dislocations) which are accompanied by AF domain walls.¹⁶ Thus, the domain structure of NiO is durable against the magnetic field application. On the other hand, considering nanocrystalline AF cores, we note that the nanocrystals of NiO can be monodomain AF particles provided they are sufficiently large to neglect some reordering at the nanocrystal surface.¹⁷ Because of the strong inter-sublattice exchange, the energy of the inter-sublattice exchange of such nanocrystals is much higher than thermal energy. Thus, unlike for nanosized ferromagnets, thermal fluctuation effect on the antiferromagnetism in nanocrystals is expected to be suppressed. Also, the energy of the single-ion anisotropy in AF NiO is high compared to thermal energy. Therefore, we propose a common description of the magnetic response from monocrystalline and nanocrystalline NiO, treating the AF domains as separate magnetic particles.

The major characteristics determining the efficiency of magnetic materials in terms of the ability of inducing the electromotive force (for energy-conversion applications) is the product of frequency and the response-function amplitude called “performance factor”.¹⁸ Due to very strong fields of the single-ion anisotropy and of the inter-sublattice exchange, the magnetic response of AFs is linear in a wide range of amplitude of the driving-field and the performance factor is well determined. Based on our previous analysis of efficiency of the response of MNP systems to high-frequency magnetic fields,^{19,20} we perform a comparison of achievable performance factors, showing values obtainable for NiO to be relatively high, thus, claiming AFs to be of potential interest with regard to the on-chip conversion of power.

The micromagnetic model of NiO-like AF is formulated in Sec. II and the results of its application to driven magnetization oscillations of NiO are presented and summarized in Sec. III.

II. MODEL

Consider a single AF domain or AF particle. Let us denote the sublattice magnetization vectors by $\mathbf{M}_1 = M\mathbf{m}_1$, $\mathbf{M}_2 = M\mathbf{m}_2$, where $M = M(T)$ and $|\mathbf{m}_1| = |\mathbf{m}_2| = 1$. The temperature dependence of the sublattice magnetization is taken in the form²¹ $M(T) = M_0(1 + T/2T_N)\sqrt{1 - T/T_N}$, with $M_0 = 550$ kA/m. Also, let us define (renormalized) magnetization $\mathbf{m} \equiv (\mathbf{m}_1 + \mathbf{m}_2)/2$ and Néel vector $\mathbf{l} \equiv (\mathbf{m}_1 - \mathbf{m}_2)/2$. The macroscopic model of two-sublattice AF relevant to a series of fcc-lattice oxides like NiO and MnO is based on the Hamiltonian density of magnetic subsystem $\mathcal{H} = \mathcal{H}_{ex} + \mathcal{H}_{an} + \mathcal{H}_Z$;

$$\begin{aligned} \mathcal{H}_{ex} &= A_1|\mathbf{m}|^2 + A_2\sum_{i=1}^3\left|\frac{\partial\mathbf{l}}{\partial x_i}\right|^2 = \frac{A_1}{2}(1 + \mathbf{m}_1 \cdot \mathbf{m}_2) \\ &+ \frac{A_2}{4}\sum_{i=1}^3\left(\left|\frac{\partial\mathbf{m}_1}{\partial x_i}\right|^2 + \left|\frac{\partial\mathbf{m}_2}{\partial x_i}\right|^2 - 2\frac{\partial\mathbf{m}_1}{\partial x_i}\frac{\partial\mathbf{m}_2}{\partial x_i}\right), \\ \mathcal{H}_{an} &= K_1[(\mathbf{m}_1 \cdot \mathbf{n})^2 + (\mathbf{m}_2 \cdot \mathbf{n})^2] + K_2\left[\prod_{i=1}^3(\mathbf{m}_1 \cdot \mathbf{n}_i)^2\right. \\ &\left. + \prod_{i=1}^3(\mathbf{m}_2 \cdot \mathbf{n}_i)^2\right], \mathcal{H}_Z = -2M\mathbf{m} \cdot \mathbf{B}. \end{aligned} \quad (1)$$

Here \mathbf{B} denotes an external field. The normal to the easy plane \mathbf{n} is one of the set $(1, 1, 1)/\sqrt{3}$, $(-1, 1, 1)/\sqrt{3}$, $(1, -1, 1)/\sqrt{3}$, $(1, 1, -1)/\sqrt{3}$. The three easy directions \mathbf{n}_1 , \mathbf{n}_2 , \mathbf{n}_3 lie in the easy plane and they deviate from each other by an angle of 120° .

In the effective fields on the sublattices

$$\mathbf{B}_{eff;1(2)} \equiv -\frac{\delta\mathcal{H}}{M\delta\mathbf{m}_{1(2)}} \equiv \mathbf{B}_{eff;1(2)}^{ex} + \mathbf{B}_{eff;1(2)}^{an} + \mathbf{B}, \quad (2)$$

the exchange parts take the form

$$\mathbf{B}_{eff;1(2)}^{ex} = \frac{4A_h}{M}\mathbf{m}_{2(1)} + \frac{2A_i}{M}\Delta\mathbf{m}_{1(2)} + \frac{A_{nhi}}{M}\Delta\mathbf{m}_{2(1)}, \quad (3)$$

where constants $A_h = -A_1/8$, $A_i = A_2/4$, $A_{nhi} = -A_2/2$ are written according to the notation of the BORIS package applied for micromagnetic simulations.²² Macroscopic (micromagnetic) parameters for NiO are established based on the microscopic Hamiltonian $\mathcal{H} = \mathcal{H}_{ex} + \mathcal{H}_{an} + \mathcal{H}_Z$;

$$\begin{aligned} \mathcal{H}_{ex} &= J_{NN}\sum_{\langle j,\delta_j \rangle}\hat{\mathbf{s}}_j \cdot \hat{\mathbf{s}}_{j+\delta_j} + J_{NNN}\sum_{\langle j,\delta'_j \rangle}\hat{\mathbf{s}}_j \cdot \hat{\mathbf{s}}_{j+\delta'_j}, \\ \mathcal{H}_{an} &= D_1\sum_j(\hat{\mathbf{s}}_j \cdot \mathbf{n})^2 + D_2\sum_j(\hat{\mathbf{s}}_j \cdot \mathbf{n}_1)^2(\hat{\mathbf{s}}_j \cdot \mathbf{n}_2)^2(\hat{\mathbf{s}}_j \cdot \mathbf{n}_3)^2, \\ \mathcal{H}_Z &= -M\delta V\sum_j\hat{\mathbf{s}}_j \cdot \mathbf{B}. \end{aligned} \quad (4)$$

Here, $J_{NN} = -2210^{-23}$ J and $J_{NNN} = 30510^{-23}$ J are the nearest-neighbor (NN) and next-nearest-neighbor (NNN) exchange integrals,²³ while the single-ion anisotropy constants are given by $D_1 = -38$ μeV and $D_2 = 320$ neV,²⁴ where δV denotes the volume per magnetic ion. The single cell of NiO crystal is visualized in Fig. 1. The numbers of NNs of a given spin which belong the same sublattice is 6 and it is equal to the number of its NN in the second sublattice. The number of NNNs of a given spin is 6 and they belong to another sublattice.^{25,26} The energy of AF exchange interactions between NNNs dominate over the NN interaction energy and the comparison of microscopic Hamiltonian (upon approximating spin

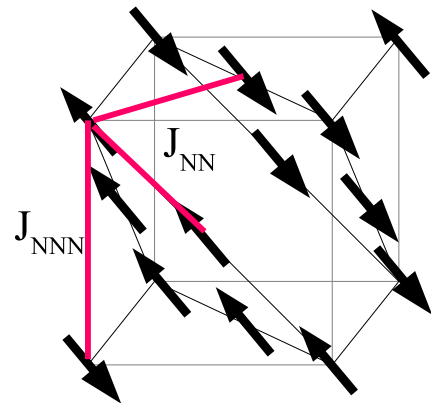


FIG. 1. The single cell of NiO crystal with connections between the nearest and next nearest neighbors indicated with red lines.

with classical vectors) to the macroscopic Hamiltonian leads us to the estimations

$$\begin{aligned}\frac{A_1}{2} &= -4A_h = \frac{6J_{NN}}{(a/\sqrt{2})^3} + \frac{6J_{NNN}}{a^3} \approx 25 \cdot 10^7 \text{ J/m}^3, \\ \frac{A_2}{2} &= -A_{nhi} = 2A_i = \frac{6J_{NN}}{a/\sqrt{2}} + \frac{6J_{NNN}}{a} \approx 4.4 \cdot 10^{-11} \text{ J/m}.\end{aligned}\quad (5)$$

In a similar way, we compare the quantum and classical anisotropy Hamiltonians and we evaluate $K_{1(2)} = 2D_{1(2)}/a^3$. It should be noted that the spin anisotropy constants for NiO or related Mott insulators is a mixture of magnetic and magneto-elastic contributions. At high frequencies and high amplitude of the sublattice magnetization oscillations (due to a strong driving field), the magneto-elastic coupling induces dynamical strain which is not relaxing during oscillation cycles. Therefore, the effective magnetic anisotropy model relevant to fast dynamics is different than the one considered for the slow dynamics description, for instance, the description of domain wall creation and domain-wall motion.²⁷ While, the latter requires dealing with simultaneous evolution of the magnetic and elastic degrees of freedom, in the former, the magnetic evolution is studied separately via averaging the lattice oscillations.

In order to implement the model to the micromagnetic (BORIS) package, it is important to express the anisotropy energy using only three constant vectors and a little algebra leads us to

$$\begin{aligned}\mathcal{H}_{an} &= 2K_1 - \frac{2}{3}K_1 \sum_{i=1}^3 [(m_1 \cdot n_i)^2 + (m_2 \cdot n_i)^2] \\ &+ K_2 \left[\prod_{i=1}^3 (m_1 \cdot n_i)^2 + \prod_{i=1}^3 (m_2 \cdot n_i)^2 \right].\end{aligned}\quad (6)$$

Within the stochastic Landau–Lifshitz–Gilbert (sLLG) approach, thermal fluctuations can be included into the considerations of the AF dynamics. By analogy to superferromagnetic systems, thermal fluctuations in AF nanoparticles could be of especial importance for their magnetic response.^{28–30} However, besides larger sizes of

AF nanoparticles than achievable for ferromagnetic nanoparticles, another factor makes thermal fluctuations negligible. We show that, unlike for typical ferromagnetic nanoparticles, the thermal energy is low compared to the exchange energy as well as to the magnetic anisotropy energy of AF nanocrystals of NiO. In particular, considering (for estimation purposes) as small AF nanocrystal of NiO as $5 \times 5 \times 5 \text{ nm}^3$ (denoting the particle volume with V), one finds characteristic switching temperatures $K_1 V/k_B = 1450 \text{ K}$ and $4|A_h|V/k_B = 2.210^6 \text{ K}$. In fact, real nanocrystals have to be considerably larger to be considered as AFs (of sufficiently large volume to surface ratio), thus, their magnetic states are even better protected against thermal fluctuations.¹⁷ The only macroscopic effect of temperature is its influence on the value of the sublattice magnetization.^{31,32}

The high value of the AF exchange field raises a problem when implementing micromagnetic code. One of the exchange lengths of AF is $l_{ex}^{AF} \equiv \sqrt{A_2/A_1} = \sqrt{-A_i/2A_h}$. For NiO, we establish $l_{ex}^{AF} = 0.42 \text{ nm}$, thus, the exchange length is equal to the lattice constant, which makes the micromagnetic approach to the ordering inhomogeneity invalid. The requirement of the summary sublattice macrospin of the computational cell to be high and the requirement of the cell edge not to be larger than the exchange length are contradictory. On the other hand, local inhomogeneities of the magnetization (which is zero except at lattice imperfections) are not expected to strongly influence the magnetic response of the AF system and we finally neglect them putting all the gradient terms in the macroscopic Hamiltonian as zero, $A_2 = 4A_i = -2A_{nhi} = 0$. Hence, we restrict the problem to homogeneous magnetization oscillations (AFMR) in a system of many AF nanocrystals or domains in a bulk AF. According to this simplification, any domain or nanocrystal is represented in simulations as a single computational cell. Let us emphasize that we simulate AF below the frequency of the spin-wave gap.

Measurements of the Gilbert damping constant for NiO have been reported in Ref. 31. They indicate the damping constant to be very low $\sim 10^{-4}$. Taking into account possible structure imperfections (especially present in polycrystalline materials), following,²⁴

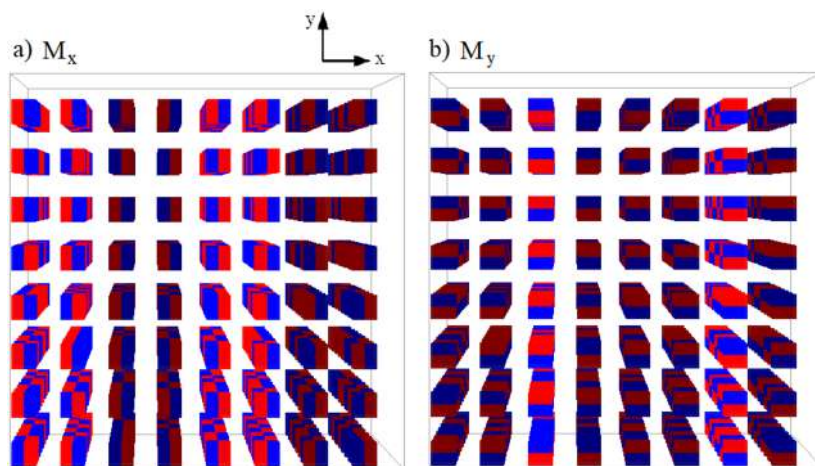


FIG. 2. Spatial distribution of magnetization components of the simulated system of single-domain particles, which are treated as isolated computational cells. Color intensities (from red to blue) correspond to the projection of macrospin of the (a) left or right and (b) upper or lower sublattices onto x -axis and y -axis, correspondingly.

we perform numerical simulations for the damping constant of $\alpha = 0.005$ which is a much higher value than reported for perfect NiO, while, being relatively small compared to those of metallic ferromagnets.

III. RESULTS AND CONCLUSION

We generate a number of isolated cubic cells and, for each cell, we draw one of four possible easy planes. For a given sublattice-plane direction, the axes of in-plane anisotropy are uniquely determined by the cell corners. The relaxed magnetization state is visualized in Fig. 2. We simulate numerically the application of a linearly-polarized driving field $\mathbf{B}(t) = [0, B \sin(2\pi\nu t), 0]$ to the system of many single-cell domains. The longitudinal (with respect to the driving field) component of the magnetization $M_y = M_{1y} + M_{2y}$ (the response function) is plotted in Figs. 3 and 4 as function of time. The amplitude of oscillations of M_y it found to be a linear function of the field amplitude B in a reasonably-wide range of the field (we considered $B = 20 \div 200$ mT), for the frequencies of 10 and 100 GHz. Also, we do not find any noticeable phase shift of the response function relative to the driving field for these frequencies, (100 GHz is one order of magnitude lower than the frequency of AFMR³³), which is desirable with respect to avoiding hysteresis loss.

Following Figs. 3 and 4, we evaluate the susceptibility $\chi = \mu_0 \text{Amp}(M_y)/B (= 0.22 \text{ mT}/200 \text{ mT}) = 1.110^{-3}$, where $\text{Amp}(M_y)$ denotes the amplitude of the response function. Though this value is low, it is constant up to the frequency of 100 GHz and almost constant up to room temperature.^{32,34} Thus, achievable performance factor takes the value $\nu\chi = 1.110^8 \text{ s}^{-1}$ at least. It is comparable to that predicted for a superparamagnetic system with susceptibility $\chi \sim 1$ at the driving-field amplitude $B = 20$ mT which can be efficiently operated at the frequencies up to $\nu \sim 0.1$ GHz, however, beyond the linear response regime.²⁰

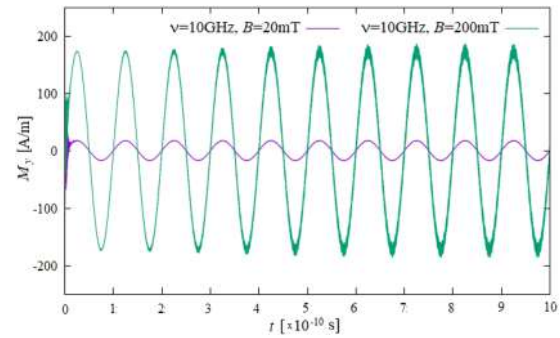


FIG. 3. Time dependence of magnetization component parallel to the linearly-polarized driving field of amplitude 20 mT (purple line) and 200 mT (green line) at frequency 10 GHz.

Besides driving with a simple linearly-polarized AC field, we have tested the application of a rotating field to driving the AF system. For similar values of the frequency and field amplitude, we obtained almost the same amplitudes of the response function as for the driving with both the linearly-polarized and rotating fields, unlike for ferromagnetic and superferromagnetic systems.¹⁹ Also, we have tested additional application of a DC field perpendicular to the driving (linear or rotating) field, which is a way of influencing the magnetic response in superparamagnetic systems, according to Ref. 20. This way also did not appear to be efficient in terms of increasing the amplitude of the response function of NiO.

Summarizing, we state that the predicted response of an AF insulator to a sub-THz field is relevant to spintronic and power transfer applications of these materials. This is due to its high performance factor and the natural insulating property present without any structural engineering.

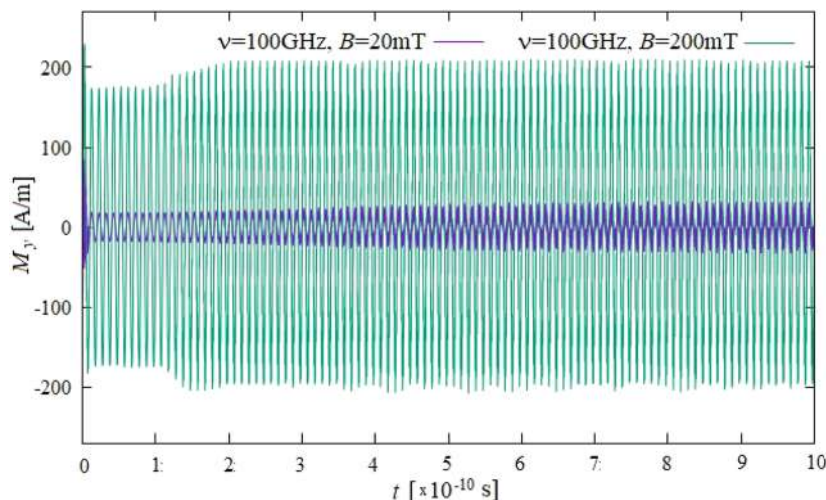


FIG. 4. Time dependence of magnetization component parallel to the linearly-polarized driving field of amplitude 20 mT (purple line) and 200 mT (green line) at frequency 100 GHz.

ACKNOWLEDGEMENTS

The authors acknowledge support of a MISTI-Poland award from MIT.

AUTHOR DECLARATIONS

Conflict of Interest

The authors have no conflicts to disclose.

Author Contributions

Kacper Brzuszek: Investigation (equal); Software (lead); Writing – original draft (supporting). **Caroline A. Ross:** Conceptualization (supporting); Project administration (equal); Writing – review & editing (equal). **Andrzej Janutka:** Conceptualization (lead); Investigation (equal); Methodology (lead); Project administration (equal); Supervision (lead); Writing – original draft (lead); Writing – review & editing (equal).

DATA AVAILABILITY

The data that support the findings of this study are available within the article.

REFERENCES

- V. Baltz, A. Manchon, M. Tsoi, T. Moriyama, T. Ono, and Y. Tserkovnyak, “Antiferromagnetic spintronics,” *Rev. Mod. Phys.* **90**(1), 015005 (2018).
- T. Jungwirth, J. Sinova, A. Manchon, X. Marti, J. Wunderlich, and C. Felser, “The multiple directions of antiferromagnetic spintronics,” *Nature Phys.* **14**, 200 (2018).
- H. Dang-ba and G.-S. Byun, “A sub-THz wireless power transfer for non-contact wafer-level testing,” *Electronics* **9**(8), 1210 (2020).
- N. Shinohara, “Trends in wireless power transfer: WPT Technology for energy harvesting, millimeter-wave/THz rectennas, MIMO-WPT, and advances in near-field WPT applications,” *IEEE Microwave Magazine* **22**(1), 46–59 (2021).
- T. J. Yen *et al.*, “Terahertz magnetic response from artificial materials,” *Science* **303**(5663), 1494–1496 (2004).
- C. Rong *et al.*, “A critical review of metamaterial in wireless power transfer system,” *IET Power Electronics* **14**(9), 1541 (2021).
- J. Zhou, P. Zhang, J. Han, L. Li, and Y. Huang, “Metamaterials and metasurfaces for wireless power transfer and energy harvesting,” *Proc. IEEE* **110**(1), 31–55 (2022).
- Y. Mukai, H. Hirori, T. Yamamoto, H. Kageyama, and K. Tanaka, “Nonlinear magnetization dynamics of antiferromagnetic spin resonance induced by intense terahertz magnetic field,” *New J. Phys.* **18**(1), 013045 (2016).
- D. M. Heligman and R. V. Aguilar, “Numerical simulation of the coupling between split-ring resonators and antiferromagnetic magnons,” arxiv.org/abs/2109.05086 (2021).
- A. Kurs, A. Karalis, R. Moffatt, J. D. Joannopoulos, P. Fisher, and M. Soljačić, “Wireless power transfer via strongly coupled magnetic resonances,” *Science* **317**(5834), 83–86 (2007).
- D. Wang *et al.*, *Nanomaterials* **12**(20), 3662 (2022).
- C. R. Sullivan, D. V. Harburg, J. Qiu, C. G. Levey, and D. Yao, “Integrating magnetics for on-chip power: A perspective,” *IEEE Trans. Power Electron.* **28**(9), 4342–4353 (2013).
- R. J. Kaplar, J. C. Neely, D. L. Huber, and L. J. Rashkin, “Generation-after-next power electronics: Ultrawide-bandgap devices, high-temperature packaging, and magnetic nanocomposite materials,” *IEEE Power Electron. Mag.* **4**(1), 36–42 (2017).
- D. Hasegawa, H. Yang, T. Ogawa, and M. Takahashi, “Challenge of ultra high frequency limit of permeability for magnetic nanoparticle assembly with organic polymer—Application of superparamagnetism,” *Journal of Magnetism and Magnetic Materials* **321**, 746–749 (2009).
- M. Kin, H. Kura, and T. Ogawa, “Core loss and magnetic susceptibility of superparamagnetic Fe nanoparticle assembly,” *AIP Advances* **6**(12), 125013 (2016).
- N. B. Weber, H. Ohldag, H. Gomonaj, and F. U. Hillebrecht, “Magnetostrictive domain walls in antiferromagnetic NiO,” *Phys. Rev. Lett.* **91**(23), 237205 (2003).
- A. C. Gandhi, H.-Y. Cheng, Y.-M. Chang, and J. G. Lin, “Size confined magnetic phase in NiO nanoparticles,” *Mater. Res. Express* **3**(3), 035017 (2016).
- A. J. Hanson, J. A. Belk, S. Lim, C. R. Sullivan, and D. J. Perreault, “Measurements and performance factor comparisons of magnetic materials at high frequency,” *IEEE Transactions on Power Electronics* **31**(11), 7909–7925 (2016).
- K. Brzuszek and A. Janutka, “High-frequency magnetic response of superferromagnetic nanocomposites,” *Journal of Magnetism and Magnetic Materials* **543**, 168608 (2022).
- K. Brzuszek, C. A. Ross, and A. Janutka, “High-frequency magnetic response of superparamagnetic composites of spherical Fe₆₅Co₃₅ nanoparticles,” *Journal of Magnetism and Magnetic Materials* **573**, 170651 (2023).
- V. Barsan and V. Kuncser, “Exact and approximate analytical solutions of Weiss equation of ferromagnetism and their experimental relevance,” *Philosophical Magazine Letters* **97**(9), 359 (2017).
- See <http://www.boris-spintronics.uk/>.
- M. T. Hutchings and E. J. Samuelsen, “Measurement of spin-wave dispersion in NiO by inelastic neutron scattering and its relation to magnetic properties,” *Phys. Rev. B* **6**(9), 3447–3461 (1972).
- T. Chirac, J.-Y. Chauveau, P. Thibaudeau, O. Gomonay, and M. Viret, “Ultrafast antiferromagnetic switching in NiO induced by spin transfer torques,” *Phys. Rev. B* **102**(13), 134415 (2020).
- I. V. Solov'yev, “Exchange interactions and magnetic force theorem,” *Phys. Rev. B* **103**(10), 104428 (2021).
- M. Hafez-Torbati, F. B. Anders, and G. S. Uhrig, “Simplified approach to the magnetic blue shift of Mott gaps,” *Phys. Rev. B* **106**(20), 205117 (2022).
- O. Gomonay and D. Bossini, “Linear and nonlinear spin dynamics in multi-domain magnetoelastic antiferromagnets,” *J. Phys. D: Appl. Phys.* **54**(37), 374004 (2021).
- B. Ouari, S. Aktaou, and Y. P. Kalmykov, “Reversal time of the magnetization of antiferromagnetic nanoparticles,” *Phys. Rev. B* **81**(2), 024412 (2010).
- Y. L. Raikher and V. I. Stepanov, “Magneto-orientational behavior of a suspension of antiferromagnetic particles,” *J. Phys.: Condens. Matter* **20**(20), 204120 (2008).
- I. S. Poperechny and Y. L. Raikher, “Low-frequency dynamic magnetic susceptibility of antiferromagnetic nanoparticles with superparamagnetic properties,” *Magnetism* **2**(4), 340 (2022).
- T. Moriyama, K. Hayashi, K. Yamada, M. Shima, Y. Ohya, and T. Ono, Intrinsic and extrinsic antiferromagnetic damping in NiO, *Phys. Rev. Materials* **3**(5), 051402 (2019).
- S. Thota, J. H. Shim, and M. S. Seehra, “Size-dependent shifts of the Néel temperature and optical band-gap in NiO nanoparticles,” *Journal of Applied Physics* **114**(21), 214307 (2013).
- Y. Shoji, E. Ohmichi, H. Takahashi, and H. Ohta, “Antiferromagnetic resonance spectroscopy of NiO in the terahertz region,” in *2022 47th International Conference on Infrared, Millimeter and Terahertz Waves (IRMMW-THz)* (Delft, Netherlands, 2022), pp. 1–2.
- G. Srinivasan and M. S. Seehra, “Magnetic susceptibilities, their temperature variation, and exchange constants of NiO,” *Phys. Rev. B* **29**(11), 6295 (1984).

PART III:
SUMMARY

Chapter 5

Summary and general conclusions

Numerical study of the dynamical magnetic response has been carried out using specialized software: Object Oriented Micromagnetic Framework [DN99], MuMAX3 [VLD+; VLD+14] and Boris Computational Spintronics [Lep20; Lep21].

Following materials were simulated:

1. four composites written in form MeDie, where Me designates metallic material constituting nanoparticles, and Die – material of which dielectric matrix consist. These materials were: $\text{Co}_{0.42}(\text{MgF}_2)_{0.58}$, $(\text{Fe}_{65}\text{Co}_{35})_{0.6}(\text{Al}_2\text{O}_3)_{0.4}$, $(\text{Fe}_{65}\text{Co}_{35})_{0.75}(\text{Al}_2\text{O}_3)_{0.25}$ and $(\text{Fe}_{65}\text{Co}_{35})_{0.57}(\text{SiO}_2)_{0.43}$. The simulated system was superferromagnetic array of densely packed cubical nanoparticles;
2. magnetic $\text{Fe}_{65}\text{Co}_{35}$ in a form of array of spherical nanoparticles. There were two systems simulated with difference between them being the distance between nanoparticles. Due to change of this distance, interparticle interaction changed magnitude leading to two different states emerging: superparamagnet and super spin glass;
3. in contrast to previous papers, cubic anisotropy materials were simulated: magnetic Fe and Fe_3O_4 (which has cubic anisotropy above 120 K). Magnetic material was in form of arrays of spherical nanoparticles;
4. magnetic $\text{Fe}_{65}\text{Co}_{35}$ in a form of arrays of flat nanodots. Such a shape induces shape anisotropy in each nanoparticle (what isn't a case in ideal spheres/cubics from previous papers);
5. antiferromagnetic NiO in form of polycrystalline monodomain medium or of nanocrystalites. NiO, thanks to significant exchange and anisotropy energies, is not susceptible to the influence of the thermal field

The conducted studies allowed us possible to evaluate values of amplitude of the magnetic response function (linear and nonlinear dynamical susceptibility) of ideal supermagnetic systems, in the high frequency range, which is difficult to access in measurements.

In the case of superferromagnets, these values turned out to be quite close to those predicted by the analytical description of the ferromagnetic response, although the possibility of deviations was recognized, such as the violation of the Snoek limit on the maximum susceptibility or the nonlinearity of the response to the rotating field.

For superparamagnetic systems, in the expected operating range of magnetic cores – high amplitude of the driving field, the nonlinearity of the dynamical response is a key factor, justifying the need for a numerical approach to describing the response. It is worth noting that efficient micromagnetic simulations of superparamagnetic systems have become possible relatively recently, thanks to the development of methods of micromagnetic simulations including thermal noise, with a variable (adaptive) time step. Only

the latest available versions of micromagnetic computing packages provide such a capability. The same is true in terms of simulations of antiferromagnetic systems, including superantiferromagnetic ones.

For an antiferromagnetic insulator, though the simulations did not show significant nonlinear effects, they made it possible to study the response of a multi-domain system without tediously averaging the response of single-domain antiferromagnets over numerous possible orientations of the spin sublattices.

It seems that employing simulations, the dynamical susceptibility of composite magnetic cores can be significantly optimized. That is important because the fabrication of the magnetic systems under consideration requires the use of complex techniques and it is difficult to be optimized just via performing experiments.

Analysis of the results of micromagnetic simulations of the dynamical response made it possible to evaluate both the amplitudes of the response function and the magnetic power losses. The possible evaluation of power losses on eddy currents is not an universal problem, since the spatial distribution of eddy currents depends on the boundary conditions. It would be necessary to reliably determine the inhomogeneous and frequency-dependent electrical conduction function, which is a separate scientific problem that is not within the scope of the conducted research.

Chapter 6

Acknowledgements

I recognize support from MIT-Poland Lockheed Martin Seed Fund grant named *Magnetic Nanocomposites for Power Conversion*.

Numerical simulations were supported by the Wrocław Center for Networking and Supercomputing, under Grant no 450.

I am grateful to Dr Serban Lepadatu for his help with BORIS package.

I recognize and I am very grateful for the immense feedback and guidance received from my supervisor, dr hab. inż. Andrzej Janutka, prof. PWr.

Cambridge, MA

Prof. Caroline A. Ross

77 Massachusetts Avenue
Cambridge, MA 02139, USA
617-258-0223
caross@mit.edu

Massachusetts Institute of Technology
Department of Materials Science and Engineering

I declare my contribution in following papers:

1. K. Brzuszek, C. A. Ross, and A. Janutka, “High-frequency magnetic response of superparamagnetic composites of spherical $\text{Fe}_{65}\text{Co}_{35}$ nanoparticles,” *Journal of Magnetism and Magnetic Materials*, vol. 573, 170651, 2023; my participation consisted of conceptualization, project administration, writing – review and editing;
2. K. Brzuszek, C. A. Ross, and A. Janutka, “High-frequency magnetic response of arrays of planar $\text{Fe}_{65}\text{Co}_{35}$ nanodots: Effects of bias field and thermal fluctuations,” *IEEE Transactions on Magnetics*, vol. 59, no. 11, 7100306, 2023; my participation consisted of conceptualization, project administration, writing – review and editing;
3. K. Brzuszek, C. A. Ross, and A. Janutka, “High-frequency magnetic response of superparamagnetic composites of spherical Fe and Fe_3O_4 nanoparticles,” *Journal of Magnetism and Magnetic Materials (submitted)*, my participation consisted of conceptualization, project administration, writing – review and editing;
4. K. Brzuszek, C. A. Ross, and A. Janutka, “High-frequency magnetic response of crystalline and nanocrystalline antiferromagnetic NiO,” *AIP Advances (accepted)*, my participation consisted of conceptualization, project administration, writing – review and editing.

Caroline A. Ross

Caroline Ross

Jan. 20, 2024

Andrzej Janutka

ul. Wybrzeże Wyspiańskiego 27
50-370 Wrocław

tel: 510754169
andrzej.janutka@pwr.edu.pl

Politechnika Wrocławska
Wydział Podstawowych Problemów Techniki
Instytut Fizyki Teoretycznej

RADA DYSCYPLINY NAUKOWEJ

nauki fizyczne

OŚWIADCZENIE WSPÓŁAUTORA, KANDYDATA DO STOPNIA DOKTORA

Oświadczam, że w publikacji:

- 1) K. Brzuszek, A. Janutka, 2022, High-frequency magnetic response of superferromagnetic nanocomposites, Journal of Magnetism and Magnetic Materials, vol. 543, 168608

mój udział polegał na: sformułowaniu zagadnienia, opracowaniu metodyki wyznaczania parametrów materiałowych, weryfikacji kodów obliczeniowych, dostosowaniu opisu analitycznego dynamiki ferromagnetyków, przygotowaniu tekstu manuskryptu

- 2) K. Brzuszek, C. A. Ross, A. Janutka, 2023, High-frequency magnetic response of superparamagnetic composites of spherical $\text{Fe}_{65}\text{Co}_{35}$ nanoparticles, Journal of Magnetism and Magnetic Materials, vol. 573, 170651

mój udział polegał na: sformułowaniu zagadnienia, weryfikacji metodyki i kodów obliczeniowych, przygotowaniu tekstu manuskryptu, współkierowaniu projektem naukowym

- 3) K. Brzuszek, C. A. Ross, A. Janutka, 2023, High-Frequency Magnetic Response of Arrays of Planar $\text{Fe}_{65}\text{Co}_{35}$ Nanodots: Effects of Bias Field and Thermal Fluctuations, IEEE Transactions on Magnetics, vol. 59, 7100306

mój udział polegał na: sformułowaniu zagadnienia, weryfikacji metodyki i kodów obliczeniowych, przygotowaniu tekstu manuskryptu, współkierowaniu projektem naukowym

- 4) K. Brzuszek, C. A. Ross, A. Janutka, 2024, High-frequency magnetic response of superparamagnetic composites of spherical Fe and Fe_3O_4 nanoparticle, (w recenzji), SSRN Abstract ID: 4709514; <https://ssrn.com/abstract=4709514>

mój udział polegał na: sformułowaniu zagadnienia, weryfikacji metodyki i kodów obliczeniowych, przygotowaniu tekstu manuskryptu, współkierowaniu projektem naukowym

- 5) K. Brzuszek, C. A. Ross, A. Janutka, 2024, High-frequency magnetic response of crystalline and nanocrystalline antiferromagnetic NiO, (zaakceptowane do AIP Advances)

mój udział polegał na: sformułowaniu zagadnienia, weryfikacji metodyki i kodów obliczeniowych, przygotowaniu tekstu manuskryptu, współkierowaniu projektem naukowym

Wrocław, 29.01.2024

(miejsowość, data)

Andrzej Janutka

(podpis współautora)

PART IV:
APPENDIX

Appendix A

High-frequency magnetic composites

Composite magnetic materials are used for numerous applications both as permanent magnets and dynamically remagnetized materials.

High-temperature resistant permanent magnets are primarily ferrite sinters. Ferrite crystals have relatively low electrical conductivity, and the discontinuous structure of the sinters provides high electrical and thermal resistivities of the bulk material. This property of ferrite sinters is very desirable in technology, despite their inferior magnetic characteristics compared to, for instance, popular neodymium magnets. However, specific sinter structure can provide it with soft-magnetic properties making it a material for transformer cores.

Used in voltage converters (power conversion) in transmission networks are ferromagnetic nanostructured alloys (amorphous alloys), the main advantage of which is narrow magnetic hysteresis loop at high saturation magnetization (the imaginary part of the magnetic permeability is a worse characteristic at relatively low operating frequencies).

Solutions of magnetic particles (ferrite materials) in dielectrics serve as absorbers of electromagnetic radiation. For these materials, the advantages are the large width of dynamical hysteresis loop and the ease of generation of eddy currents at simultaneous high values of the imaginary part of the dielectric permeability. In ferrite-based absorbers, the size of magnetic particles is relatively large (on the order of several hundred nanometers) and domain structure in them is desired, this results in creation of intraparticle eddy currents. The operating range of frequencies corresponds to the vicinity of ferromagnetic resonance, in which the magnetic permeability is essentially imaginary.

Finally, solutions of small ferromagnetic nanoparticles in dielectric matrices (epoxy resin can be used – [LWY18; XSD+14]) are being considered as materials for magnetic cores for high frequency applications (the limitation is the frequency of magnetic resonance). The small size of nanoparticles ensures the absence of internal domain structure. With structurally hard materials for dielectric matrix (e.g. MgO [TEGJ10; UWN+07], SiO₂ [JZW+04], Al₂O₃ [LFL+20; PYL+16; YTHJ13; ZZL+20], MgF₂ [YGZ+10]), dynamical magnetostrictive effects are weakened.

The aspiration of technologists is to isolate each magnetic particle in order to eliminate current flows between particles. When the content of magnetic phase in a nanocomposite is high enough, part of the magnetic ions localize in the matrix and the whole system becomes superferromagnetic, due to exchange interactions. This makes it possible to achieve high values of the real part of the magnetic permeability, especially for nanoparticles of high saturation magnetization. The cost of metal ion content in the matrix is a nonnegligible electrical conductivity. Superferromagnets have been considered for spintronic applications, as materials of high magnetoresistance the source of which is the tunneling

of electrons between nanoparticles through dielectric barriers (matrix). Below a certain threshold of the magnetic phase concentration, the system is superparamagnetic, which is associated with low values of magnetic susceptibility, but with increased electrical resistance.

The material of the magnetic phase (nanoparticles) can be chosen for its price, high saturation magnetization (Fe, Co, FeCo alloys), high electrical resistivity (FeSi), high magnetic permeability (FeNi, ferrites based on NiZn, MnZn, Ba, amorphous alloys - $\text{Fe}_{78}\text{Si}_9\text{B}_{13}$) – [KCT+15; SJ07; ST17; ZWX15].

There is a wide range of methods for producing (nano)magnetic composites as presented in the review papers [GXS+05; PWKF18; SJ07; ST17; TSB+21]. Important problems in the production of composites are

- regular distribution of magnetic nanoparticles, aggregations negatively affect the magnetic response – [HP11; SÁP+06];
- preservation of uniformity of shapes and sizes of nanoparticles – [GLW08; JH21; VWS+15];
- preservation of a constant size distribution of nanoparticles – [JH21];
- possible internal stresses in the composite created during the pressing process. These can be lifted off by annealing the material – [ZWY16].

When discussing ways of manufacturing magnetic nanocomposites, it is important to mention several methods for producing ferromagnetic nanoparticles (nanopowders) with controlled sizes.

- precipitation from particles produced in a chemical reaction ([KLKY17; RESM12; SKK+07]). The size and crystal ordering depend on the reaction temperature. However, the nanoparticles formed are relatively large;
- sol-gel autocombustion method uses an exothermic reaction between a metal salt and a suitable organic fuel ([SMAY14]);
- the method of long-term (from a few hours to more than a week) milling of crystals using balls allows to control the size of nanoparticles by means of milling time and selection (weight) of spheres ([BJM99; CS09; ddM+13; SBA+14]). To counteract oxidation, grinding can be carried out in a noble gas atmosphere;
- deposition of self-organized magnetic nanorods on substrate layers under high vacuum conditions ([HWY+08; LGG+09; LWH+06; LWH+10]). For example, the work [MJVM15] reported alternate deposition of Al_2O_3 and Fe layers on a silicon substrate and yielded nanoparticles with a diameter of 2.5 nm, and therefore very fine, with a magnetic phase content of 6 %.

The synthesis of magnetic nanocomposites can also be carried out by pressing nanopowders.

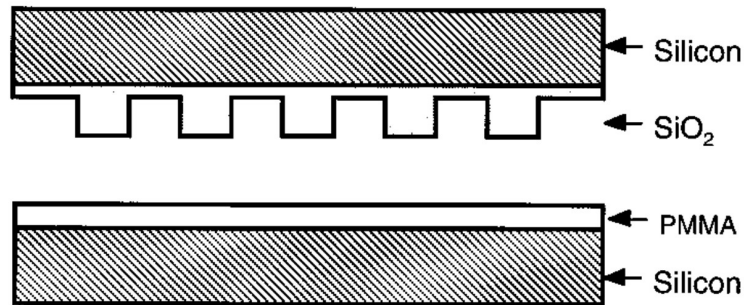
Of particular interest with regard to the present analyses, because they allow the formation of very regular arrays of small magnetic nanoparticles, are lithographic methods: *nanoimprint lithography* and *block-copolymer lithography*.

Nanoimprint lithography (NIL) ([BL16; CKR96; Guo07; Sch08; TLT16; WSL16]) is characterized by [WSL16] low cost, high production speed, and very high resolution (period 10 nm) using, for example, molds of small carbon nanotubes ([HSG+04]). To minimize the effect of air caught in the mold, elastomeric materials can be used, such as poly(dimethylsiloxane) (PDMS) – [BL16]. In the work [CKR95], polymethylmethacrylate (PMMA) was used, while the process (fig. A.1) consists of:

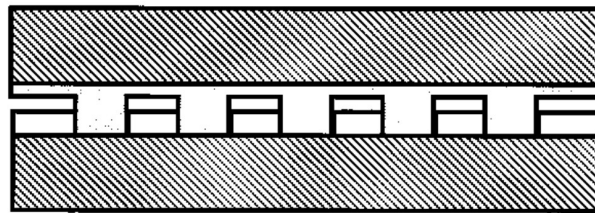
1. heating a thin layer of thermoplastic polymer above the glass transition temperature T_g . For PMMA layers, this is slightly above 100 °C – [PB00];

2. pressing the gouged mold into the liquid PMMA;
3. leaving the mold to cool below T_g ;
4. pulling out the mold and removing the excess PMMA by reactive ion etching (RIE – [Oeh86]), in [CKR96] oxygen was used for this purpose.

1. Initial Setup



2. Nanoimprinting



3. Mold Removal

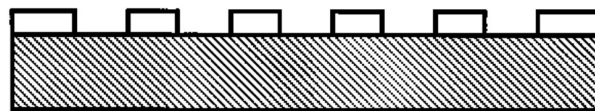


Figure A.1: Schematic representation of the NIL process – [CKR95]

There are numerous variants of this method (using UV or lasers, among others) – these methods are suitable for producing 2D and 2.5D materials ([WSL16]).

Block-copolymer lithography (BCL), ([BMJ+14; HPF03; HR05; NGM13; NM13; TD10; TLF+08]) is a method in which periodic blocks of nanostructures made of two different polymers form spontaneously with a resolution (period) of up to several nanometers ([BF90]).

There are two parameters that determine the interaction between the copolymer phases that form the blocks:

- Flory-Huggins parameter determined by the interaction between the monomers of each phase;
- N – polymerization factor.

Depending on the product χN , there are three regimes of ordering ([BMJ+14]):

$$\chi N \begin{cases} \ll 10.5 & \text{– disorder regime;} \\ \approx 10.5 & \text{– Weak Segregation Limit (WSL);} \\ \gg 10.5 & \text{– Strong Segregation Limit (SSL);} \end{cases}$$

The most favorable regime is the one of strong ordering due to the sharp and clear boundaries [BF90; BMJ+14] as seen in fig. A.2. In both cases, one can see oscillations of the A phase concentration (φ_A) around the global average denoted by f , but nevertheless clear differences in the phase profile are apparent – in SSL, the transition from the A phase-rich zone to the B phase-rich zone is over a short distance, and the function becomes saturated quickly. In WSL, the transition is continuous, and the difference between minimum and maximum is not significant.

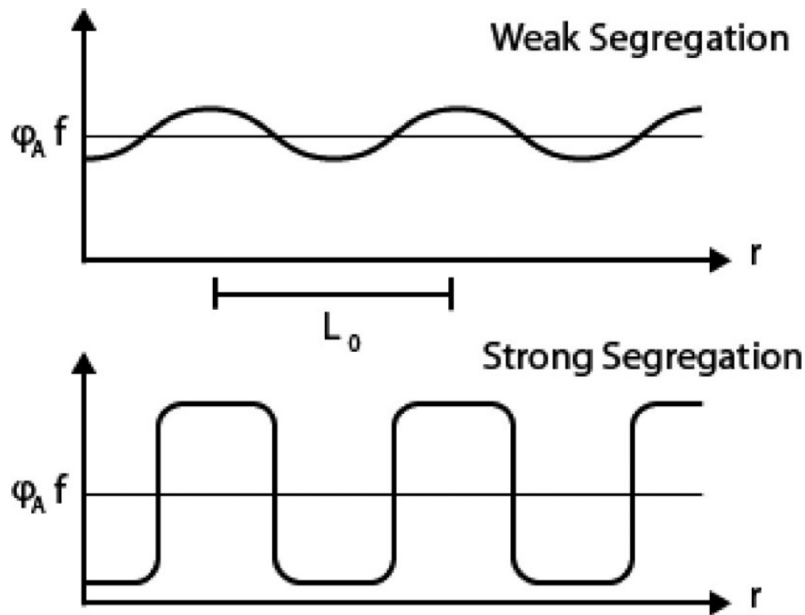


Figure A.2: Concentration (local and global) of A phase in copolymer depending on position – [BF90]

There is quite rich literature treating about blending magnetic nanoparticles into block copolymers: [HBN+23; HZN+10; MOT+17], including whole PhD dissertations: [Ola16; Zho10].

There are two approaches to embedding MNPs in BCP:

- *in situ* – synthesis of nanoparticles occurs within copolymer (e.g. [BJE+14; SYH+12], a method allowing combination of Fe_3O_4 and PMMA was proposed in [AKD+11]), which comes with obvious downside of complicating whole process and losing control of particle sizes and their ordering [HBN+23];
- *ex situ* – pre-synthesized MNPs are added to BCP solution as in [HZN+10].

In that paper alternative method of combining Fe_3O_4 nanoparticles with poly(styrene-*b*-vinylpyridine) (PS-*b*-PVP) is presented – it needs no functionalisation of MNPs surface nor usage of extra ingredients:

- BCPs are dissolved in solvent (usage of tetrahydrofuran is reported) to create low-percentage ($< 3\%$ content);
- then MNPs are added to solution – their mass content is $\leq 10\%$;

- mixture is sonicated and then mixed for 24 h;
- next mixture is filtered through small mesh (0.2 μm) membrane and solution is ready to be deposited;
- filtrate is deposited onto thoroughly cleaned silicone wafer using spin-coating;
- finally solvent vapor annealing is performed in glass chamber filled with 1,4-dioxane or chloroform vapor for up to three days.

Magnetic nanocomposites are materials widely applicable in industry [LSS07; Sen20], voltage conversion [LOM12; SFHM18; SPK21] and electromagnetic radiation absorption [KBF+13; SJ07]. They are potentially applicable in medicine for annealing (cancer) cells using the phenomenon of magnetic hyperthermia, similarly to magnetic fluids [FLD+19; LZW+20; MXL19]. In this dissertation, composites of magnetic particles with ideal shape, size and perfectly periodic dispersion are considered. The closest magnetic nanostructures to such a situation are, produced by NIL and BCL methods, systems for super-dense magnetic recording known as *bit-patterned media* ([AAA+15; TGH+12]).

Bibliography

- [AAA+15] T. R. Albrecht, H. Arora, V. Ayanoor-Vitikkate, et al. “Bit-patterned magnetic recording: Theory, media fabrication, and recording performance”. In: *IEEE Transactions on Magnetism*, vol. 51, no. 5 (2015), pp. 1–42. DOI: 10.1109/TMAG.2015.2397880 (cit. on p. 93).
- [ABC78] R. Alben, J. J. Becker, and M. C. Chi. “Random anisotropy in amorphous ferromagnets”. In: *Journal of Applied Physics*, vol. 49, (1978), pp. 1653–1658. DOI: 10.1063/1.324881 (cit. on p. 12).
- [AD08] O. Acher and S. Dubourg. “Generalization of Snoek’s law to ferromagnetic films and composites”. In: *Phys. Rev. B*, vol. 77, (issue 10, Mar. 2008), p. 104440. DOI: 10.1103/PhysRevB.77.104440 (cit. on p. 17).
- [AKD+11] M. M. Abul Kashem, G. Kaune, A. Diethert, et al. “Selective Doping of Block Copolymer Nanodomains by Sputter Deposition of Iron”. In: *Macromolecules*, vol. 44, no. 6 (2011), pp. 1621–1627. DOI: 10.1021/ma102690b (cit. on p. 92).
- [Ber88] G. Bertotti. “General properties of power losses in soft ferromagnetic materials”. In: *IEEE Transactions on Magnetism*, vol. 24, no. 1 (1988), pp. 621–630. DOI: 10.1109/20.43994 (cit. on p. 9).
- [BF90] F. S. Bates and G. H. Fredrickson. “Block copolymer thermodynamics: theory and experiment”. In: *Annual review of physical chemistry*, vol. 41, no. 1 (1990), pp. 525–557. DOI: 10.1146/annurev.pc.41.100190.002521 (cit. on pp. 91, 92).
- [BJE+14] J. S. Basuki, A. Jacquemin, L. Esser, et al. “A block copolymer-stabilized co-precipitation approach to magnetic iron oxide nanoparticles for potential use as MRI contrast agents”. In: *Polym. Chem.* Vol. 5, (issue 7, 2014), pp. 2611–2620. DOI: 10.1039/C3PY01778H (cit. on p. 92).
- [BJM99] C. Bender Koch, J. Z. Jiang, and S. Mørup. “Mechanical milling of Fe₃O₄/SiO₂: Formation of an amorphous Fe(II)-Si-O-containing phase”. In: *Nanostructured Materials*, vol. 12, no. 1 (1999), pp. 233–236. DOI: 10.1016/S0965-9773(99)00106-3 (cit. on p. 90).
- [BL16] S. Barcelo and Z. Li. “Nanoimprint lithography for nanodevice fabrication”. In: *Nano Convergence*, vol. 3, no. 1 (2016), pp. 1–9. DOI: 10.1186/s40580-016-0081-y (cit. on p. 90).
- [BMJ+14] C. M. Bates, M. J. Maher, D. W. Janes, et al. “Block copolymer lithography”. In: *Macromolecules*, vol. 47, no. 1 (2014), pp. 2–12. DOI: 10.1021/ma401762n (cit. on pp. 91, 92).

- [Bro59] W. F. Brown. “Relaxational behavior of fine magnetic particles”. In: *Journal of Applied physics*, vol. 30, no. 4 (1959), S130–S132. DOI: 10.1063/1.2185851 (cit. on p. 26).
- [Bro63] W. F. Brown. “Thermal Fluctuations of a Single-Domain Particle”. In: *Phys. Rev.* Vol. 130, (issue 5, June 1963), pp. 1677–1686. DOI: 10.1103/PhysRev.130.1677 (cit. on pp. 17, 26).
- [CKR95] S. Y. Chou, P. R. Krauss, and P. J. Renstrom. “Imprint of sub-25 nm vias and trenches in polymers”. In: *Applied physics letters*, vol. 67, no. 21 (1995), pp. 3114–3116. DOI: 10.1063/1.114851 (cit. on pp. 90, 91).
- [CKR96] S. Y. Chou, P. R. Krauss, and P. J. Renstrom. “Nanoimprint lithography”. In: *Journal of Vacuum Science & Technology B: Microelectronics and Nanometer Structures Processing, Measurement, and Phenomena*, vol. 14, no. 6 (1996), pp. 4129–4133. DOI: 10.1116/1.588605 (cit. on pp. 90, 91).
- [Coe10] J. M. D. Coey. *Magnetism and Magnetic Materials*. Cambridge University Press, 2010. DOI: 10.1017/CB09780511845000 (cit. on pp. 13, 15).
- [CRD21] R. Corcolle, X. Ren, and L. Daniel. “Effective properties and eddy current losses of soft magnetic composites”. In: *Journal of Applied Physics*, vol. 129, no. 1 (2021), p. 015103. DOI: 10.1063/5.0031226 (cit. on p. 9).
- [CS09] M. D. Chermahini and H. Shokrollahi. “Milling and subsequent thermal annealing effects on the microstructural and magnetic properties of nanostructured Fe₉₀Co₁₀ and Fe₆₅Co₃₅ powders”. In: *Journal of Alloys and Compounds*, vol. 480, no. 2 (2009), pp. 161–166. DOI: 10.1016/j.jallcom.2009.01.088 (cit. on p. 90).
- [DDF07] M. D. De Sihues, C. Durante-Rincón, and J. Fermin. “A ferromagnetic resonance study of NiFe alloy thin films”. In: *Journal of Magnetism and Magnetic Materials*, vol. 316, no. 2 (2007), e462–e465. DOI: 10.1016/j.jmmm.2007.02.181 (cit. on p. 15).
- [ddM+13] J. F. de Carvalho, S. N. de Medeiros, M. A. Morales, et al. “Synthesis of magnetite nanoparticles by high energy ball milling”. In: *Applied Surface Science*, vol. 275, (2013). NANOSMAT 2012, pp. 84–87. DOI: 10.1016/j.apsusc.2013.01.118 (cit. on p. 90).
- [DN99] M. Donahue and National Institute of Standards and Technology (U.S.) *OOMMF User’s Guide, Version 1.0*. NISTIR; NIST IR; NIST interagency report; NIST internal report, U.S. Department of Commerce, National Institute of Standards and Technology, 1999. DOI: 10.6028/NIST.IR.6376 (cit. on p. 81).
- [DWL+23] R. Das, G.-N. Wei, D. Lordan, et al. “Enhanced soft magnetic properties in N-doped amorphous FeCo thin film”. In: *IEEE Transactions on Magnetics*, (2023). DOI: 10.1109/TMAG.2023.3287682 (cit. on p. 7).
- [FLD+19] F. Fabris, E. Lima, E. De Biasi, et al. “Controlling the dominant magnetic relaxation mechanisms for magnetic hyperthermia in bimagnetic core–shell nanoparticles”. In: *Nanoscale*, vol. 11, (issue 7, 2019), pp. 3164–3172. DOI: 10.1039/C8NR07834C (cit. on p. 93).

- [Fok14] A. D. Fokker. “Die mittlere Energie rotierender elektrischer Dipole im Strahlungsfeld”. In: *Annalen der Physik*, vol. 348, no. 5 (Jan. 1914), pp. 810–820. DOI: 10.1002/andp.19143480507 (cit. on p. 17).
- [FPW16] V. Flovik, B. H. Pettersen, and E. Wahlström. “Eddy-current effects on ferromagnetic resonance: Spin wave excitations and microwave screening effects”. In: *Journal of Applied Physics*, vol. 119, no. 16 (2016), p. 163903. DOI: 10.1063/1.4948302 (cit. on p. 15).
- [GHJM98] L. Gammaitoni, P. Hänggi, P. Jung, et al. “Stochastic resonance”. In: *Rev. Mod. Phys.* Vol. 70, (issue 1, Jan. 1998), pp. 223–287. DOI: 10.1103/RevModPhys.70.223 (cit. on pp. 20, 21).
- [Gil04] T. L. Gilbert. “A phenomenological theory of damping in ferromagnetic materials”. In: *IEEE Transactions on Magnetics*, vol. 40, no. 6 (2004), pp. 3443–3449. DOI: 10.1109/TMAG.2004.836740 (cit. on p. 11).
- [Gil55] T. L. Gilbert. “A Lagrangian formulation of the gyromagnetic equation of the magnetization field”. In: *Physical Review*, vol. 100, no. 4 (Oct. 1955) (cit. on p. 11).
- [GLW08] F. Gazeau, M. Lévy, and C. Wilhelm. “Optimizing magnetic nanoparticle design for nanothermotherapy”. In: *Nanomedicine*, vol. 3, no. 6 (2008). PMID: 19025457, pp. 831–844. DOI: 10.2217/17435889.3.6.831 (cit. on p. 90).
- [Guo07] L. J. Guo. “Nanoimprint lithography: methods and material requirements”. In: *Advanced materials*, vol. 19, no. 4 (2007), pp. 495–513. DOI: 10.1002/adma.200600882 (cit. on p. 90).
- [GXS+05] B. D. Gates, Q. Xu, M. Stewart, et al. “New approaches to nanofabrication: molding, printing, and other techniques”. In: *Chemical reviews*, vol. 105, no. 4 (2005), pp. 1171–1196. DOI: 10.1021/cr030076o (cit. on p. 90).
- [HBN+23] F. Hartmann, M. Bitsch, B.-J. Niebuur, et al. “Self-Assembly of Polymer-Modified FePt Magnetic Nanoparticles and Block Copolymers”. In: *Materials*, vol. 16, no. 16 (2023), p. 5503. DOI: 10.3390/ma16165503 (cit. on p. 92).
- [Her05] G. Herzer. “The Random Anisotropy Model”. In: *Properties and Applications of Nanocrystalline Alloys from Amorphous Precursors*. Ed. by B. Idzikowski, P. Švec, and M. Miglierini. Dordrecht: Springer Netherlands, 2005, pp. 15–34. DOI: 10.1007/1-4020-2965-9_2 (cit. on p. 12).
- [HP11] J. Hári and B. Pukánszky. “8 – Nanocomposites: Preparation, Structure, and Properties”. In: *Applied Plastics Engineering Handbook*. Ed. by M. Kutz. Plastics Design Library, Oxford: William Andrew Publishing, 2011, pp. 109–142. DOI: 10.1016/B978-1-4377-3514-7.10008-X (cit. on p. 90).
- [HPF03] N. Hadjichristidis, S. Pispas, and G. Floudas. *Block Copolymers: Synthetic Strategies, Physical Properties, and Applications*. Wiley, 2003. URL: https://books.google.pl/books?id=RN4L8ifv_2kC (cit. on p. 91).
- [HR05] C. J. Hawker and T. P. Russell. “Block copolymer lithography: Merging “bottom-up” with “top-down” processes”. In: *MRS bulletin*, vol. 30, no. 12 (2005), pp. 952–966. DOI: 10.1557/mrs2005.249 (cit. on p. 91).

- [HSG+04] F. Hua, Y. Sun, A. Gaur, et al. “Polymer imprint lithography with molecular-scale resolution”. In: *Nano letters*, vol. 4, no. 12 (2004), pp. 2467–2471. DOI: 10.1021/nl048355u (cit. on p. 90).
- [HWY+08] P.-J. Hsu, C.-B. Wu, H.-Y. Yen, et al. “Electronically patterning through one-dimensional nanostripes with high density of states on single-crystalline Al₂O₃ domain”. In: *Applied Physics Letters*, vol. 93, no. 14 (2008). DOI: 10.1063/1.2996578 (cit. on p. 90).
- [HWZ+21] Y. He, R. Wu, Z. Zhong, et al. “On-chip coupled solenoid inductors for integrated power conversion”. In: *IEEE Transactions on Electron Devices*, vol. 68, no. 12 (2021), pp. 6292–6295. DOI: 10.1109/TED.2021.3119260 (cit. on p. 7).
- [HZN+10] A. Horechyy, N. E. Zafeiropoulos, B. Nandan, et al. “Highly ordered arrays of magnetic nanoparticles prepared via block copolymer assembly”. In: *J. Mater. Chem.* Vol. 20, (issue 36, 2010), pp. 7734–7741. DOI: 10.1039/C0JM01103G (cit. on p. 92).
- [Iga17] H. Igarashi. “Semi-Analytical Approach for Finite-Element Analysis of Multi-Turn Coil Considering Skin and Proximity Effects”. In: *IEEE Transactions on Magnetics*, vol. 53, no. 1 (2017), pp. 1–7. DOI: 10.1109/TMAG.2016.2601066 (cit. on p. 9).
- [JB18a] A. Janutka and K. Brzuszek. “Domain-wall-assisted asymmetric magnetoimpedance in ferromagnetic nanostripes”. In: *Journal of Physics D: Applied Physics*, vol. 52, (2018). DOI: 10.1088/1361-6463/aae6b4 (cit. on p. 1).
- [JB18b] A. Janutka and K. Brzuszek. “Domain-wall-assisted giant magnetoimpedance of thin-wall ferromagnetic nanotubes”. In: *Journal of Magnetism and Magnetic Materials*, vol. 465, (2018), pp. 437–449. DOI: 10.1016/j.jmmm.2018.06.007 (cit. on p. 1).
- [JB19] A. Janutka and K. Brzuszek. “Double-Vortex-Assisted Asymmetric Magnetoreactance in H-Shaped Nanomagnets”. In: *IEEE Magnetics Letters*, vol. 10, (2019), pp. 1–5. DOI: 10.1109/LMAG.2019.2912964 (cit. on p. 1).
- [JB20] A. Janutka and K. Brzuszek. “Giant magnetoreactance in magnetic nanowires”. In: *Journal of Magnetism and Magnetic Materials*, vol. 515, (2020), p. 167297. DOI: 10.1016/j.jmmm.2020.167297 (cit. on p. 1).
- [JH21] M. Jafari Eskandari and I. Hasanzadeh. “Size-controlled synthesis of Fe₃O₄ magnetic nanoparticles via an alternating magnetic field and ultrasonic-assisted chemical co-precipitation”. In: *Materials Science and Engineering: B*, vol. 266, (2021), p. 115050. DOI: 10.1016/j.mseb.2021.115050 (cit. on p. 90).
- [JZW+04] H. Jiang, W. Zhong, X. Wu, et al. “Direct and alternating current magnetic properties of FeNi particles coated with SiO₂”. In: *Journal of Alloys and Compounds*, vol. 384, no. 1 (2004), pp. 264–267. DOI: 10.1016/j.jallcom.2004.04.078 (cit. on p. 89).

- [KBF+13] P. Kollár, Z. Birčáková, J. Füzér, et al. “Power loss separation in Fe-based composite materials”. In: *Journal of Magnetism and Magnetic Materials*, vol. 327, (2013), pp. 146–150. doi: 10.1016/j.jmmm.2012.09.055 (cit. on pp. 8, 9, 93).
- [KCT+15] A. Krings, M. Cossale, A. Tenconi, et al. “Characteristics comparison and selection guide for magnetic materials used in electrical machines”. In: *2015 IEEE International Electric Machines & Drives Conference (IEMDC)*. 2015, pp. 1152–1157. doi: 10.1109/IEMDC.2015.7409206 (cit. on p. 90).
- [Kit48] C. Kittel. “On the Theory of Ferromagnetic Resonance Absorption”. In: *Phys. Rev.* Vol. 73, (issue 2, Jan. 1948), pp. 155–161. doi: 10.1103/PhysRev.73.155 (cit. on p. 14).
- [Kit51] C. Kittel. “Ferromagnetic resonance”. In: *J. Phys. Radium*, vol. 12, no. 3 (1951), pp. 291–302. doi: 10.1051/jphysrad:01951001203029100 (cit. on p. 14).
- [KLKY17] M. Kishimoto, H. Latiff, E. Kita, et al. “Characterization of FeCo particles synthesized via co-precipitation, particle growth using flux treatment and reduction in hydrogen gas”. In: *Journal of Magnetism and Magnetic Materials*, vol. 432, (2017), pp. 404–409. doi: 10.1016/j.jmmm.2016.12.078 (cit. on p. 90).
- [KM18] C. Kittel and P. McEuen. *Introduction to solid state physics*. John Wiley & Sons, 2018. doi: 10.1119/1.1974177 (cit. on p. 13).
- [KTPT92] E. E. Kriezis, T. D. Tsiboukis, S. M. Panas, et al. “Eddy currents: theory and applications”. In: *Proceedings of the IEEE*, vol. 80, no. 10 (1992), pp. 1559–1589. doi: 10.1109/5.168666 (cit. on p. 9).
- [Lep20] S. Lepadatu. “Boris computational spintronics - High performance multi-mesh magnetic and spin transport modeling software”. In: *Journal of Applied Physics*, vol. 128, (Dec. 2020), p. 243902. doi: 10.1063/5.0024382 (cit. on p. 81).
- [Lep21] S. Lepadatu. *Boris Computational Spintronics User Manual*. Oct. 2021. doi: 10.13140/RG.2.2.31496.88322/1 (cit. on p. 81).
- [LFL+20] F. Luo, X. Fan, Z. Luo, et al. “Microstructure, formation mechanism and magnetic properties of $\text{Fe}_{1.82}\text{Si}_{0.18}@\text{Al}_2\text{O}_3$ soft magnetic composites”. In: *Journal of Magnetism and Magnetic Materials*, vol. 493, (2020), p. 165744. doi: 10.1016/j.jmmm.2019.165744 (cit. on p. 89).
- [LGG+09] W.-C. Lin, Z. Gai, L. Gao, et al. “Nanoscale magnetic configurations of supported Fe nanoparticle assemblies studied by scanning electron microscopy with spin analysis”. In: *Physical Review B*, vol. 80, no. 2 (2009), p. 024407. doi: 10.1103/PhysRevB.80.024407 (cit. on p. 90).
- [LL37] L. Landau and E. Lifshitz. “On the theory of the dispersion of magnetic permeability in ferromagnetic bodies”. In: *Physikalische Zeitschrift der Sowjetunion*, vol. 8, (1937), pp. 153–169. doi: 10.1016/B978-0-08-036364-6.50008-9 (cit. on p. 11).

- [LOM12] A. Leary, P. Ohodnicki, and M. McHenry. “Soft Magnetic Materials in High-Frequency, High-Power Conversion Applications”. In: *JOM Journal of the Minerals*, vol. 64, (July 2012). DOI: 10.1007/s11837-012-0350-0 (cit. on p. 93).
- [LSS07] A.-H. Lu, E. L. Salabas, and F. Schüth. “Magnetic Nanoparticles: Synthesis, Protection, Functionalization, and Application”. In: *Angewandte Chemie International Edition*, vol. 46, no. 8 (2007), pp. 1222–1244. DOI: 10.1002/anie.200602866 (cit. on p. 93).
- [LWH+06] W.-C. Lin, S.-S. Wong, P.-C. Huang, et al. “Controlled growth of Co nanoparticle assembly on nanostructured template Al₂O₃/NiAl (100)”. In: *Applied physics letters*, vol. 89, no. 15 (2006). DOI: 10.1063/1.2358926 (cit. on p. 90).
- [LWH+10] W.-C. Lin, C. Wu, P.-J. Hsu, et al. “Coverage dependence of magnetic domain structure and magnetic anisotropy in supported Fe nanoparticles on Al₂O₃/NiAl (100)”. In: *Journal of Applied Physics*, vol. 108, no. 3 (2010). DOI: 10.1063/1.3457794 (cit. on p. 90).
- [LWY18] D. Luo, C. Wu, and M. Yan. “Incorporation of the Fe₃O₄ and SiO₂ nanoparticles in epoxy-modified silicone resin as the coating for soft magnetic composites with enhanced performance”. In: *Journal of Magnetism and Magnetic Materials*, vol. 452, (2018), pp. 5–9. DOI: 10.1016/j.jmmm.2017.12.005 (cit. on p. 89).
- [LZW+20] X. Liu, Y. Zhang, Y. Wang, et al. “Comprehensive understanding of magnetic hyperthermia for improving antitumor therapeutic efficacy”. In: *Theranostics*, vol. 10, no. 8 (2020), p. 3793. DOI: 10.7150/thno.40805 (cit. on p. 93).
- [MJVM15] D. Miu, S. Jinga, B. Vasile, et al. “Out of plane superferromagnetic behavior of quasi two-dimensional Fe/Al₂O₃ multilayer nanocomposites”. In: *Journal of Applied Physics*, vol. 117, no. 7 (2015). DOI: 10.1063/1.4908219 (cit. on p. 90).
- [MOT+17] M. Morcrette, G. Ortiz, S. Tallegas, et al. “Fabrication of monodisperse magnetic nanoparticles released in solution using a block copolymer template”. In: *Journal of Physics D: Applied Physics*, vol. 50, no. 29 (June 2017), p. 295001. DOI: 10.1088/1361-6463/aa790b (cit. on p. 92).
- [MSS+15] A. Moazenzadeh, F. Suárez Sandoval, N. Spengler, et al. “3-D Micro-transformers for DC–DC On-Chip Power Conversion”. In: *IEEE Transactions on Power Electronics*, vol. 30, no. 9 (2015), pp. 5088–5102. DOI: 10.1109/TPEL.2014.2368252 (cit. on p. 7).
- [MXL19] J. Mohapatra, M. Xing, and J. P. Liu. “Inductive Thermal Effect of Ferrite Magnetic Nanoparticles”. In: *Materials*, vol. 12, no. 19 (2019). DOI: 10.3390/ma12193208 (cit. on p. 93).
- [Née49a] L. Néel. “Influence des fluctuations thermiques sur l’aimantation de grains ferromagnétiques très fins”. In: *Comptes Rendus Hebdomadaires Des Seances De L Academie Des Sciences*, vol. 228, no. 8 (1949), pp. 664–666 (cit. on p. 26).

- [Née49b] L. Néel. “Théorie du traînage magnétique des ferromagnétiques en grains fins avec application aux terres cuites”. In: *Annales de géophysique*. Vol. 5, 1949, pp. 99–136 (cit. on p. 26).
- [NGM13] A. Nunns, J. Gwyther, and I. Manners. “Inorganic block copolymer lithography”. In: *Polymer*, vol. 54, no. 4 (2013), pp. 1269–1284. DOI: 10.1016/j.polymer.2012.11.057 (cit. on p. 91).
- [NM13] A. Noshay and J. McGrath. *Block Copolymers: Overview and Critical Survey*. Elsevier Science, 2013. DOI: 10.1002/pol.1978.130160313 (cit. on p. 91).
- [NSSP19] M. Najgebauer, J. Szczyglowski, B. Slusarek, et al. “Scaling algorithms in modelling of power loss in soft magnetic composites”. In: *COMPEL - The international journal for computation and mathematics in electrical and electronic engineering*, vol. 38, (June 2019). DOI: 10.1108/COMPEL-10-2018-0412 (cit. on p. 8).
- [Oeh86] G. S. Oehrlein. “Reactive-Ion Etching”. In: *Physics Today*, vol. 39, no. 10 (1986), pp. 26–33. DOI: 10.1063/1.881066 (cit. on p. 91).
- [Ola16] I. B. Olaetxea. “Synthesis and Characterization of hybrid nanomaterials based on block copolymers and magnetic nanoparticle”. PhD thesis. Engineering College, Gipuzkoa, 2016 (cit. on p. 92).
- [P1] K. Brzuszek and A. Janutka. “High-frequency magnetic response of superferromagnetic nanocomposites”. In: *Journal of Magnetism and Magnetic Materials*, vol. 543, (2022), p. 168608. DOI: 10.1016/j.jmmm.2021.168608 (cit. on pp. 1, 12, 23, 26).
- [P2] K. Brzuszek, C. A. Ross, and A. Janutka. “High-frequency magnetic response of superparamagnetic composites of spherical Fe₆₅Co₃₅ nanoparticles”. In: *Journal of Magnetism and Magnetic Materials*, vol. 573, (2023), 170651. DOI: 10.1016/j.jmmm.2023.170651 (cit. on pp. 1, 12, 26, 28, 32).
- [P3] K. Brzuszek, C. A. Ross, and A. Janutka. “High-frequency magnetic response of superparamagnetic composites of spherical Fe and Fe₃O₄ nanoparticles”. DOI: 10.2139/ssrn.4709514 (cit. on pp. 1, 12, 28, 32).
- [P4] K. Brzuszek, C. A. Ross, and A. Janutka. “High-Frequency Magnetic Response of Arrays of Planar Fe₆₅Co₃₅ Nanodots: Effects of Bias Field and Thermal Fluctuations”. In: *IEEE Transactions on Magnetics*, vol. 59, no. 11 (2023), 7100306. DOI: 10.1109/TMAG.2023.3313871 (cit. on pp. 1, 12, 30, 32).
- [P5] K. Brzuszek, C. A. Ross, and A. Janutka. “High-frequency magnetic response of crystalline and nanocrystalline antiferromagnetic NiO”. In: *AIP Advances*, vol. 14, no. 2 (Feb. 2024), p. 025222. DOI: 10.1063/9.0000781 (cit. on pp. 1, 12, 32).
- [PB00] C. E. Porter and F. D. Blum. “Thermal characterization of PMMA thin films using modulated differential scanning calorimetry”. In: *Macromolecules*, vol. 33, no. 19 (2000), pp. 7016–7020. DOI: 10.1021/ma0003021 (cit. on p. 90).

- [Pla17] V. M. Planck. “Über einen Satz der statistischen Dynamik und seine Erweiterung in der Quantentheorie”. In: *Sitzungsberichte der Königlich-Preussischen Akademie der Wissenschaften zu Berlin* (1917) (cit. on p. 17).
- [PWKF18] E. A. Périgo, B. Weidenfeller, P. Kollár, et al. “Past, present, and future of soft magnetic composites”. In: *Applied Physics Reviews*, vol. 5, no. 3 (2018), p. 031301. DOI: 10.1063/1.5027045 (cit. on pp. 8, 9, 90).
- [PYL+16] Y. Peng, Y. Yi, L. Li, et al. “Iron-based soft magnetic composites with Al₂O₃ insulation coating produced using sol–gel method”. In: *Materials & Design*, vol. 109, (2016), pp. 390–395. DOI: 10.1016/j.matdes.2016.07.097 (cit. on p. 89).
- [RESM12] R. Raeisi Shahraki, M. Ebrahimi, S. A. Seyyed Ebrahimi, et al. “Structural characterization and magnetic properties of superparamagnetic zinc ferrite nanoparticles synthesized by the coprecipitation method”. In: *Journal of Magnetism and Magnetic Materials*, vol. 324, no. 22 (2012), pp. 3762–3765. DOI: 10.1016/j.jmmm.2012.06.020 (cit. on p. 90).
- [SÁP+06] L. Százdí, Á. Ábrányi, B. Pukánszky Jr., et al. “Morphology Characterization of PP/Clay Nanocomposites Across the Length Scales of the Structural Architecture”. In: *Macromolecular Materials and Engineering*, vol. 291, no. 7 (2006), pp. 858–868. DOI: 10.1002/mame.200600026 (cit. on p. 90).
- [SBA+14] P. Sirvent, E. Berganza, A. M. Aragón, et al. “Effective high-energy ball milling in air of Fe₆₅Co₃₅ alloys”. In: *Journal of Applied Physics*, vol. 115, no. 17 (2014). DOI: 10.1063/1.4862220 (cit. on p. 90).
- [Sch08] H. Schiff. “Nanoimprint lithography: An old story in modern times? A review”. In: *Journal of Vacuum Science & Technology B: Microelectronics and Nanometer Structures Processing, Measurement, and Phenomena*, vol. 26, no. 2 (2008), pp. 458–480. DOI: 10.1116/1.2890972 (cit. on p. 90).
- [Sen20] M. Sen. “Nanocomposite materials”. In: *Nanotechnology and the Environment*, (2020), pp. 1–12. DOI: 10.5772/intechopen.93047 (cit. on p. 93).
- [SFHM18] J. M. Silveyra, E. Ferrara, D. L. Huber, et al. “Soft magnetic materials for a sustainable and electrified world”. In: *Science*, vol. 362, no. 6413 (2018), eaao0195. DOI: 10.1126/science.aao0195 (cit. on p. 93).
- [SJ07] H. Shokrollahi and K. Janghorban. “Soft magnetic composite materials (SMCs)”. In: *Journal of Materials Processing Technology*, vol. 189, no. 1 (2007), pp. 1–12. DOI: 10.1016/j.jmatprotec.2007.02.034 (cit. on pp. 90, 93).
- [SKK+07] S. J. Shin, Y. H. Kim, C. W. Kim, et al. “Preparation of magnetic FeCo nanoparticles by coprecipitation route”. In: *Current Applied Physics*, vol. 7, no. 4 (2007), pp. 404–408. DOI: 10.1016/j.cap.2006.09.012 (cit. on p. 90).
- [SMAY14] S. A. Seyyed Ebrahimi, S. M. Masoudpanah, H. Amiri, et al. “Magnetic properties of MnZn ferrite nanoparticles obtained by SHS and sol-gel auto-combustion techniques”. In: *Ceramics International*, vol. 40, no. 5 (2014), pp. 6713–6718. DOI: 10.1016/j.ceramint.2013.11.133 (cit. on p. 90).

- [SML+21] D. S. Schmool, D. Markó, K.-W. Lin, et al. “Ferromagnetic Resonance Studies in Magnetic Nanosystems”. In: *Magnetochemistry*, vol. 7, no. 9 (2021). DOI: 10.3390/magnetochemistry7090126 (cit. on p. 15).
- [Smo16a] M. Smoluchowski. “Drei Vorträge über Diffusion, Brownsche Bewegung und Koagulation von Kolloidteilchen”. In: *Zeitschrift für Physik*, vol. 17, (Jan. 1916), pp. 557–585 (cit. on p. 17).
- [Smo16b] M. Smoluchowski. “Über Brownsche Molekularbewegung unter Einwirkung äußerer Kräfte und deren Zusammenhang mit der verallgemeinerten Diffusionsgleichung”. In: *Annalen der Physik*, vol. 353, no. 24 (1916), pp. 1103–1112 (cit. on p. 17).
- [Sno48] J. L. Snoek. “Dispersion and absorption in magnetic ferrites at frequencies above one Mc/s”. In: *Physica*, vol. 14, no. 4 (1948), pp. 207–217. DOI: 10.1016/0031-8914(48)90038-X (cit. on p. 17).
- [SPK21] B. Sai Ram, A. Paul, and S. Kulkarni. “Soft magnetic materials and their applications in transformers”. In: *Journal of Magnetism and Magnetic Materials*, vol. 537, (2021), p. 168210. DOI: 10.1016/j.jmmm.2021.168210 (cit. on p. 93).
- [SSNW07] K. Sokalski, J. Szczyglowski, M. Najgebauer, et al. “Losses scaling in soft magnetic materials”. In: *COMPEL: The International Journal for Computation and Mathematics in Electrical and Electronic Engineering*, vol. 26, (June 2007), pp. 640–649. DOI: 10.1108/03321640710751118 (cit. on p. 8).
- [ST17] K. J. Sunday and M. L. Taheri. “Soft magnetic composites: recent advancements in the technology”. In: *Metal Powder Report*, vol. 72, no. 6 (2017), pp. 425–429. DOI: 10.1016/j.mprp.2016.08.003 (cit. on p. 90).
- [Ste92] C. P. Steinmetz. “On the Law of Hysteresis”. In: *Transactions of the American Institute of Electrical Engineers*, vol. IX, no. 1 (1892), pp. 1–64. DOI: 10.1109/T-AIEE.1892.5570437 (cit. on p. 8).
- [SYH+12] S. K. Suh, K. Yuet, D. K. Hwang, et al. “Synthesis of Nonspherical Superparamagnetic Particles: In Situ Coprecipitation of Magnetic Nanoparticles in Microgels Prepared by Stop-Flow Lithography”. In: *Journal of the American Chemical Society*, vol. 134, no. 17 (2012). PMID: 22462394, pp. 7337–7343. DOI: 10.1021/ja209245v (cit. on p. 92).
- [TD10] Y.-C. Tseng and S. B. Darling. “Block Copolymer Nanostructures for Technology”. In: *Polymers*, vol. 2, no. 4 (2010), pp. 470–489. DOI: 10.3390/polym2040470 (cit. on p. 91).
- [TEGJ10] A. H. Taghvaei, A. Ebrahimi, K. Gheisari, et al. “Analysis of the magnetic losses in iron-based soft magnetic composites with MgO insulation produced by sol–gel method”. In: *Journal of Magnetism and Magnetic Materials*, vol. 322, no. 23 (2010), pp. 3748–3754. DOI: 10.1016/j.jmmm.2010.07.032 (cit. on p. 89).
- [TGH+12] A. Tavakkoli KG, K. Gotrik, A. Hannon, et al. “Templating three-dimensional self-assembled structures in bilayer block copolymer films”. In: *Science*, vol. 336, no. 6086 (2012), pp. 1294–1298. DOI: 10.1126/science.1218437 (cit. on p. 93).

- [TLF+08] C. Tang, E. M. Lennon, G. H. Fredrickson, et al. “Evolution of block copolymer lithography to highly ordered square arrays”. In: *Science*, vol. 322, no. 5900 (2008), pp. 429–432. DOI: 10.1126/science.1162950 (cit. on p. 91).
- [TLT16] M. C. Traub, W. Longsine, and V. N. Truskett. “Advances in nanoimprint lithography”. In: *Annual review of chemical and biomolecular engineering*, vol. 7, (2016), pp. 583–604. DOI: 10.1146/annurev-chembioeng-080615-034635 (cit. on p. 90).
- [TSB+21] A. Talaat, M. Suraj, K. Byerly, et al. “Review on soft magnetic metal and inorganic oxide nanocomposites for power applications”. In: *Journal of Alloys and Compounds*, vol. 870, (2021), p. 159500. DOI: 10.1016/j.jallcom.2021.159500 (cit. on p. 90).
- [UWN+07] G. Uozumi, M. Watanabe, R. Nakayama, et al. “Properties of soft magnetic composite with evaporated MgO insulation coating for low iron loss”. In: *Materials science forum*. Vol. 534, Trans Tech Publ. 2007, pp. 1361–1364. DOI: 10.4028/www.scientific.net/MSF.534-536.1361 (cit. on p. 89).
- [VK14] L. Varga and J. Kováč. “Minor loop scaling rules for finemet type soft magnetic cores”. In: *Acta Physica Polonica A*, vol. 126, no. 1 (2014), pp. 156–157. DOI: 10.12693/APhysPolA.126.156 (cit. on p. 8).
- [VLD+] A. Vansteenkiste, J. Leliaert, M. Dvornik, et al. *mumax³ GPU-accelerated micromagnetism*. Ghent University. URL: <https://mumax.github.io/api.html> (cit. on p. 81).
- [VLD+14] A. Vansteenkiste, J. Leliaert, M. Dvornik, et al. “The design and verification of MuMax3”. In: *AIP Advances*, vol. 4, no. 10 (Oct. 2014), p. 107133. DOI: 10.1063/1.4899186 (cit. on p. 81).
- [VWS+15] E. C. Vreeland, J. Watt, G. B. Schober, et al. “Enhanced Nanoparticle Size Control by Extending LaMer’s Mechanism”. In: *Chemistry of Materials*, vol. 27, no. 17 (2015), pp. 6059–6066. DOI: 10.1021/acs.chemmater.5b02510 (cit. on p. 90).
- [WDS+16] N. Wang, B. B. Doris, A. B. Shehata, et al. “High-Q magnetic inductors for high efficiency on-chip power conversion”. In: *2016 IEEE International Electron Devices Meeting (IEDM)*. IEEE. 2016, pp. 35.3.1–35.3.4. DOI: 10.1109/IEDM.2016.7838547 (cit. on p. 7).
- [WMZL12] S. Wang, J. Ma, X. Zhang, et al. “Magnetic softness and interparticle exchange interactions of $(\text{Fe}_{65}\text{Co}_{35})_{1-x}(\text{Al}_2\text{O}_3)_x$ ($x=0-0.50$) nanogranular films”. In: *Thin Solid Films*, vol. 520, no. 15 (2012), pp. 5046–5052. DOI: 10.1016/j.tsf.2012.03.025 (cit. on p. 13).
- [WSL16] D. Wu, N. S Rajput, and X. Luo. “Nanoimprint lithography – the past, the present and the future”. In: *Current Nanoscience*, vol. 12, no. 6 (2016), pp. 712–724. DOI: 10.2174/1573413712666160530120432 (cit. on pp. 90, 91).

- [XSD+14] L. Xiao, Y. Sun, C. Ding, et al. “Annealing effects on magnetic properties and strength of organic-silicon epoxy resin-coated soft magnetic composites”. In: *Proceedings of the Institution of Mechanical Engineers, Part C: Journal of Mechanical Engineering Science*, vol. 228, no. 12 (2014), pp. 2049–2058. DOI: 10.1177/0954406213515112 (cit. on p. 89).
- [Yal13] O. Yalçın. “Ferromagnetic Resonance”. In: *Ferromagnetic Resonance*. Ed. by O. Yalcin. Rijeka: IntechOpen, 2013. DOI: 10.5772/56134 (cit. on pp. 13, 15).
- [YGZ+10] D.-S. Yao, S.-H. Ge, X.-Y. Zhou, et al. “Soft Magnetism and High Frequency Properties of Fe₆₅Co₃₅–MgF₂ Granular Thin Films”. In: *Chinese Physics Letters*, vol. 27, no. 6 (2010), p. 067502. DOI: 10.1088/0256-307X/27/6/067502 (cit. on p. 89).
- [YTHJ13] M. Yaghtin, A. H. Taghvaei, B. Hashemi, et al. “Effect of heat treatment on magnetic properties of iron-based soft magnetic composites with Al₂O₃ insulation coating produced by sol–gel method”. In: *Journal of Alloys and Compounds*, vol. 581, (2013), pp. 293–297. DOI: 10.1016/j.jallcom.2013.07.008 (cit. on p. 89).
- [Zho10] Z. Zhou. “Hybrid Materials of Block Copolymers and Magnetic Nanoparticles”. PhD thesis. Queen’s University, Kingston, Ontario, Canada, 2010 (cit. on p. 92).
- [ZWX15] Y. Y. Zheng, Y. G. Wang, and G. T. Xia. “Amorphous soft magnetic composite-cores with various orientations of the powder-flakes”. In: *Journal of Magnetism and Magnetic Materials*, vol. 396, (2015), pp. 97–101. DOI: 10.1016/j.jmmm.2015.08.036 (cit. on p. 90).
- [ZWY16] G. Zhao, C. Wu, and M. Yan. “Evolution of the insulation matrix and influences on the magnetic performance of Fe soft magnetic composites during annealing”. In: *Journal of Alloys and Compounds*, vol. 685, (2016), pp. 231–236. DOI: 10.1016/j.jallcom.2016.05.277 (cit. on p. 90).
- [ZZL+20] J. Zheng, H. Zheng, J. Lei, et al. “Magnetic properties and microstructure of iron-based soft magnetic composites with Al₂O₃ insulating coating by one-pot synthesis method”. In: *Journal of Magnetism and Magnetic Materials*, vol. 499, (2020), p. 166255. DOI: 10.1016/j.jmmm.2019.166255 (cit. on p. 89).

List of Figures

2.1	Hysteresis losses are directly related to area of hysteresis – [PWKF18]	8
2.2	Possible paths of eddy currents in magnetic nanocomposite – origin of eddy currents losses – [PWKF18]	9
3.1	Angles for determining ferromagnetic resonance frequencies from eq. (3.2.2) – [DDF07]	15
3.2	Average amplitude \bar{x} is a function of noise intensity D – [GHJM98]	21
3.3	Transformation of wells given by eq. (3.2.6) – [GHJM98]	21
4.1	Comparison of analytical and simulated values of magnetic permeability components for two selected superferromagnetic composites – breakthrough on the Snoek limit	24
4.2	Strong response of $(\text{Fe}_{65}\text{Co}_{35})_{0.6}(\text{Al}_2\text{O}_3)_{0.4}$ to the rotating field of 2 kA m^{-1} in the plane, components of m_x and m_y are shown.	25
4.3	Response of superparamagnetic composite as a function of system temperature – highlighting low and high energy barrier regimes	27
4.4	Stabilization of the response of Fe_3O_4 as a function of nanoparticle size and temperature	28
4.5	Dynamical hystereses for different sizes of nanoparticles of Fe_3O_4 – an increase in size leads to opening the hysteresis loop and therefore to an increase in losses	29
4.6	Averaged loops of hystereses for different sizes of nanoparticles of Fe_3O_4	29
4.7	Relaxed magnetization for an array of $4 \times 4 \times 4$ nanodiscs with a diameter of 5 nm and a height of 1 nm (RIA-I). Random orientations of the anisotropy axes	30
4.8	Response amplitude function for RIA-I as a function of perpendicular field	31
A.1	Schematic representation of the NIL process – [CKR95]	91
A.2	Concentration (local and global) of A phase in copolymer depending on position – [BF90]	92